View metadata, citation and similar papers at core.ac.uk
brought to you by CORE
provided by Thèses en ligne de l'Université Toulouse III - Paul Sabatier

THÈSE

En vue de l'obtention du

DOCTORAT DE L'UNIVERSITÉ DE TOULOUSE

Délivré par *l'Université Toulouse III - Paul Sabatier*
Discipline ou spécialité : *Physico-chimie théorique*

Présentée et soutenue par *Rémi MAURICE*
Le *lundi 20 juin 2011*

Titre : *Zero-Field Anisotropic Spin Hamiltonians in First-Row Transition Metal Complexes: Theory, Models and Applications*

JURY
Pr. Mark R. Pederson (rapporteur)
Pr. John E. McGrady (rapporteur)
Pr. Ria Broer-Braam (examinatrice)
Dr. Jean-Pascal Sutter (président)
Pr. Rosa Caballol (examinatrice)
Pr. Nathalie Guihéry (directrice de thèse)
Dr. Coen de Graaf (directeur de thèse)

Ecole doctorale : *Sciences de la Matière (EDSDM)*
Unité de recherche : *Laboratoire de Chimie et de Physique Quantiques*
Directeur(s) de Thèse : *Pr. Nathalie Guihéry (Toulouse) et Dr. Coen de Graaf (Tarragone)*
Rapporteurs : *Pr. Mark R. Pederson et Pr. John E. McGrady*

Rémi Maurice

ZERO-FIELD ANISOTROPIC SPIN HAMILTONIANS IN FIRST-ROW TRANSITION METAL COMPLEXES: THEORY, MODELS AND APPLICATIONS

TESI DOCTORAL

dirigida pels Drs. Coen de Graaf i Nathalie Guihéry

Departament de Química Física i Inorgànica

UNIVERSITAT ROVIRA I VIRGILI

Tarragona

Juny 2011

Resumen de la tesis

La anisotropía magnética es una propiedad física que se encuentra en sistemas con electrones desapareados, como complejos de coordinación, moléculas orgánicas, o materiales, que puede aparecer sin la presencia de un campo magnético externo en sistemas no degenerados de baja simetra y de espín superior a 1/2. En este caso, la interacción espín-órbita desdobla los niveles del estado fundamental (o de los estados magnéticos los mas bajos en energía en sistemas polinucleares): es el denominado "Zero-Field Splitting" (ZFS). Este efecto se puede describir con un Hamiltoniano de espín, es decir que el grado de libertad principal es el espín dado que los niveles más bajos que resultan del desdoblamiento espín-órbita tienen una parte orbital muy parecida.

Los Hamiltonianos modelos de espín que se suelen utilizar son fenomenológicos e introducen parámetros de ZFS extraídos de experimentos o de cálculos teóricos. El objetivo principal de la tesis consiste en la validación de estos modelos de manera rigurosa, utilizando la teoría de los Hamiltonianos efectivos. Para llegar a este objetivo, una primera etapa consiste en elegir y validar un método de cálculo que proporcione la parte baja del espectro espín-órbita. Para este estudio se han considerado varios complejos mononucleares, y los resultados obtenidos presentan un buen acuerdo con los valores experimentales. La metodología de cálculo elegida, ab initio con inclusión de la correlación electrónica y relativista, se basa en métodos de función de onda y se efectúa en dos etapas. Primero, una colección de estados libres de interacción espín-órbita se calculan al nivel "Complete Active Space Self Consistent Field" (CASSCF) para dar cuenta de la correlación non dinámica. En segundo lugar, se construye una matriz de interacción entre los componentes espín-órbita de los estos estados que posteriormente se diagonaliza. Los efectos de correlación dinámica se incluyen modificando los elementos diagonales de la matriz con las energías obtenidas a un nivel "post-CASSCF". Se estudiaron

los diferentes grados de libertad de este método, los resultados obtenidos en una seria de complejos mono- y bi-nucleares mostraron buen acuerdo con la experiencia.

Los Hamiltonianos anisotrópicos se extraen mediante la teoría de los Hamiltonianos efectivos. Este método de extracción permite la validación o la mejora de los modelos fenomenológicos, validando el espacio modelo y los operadores utilizados en el modelo. Las ventajas de utilizar este método de extracción han sido varias. En primer lugar, en complejos mononucleares, pueden extraerse los parámetros de ZFS y los ejes magnéticos a partir de cualquier sistema de ejes arbitrario para cualquier configuración d^n. En segundo lugar, en sistemas binucleares, pueden extraerse los términos antisimétricos del Hamiltoniano multiespín, lo que se ha hecho por primera vez en este trabajo a partir de cálculos ab initio para la configuración $d^9 - d^9$. Finalmente, se han podido mejorar los modelos usuales multiespín y de espín gigante para configuraciones $d^8 - d^8$, lo que ha llevado a nuevos modelos. Analizando todos los datos obtenidos para la variedad de configuraciones estudiadas, se pueden generar todos los modelos mono- y bi-nucleares.

Otro objetivo importante de esta tesis consiste en proponer racionalizaciones de la anisotropía en varios casos de interés. Los Hamiltonianos de espín se derivaron analíticamente, usando la teoría del campo del ligando. Se revisaron los trabajos pioneros de Abragam y Bleaney y se extendieron a sistemas mono- y bi-nucleares. Los resultados son de especial interés para poder proponer explicaciones simples a los grupos experimentales, permitiendo un ajuste de la propiedad con la estructura electrónica. Se ha mostrado que las reglas empíricas estándar para mejorar la anisotropía no son aplicables a complejos de Mn(III), lo que permite entender que no sea posible encontrar una anisotropía muy grande para esta configuración. En complejos binucleares, como el conocido caso del acetato de cobre, se ha observado que la correlación dinámica tiene un papel importante.

Este trabajo también ha permitido evidenciar las limitaciones metodológicas, cuando no sólo el átomo metálico sino también el ligando pueden participar en el ZFS por efectos de covalencia y transferencia de carga. Aunque se puede entender de manera intuitiva que estos efectos participan en el ZFS, su racionalización y tratamiento teórico son problemáticos. En particular, se ha mostrado en una seria de complejos modelo que el método utilizado en esta tesis no es válido en este caso. Este trabajo abre pues perspectivas metodológicas, que consisten en desarrollar e implementar un método válido para estos casos.

Otra perspectiva de interés es de extender el estudio de la anisotropía asimétrica a sistemas polinucleares, a sistemas orgánicos y a materiales de estructura más compleja.

Résumé de la thèse

Introduction

L'anisotropie magnétique est une propriété physique qui peut apparaître dans divers systèmes moléculaires tels les complexes de métaux de transition et les systèmes organiques, ou encore certains matériaux. Cette propriété nécessite un état fondamental de nombre quantique de spin S supérieur ou égal à un dans les systèmes mononucléaires, et la présence d'au moins deux électrons célibataires dans les complexes polynucléaires. Si la symétrie du système le permet, les états électroniques se mélangent et s'éclatent sous l'effet conjoint du champ de ligand et du couplage spin-orbite: c'est l'éclatement en champ nul, "Zero-Field Splitting" (ZFS).

Cet effet est souvent caractérisé de façon expérimentale par la Résonance Paramagnétique Electronique (RPE), qui permet d'extraire les paramètres d'anisotropie en ajustant spectres modèles et expérimentaux. Depuis les premières extractions concernant par exemple l'acétate de cuivre monohydraté, cette méthode a évolué gràce à l'usage de hautes fréquences et hauts champs magnétiques (RPE-HF), permettant d'atteindre une précision remarquable dans la détermination des paramètres d'anisotropie dans la plupart des cas intéressants. D'autres avancées significatives concernent les matériaux, et les modèles pour décrire les interactions intersites. Après l'introduction des termes antisymétriques dans le modèle multispin par Dzyaloshinskii en 1958, Moriya rationalisa les termes de ce modèle en géneralisant la théorie du superéchange de Anderson.

La découverte des aimants moléculaires, par la caractérisation du Mn_{12} au début des années 90, a enfin renouvelé la thématique en suscitant de nouveaux travaux de la part de chimistes et physiciens, expérimentateurs et théoriciens. Ces molécules particulières se comportent comme des aimants à très basse température, et ont notamment permis d'étudier de façon intensive l'effet tunnel quantique à une échelle mésoscopique ou nanoscopique. Un des grands enjeux

actuels, qui permettrai d'envisager des applications technologiques viables, serait d'augmenter la température de blocage des ces aimants, et donc de favoriser l'anisotropie axiale tout en inhibant l'anisotropie rhombique, et d'augmenter les barrières d'anisotropie. Pour construire de façon rationnelle ce type de système idéal, le chimiste doit mieux comprendre le lien entre structure et propriété.

Jusqu'à présent, la plupart des travaux reliant structure et propriété, ou rationalisant le ZFS concernent les complexes mononucléaires. Abragam et Bleaney par exemple, dans leur fameux livre, ont proposé des rationalisations qualitatives pour toutes les configurations d^n dans des geométries octahédriques distordues. Puisqu'aujourd'hui de nombreux résultats expérimentaux sont disponibles, une étude théorique sérieuse et systématique serait donc bienvenue.

La réalisation d'une telle étude nécessite de disposer de méthodes de calculs fiables permettant une bonne comparaison aux valeurs expérimentales. Un des objectifs majeurs de cette thèse est de définir et tester quelques méthodes de calcul du ZFS.

Méthodologie

Dans la mesure où les méthodes basées sur la fonction d'onde peuvent permettre de décrire proprement le caractère multidéterminental de la fonction d'onde, ce sont les méthodes de choix pour le calcul du ZFS. Les méthodologies de calcul utilisées comportent deux étapes. Dans la première, un nombre choisi d'états spin-orbite "free" est calculé au niveau CASSCF ("Complete Active Space Self-Consistent Field"), CASPT2 ("Complete Active Space Second-Order Perturbation Theory") ou MRCI ("Multi-Reference Configuration Interaction") pour rendre compte des effets de corrélation non dynamique et dynamique. Dans la deuxième, la matrice d'interaction, entre les composantes M_S des différents états construit précédemment, incluant les effets du couplage spin-orbite et parfois spin-spin, est construite et diagonalisée. La prise en compte des effets de corrélation dynamique se fait par l'utilisation des énergies corrélées sur la diagonale de la matrice d'interaction. Cette méthodologie de calcul comporte plusieurs degrés de liberté, qui doivent être ajustés en fonction de la configuration d^n et de la structure considérée. Les complexes binucléaires, quant à eux, étant plus sujets à la correlation dynamique, nécessiteront plus d'attention sur le plan méthodologique.

Afin de pouvoir extraire de façon rigoureuse les hamiltoniens de spin anisotropes, la théorie

des hamiltoniens effectifs est utilisée. Cette théorie tire profit des informations contenues dans les energies des états de basse énergie ainsi que des fonctions d'onde projetées sur un espace modèle, defini au préalable. En projetant explicitement l'information contenue dans le hamiltonien électronique exact sur l'espace modèle, la validité de ce dernier peut être vérifiée en contrôlant la norme de la projection pour chaque état (ici les états spin-orbite de basse énergie). De plus, en comparant terme à terme les matrices d'interaction modèle et effective, la validité des opérateurs utilisés dans le hamiltonien modèle peut être remise en question et les modèles usuels éventuellement améliorés, ce qui s'est avéré nécéssaire pour les complexes binucléaires pour lesquels les modèles usuels ne sont pas pertinents.

Afin de rationaliser le ZFS, un modèle intermédiaire entre les approches de Abragam et Bleaney et le modèle de Racah doit être envisagé. Ces deux approches se basent sur la théorie du champ cristallin, et ont toutes deux leurs avantages et inconvénients. Dans l'approche d'Abragam et Bleaney, le champ cristallin est traité en tant que perturbation du hamiltonien de l'ion libre. Seuls les effets du champ au premier order de perturbation sont considérés, c'est à dire l'éclatement du multiplet fondamental de l'ion libre dû au champ cristallin. Les effets du couplage spin-orbite sont ensuite traités, mais la contribution au ZFS des états provenant de multiplets excités dans l'ion libre est négligée, ce qui n'est pas toujours une approximation valable. L'approche de Racah permet quant à elle d'inclure de telles contributions, mais est souvent trop compliquée pour un traitement à la main du problème car il s'agit de diagonaliser un hamiltonien comprenant les termes de l'ion libre ainsi qu'un opérateur monoélectronique de champ cristallin. L'approche utilisée prend en compte le meilleur des deux mondes, en incluant uniquement les effets de premier ordre du champ cristallin (comme Abragam et Bleaney), mais en permettant d'introduire des états provenants de n'importe quel multiplet de l'ion libre (comme Racah). Pour cela, les états spin-orbite "free" sont exprimés dans la base des orbitales réelles et couplés par un opérateur monoélectronique de couplage spin-orbite.

Complexes mononucléaires

Dans les complexes mononucléaires ayant un état fondamental de spin S égal à un ou trois demi, le ZFS peut être décrit par le hamiltonien modèle suivant:

$$\hat{H}_{mod} = \hat{\mathbf{S}}\overline{\overline{D}}\hat{\mathbf{S}} \tag{1}$$

où $\overline{\overline{D}}$ est le tenseur symétrique de ZFS de rang deux. En confrontant terme à terme la matrice d'interaction modèle (obtenue en développant et applicant $\hat{H}_{mod}$ à l'espace modèle) à la matrice d'interation effective, il est montré dans un premier temps que la théorie des hamiltoniens effectifs permet d'extraire le tenseur de ZFS pour les configurations d^8 et d^7 dans un repère d'axes arbitraire. Les axes propres magnétiques et les paramètres d'anisotropie axiaux et rhombiques peuvent donc être obtenus à partir d'un calcul *ab initio* unique et ce même en cas de dégénérescence de Kramers. En utilisant un calcul spin-orbite de type variation/perturbation, cette méthode d'extraction a permis pour la première fois d'inclure des effets d'ordre supérieur à deux dans le calcul des paramètres d'anisotropie pour les états fondamentaux de spin demi-entier.

Au travers de l'étude de deux complexes, $[Ni(HIM2\text{-}Py)_2NO_3]^+$ et $[Co(PPh_3)_2Cl_2]$, pour lesquels des études expérimentales précises par RPE-HF existent, les degrés de liberté principaux de la méthode utilisée ont été étudiés. Il a été notamment montré que pour obtenir des résultats en bon accord avec l'expérience, un compromis est nécéssaire: traiter le mieux possible les états qui contribuent le plus au ZFS, tout en maintenant un équilibre des excitations dans les différentes directions de l'espace. L'ajout des configurations de type transfert de charge ligand-métal permet de réduire la surestimation des effets du couplage spin-orbite liée au champ moyen (CASSCF), et la corrélation dynamique doit être prise en compte en utilisant des énergies obtenues à un niveau CASPT2 ou NEVPT2 ("N-Electron Valence Perturbation Theory") par exemple sur la diagonale de la matrice d'interaction d'états afin d'obtenir des valeurs précises. Dans la mesure où les paramètres calculés sont modérément affectés par les degrés de liberté, il est aussi montré que des résultats semi-quantitatifs peuvent être obtenus pour un coût calculatoire raisonnable. De tels calculs ont permis de proposer des rationalisations et des corrélations magnéto-structurales dans les complexes mononucléaires.

Lorsque quatre électrons célibataires ou plus sont présents dans l'état fondamental (S supérieur ou égal à deux), des interactions issues d'opérateurs biquadratiques apparaissent dans le hamiltonien effectif et doivent donc être introduits dans le hamiltonien modèle. Si la matrice d'interaction *ab initio* construite dans la deuxième étape prend en compte simultanément les couplages spin-spin et spin-orbite, alors il devient impossible de définir formellement un système d'axes propres magnétiques dans les cas non symétriques. Dans cette thèse, le couplage spin-spin est donc en général négligé, puisque sa contribution est souvent bien

moindre que celle du couplage spin-orbite. Les axes propres magnétiques sont donc définis à partir des axes engendrés par le couplage spin-orbite uniquement. Il est ensuite montré que dans ce système d'axes, un modèle basé sur les opérateurs de Stevens est parfaitement adequat, validant le modèle pour l'ensemble des complexes mononucléaires.

Un des objectifs principaux de cette thèse était de proposer des rationalisations du ZFS. Souvent, les chimistes essaient d'augmenter l'anisotropie de leurs systèmes en distordant la géométrie gràce à l'utilisation: de ligands de natures diffèrentes ou en imposant des sphères de coordinations exotiques aux métaux de transition. Une analyse plus fine, considérant que le ZFS est un effet du second ordre des perturbations, mène à la conclusion que stabiliser les états d^n excités par rapport à l'état fondamental peut aussi être une bonne stratégie. Pour cela, on peut utiliser des ligands π-accepteur dans les complexes pseudo-octaédriques par exemple. En dérivant des formules analytiques pour décrire le ZFS à partir de la théorie du champ cristallin, il a été montré que les complexes six fois coordinés de Ni(II) suivent ces règles, alors que les complexes de Mn(III) ont un comportement moins intuitif. En effet, pour ces derniers, les paramètres d'anisotropie sont plus importants proche de l'octaédre, rendant inutile de chercher à favoriser de grandes distortions.

Enfin, la méthodologie de calcul a été mise en défaut dans le cas des ligands lourds. En effet, dans cette situation, le ligand peut contribuer au couplage spin-orbite et donc au ZFS de façon non évidente, de par les états d^n ainsi que par les états à transfert de charge, ce qui rend problématique l'utilisation d'une méthode tronquée en deux étapes en plus de rendre crucial le rôle de la correlation dynamique. Ce problème méthodologique est toujours d'actualité et devra être résulu par les méthodologistes dans un avenir proche.

Complexes binucléaires

Les complexes binucléaires présentent un peu plus de difficultés que les mononucléaires tant d'un point de vue *ab initio* que de celui des hamiltoniens modèles. Trois situations sont étudiées rendant compte des principales difficultées rencontrées dans de nombreux complexes binucléaires.

La première étude concerne l'acétate de cuivre monohydraté. Cette molécule, trés connue, a été étudiée de nombreuses fois depuis les premières études de susceptibilité magnétique menées par Guha en 1951. D'après les courbes obtenues, l'hypothèse d'un complexes bin-

ucléaire (et non mononucléaire) a pu être émisse avant la détermination de la structure cristallographique, et validée un an plus tard par l'étude RPE de Bleaney et Bowers. Ces derniers avaient pu montrer qu'un état triplet présentant du ZFS était peuplé à température ambiante et avaient rationalisé ce ZFS par des dérivations analytiques. Ces travaux ont ensuite été repris et améliorés, mais le signe positif du paramètre axial de ZFS avait toujours été determiné de façon indirecte à partir de formules analytiques. Récemment, Ozarowski a montré par RPE-HF que le signe était incorrect, mettant en doute les formules analytiques et leur application dans les précédents travaux. En démontrant de nouveau une formule similaire, il est montré dans cette thèse que le ZFS est susceptible d'être très sensible aux effets de la corrélation dynamique. Une étude méthodologique poussée a pu monter qu'un calcul variationnel de type DDCI ("Difference Dedicated Configuration Interaction") était nécessaire dans la première étape du calcul *ab initio*, et que le couplage spin-spin devait être inclu afin de reproduire les valeurs expérimentales. Les formules analytiques précédemment utilisées ont été validées, montrant que l'usage de valeurs erronées des couplages magnétiques des états excités était la source de l'erreur sur le signe du paramètre axial de ZFS.

Une autre application importante de la configuration $d^9 - d^9$ concerne l'étude des termes antisymétriques du hamiltonien multispin. Dans cette configuration, le modèle multispin s'écrit de la façon suivante:

$$\hat{H}_{mod} = J\hat{\mathbf{S}}_a \cdot \hat{\mathbf{S}}_b + \hat{\mathbf{S}}_a \overline{\overline{D}}_{ab} \hat{\mathbf{S}}_b + \overline{d} \cdot \hat{\mathbf{S}}_a \times \hat{\mathbf{S}}_b \tag{2}$$

où J est le terme de couplage isotrope, $\hat{\mathbf{S}}_a$ et $\hat{\mathbf{S}}_b$ sont les spins locaux (sur les sites a et b respectivement), $\overline{\overline{D}}_{ab}$ est l'échange symétrique et $\overline{d}$ le pseudo-vecteur de Dzyaloshinskii-Moriya. Ce modèle fait intervenir trop de paramètres pour permettre une extraction à partir des énergies seulement. En utilisant la théorie des hamiltonien effectifs, il est montré que l'ensemble des paramètres peut être extrait à partir d'un calcul *ab initio* dans un repère arbitraire. En étudiant des déformations présentes dans le matériau réel CuO, des corrélations magneto-structurales sont proposées, et les principaux mécanismes menant à l'échange antisymétrique sont étudiés. Ce travail poursuit donc les premières études mécanistiques portant sur l'échange antisymétrique menées dans un premier temps par Moriya et récemment poursuivies par Moskvin.

La dernière étude de cette thèse concerne le composé $[Ni_2(en)_4Cl_2]^{2+}$ (en=ethylène di-

amine). Ce complexe centrosymétrique, récemment caractérisé par mesures magnétiques et RPE-HF, relève de la limite de l'échange faible. Dans ce cas, l'échange isotrope et les termes anisotropes ont le même ordre de grandeur, et l'extraction des paramètres d'anisotropie du hamiltonien multispin à partir des énergies (et donc d'une expérience) est problématique. En suivant la stratégie recommandée par Boča, mais jamais mise en pratique, ce problème est pour la première fois résolu dans cette thèse. Cependant, l'application de la théorie des hamiltoniens effectifs montre clairement ensuite que le modèle multispin standard n'est pas correct dans cette configuration, et qu'il manque un terme d'échange biquadratique anisotrope. L'introduction de ce terme dans le hamiltonien modèle rend l'extraction du hamiltonien multispin impossible en pratique (plus de paramètres que d'équations). Il est donc nécessaire d'utiliser des modèles de type spin géant (qui se concentre sur l'état fondamental de spin) ou de type spin bloc (qui traite l'ensemble des états de spin au travers d'une matrice modèle bloc diagonale). Cependant, afin de prendre en compte les termes de "spin-mixing" (couplage entre les différents blocs de spin, ici entre le quintet et le singulet) de façon effective et cohérente, ces termes ont été analytiquement dérivés à partir du modèle multispin. Ce travail analytique a montré que les opérateurs de Stevens ne sont pas appropriés à la description du spin-mixing dans les composés polynucléaires, contrairement à ce qui est supposé par la communauté des expérimentateurs, et les modèles de spin géant et spin bloc ont donc aussi été révisés.

Conclusion et perspectives

D'un point de vue méthodologique, ce travail a montré qu'une méthode de calcul en deux étapes, incluant les effects relativistes responsables du ZFS (couplages spin-spin et/ou spin-orbite) *a posteriori*, permet d'obtenir des résultats en bon accord avec l'expérience lorsque les degrés de liberté de la méthode sont bien maîtrisés. Cette méthode de calcul n'a été mise en défaut que dans le cas des ligands lourds, ce qui constitue un réel défi pour les méthodologistes.

Dans les complexes mononucléaires, il a été montré que les modèles usuels sont appropriés pour décrire le ZFS. Des rationalisations analytiques ont permis de mieux comprendre comment jouer sur le ZFS, et en particulier d'expliquer pourquoi les complexes de Mn(III) ne présentent jamais de paramètres d'anisotropie importants, contrairement aux autres configurations. Par des exemples bien choisis, l'intérêt des coordinations exotiques a pu être mis en évidence, ouvrant la voie à de nouveaux travaux de synthèse en collaboration avec des

expérimentateurs.

Concernant les systèmes binucléaires, plusieurs cas de figure peuvent se présenter. Lorsque le modèle multispin est utilisable en pratique, comme dans les complexes Cu(II)-Cu(II), la théorie des hamiltonien effectifs permet d'extraire tous les paramètres d'anisotropie, y compris les termes antisymétriques, qui pour la première fois dans ce travail ont été extraits à un haut niveau de calcul. Lorsque le modèle multispin est inutilisable en pratique, il est nécéssaire d'utiliser des modèles un peu plus approchés tels les modèles de spin géant ou spin bloc. Le rôle crucial de la corrélation dynamique dans les complexes polynucléaires a pu être mis en évidence au travers de l'étude de l'acétate de cuivre monohydraté, montrant une fois encore que le traitement théorique de l'anisotropie magnétiquepeut constituer un vrai défi méthodologique.

Outre la poursuite des travaux vers de nouvelles configurations, cette thèse ouvre des perspectives vers les matériaux ou vers des systèmes pour lesquels le degré de liberté orbitalaire joue un rôle plus important (proche dégénérescence et couplage spin-orbite au premier ordre, lanthanides, ...).

Acknowledgements

First, I would like to thank very much all university teachers that made me appreciate chemistry and physics, and in particular transition metal chemistry, spectroscopy and theoretical chemistry. Without their passionating lectures, I would have never known these particular fields, and I would not have realized this thesis. I am convinced that science is much more beautiful when taught, and I would like to become a lecturer to transmit my enthusiasm to students.

I would like to acknowledge my supervisors, Nathalie and Coen, for allowing me to deal (sometimes even fight!) with such an interesting project, started during my master studies. They have been of great help and support during all these years, and I will always remember our common interest and passion in our numerous discussions. I hope that we will still collaborate for a long time since it has been a pleasure to work together.

I thank Pr. Neese for inviting me one month in his group in Bonn. Despite the cold german weather in january, it has been a pleasure to go there and work, all people being warm and friendly. I thank Pr. Broer for initiating our collaboration and inviting me one week in Groningen. It has been also a joy to work with her PhD student Abdul Muizz Pradipto in Tarragona, and introduce him to magnetic anisotropy. I thank Pr. Mallah for his interest in this theoretical work, for helpful discussions, and for suggesting interesting systems to study.

I thank very much the members of the jury and in particular the referees of the thesis, that have accepted to evaluate this work and to come for the defense even from overseas countries. All the questions and remarks have been particularly interesting and helpful, and I am opened to further discuss and collaborate with all of them.

I also particularly thank Pr. Caballol for her help in establishing the codirection of thesis between France and Spain.

I acknowledge all members of the "Laboratoire de Chimie et de Physique Quantiques" in Toulouse and of the quantum chemistry group of the "Departament de Química Física i Inorgànica" in Tarragona for integrating me in their structures and for all good moments, discussions and support that they have provided me during my master and doctorate studies.

Finally, I thank very much all colleagues, friends, relatives and particularly my parents that have supported me, allowing me to start and achieve this thesis, and I wish good luck to Renaud Ruamps that will pursue in the directions opened by this work.

List of Abbreviations

AIMP	*Ab Initio* Model Potentials
AMFI	Atomic Mean-Field Integrals
ANO-RCC	Atomic Natural Orbitals Relativistically Core Correlated
CAS(SCF/PT)	Complete Active Space (Self-Consistent Field/Perturbation Theory)
(MR)CI(-SD)	(Multi-Reference) Configuration Interaction (with Single and Double excitations)
(I)DDCI	Iterative Difference Dedicated Configuration Interaction
(S)DFT	(Spin) Density Functional Theory
DKH	Douglas-Kroll-Hess
DM (vector)	Dzyaloshinskii-Moriya (pseudo vector)
(HF-)EPR	(High-Field, High-Frequency) Electron Paramagnetic Resonance
GSH	Giant Spin Hamiltonian
HDVV	Heisenberg-Dirac-Van Vleck
INS	Inelastic Neutron Scattering
IP-EA	Ionization Potential - Electron Affinity
LF(T)	Ligand Field (Theory)
LMCT	Ligand-to-Metal Charge Transfer
LRT	Linear Response Theory
MO	Molecular Orbital
(PC/SC-)NEVPT	(Partially/Strongly Contracted) N-Electron Valence Perturbation Theory
NMR	Nuclear Magnetic Resonance
PK	Pederson and Khanna
POM	Polyoxometalate
(QD)PT	(Quasi-Degenerate) Perturbation Theory

QRA	Quasi-Restricted Approach
(RAS)SI(-SO)	(Restricted Active Space) State Interaction (Spin-Orbit coupling)
SMM	Single Molecule Magnet
SOC	Spin-Orbit Coupling
SSC	Spin-Spin Coupling
TM	Transition Metal
WFT	Wave-Function Theory
ZFS	Zero-Field Splitting

List of Figures

List of Tables

List of Publications

1. R. Maurice, R. Bastardis, C. de Graaf, N. Suaud, T. Mallah, and N. Guihéry, *Universal theoretical approach to extract anisotropic spin Hamiltonians*, J. Chem. Theo. Comput. **5**, 2977-2984 (2009).

2. R. Maurice, N. Guihéry, R. Bastardis, and C. de Graaf, *Rigorous extraction of the anisotropic multispin Hamiltonian in bimetallic complexes from the exact electronic Hamiltonian*, J. Chem. Theo. Comput. **6**, 55-65 (2010).

3. R. Maurice, C. de Graaf, and N. Guihéry, *Magnetic anisotropy in binuclear complexes in the weak-exchange limit: From the multispin to the giant spin Hamiltonian*, Phys. Rev. B. **81**, 214427 (2010).

4. R. Maurice, C. de Graaf, and N. Guihéry, *Magnetostructural relations from a combined ab initio and ligand field analysis for the nonintuitive zero-field splitting in Mn(III) complexes*, J. Chem. Phys. **133**, 084307 (2010).

5. R. Maurice, A. M. Pradipto, N. Guihéry, R. Broer, and C. de Graaf, *Antisymmetric magnetic interactions in oxo-bridged copper(II) bimetallic systems*, J. Chem. Theo. Comput. **6**, 3092-3101 (2010).

6. R. Maurice, K. Sivalingam, D. Ganyushin, N. Guihéry, C. de Graaf, and F. Neese, *Theoretical determination of the zero-field splitting in copper acetate monohydrate*, Inorg. Chem. **50**, 6229-6236 (2011).

Contents

Introduction

Magnetic anisotropy is a physical property that arises under certain spin and symmetry conditions in several types of systems. When the spin becomes anisotropic, its projection is no longer equivalent in all directions of space. Such effect is related to the mixing and loss of degeneracy of the spin-orbit components of the electronic ground state(s). Evidence for magnetic anisotropy has been encountered in many molecules and materials over the years. The evolution of this particular field of magnetism is strongly connected to the Electron Paramagnetic Resonance (EPR) spectroscopy, among other experimental techniques. One of the first evidences for magnetic anisotropy in transition metal compounds came from the well-known copper acetate monohydrate complex. In 1951, Guha published the susceptibility curve of this molecule [1], which was clearly incompatible with the assumption of a mononuclear complex (*i.e.* presenting only one magnetic center). The explanation came one year later from Bleaney and Bowers by means of a detailed EPR study [2]. They questioned the structure of the molecule and formulated the hypothesis of coupled pairs of magnetic centers, which was validated one year later by the determination of the crystal structure [3]. They also introduced an analytical derivation in order to explain the magnetic anisotropy of the excited triplet state.

A second important advance concerns the works of Dzyaloshinskii and Moriya on the models for magnetic anisotropic intersite interactions. Dzyaloshinskii explained phenomenologically the weak ferromagnetism of α-Fe_2O_3 by introducing an antisymmetric interaction in the model in 1958 [4]. Two years later, Moriya rationalized the presence of this term [5], validating the work of Dzyaloshinskii. In 1961, the anisotropic parameters were extracted for the first time in an organic molecule using the EPR spectroscopy, namely in the excited triplet of naphtalene [6]. The last major breakthrough to be quoted concerns the so-called Single Molecule Magnets (SMMs). The first example of this class of molecules is the Mn_{12}

complex, synthesized in 1980 [7], and characterized in the early nineties [8–10]. This new type of molecules present a magnet-like behaviour at very low temperature, and allowed to evidence quantum effects like the quantum tunneling of the magnetization, coherence and interference effects. The first examples of this type of molecules, namely the Mn_{12} and Fe_8 clusters were extensively studied. However, the Mn_{12} molecule suffers one major drawback: the interesting behaviour is lost when the molecule is deposited on a surface and interest has shifted to other molecules (eg. Mn_6 clusters) that do not loose their magnetic properties when connected to a surface.

Until now, the use of SMMs in real technological applications is severely hindered by the fact that all known clusters present their extraordinary properties only at extremely low temperatures. A deep understanding of the interactions between the magnetic sites is far from being achieved [11], and consequently, the properties of such systems are not totally understood from a microscopic point of view. This lack of understanding makes it rather difficult to make predictions along what lines research should be concentrated to design clusters with higher blocking temperatures. Moreover, it has been claimed that the essential ingredients for SMM behaviour, namely a ground state with both a large spin moment and a large magnetic anisotropy is difficult to achieve [12]. This assumption corroborated a previous attempt to define criteria to enlarge the anisotropy in SMMs, which showed that increasing the total spin of the ground state S is not useful while enlarging the local spin moments appeared more promising [13]. New insights are therefore necessary to predict and fine tune the property of SMMs. A theoretical study allowing one to evaluate, modelize, and rationalize the property would allow one to better understanding of the physics of SMMs.

As underlined by Telser in a recent review [14], a large amount of experimental data already exists on mononuclear complexes, and theoretical chemistry can be used to accurately reproduce these data. However, a simple ligand-field analysis can also provide information on the property in the sense that it allows to understand deeply the origin and magnitude of the anisotropy. Such studies have been performed in the famous book of Abragam and Bleaney for all d^n configurations [15], but this work was only qualitative and quantum chemistry can now provide quantitative information on all contributions to the anisotropy. Usefull tools necessary in order to revise and improve such studies are now available. Concerning the intersite interaction, only few ligand-field analysis are available in the literature, and mainly

concern copper acetate. Hence, rationalizations of the anisotropic intersite interactions are highly desirable.

The present thesis aims to perform a theoretical study of mono- and bi-nuclear complexes and has the following objectives:

1. Choose and validate a methodology of calculation of the anisotropic parameters.
2. Extract rigorously the anisotropic spin Hamiltonians using effective Hamiltonian theory.
3. Propose rationalizations of the property and magneto-structural correlations for several configurations.
4. Establish the limits of applicability of the methodology.

The dissertation is organized in four chapters. Chapter 1 presents a short review of the information present in the literature dealing with the magnetic anisotropy and especially oriented to first-row transition metal complexes. The model Hamiltonians commonly used by experimentalists and theorists will be presented, as well as the experimental and theoretical approaches used to determine anisotropic parameters. Chapter 2 presents the methodology of calculation, the extraction and the way to derive analytically the anistropic parameters. Chapter 3 deals with mononuclear complexes. After validating the methodology and the model Hamiltonians, rationalizations will be proposed for two different configurations, namely the d^8 and d^4 configurations. The case of heavy atom ligands is examined through the example of a series of Ni(II) complexes. Chapter 4 deals with binuclear complexes. The d^9-d^9 configuration is presented first, followed by the d^8-d^8 one. Finally perspectives will be discussed on some topics that could be investigated in the near future.

Chapter 1

Literature Survey: an Introduction to Magnetic Anisotropy

1.1 From Single Molecule Magnets to Spin Hamiltonians

Single Molecule Magnets (SMMs) are coordination complexes having interesting magnetic properties. Usually these complexes are polynuclear complexes, *i.e.* they present several magnetic centers. The first example of such molecules, the Mn_{12} cluster, has been synthesized in 1980 [7]. This molecule possess eight Mn(III) sites antiferromagnetically coupled to four Mn(IV) sites, resulting in a S=10 spin ground state [8]. At very low temperature, the magnetization can be oriented in a particular direction, which can be maintained for a long time, meaning that the molecule behaves as a permanent magnet.

The magnetization may be relaxed either thermally or by tunneling effects [9, 10]. At zero field, the energy required to reverse the orientation of the magnetization is called U. In the absence of tunneling effects, the magnetization can only be relaxed when the thermal energy is larger than U. When a magnetic field is applied along the orientation of the molecular magnetization, the energy barrier is lowered and if the magnetic field is strong enough, the magnetization is reversed. The reverse process happens of course at opposite external field and in this way a hysteresis opens in the magnetization versus field curve. However, the hysteresis curves of SMMs have a peculiarity compared to ordinary magnets, they present staircases for some particular values of the magnetic field. This behaviour has been explained

by quantum tunneling of the magnetization [9, 10], which can occur at particular magnetic field values. The scan speed of the magnetic field influences the heights of the staircases, *i.e.* the probability of tunneling depends on the scan speed. The magnetization tunneling can also be thermally assisted as shown by the temperature dependance of the hysteresis curves [9, 10].

The bistability explains the envisaged applications of these systems. These molecules could be used for information storage with one bit of information recorded only on one molecule. If technically possible (one has to write and read the memory on only one molecule), this would lead to a next step in the miniaturization of computer devices. Another potential application of SMMs is the so-called quantum computing [16]. However, these complexes are also studied for fundamental purposes, since they allow one to study and put into evidence quantum effects like tunneling, coherence, decoherence and interference. Since the blocking temperatures of the SMMs are extremely low, technological applications are not yet possible, and therefore, the main interest of these systems remains fundamental.

The first examples of SMMs, namely the Mn_{12} and Fe_8 clusters, have been extensively studied for a long time, but are nowadays replaced by other clusters. At the moment, the largest energy barrier U has been encountered in a Mn_6 cluster [17], showing that enlarging the number of magnetic sites is not the clue to enlarge U [12]. To gain insight on the magnetic behaviour of these clusters, the prediction of the energy barrier value as well as the tunneling probabilities are of utmost importance but is far from being a trivial task. A rigorous theoretical study of these systems could help in this respect and the present thesis will concentrate mostly on mono- and bi-nuclear complexes. These smaller systems contain the same kind of microscopic ingredients as those governing the magnetic properties of SMMs (*i.e.* local and intersite anisotropic interactions) while their theoretical description is accessible with state-of-the-art Wave-Function Theory (WFT) based methodologies. This work should be seen as a first step in a bottom-up theoretical approach of large polynuclear complexes.

The SMMs are usually described by projecting the lowest-lying spin-orbit states onto the spin part of the ground state, and using a spin model Hamiltonian. The model space is constituted of the M_S components of the ground state in the absence of orbital degeneracy or near degeneracy. These M_S components are split if the system is anisotropic, leading to a spectrum that can be modelled by an anisotropic spin Hamiltonian. In fact, a Giant Spin Hamiltonian (GSH) is commonly used in order to study such systems. This Hamiltonian will

be described in section 1.4.2.

1.2 Applications of Spin Hamiltonians

1.2.1 A Brief History of Spin Hamiltonians

The first spin Hamiltonian in the literature was presented by Van Vleck in his famous book in 1932 [18]. Inspired by Heisenberg's and Dirac's works, he derived the Heisenberg-Dirac-Van Vleck (HDVV) Hamiltonian, presented here for a pair of spins located on two different nuclei:

$$\hat{H} = -2J_{kl}\mathbf{S}_k.\mathbf{S}_l \tag{1.1}$$

where J_{kl} is the coupling constant or exchange integral and $\mathbf{S}_k$ and $\mathbf{S}_l$ are the spin operators of the electrons k and l respectively. This Hamiltonian only involves spin degrees of freedom, and hence would be qualified nowadays as a 'spin Hamiltonian'. However, Van Vleck did not introduce the expression of 'spin Hamiltonian', he just referred to the 'Hamiltonian' of the system at that time.

Actually, the name of 'spin Hamiltonian' appeared in a serie of theoretical papers by Abragam and Pryce in the early fifties. The necessity of introducing such a vocabulary and developing the theory of such models emerged in the late forties for the interpretation of the results of EPR and Nuclear Magnetic Resonance (NMR) spectroscopies. In 1950, Pryce referred to an 'effective Hamiltonian' able to describe the energy levels of paramagnetic ions in a crystal [19]. By introducing the nuclear hyperfine structure, *i.e.* the splitting of the electronic levels due to the interaction with the spin of the nucleus of the considered ion, Abragam and Pryce mostly mention the term 'fine structure Hamiltonian' in a first paper [20] (one should note that the 'fine structure Hamiltonian' included the 'hyperfine structure' in this paper, contrary to the common usage nowadays). The expression 'spin Hamiltonian' is introduced in the discussion of the Mn(III) ion, which has a non-degenerate ground state, and for which quadratic terms appear in the Hamiltonian. Actually, they used the expression 'quartic spin Hamiltonian' to refer to these particular terms of the Hamiltonian. In a following paper [21], they currently used the expression 'spin Hamiltonian', which was rapidly accepted in the literature as can be seen in a review of Bleaney and Stevens that was published two years later [22].

One should note that the above presented HDVV Hamiltonian is still extensively used for the description of the isotropic interactions between different magnetic sites. More sophisticated operators and terms have been introduced for isotropic intersite interactions in some particular cases [23]. However, these terms are out of the scope of the present thesis. Spin Hamiltonians are still extensively used in the EPR and NMR spectroscopies, the former case will be commented in section 1.2.2. One should also mention that spin Hamiltonians are widely used in nuclear magnetism as well [24].

1.2.2 The Spin Hamiltonian in Electron Paramagnetic Resonance Spectroscopy

The interpretation of EPR spectra completely relies on the use of spin Hamiltonians. The sample is exposed to an external magnetic field and electrons are excited to higher energy levels (resonance phenomena). For orbitally non-degenerate ions, the spectra may be interpreted using a spin Hamiltonian since most of the physics can be projected onto spin degrees of freedom only. Several effective interactions may be introduced in the Hamiltonian, responsible for the different structures in the spectrum. These interactions can be written in order of decreasing importance [15]:

- The Zeeman interaction, *i.e.* the interaction between the external magnetic field and the magnetic moments of the electrons.

- The fine structure, *i.e* the splitting of the energy levels in the absence of magnetic field, usually called 'Zero-Field Splitting' (ZFS).

- The hyperfine structure, *i.e.* the effect on the spectrum of the interaction between the magnetic moments of the nuclei of the magnetic centers and the magnetic moments of the electrons.

- The superhyperfine structure, *i.e.* the effect on the spectrum of the interaction between the magnetic moments of other nuclei and the magnetic moments of the electrons.

- The Zeeman interaction of the nuclei, *i.e.* the interaction between the external magnetic field and the magnetic moments of the nuclei, often called 'paramagnetic shift'.

The parameters characteristic of all these interactions can be extracted by fitting a model spectrum to the experimental one. One should note that the ZFS parameters are extracted in the presence of a magnetic field. More considerations on the experimental extractions will be presented in section 1.4. At this stage, it is important to note that the EPR spectra of non-degenerate ions are usually interpreted using a spin Hamiltonian. In the remainder of this dissertation, only the zero-field part of the Hamiltonian dealing with the spin of the electrons only will be considered. The expression 'anisotropic spin Hamiltonians' is then used here to refer to the ZFS.

1.3 The Anisotropic Spin Hamiltonian in Mononuclear Systems

1.3.1 Model Hamiltonian

In mononuclear complexes, magnetic anisotropy can be observed in the absence of magnetic field if the spin angular momentum of the ground state is larger or equal to one and if the symmetry of the system is not too high. The associated ZFS can be described by a spin Hamiltonian if the ground state is not degenerate and well separated in energy to all other excited states. Actually, in this case, the low-lying eigenfunctions of the relativistic Hamiltonian can be limited to the spin part of the ground state, and hence, the $|S, M_S\rangle$ components of the ground state form the basis of the corresponding model Hamiltonians. When the spin quantum number of the ground state S is one or one and a half, the following Hamiltonian describes all features of the ZFS:

$$\hat{H}_{mod} = \hat{\mathbf{S}}.\overline{\overline{D}}.\hat{\mathbf{S}} \tag{1.2}$$

where $\mathbf{S}$ refers to the spin of the ground state and $\overline{\overline{D}}$ is the second-order symmetric ZFS tensor [25]. This tensor has six different parameters in an arbitrary frame and for a system of C_1 symmetry.

However, the relations between some of the ZFS tensor components that exist in systems of higher symmetry and/or in particular axes frames may reduce the number of parameters. The presence of anisotropy is directly related to the symmetry of the system through Neumann's

principle. This principle specifies that any physical property should have at least the same symmetry elements as the system. If one or three particular orientations of a certain system can be defined in an orthonormal axes frame, the spin of the ground state is necessarily anisotropic. For instance, in the O_h point group, no particular orientations can be defined whatever the axes frame is. Hence, in this point group, the extradiagonal terms of the ZFS tensor vanish independently of the orientation, and $D_{xx} = D_{yy} = D_{zz}$. This means that all $|S, M_S\rangle$ components of an orbitally non-degenerate ground state are degenerate in the O_h symmetry point group.

In C_1 symmetry, when all six parameters of the ZFS tensor may have different values in an arbitrary axes frame, the magnetic axes frame is defined as one of the axes frame that diagonalizes the $\overline{\overline{D}}$ tensor. However, the attributions of the X, Y and Z magnetic axes require some additional conventions [11]. These conventions are related to the definition of an axial D parameter and a rhombic E parameter. In the magnetic axes frame, the standard conventions specify that $|D| > 3E$ and $E > 0$ while the D and E parameters are defined as follow:

$$D = D_{ZZ} - \frac{1}{2}(D_{XX} + D_{YY}) \tag{1.3}$$

$$E = \frac{1}{2}(D_{XX} - D_{YY}) \tag{1.4}$$

This means that a magnetic Z axis can be defined for a non-zero D parameter, and that the X and Y axes can only be defined when E is not equal to zero.

D and E completely define the ZFS when the spin of the ground state is one or one and a half. However, when $S \geq 2$, higher order terms may appear in the model Hamiltonian, which can be expressed using the so-called standard Stevens operators when the system is oriented in its magnetic axes frame. These operators were originally defined first in order to describe the splitting of the non-relativistic energy levels associated with the crystal field potential created by the valence electrons of the ligands, underlining the close relation between the crystal field potential and the ZFS. This strong relation will be introduced in deeper details in section 1.3.2. The more general equation of the ZFS Hamiltonian in terms of Stevens operators is:

$$\hat{H} = \sum_{n,k} B_k^n \cdot \hat{O}_k^n \tag{1.5}$$

where B_k^n are the ZFS parameters associated with the $\hat{O}_k^n$ standard Stevens operators [11, 15]. k is the order of the spherical tensor involved and cannot be larger than 2S, n is the type of anisotropy and is never larger than k. In mononuclear transition metal complexes, k can only be equal to two or four since it has to be even in order to respect the inversion symmetry around the magnetic center and the Kramers' degeneracy in case of odd number of electrons. Therefore, n is restricted to the 0, 2, and 4 values where 0 is associated with an axial anisotropy, 2 with a rhombic one and 4 with a tetragonal anisotropy. When only second order operators are allowed, this Hamiltonian is equivalent to the one defined in Eq. 1.2 (axial and rhombic anisotropies are defined). Even when fourth order terms are allowed in the Hamiltonian ($S = 2$ or $S = \frac{5}{2}$), relations appear between the Stevens and the previously defined parameters due to the expression of the operators used:

$$D = 3B_2^0 \tag{1.6}$$

$$E = B_2^2 \tag{1.7}$$

These relations are valid whatever the configuration is. Hence, for mononuclear complexes, in the magnetic axes frame, the D and E parameters will be used for second-order terms, and the B_4^n parameters (n=0,2,4) for the fourth order ones when allowed ($2 \leq S \leq \frac{5}{2}$). One should keep in mind that these ZFS parameters have never been derived from the exact electronic Hamiltonian. Nevertheless, all model Hamiltonians presented in this chapter are always considered as valid by theorists and experimentalists. One of the objective of the present thesis is to validate and/or improve these phenomenological Hamiltonians and give them a firm basis. Section 2.2 will present a computational approach that allows one to check the validity of model Hamiltonians, and some applications of this method dealing with mononuclear complexes will be presented in section 3.1.

1.3.2 The Origin of the Zero-Field Splitting Parameters

For decades it is known that the ZFS arises from the spin-orbit coupling (SOC) and the spin-spin coupling (SSC) [26]. Even though other relativistic effects may also contribute to the ZFS [27], these two interactions are by far the dominant ones. Even in first-row transition metal

complexes, the SOC effects are larger than the SSC ones, and hence a theoretical study dealing only with the SOC interaction is precise enough for rationalization purposes. As underlined by Telser in 2006 [14], nowadays a large amount of experimental data is available from EPR spectroscopy measurements, and there is a need for rationalization based on simple ligand-field approaches in order to interpret them. Even if advanced computational methodologies exist, nothing can replace a deep understanding based on simple models.

Actually, one of the major efforts concerning the analytical derivation of ZFS parameters is presented in the book of Abragam and Bleaney [15]. This book published in 1970, aims to explain experimental data obtained for all different d^n configurations. However, at that time, neither detailed optical spectra nor computational methodologies were available in order to provide deep information on the origin of the ZFS parameters. Hence their work was only qualitative and often limited to explain the sign of the D parameter as a function of the symmetry lowering for instance. However this work is still an important reference, and therefore, their approach is explained in some details in the following.

Abragam and Bleaney started with the case of 6-fold coordinated complexes with an O_h symmetry point group. The symmetry was lowered to the D_{4h} and D_{2h} symmetry point groups to introduce anisotropy. They only considered the spin-orbit free states belonging to the spectroscopic term of the free-ion ion ground state. For non-degenerate ions, the ZFS parameters were derived through a two-step approach. The first step consists in describing the splitting of the free-ion multiplet under the action of the crystal-field potential. This potential is created by the valence electrons of the ligand and is responsible for the energy splitting of the levels of a given multiplet. In this approach, the covalency effects are only treated effectively through the crystal field, and therefore, the approach is only valid when the covalency effects are not too strong (*i.e.* the "d" orbitals can be considered to be mainly localized on the magnetic center) and when the spin-orbit coupling is only brought by the metal atom.

Energies and wavefunctions of molecular complexes were described using the so-called Stevens operators acting on the $|L, M_L\rangle$ configurations. One has to note that this rigorous treatment of the crystal-field is not equivalent to the simpler standard model of the splitting of the d orbitals under the action of the crystal-field. These two visions are only strictly equivalent for the d^1 configuration for which the energy levels directly correspond to the energy

of the d orbitals in a monoelectronic picture. However, due to the Kramers' degeneracy, this configuration is not of interest for the present work focussing on magnetic anisotropy. For the other d^n configurations, it is necessary to treat the crystal-field using Stevens operators in order to describe the multideterminental character of the crystal-field states (see section 2.3.3).

In the second step, the spin-orbit coupling interaction is introduced using second-order perturbation theory. The following spin-orbit coupling Hamiltonian is used:

$$\hat{H}_{SOC} = \lambda \hat{\mathbf{L}}.\hat{\mathbf{S}} \tag{1.8}$$

where λ is the polylectronic spin-orbit coupling constant and where $\hat{\mathbf{L}}$ and $\hat{\mathbf{S}}$ refer to the orbital momentum and spin operators of the considered states. This Hamiltonian works in the basis of the $|L, M_L, S, M_S\rangle$ configurations belonging to the multiplet of the free-ion ground state. The expressions of the crystal-field states built in the first step are used in this step as basis to act upon with the spin-orbit operator. In this way, analytical expression for the ZFS parameters are obtained as functions of the polyelectronic spin-orbit coupling constant λ and the relative energies of the considered states. In practice, it is not always necessary to take all states belonging to the free-ion multiplet, it is often possible to reduce the number of states to just a few of them. However, the number of states is not totally arbitrary, the excitations have to be balanced according to all orientations of space since an anisotropic property is considered, which can easily be affected by any unbalanced choice of excited states included in the treatment.

The following approximations are inherent to the method of Abragam and Bleaney:

- The overlap between the metal d orbitals and the ligand orbitals is not treated explicitely.
- Only spin-orbit free states belonging to the same multiplet in the free-ion are considered. This implies that the SOC interaction with other spin-orbit free states is not treated.
- The low-lying states considered in the derivation are not necessarily eigenvectors of the considered electronic Hamiltonian (*i.e.* the crystal-field potential added to the free-ion Hamiltonian). Actually, in a given symmetry point group, the electronic Hamiltonian can introduce important mixings between configurations belonging to different multiplets

of the free-ion. This effect is neglected in the derivations of Abragam and Bleaney, in other words the orbital momentum of the considered states L is considered as a good quantum number before the introduction of the SOC.

Other approximations are made in the derivation but these are less questionable. For instance, the two-step approach is perfectly justified for first-row transition metal complexes, since the SOC is only a perturbation of the Hamiltonian in this case. Nowadays accurate methodologies exists for the calculation of the ZFS parameters, and hence, the quantitative impact of the previously exposed approximations can be evaluated *ab initio*, allowing one to bypass some of these to reach to a more quantitative description if necessary in some specific cases. Section 2.3 presents an alternative approach to the one of Abragam, and examples of rationalizations that can be done by applying this approach on mononuclear complexes will be presented in section 3.2. The obtained results will be compared to the ones of Abragam and Bleaney for the d^8 and d^4 configurations. This kind of work is particularly promising and of interest for the scientific community according to some recent literature on the subject dealing with ligand-field and magneto-structural correlations [14, 28, 29].

1.4 The Anisotropic Spin Hamiltonian in Polynuclear Systems

1.4.1 The Multispin Hamiltonian and the Strong-Exchange Limit

Two model Hamiltonians are commonly used in the literature for polynuclear complexes, namely the multispin and the giant spin Hamiltonians. In the former case, local anisotropies as well as the intersite interactions are considered while the giant spin Hamiltonian only considers the ZFS in the ground state of the complex (see section 1.4.2). Taking into account the antisymmetric intersite interactions (introduced by Dzyaloshinskii in 1958 [4] and refined by Moriya two years later [5]), leads to the following multispin model Hamiltonian for binuclear complexes with one unpaired electron in each magnetic site:

$$\hat{H}_{mod} = J\hat{\mathbf{S}}_a \cdot \hat{\mathbf{S}}_b + \hat{\mathbf{S}}_a \overline{\overline{D}}_{ab} \hat{\mathbf{S}}_b + \overline{d} \cdot \hat{\mathbf{S}}_a \times \hat{\mathbf{S}}_b \tag{1.9}$$

where $\hat{\mathbf{S}}_a$ and $\hat{\mathbf{S}}_b$ are the local spins on site a and b respectively, J is the isotropic exchange coupling, $\overline{\overline{D}}_{ab}$ is the symmetric anisotropic exchange tensor, and $\overline{d}$ the Dzyaloshinskii-Moriya

pseudo vector. The isotropic term is equivalent to the Heisenberg-Dirac-Van Vleck Hamiltonian. The expression $J\hat{\mathbf{S}}_a \cdot \hat{\mathbf{S}}_b$ is more commonly used in the studies of magnetic anisotropy than the one presented in section 1.2.1. By defining $J_{ii} = J + D_{ii}^{ab}$ and $J_{ij} = D_{ij}^{ab}$, the $\overline{\overline{J}}_{ab}$ coupling tensor is generated, which gives rise to the J_{XYZ} model in the magnetic axes frame. The Dzyaloshinskii-Moriya pseudo-vector corresponds to the antisymmetric part of the total second-order anisotropic tensor. Its orientation is defined, contrarily to its direction which cannot be determined.

When at least one of the local ground states of the magnetic centers has two or more magnetic electrons, local anisotropic tensors appear in the same way as in mononuclear complexes. The standard multispin Hamiltonian can be written as follows for binuclear complexes [11, 23, 25]:

$$\hat{H}_{mod} = J\hat{\mathbf{S}}_a \cdot \hat{\mathbf{S}}_b + \hat{\mathbf{S}}_a\overline{\overline{D}}_a\hat{\mathbf{S}}_a + \hat{\mathbf{S}}_b\overline{\overline{D}}_b\hat{\mathbf{S}}_b + \hat{\mathbf{S}}_a\overline{\overline{D}}_{ab}\hat{\mathbf{S}}_b + \overline{d} \cdot \hat{\mathbf{S}}_a \times \hat{\mathbf{S}}_b \tag{1.10}$$

where $\overline{\overline{D}}_a$ and $\overline{\overline{D}}_b$ are the local anisotropic tensors, while the other terms keep their usual meaning. This Hamiltonian is considered valid for systems with less than four local magnetic electrons in each magnetic center.

This model can be applied in a straightforward way in the strong-exchange limit, *i.e.* when the isotropic exchange is much larger than the anisotropic effects. Considering that all tensors are traceless and that they share the same magnetic axes frame, the eigenvalues and eigenvectors of this Hamiltonian can be expressed using coupling coefficients [11, 23, 25]. A tensor is actually attributed to each spin state:

$$\overline{\overline{D}}_S = C_a\overline{\overline{D}}_a + C_b\overline{\overline{D}}_b + C_{ab}\overline{\overline{D}}_{ab} \tag{1.11}$$

where S is the total spin of the state considered, and C_a, C_b and C_{ab} are the coupling coefficients. These coefficients can be generated using explicit formula [23, 30], and fulfil the following relation:

$$C_a + C_b + 2C_{ab} = 1 \tag{1.12}$$

The anisotropic part of the Hamiltonian is then separated in several parts, each part acting on the $|S, M_S\rangle$ components of one particular spin state, and can be written as:

$$\hat{H}_S = \hat{\mathbf{S}}\overline{\overline{D}}_S\hat{\mathbf{S}} \tag{1.13}$$

In this approach, the mixing between spin-orbit states of different spin multiplicities is neglected. It is considered that the anisotropic interactions are only small perturbations of the isotropic ones, and that the anisotropic terms only split and mix the $|S, M_S\rangle$ components of one spin state. This approach can be seen as a 'block spin Hamiltonian', since the coupling between all spin states is neglected while the splitting and mixing of all $|S, M_S\rangle$ components of each subspace is treated. Hence, in the strong-exchange limit, the model Hamiltonian of Eq. 1.10 can be written as the sum of the isotropic part $\hat{H}_{iso}$ and the block spin parts $\hat{H}_S$:

$$\hat{H}_{mod} = \sum_S (\hat{H}_{iso} + \hat{H}_S) = \sum_S [\frac{1}{2}(\hat{\mathbf{S}}^2 - \hat{\mathbf{S}}_a^2 - \hat{\mathbf{S}}_b^2)J + \hat{\mathbf{S}}\overline{\overline{D}}_S\hat{\mathbf{S}}] \tag{1.14}$$

The symmetry rules for the appearance of the terms of the multispin Hamiltonian are well established. The local anisotropic tensors obain the same symmetry rules as in the mononuclear complexes; the symmetry rules for the appearence of non-zero symmetric and antisymmetric intersite interactions are presented in reference [31]. Binuclear complexes always have an axial anisotropic interaction, the intermetallic axis is necessarily different than the perpendicular directions to this axis. If the symmetry is further lowered, a rhombic term as well as an antisymmetric term may appear in the intersite anisotropic Hamiltonian (and the intermetallic axis may not correspond to any of the anisotropy axes). Examples of antisymmetric term contributions related to peculiar symmetry lowering will be presented in section 4.1.

The intersite anisotropic interactions arise from the SSC and the SOC. In the former case, the interaction is dominated by the direct coupling between the magnetic electrons. This coupling can arise directly through space or pass through a spin delocalization on the bridging ligands [32]. This interaction is usually weak, but should be considered in some specific cases such as the copper acetate monohydrate complex [33] for instance, and when the ZFS is small anyway. The SOC is a very local effect which in fact becomes more important near the nucleus. Hence, the anisotropic intersite interaction requires the joined effects of the SOC and the direct exchange and kinetic exchange between the magnetic sites. More comments on these points will be the subject of a further analysis in section 4.1. The origin of the antisymmetric

interaction has also been discussed in the literature [5, 34], and will be also reviewed in section 4.1. The relevance of the model Hamiltonian in the $d^8 - d^8$ and other configurations will be checked and commented in section 4.2. The study of the anisotropic intersite interaction is actually one of the major objectives of the present thesis.

1.4.2 The Giant Spin Hamiltonian in the Strong-Exchange Limit

The second model used to describe polynuclear complexes is based on the giant spin Hamiltonian. In this model, only the ground spin state is considered. The Hamiltonian is often used for the study of large SMMs (*i.e.* including four or more magnetic centers). The local and intersite interaction information is lost, since only the ZFS of the ground spin state is described. The model Hamiltonian involves a sum of Stevens operators as in mononuclear complexes, and can be written as follows in the magnetic axes frame:

$$\hat{H}_{mod} = D\hat{S}_z^2 + E(\hat{S}_x^2 - \hat{S}_y^2) + \sum_{n,k\geq 4} B_k^n \cdot \hat{O}_k^n \tag{1.15}$$

The first two terms represent the usual axial and rhombic parameters. Next, the Stevens B_k^n operators are introduced, where k is even and $4 \leq k \leq 2S$, S is the spin of the ground state and $0 \leq n \leq k$, while k and n have the same meaning as descrived in Section 1.3.1. The physical origin of the terms with $k \geq 4$ is not clear in the literature, even if it is often claimed that these parameter originates from spin-mixing effects [35–37]. The limitations of the giant spin approach are often underlined [38], the main criticism concerns the physical origin of the higher order terms. When a giant spin approach is chosen, it is assumed that the first excited spin state lies high in energy, *i.e.* that the spin mixing is negligible. Hence, the interpretation of the high order terms origin is still under question. Keeping in mind that these high order terms govern the magnetization tunneling in SMMs [39], a theoretical study aiming to clarify the physical meaning of the high order terms in the giant spin Hamiltonian is desirable. Such a study will be presented in section 4.2 by analyzing in deep details the case of a Ni(II) binuclear complex.

If only axial anisotropy is present by symmetry, and if only second-order terms are used in the model Hamiltonian, the ZFS of the ground state can be described using the following model Hamiltonian:

$$\hat{H}_{mod} = D\hat{S}_z^2 \tag{1.16}$$

The eigenvectors of this Hamiltonian are directly the $|S, M_S\rangle$ components of the ground state. If S is even, the $|S, 0\rangle$ state is taken as the zero of energy. The $|S, M_{Smax}\rangle$ and $|S, -M_{Smax}\rangle$ states are then associated to an energy of M_{Smax}^2 which is equal to S^2. It is then easy to note that in this case, the energy barrier can be expressed as:

$$U = |D|S^2 \tag{1.17}$$

According to the expression of the model Hamiltonian, the existence of an energy barrier between the $|S, M_{Smax}\rangle$ and $|S, -M_{Smax}\rangle$ states necessitates a negative D parameter. In case of a positive D parameter, the ground state is the $|S, 0\rangle$ state and no energy barrier can exist. When S is odd or when others terms are allowed in the model Hamiltonian, the previous energy barrier expression does not apply anymore. However, the axial D parameter always dominates the value of the energy barrier in the absence of external magnetic field. Hence, this parameter is very important in order to describe the property, and the SMM behaviour is associated with a negative D.

1.4.3 The Weak-Exchange Limit

In the weak-exchange limit, the isotropic and the anisotropic terms of the multispin Hamiltonian are of same order of magnitude. As mentioned by Boča, in this situation there is no advantage in using the coupling coefficients as presented in section 1.4.1 [11]. Actually, in this case, the spin-orbit projected states belonging to different spin-orbit free states can mix by spin-orbit coupling. This effect is called spin-mixing. To proceed in the weak-exchange limit, Boča suggested to built a complete interaction matrix of the multispin model in the uncoupled $|S_a, M_{Sa}, S_b, M_{Sb}\rangle$ basis set, and transform it into the coupled $|S, M_S\rangle$ basis set. This procedure has never been used in the literature even if it looks reasonable and feasible. The weak-exchange limit is still today a theoretical challenge. One of the objectives of this thesis is to solve this problem. In section 4.2 the resolution of the weak-exchange limit case will be presented in the case of the $d^8 - d^8$ configuration. Moreover, the accuracy of the giant spin model will be checked in the weak-exchange limit, where its validity is questionable.

1.5 Experimental Determinations of the Zero-Field Splitting Parameters

1.5.1 The Various Techniques

The ZFS parameters can directly or indirectly be determined from several experimental techniques, which are reviewed in detail by Boča [11]: Magnetic susceptibility, Magnetization vs field, EPR, Calorimetry, Far infrared spectroscopy, Inelastic neutron scattering (INS), Nuclear magnetic relaxation dispersion and Magnetic circular dichroism. In this dissertation, all the experimental ZFS parameters to which the theoretical results are compared are coming from magnetic susceptibility measurements, magnetization vs field curves and/or EPR spectroscopy. Since most of the data arise from EPR spectroscopy, and since historically this method has been particularly important, it will be commented in some details in the next section. The determination of the ZFS parameters is not trivial whatever the technique used is. This is the reason why in many experimental works, at least two methods are used to extract the ZFS parameters.

Most of the experimental data come from magnetic susceptibility measurements since it is available in almost all experimental groups. However, this method has a major drawback: the sign of D is very difficult to determine. Actually, in most of the cases, the susceptibility curves can be fitted with a similar agreement factor for D being either positive or negative [11]. However, the absolute value of D can be accurate and can be used to check the results obtained with other techniques.

The magnetization vs field studies suffer the same problem if measurements are restricted to a single temperature. However, in practice, when measurements are performed at various temperatures, a single set of parameters can be extracted with a good accuracy, and the sign of D is univocally determined [40]. If the sample is a single crystal, this method also allows one to determine the magnetic anisotropy axes [41].

Contrarily to the other techniques, the far infrared spectroscopy gives direct access to the ZFS [11]. Although some uncertainty in the extracted parameters is unavoidable due to the band width of the observed transition between the low-lying spin-orbit states, it allows one to determine unambiously the sign of the D parameter and always give a reliable information

on the spectrum.

1.5.2 The High-Field, High-Frequency Electron Paramagnetic Resonance Spectroscopy

Nowadays, EPR spectroscopy is recognized as the most accurate experimental method for the extraction of ZFS parameters [42]. The use of High-Field, High-Frequency EPR (HF-EPR) allows one to extract ZFS parameters even for some 'EPR-silent' species. Actually, if standard EPR conditions are used, only transitions of the order of the cm^{-1} can be observed [42]. By using high fields and high frequencies, this problem is solved and HF-EPR allows one to extract the ZFS in most of the transition ions, *i.e.* in all cases for which the use of a spin Hamiltonian is relevant.

In case of ions with orbitally non-degenerate ground states, the giant spin Hamiltonian in the magnetic axes frame is:

$$\hat{H}_S = \overline{\overline{g}}\beta\vec{B}\hat{\mathbf{S}} + D\hat{S}_z^2 + E(\hat{S}_x^2 - \hat{S}_y^2) + \sum_{n,k\geq 4} B_k^n \cdot \hat{O}_k^n \tag{1.18}$$

where $\overline{\overline{g}}$ is the magnetogyric ratio matrix, β is the Bohr magneton, $\vec{B}$ is the applied magnetic field, S is the spin of the ground state, and D, E and B_k^n are the ZFS parameters defined in sections 1.3.1 and 1.4.2. According to the selection rules, the intense transitions observed in the spectrum are the ones for which $\Delta M_S = \pm 1$.

The extraction of the ZFS parameters in HF-EPR spectroscopy is based on a simulation of the spectrum with a first set of ZFS parameters that are adjusted to reproduce as accurate as possible the experimental spectrum. The extraction is facilitated if the first set of parameters comes from other experimental techniques (magnetization vs field for instance). Nowadays, in order to extract more reliable information, the adjustment can be done on a two-dimensional dataset (spectra obtained as functions of the field and frequency) [42]. An exceptional accuracy of ± 0.01 cm^{-1} can be reached in a rather routine like way, and the rhombic and some fourth-order terms can be extracted [42].

However, since since in general only the $\Delta M_S = \pm 1$ transitions are observed, not all the high-order terms of the ZFS Hamiltonian are available. Hence, when necessary, the extraction process might include information coming from other experimental techniques. In particular,

in the case of a high-spin d^4 mononuclear complex in which five ZFS parameters are allowed by symmetry, the EPR spectroscopy only gives access to four energy transitions when the magnetic field is applied in the parallel direction [11]. By combining the information of INS and EPR experiments, all five parameters were accurately determined in 2008 for the first time [43]. In the case of dinuclear complexes, the ZFS parameters have been extracted for instance in the $[Ni_2Cl_2(en)_4]^{2+}$ complex (where 'en' stands for ethylenediamine) by using magnetic and two-dimensionnal EPR data [44]. A detailed theoretical study of this molecule will be presented in section 4.2 being the first case for which local and intersite anisotropies are extracted with HF-EPR in a binuclear compound. Actually, the importance of the intersite anisotropy has already been highlighted in larger polynuclear compounds [45], but such large systems are out of the scope of the present work.

1.6 State-of-the-Art Theoretical Approaches for the Calculation of the Zero-Field Splitting Parameters

1.6.1 Density Functional Theory Based Methods

Several methods have been developed, implemented and used in the last decades for the calculations of the ZFS parameters. Some of them are based on Density Function Theory (DFT). Contrary to the WFT based approaches, the standard Kohn-Sham DFT implementations cannot handle the multideterminental character of the spin eigenfunctions involved in the ZFS [46]. Hence, most DFT based methodologies do not directly calculate the low-lying spin-orbit spectrum, but evaluate the ZFS tensor to reconstruct the model spectrum *a posteriori*. Hence, these methods can be used to evaluate the second-order ZFS tensor in mononuclear complexes as well as the second-order giant spin ZFS tensor in polynuclear compounds. Several major implementations have been proposed:

- In 1999, Pederson and Khanna developed the first DFT based approach method of calculation of the ZFS parameters. Starting from a spin-unrestricted ground state determinant, they compute the second-order SOC contribution to the second-order ZFS tensor [47]. By diagonalizing the ZFS tensor, they determine the magnetic anisotropy axes and the anisotropic energies.

- In 2003, Atanasov *et al.* presented a hybrib LF-DFT scheme [48]. First, a spin-restricted DFT calculation that averages the occupation of the d orbitals is performed. Second, these Kohn-Sham orbitals are used in a spin-unrestricted calculation of all Slater determinants that can be built in the d^n configuration in order to extract the ligand-field parameters. Then, these parameters are used in a ligand-field program in order to compute the d^n states. Finally, the effect of the spin-orbit coupling is introduced in order to compute the ZFS [49].

- In 2005, Aquino and Rodriguez implemented a combined spin-DFT and perturbation theory (SDFT-PT) method [50] similar than the pioneering one of Pederson and Khanna.

- In 2006, Neese developed an alternative approach following a different line of reasoning. Although the equations derived look similar to the ones of Pederson and Khanna, apart from some prefactors [51], this implementation follows a Quasi-Restricted Approach (QRA) and computes the second-order SOC contribution to the second-order ZFS tensor.

- In 2007, Neese solved the coupled-perturbed equations and proposed a linear response approach for the calculation of the second-order ZFS tensor [52]. This method accounts for the SOC and SSC contributions to the ZFS. The application of linear response theory (LRT) avoids the truncation problem inherent to the previously exposed perturbation approaches. Among the five methods, this one is therefore the most sophisticated one.

The Pederson and Khanna (PK) method has been successfully applied to various polynuclear compounds [53–58]. In Mn(II) mononuclear complexes, it has been shown that the LRT improves the result compared to the QRA [59, 60], leading to a good agreement with experiment. Although in this specific configuration, DFT is more accurate than WFT [60], the latter gives in general better results than DFT for mononuclear complexes [46, 51, 61].

1.6.2 Wave-Function Based Methods

WFT allows one to calculate the ZFS parameters in different ways. Some attempts have been presented in the literature to calculate the ZFS within monodeterminental WFT based approaches [52, 62]. However, by using the Hartree-Fock method, the multideterminantal character of the ground state is not well described and an important part of the electron

correlation is missed. Hence, these implementations are not the most appropriate ones for the calculation of the ZFS in transition metal complexes, even in combination with LRT. Hence, in the present work, WFT methods that take into account the multideterminantal nature of the electronic states are used, namely Complete Active Space Self-Consistent Field (CASSCF) and post-CASSCF methods.

Usually, the WFT based methods which are used to compute the ZFS proceeds in two steps. In a first step, a set of spin-orbit free states is computed at either a CASSCF or a post-CASSCF level. In the second step, the low-lying spin-orbit spectrum can be (i) directly calculated through a state interaction (SI) method, or, as in some previously reported DFT schemes, (ii) constructed from the second-order ZFS tensor previously computed at second order of perturbation.

(i) When the low-lying spin-orbit spectrum is computed by diagonalizing the SOC matrix, two situations occur. In case of an even number of unpaired electrons, the second-order ZFS parameters can be extracted directly from the spectrum. In a pioneering application on $H_2Ti(\mu$-$H)_2TiH_2$, Webb and Gordon evaluated in this way the ZFS parameters [63]. However, in the case of an odd number of unpaired electrons, the ZFS parameters cannot be extracted from the information contained in the spectrum only due to the Kramers' degeneracy (see section 2.2) [64]. It is then necessary to use the information contained in the wavefunction in order to extract the ZFS parameters (see section 2.2).

(ii) Ganyushin *et al.* implemented a method to calculate the second-order ZFS tensor at second-order of perturbation starting from a CASSCF or post-CASSCF method, including the SOC and the SSC contribution to the ZFS [46]. One may notice that similar works have been reported in the literature, see for instance Sugisaki *et al.* [65].

Applications concerning mononuclear complexes led to a good agreement with experiment [51, 61]. Concerning polynuclear compounds, some brave test calculations on binuclear compounds were not very totally conclusive [64, 66], showing the difficulty to calculate ZFS parameters in such compounds. WFT calculations have also been used to calculate local anisotropies of mononuclear units in polynuclear complexes [67–70]. However, the relevance of the approximations used in these works and the validity of the multispin model Hamiltonian needs to be checked in a systematic way. New and challenging applications concerning both mononuclear complexes and binuclear complexes will be presented in sections 3 and 4,

respectively.

Summary

For a non-degenerate ground state, the low-lying spin-orbit spectrum of transition metal complexes can be described by a 'spin Hamiltonian', in which only spin degrees of freedom are considered. If the symmetry is not too high, the system can show magnetic anisotropy, even in the absence of an external magnetic field. This effect is called 'Zero-Field Splitting' (ZFS), and is described using phenomenological Hamiltonians. In binuclear complexes, the model Hamiltonians that describe this effect are questionable. While the physical origin of the ZFS is known for decades, the link between the structure and the property is not obvious in polynuclear complexes. There is clearly a need for a detailed theoretical study of the magnetic anisotropy to gain more insights that may eventually lead to a tuning of the property. However, the computational treatment of the ZFS is far from being trivial. Wave-Function Theory (WFT) based approaches are particularly promising for an extended theoretical study since they: (i) permit in most of the cases to find a better agreement with experiment than the DFT based ones, (ii) are powerful for interpretation purposes since they give access to the wavefunction, and (iii) allow one to check the relevance of the used model Hamiltonians (see section 2.2).

Chapter 2

Theory and Methods

2.1 *Ab Initio* Calculations

As mentioned in the previous chapter, the ZFS arises from the joint effects of the ligand field and the relativistic effects such as the SOC and SSC. In general, many of the electronic states belonging to the d^n manifold of the transition metal ions in the complexes with ZFS are strongly multiconfigurational. Furthermore, it is well-known that the relative energies of these states strongly depend on electron correlation. Hence, one need, in principle, a relativistic, WFT based correlated multideterminantal method for a correct description of the ZFS.

Except for small systems, such calculations are unaffordable, and obviously, some approximations are required to find a methodology applicable to most of complexes. As in transition metal complexes the relativistic effects are less important than the non-relativistic ones (crystal-field, ligand-field, electron correlation, *etc.*), one way to include the relativistic effects consits in a two-step strategy:

- In the first step, the spin-independent part of the Hamiltonian is treated. The spin part is included "ad-hoc".

- In the second step, the SOC and/or SSC terms are treated in a 'variation/perturbation' scheme, where 'variation' means that an interaction matrix is diagonalized and 'perturbation' means that the introduced effets are considered as a perturbation of the terms introduced in the first step.

2.1.1 The Treatment of the Electronic Part of the Hamiltonian

The CASSCF Method

The Complete Active Space Self-Consistent Field (CASSCF) is the method of choice to treat multiconfigurational wavefunctions as they occur in: dissociation and bond breakings, orbitally degenerate or nearly degenerate states, magnetic interactions, diradicals, excited states, etc. This method has several advantages that make its application particularly interesting: it is variational, size-consistent, generally applicable and highly efficient computationally speaking.

The key feature of CASSCF consists in a partition of the molecular orbital (MO) space in three subspaces: the inactive orbitals (doubly occupied orbitals in all configurations), the active orbitals and the virtual orbitals (unoccupied in all configurations). The active space is constructed by distributing the active electrons (total number of electrons minus twice the number of inactive orbitals) in all possible ways over the active orbitals. A correct description of the property under study depends therefore critically on the choice of the active space. The most general option for selecting the active orbitals is to include all the valence orbitals of the system in the active space. However, this definition is not feasible in practise due to the computational cost since too many orbitals would be involved. Hence, a further reduction of the active space is required. For the calculation of isotropic magnetic couplings, the smallest active space is constituted of the unpaired electrons and the corresponding magnetic orbitals.

With this active space, all spin multiplicity states from a given orbital configuration can be computed, and from there the magnetic coupling parameter J can be determined. Starting from the HDVV Hamiltonian:

$$\hat{H}_{HDVV} = J\hat{\mathbf{S}}_a \cdot \hat{\mathbf{S}}_b \tag{2.1}$$

it can be shown that the magnetic coupling parameter can be extracted using the following expression:

$$J = \frac{E(S) - E(S-1)}{S} \tag{2.2}$$

where E(S) is the energy of a state with spin multiplicity S, and E(S-1) the energy of a state of S-1 spin multiplicity. Hence, the CASSCF energies of two (consecutive) spin states arising from the HDVV Hamiltonian are sufficient to extract J. In some cases, deviations to the HDVV

Hamiltonian are observed: the J value extracted from different pairs of consecutive spin states are not equal. These deviations are actually directly accessible using the energies computed at the CASSCF level if all spin states generated by the HDVV Hamiltonian are computed and can also be characterized through a parameter. The physical origin of both J [71–73] and deviations to the HDVV [74] have been studied in details, showing that dynamic correlation plays a crucial role on these parameters. Hence, the CASSCF method, which only introduces non-dynamic correlation is not accurate enough for a quantitative calculation of magnetic parameters, and one has to go beyond the mean-field approach. The main post-CASSCF methods used in magnetism will be presented in the next paragraphs.

Perturbative Post-CASSCF Methods

In perturbative post-CASSCF methods, the CASSCF wavefunction is chosen as the zeroth-order wavefunction, and the effect of the configurations external to the CAS on the energy and wavefunction is estimated through perturbation theory. The most popular methods used are the Complete Active Space Perturbation Theory (CASPT) and the N-Electron Valence Perturbation Theory (NEVPT). Usually, the perturbation is done at second-order, leading to the so-called CASPT2 [75] and NEVPT2 [76] methods.

While these two methods obviously have some points in common, one important difference has to be mentioned, namely the definition of the zeroth order Hamiltonian. In CASPT2, various zeroth order Hamiltonians have been used over the years. All are Fock-type (monoelectronic) Hamiltonians. The approximate nature of these Hamiltonians can cause the appearance of intruder states. In order to avoid this, a level-shifting technique is usually employed [77]. However, one has to note that the correlated energies are moderately dependent on the applied level-shift. In NEVPT2, the zeroth-order Hamiltonian has a bielectronic nature. It is indeed a Dyall's model Hamiltonian that is equivalent to the full Hamiltonian in the CAS space since it includes all two-electron components among the active electrons. This definition of the zeroth order Hamiltonian prevents the appearance of intruder states and ensures that dynamic correlation can be treated as a perturbation.

Since both methods treat dynamic correlation at second order of perturbation, they include all single and double excitations involving at least one inactive or one virtual orbital. Both methods are internally contracted, *i.e.* they do not revise the coefficients of the reference

wavefunction under the effect of the dynamic correlation. One should note that internally uncontracted schemes have been proposed based on either CASPT2 or NEVPT2, but are not considered in the present work. CASPT2 and NEVPT2 are both externally contracted, *i.e.* some fixed relations appear between the perturber coefficients in the correlated wavefunctions. Two external contraction shemes have been introduced in NEVPT2, namely the Partially Contracted (PC) and the Strongly Contracted (SC) approaches. While the PC-NEVPT2 approach is closer to the CASPT2 contraction scheme, the more approximate SC-NEVPT2 approach gives usually similar results as the PC-NEVPT2 approach provided that the zeroth order wavefunction is adequate [78]. Hence, in most applications the SC-NEVPT2 approach is accurate enough, and 'NEVPT2' usually refers to the 'SC-NEVPT2' approach in the literature.

As often reported, both CASPT2 and NEVPT2 are unable to give quantitative estimates of J for weakly coupled spin moments [79]. This problem lies in the fact that fourth- and higher-order corrections to the energies significantly enhance the metal-ligand delocalization, leading to important changes in the magnetic coupling [73]. Moreover, both approaches are susceptible to introduce artificial deviations to the Landé intervals due to their perturbative character [79]. The study of deviations to the HDVV Hamiltonian is then restricted to variational methods. Hence, when small magnetic effects are studied, variational or mixed variational and perturbative approaches are required.

Variational Post-CASSCF Methods

To increase the accuracy in the computation of magnetic coupling parameters, one has to go to Multi-Reference Configuration Interaction (MRCI) methods. However, the cost of the calculation increases dramatically with the number of determinants included in the CI expansion. If one takes into account all possible excitations included in the CASPT2 and NEVPT2 methods, one arrives at the MRCI-SD method where SD stands for Single and Double excitations. Since these excitations are too numerous for any real system, it is necessary to truncate the MRCI-SD space.

In order to further describe some possible reductions of the MRCI-SD space, it is convenient to introduce first the different classes of excitations and their corresponding number of degrees of freedom. A degree of freedom corresponds to the annihilation of an electron in the inactive orbitals or the creation of an electron in the virtual orbitals. One has to remember that such

n	Class	Excitation
0	None	p → q
		pq → rs
1	1h	i → p
		ip → qr
	1p	p → a
		pq → ra
2	1h-1p	i → a
		ip → qa
	2h	ij → pq
	2p	pq → ab
3	2h-1p	ij → pa
	1h-2p	ip → ab
4	2h-2p	ij → ab

Table 2.1: Classification of the different excitations that generate the determinants in the CI expansion of MRCI-SD and truncated MRCI-SD approaches. i and j correspond to inactive orbitals, p, q, r and s to active orbitals while a and b correspond to virtual orbitals. n is the number of degree of freedom.

an excitation can be accompanied by an excitation within the active space. According to this definition, the CASSCF method has no degrees of freedom, and the MRCI-SD methods includes all excitations with 0, 1, 2, 3 and 4 degrees of freedom. The number of degrees of freedom does not correspond to the number of excitations. However, for 3 or 4 degrees of freedom, only diexcitations can be envisaged. The excitations can also be classified with regard to the holes and particles created by the excitation. If one electron is promoted from one inactive orbital, one hole (h) is created, and if one electron is promoted to a virtual orbital, one particle (p) is created. Table 2.1 recalls all types of excitations of a truncated MRCI-SD and their nomenclature according to these two conventions.

When an energy difference between two correlated states belonging to the CAS reference space has to be computed, the 2h-2p can be neglected since they cannot contribute to this en-

ergy difference in a quasi-degenerate second order treatment of the dynamic correlation. This approximation gives rise to the so-called DDCI3 method, where 3 represents the maximum number of degrees of freedom [80]. In the DDCI2 method, the 2h-1p and 1h-2p excitations are further neglected compared to the DDCI3 method. The role of all different types of excitations on the magnetic coupling parameters has been extensively studied [71–73], showing that the 2h-1p and 1h-2p excitations play a crucial role in the energy difference. Usually the LMCT configurations, that are introduced through the 1h excitations, are inhibited due to the Brillouin's theorem. However, when the 2h-1p and 1h-2p excitations are added to the variational space, the weight of the LMCT excitations in the wavefunctions are increased, resulting in a better description of the covalency effects. For binuclear compounds having bridging ligands, no reliable estimate of the magnetic couplings can be obtained below the DDCI3 level, since the magnetic orbitals are not sufficiently delocalized on the ligands. However, even the DDCI3 methods rapidly becomes very expensive computationally speaking. Hence, several approximations to the DDCI3 treatment have been explored over the years. One of these consists in mixing the variation and the perturbation, and is presented in the next paragraph.

Hybrid Variational and Perturbative Post-CASSCF Methods

Although algorithms that mixes variational and perturbative approaches are available [81, 82], their application in magnetism can be dangerous. Usually these kind of approaches start with a perturbative estimate of all single and double excitations to the total energy. If this contribution is smaller than a certain threshold, the excitation will be treated by perturbation, otherwise it will be considered in the CI space. However, it is easy to imagine that this threshold value must be very small to obtain accurate magnetic coupling parameters. Indeed, as explained in the previous paragraph, the 2h-1p and 1h-2p excitations play a crucial role in the relaxation process of the 1h and 1 p excitations. These 1h and 1p excitations have rather small contributions to the total energy in the perturbative estimate performed at the beginning of the process. Hence, in order to take them into account in the CI process, a very small threshold is needed, limiting drastically the gain in the computational cost. After obtaining the CI wavefunctions and energies, the effect of excitations neglected in the CI process can be treated perturbatively. With an adequate threshold, one may expect the same accuracy than the DDCI3 level, providing a good agreement with experiment in most cases.

2.1.2 *A Posteriori* Inclusion of Relativistic Effects

As already mentionned, one of the objectives of the present thesis is to compute the ZFS parameters in a two-step approach. As shown previously, (post-)CASSCF methods present several advantages for the calculation of the energies and wavefunctions of the electronic states relevant for determining magnetic couplings. Hence, the point is to include these approaches in an approximate relativistic framework. This can be obtained by dealing in a first step with all spin-orbit independent terms, and all spin-orbit dependent terms can be treated in the second step. One popular scheme is already presented in details elsewhere in the literature [83], and is also briefly presented in this section.

From the Dirac Hamiltonian to the Douglas-Kroll-Hess Hamiltonian

The Douglas-Kroll transformation [84] aims to eliminate the coupling between the small and large components of the Dirac one-electron Hamiltonian. The Dirac Hamiltonian may be written as:

$$\hat{H}_D = \hat{V} + m_e c^2 \hat{\boldsymbol{\beta}} + c\hat{\mathbf{p}}_k \hat{\boldsymbol{\alpha}}_k \tag{2.3}$$

where $\hat{V}$ is the one-electron external potential, m_e the electron mass, c the speed of the light, $\mathbf{p}$ the momentum operator, $\boldsymbol{\alpha}$ and $\boldsymbol{\beta}$ the 4x4 Dirac matrices, and k an index ranging from 0 to 3. The eigenfunctions of this Hamiltonian involve four components, two small ones, the positrons, and two large ones, the electrons. The Douglas-Kroll transformation is based on an expansion in orders of the external potential $\hat{V}$ and on a series of unitary transformations. At an infinite order, two uncoupled two-components parts are generated and their energy difference reproduces exactly the splitting of the Dirac Hamiltonian. In practice, the transformation is done at second order, leading to the so-called Douglas-Kroll-Hess Hamiltonian [84–86]. As soon as the small and large components are decoupled, one may consider only the large components, leading to the no-pair Hamiltonian. At this point the Hamiltonian can be separated in two parts, the spin-independent part and the spin-orbit dependent part. These two parts can be treated in two steps, each part having its specificities and further approximations that will be presented in the following paragraphs.

The Treatment of the Spin-Orbit Free States

The spin-orbit free states are calculated within a pseudo-relativistic framework. For light atoms such as the first-row transition metal complexes, it is usually assumed that the scalar relativistic corrections to the non-relativistic Hamiltonian can be treated in the monoelectronic part of the Hamiltonian. Hence in practice, a Hamiltonian is built by summing the spin independent no-pair Hamiltonian and the non-relativistic bi-electronic Coulomb interaction which can be used in standard calculations such as CASSCF and CASPT2 for instance, allowing one to treat consistently the major part of the scalar relativistic effects in the spin-orbit free states.

As discussed in section 1.3.2, a correct account of the ZFS requires a balanced consideration of the spin-orbit free states. The safest procedure is to perform a state-average CASSCF calculation for all the states of the d^n manifold, eventually followed by CASPT2 or another post-CASSCF method.

The Spin-Orbit Coupling within the Variation/Perturbation Scheme

Knowing the wavefunctions and energies of a set of spin-orbit free states obtained in the first step, the SOC can be calculated. The SOC Hamiltonian is considered as a perturbation of the spin-orbit free Hamiltonian, and hence the wavefunction coefficients of the spin-orbit free states are not modified under the action of the SOC. However, some flexibility is introduced since the SOC matrix between all M_S components of all spin-orbit free states is computed and diagonalized.

The SOC Hamiltonian is usually an approximate version of the Breit-Pauli Hamiltonian. Knowing that the multi-center SOC integrals are negligible and that the mono-center bielectronic integrals can be treated by a mean-field approximation [87], one can use the so-called Atomic Mean Field Integrals (AMFI) [88] to include SOC effects in the Hamiltonian. By diagonalizing the resulting SI matrix, the eigenvalues and eigenvectors of the SOC Hamiltonian can be found.

The Inclusion of Dynamic Correlation Effects

In the two-step approach outlined above, dynamic correlation can play a role on the ZFS parameters by modifying (i) the wavefunction of the spin-orbit free states and therefore the off-diagonal SOC matrix elements and (ii) the relative energies of the spin-orbit free states and therefore the diagonal energies of the SOC matrix. However, as it will be seen in section 4.1, the inclusion of (i) in the SOC calculation is problematic. Hence, at this stage, it is considered that dynamic correlation effects are safely included only by replacing the diagonal energies of the SOC matrix by the energies obtained at a post-CASSCF level [89]. This treatment is not completely rigorous since the CASSCF wavefunctions are used in the computation of the extradiagonal terms of the SOC matrix, and may become questionable, especially when dynamic correlation effects cause large changes in the relative weights of the most important configurations in the wavefunction.

2.2 Extraction of the Spin Hamiltonian Interactions

2.2.1 On the Extraction of Model Interactions Using Effective Hamiltonian Theory

Having obtained the energies and wavefunctions of the low-lying spin-orbit states, the last step consists in extracting the ZFS parameters. The extraction procedure is based on the effective Hamiltonian theory [90, 91]. It extracts the full ZFS tensor which means that the use of an arbitrary axes frame in the *ab initio* calculation is not problematic. Furthermore, the mapping between the full electronic Hamiltonian and the simpler spin Hamiltonians provided by the effective Hamiltonian procedure allows one to check the accuracy of any model Hamiltonians. This aspect is especially important for polynuclear systems for which the proposed Hamiltonians lack firm theoretical foundation.

Although the effective Hamiltonian can be constructed without any assumption on the model Hamiltonian operators, extractions often start by writing down a supposedly relevant model Hamiltonian. This choice defines the dimension and the basis of the model space. The construction of the model interaction matrix paves the way for the extraction procedure and subsequent validation of the model Hamiltonian.

For instance, to describe the ZFS in mononuclear complexes with two or three unpaired electrons, the following model Hamiltonian applies (already introduced in section 1.3.1):

$$\hat{H}_{mod} = \hat{\mathbf{S}}.\overline{\overline{D}}.\hat{\mathbf{S}} \tag{2.4}$$

provided that the ground state is non-degenerate. Hence, in order to build the model interaction matrix, the model Hamiltonian is expanded:

$$\hat{H}_{mod} = \begin{pmatrix} \hat{S}_x & \hat{S}_y & \hat{S}_z \end{pmatrix} . \begin{pmatrix} D_{xx} & D_{xy} & D_{xz} \\ D_{xy} & D_{yy} & D_{yz} \\ D_{xz} & D_{yz} & D_{zz} \end{pmatrix} . \begin{pmatrix} \hat{S}_x \\ \hat{S}_y \\ \hat{S}_z \end{pmatrix} \tag{2.5}$$

and the $\hat{S}_x$ and $\hat{S}_y$ operators are replaced by the adequate linear combinations of the $\hat{S}_+$ and $\hat{S}_-$ operators. By applying this Hamiltonian on the basis of the model space (in this case all the $|S, M_S\rangle$ components of the ground state) the interaction matrix is constructed. Examples of interaction matrices will be presented in sections 3.1, 4.1 and 4.2.

Construction of the Effective Interaction Matrix

The construction of the effective Hamiltonian relies on the information contained in both the energies and the wavefunctions of the low-lying spin-orbit states. According to Bloch's formalism [90], the effective Hamiltonian reproduces the energy levels of the "exact" Hamiltonian E_k and the wavefunctions of the low-lying states projected onto the model space $\widetilde{\Psi}_k$:

$$\hat{H}_{eff}|\widetilde{\Psi}_k\rangle = E_k|\widetilde{\Psi}_k\rangle \tag{2.6}$$

Here the "exact" Hamiltonian corresponds to the *ab initio* Hamiltonian introduced in the previous section. A formulation of such Hamiltonian has been proposed by Bloch [90] and involves the biorthonormal vectors $\widetilde{\Psi}_k^{\downarrow}$:

$$\hat{H}_{eff} = \sum_k |\widetilde{\Psi}_k\rangle E_k \langle\widetilde{\Psi}_k^{\downarrow}| \tag{2.7}$$

where the biorthonormal set of vectors is constructed as follows:

$$|\widetilde{\Psi}_k^{\downarrow}\rangle = |S^{-1}\widetilde{\Psi}_k\rangle \tag{2.8}$$

and where S is the overlap matrix between the projected vectors. Hence, Bloch's Hamiltonian can be directly written as follows:

$$\hat{H}_{eff} = \sum_k |\widetilde{\Psi}_k\rangle E_k \langle S^{-1}\widetilde{\Psi}_k| \tag{2.9}$$

which ensures that the effective Hamiltonian reproduces the energies of the exact Hamiltonian.

However, in this approach, the projected vectors are not always orthogonal to each other, leading to a non-Hermitian effective Hamiltonian. Since all model Hamiltonians are Hermitian, the des Cloizeaux formalism is used [91]. In des Cloizeaux' formalism, the projected vectors are symmetrically orthonormalized and the resulting effective Hamiltonian is by construction Hermitian while it still reproduces the energies of the exact Hamiltonian and the orthonormalized projected wavefunctions. This Hamiltonian can be written as:

$$\hat{H}_{eff} = \sum_k |S^{-\frac{1}{2}}\widetilde{\Psi}_k\rangle E_k \langle S^{-\frac{1}{2}}\widetilde{\Psi}_k| \tag{2.10}$$

The overlap matrix between the projected vectors (before orthonormalization) provides a first simple check of the validity of the model Hamiltonian. If the norm of the projections is too small, the model space is probably not adequate. For example, when the SOC induces large contributions of M_S components of excited spin-orbit free state(s), the norm of the projections onto the model space becomes small, which can be associated to an inadequate and too small model space. Such problems occur due to an orbital degeneracy or near-degeneracy. In this case, the model space must include all M_S components of the degenerate or nearly degenerate spin-orbit free states to obtain a reliable model description of the lowest spin-orbit states.

If the model space is adequate, the effective interaction matrix can be constructed as follows:

$$\langle\Phi_i|\hat{H}_{eff}|\Phi_j\rangle = \langle\Phi_i|\sum_k |S^{-\frac{1}{2}}\widetilde{\Psi}_k\rangle E_k \langle S^{-\frac{1}{2}}\widetilde{\Psi}_k|\Phi_j\rangle \tag{2.11}$$

where Φ_i and Φ_j are determinants belonging to the model space. This effective interaction matrix has to be carefully compared to the model interaction matrix for a definite justification of the model Hamiltonian. Three cases can be encountered:

- Both effective and model matrices perfectly match. This case is obviously the preferable

one, and then both the dimension and nature of the model space and the operators used in the model Hamiltonian have been rigorously defined.

- Small differences appear between the model and the effective Hamiltonian matrices. In this case, the model Hamiltonian can be considered to be appropriate, even if it should be mentioned that the model is unable to reproduce precisely effective interactions arising from the exact Hamiltonian.

- Large differences that cannot be denied appear between both interaction matrices. It is obviously the worst case scenario indicating that some important effective interactions are neglected in the initial model Hamiltonian. An example of this scenario will be presented in section 4.2. If this happens, one should question the validity of the model Hamiltonian, and the model must be refined.

Model Interaction Extraction

If no deviations between the model and the effective interaction matrices are observed, the model interactions can be extracted by solving the system of independent equations generated by the one-to-one correspondance of the matrix elements. Since the effective Hamiltonian reproduces by definition the splitting between the low-lying energy levels of the exact Hamiltonian, the corresponding model Hamiltonian also reproduces this low-lying spectrum perfectly.

In the case of small deviations between the model and effective interaction matrices, the extracted model Hamiltonian does not reproduce anymore the splitting of the energy levels of the exact Hamiltonian. In this case, the deviation between both spectra is calculated to quantify the importance of the missing interactions in the model. In the present thesis the error ϵ is defined as follows [92]:

$$\epsilon = \frac{\sum_k^N |E_k^{exact} - E_k^{model}|}{N \times 100 \times \Delta E^{exact}} \tag{2.12}$$

where N is the number of states considered, E_k^{exact} and E_k^{model} the eigenvalues of the exact and model Hamiltonians, respectively, and ΔE^{exact} the energy difference between the highest and lowest energy eigenvalues of the exact Hamiltonian.

2.2.2 Towards an Approximate Treatment of Large Systems

At present, an *ab initio* treatment of SMMs is impossible due to the elevated computational cost. However, the combination of effective Hamiltonian theory and model Hamiltonians can provide accurate model spectra for such large systems. A necessary condition to proceed along this line is that the system can be described using operators acting on small fragments of the whole system (for instance only considering one- and two-center operators), and that the corresponding parameters can be accurately calculated from small fragments (*i.e.* the parameters extracted in the fragments are transferable to the whole system).

In the fragment calculations, the rest of the molecule has to be taken implicitly into account. Usually, the embedding is treated by means of *Ab Initio* Model Potentials (AIMPs) for the atoms closest to the fragment and point charges for the rest of the system. Subsequently, a model Hamiltonian of the complete system can be built using the fragment parameters. The diagonalization of this Hamiltonian gives the model spectrum that can be used to study the properties of the whole system.

Such studies have been successfully applied to several polyoxometalates for instance [93–95], for which the magnetic coupling parameters as well as the electron transfer integrals were evaluated in binuclear fragments (and in some cases in tri- or tetra-nuclear fragments). The magnetic susceptibility of some polyoxometalates (POMs) could be reproduced with the model Hamiltonian built from the parameters extracted from the fragment calculations [94], demonstrating the power of effective Hamiltonian theory and model Hamiltonian approaches.

Concerning the magnetic anisotropy and the SMMs, such an approach is certainly interesting. However, one should carefully validate the minimal size of the fragment to consistently extract anisotropic parameters. Usually, it is considered that the mono- and bi-centric anisotropic tensors dominates the physics. However, this assertion has never been checked, and the transferability of the extracted parameters is not guaranteed. Hence, at this stage, this possibility is kept in mind as a long-term perspective.

2.3 Analytical Derivations of the Spin Hamiltonian Parameters as a Tool for Rationalization

One of the objectives of this thesis is to revisit and improve the rationalizations of the ZFS performed by Abragam and Bleaney [15]. Most of their work concerns nearly octahedral complexes under intermediate crystal fields. In this case, the d^n configurations can be divided in three groups. While the d^1 and d^9 configurations cannot present any anisotropy due to the Kramers' degeneracy, the high spin d^3, d^4, d^5 and d^8 configurations in an octahedral coordination lead to magnetic anisotropy if a distortion is applied. The remaining high spin d^2, d^6 and d^7 configurations have a first order orbital momentum in the octahedral situation. Hence, even when applying a distortion, the orbital momentum is not totally quenched, and spin Hamiltonians are not models of choice.

Keeping in mind these general considerations concerning the first-row transition metal complexes, an analytical way of deriving spin Hamiltonians has to be defined for our rationalizing purpose. Most of the approximations introduced in the analytical treatment of ZFS by Abragam and Bleaney (see section 1.3.2) are well established and will also be applied here. However, the contribution to the ZFS arising from spin-orbit free states belonging to excited multiplets of the free-ion has sometimes to be included in the treatment to become quantitative. To include such contributions in the treatment, the polyelectronic SOC Hamiltonian $\lambda\hat{\mathbf{L}}.\hat{\mathbf{S}}$ cannot be used anymore since the spin-orbit interaction might then couple states having a different quantum number L in the free-ion. Nevertheless, a monoelectronic spin-orbit Hamiltonian can be used:

$$\hat{H}_{SOC} = \zeta \sum_i \hat{\mathbf{l}}_i.\hat{\mathbf{s}}_i \tag{2.13}$$

where ζ is the effective spin-orbit coupling constant, and where the sumation runs over the considered electrons (or holes). Consequently, the spin-orbit free states cannot be expressed using the $|L, M_L\rangle$ configurations anymore and the first step of the analytical derivation has to be adapted. In the following, the new derivation process is explained in detail.

2.3.1 The Crystal Field Somewhere in between Stevens and Racah's Languages

The Intermediate Crystal Field Approach in Stevens Language

Abragam and Bleaney take the free-ion Hamiltonian as zeroth-order description and the crystal field as perturbation. Taking into account only the first-order corrections, the effect of the crystal field is limited to a splitting of the free-ion multiplets without further modifications to the wavefunctions. Due to the fact that the zeroth-order Hamiltonian only defines a zero of energy, it can be omitted in the analytical treatment of the crystal field. This makes that the crystal field Hamiltonian, expressed in terms of extended Stevens operators [96], reads as:

$$\hat{H}_{ligand} = \sum_{k=2,4} \sum_{q=-k}^{k} B_k^q \hat{O}_k^q \tag{2.14}$$

where k is the order of the operator and q indexes the type (symmetry) of the crystal field. The explicit form of the operators is given in the book of Abragam and Bleaney [15]. Contrary to the spin Hamiltonian that describes the ZFS for mononuclear complexes presented in section 1.3.1, k can be odd for non-centrosymmetric complexes and also negative values for q are possible depending on the symmetry of the crystal field.

This treatment accounts for the splitting and possible mixing of the $|L, M_L\rangle$ configurations of a same multiplet of the free-ion consistently, but remains very simple. In practice the model can be solved analytically. Subsequently, the spin-orbit coupling can be calculated perturbatively using the polyelectronic version of the SOC Hamiltonian.

However, the major drawback on this approach is that the mixing between the $|L, S\rangle$ and $|L', S\rangle$ configurations belonging to different multiplets of the free-ion is neglected. While such interaction could be actually introduced at second-order in Stevens formalism [15], the interest of using this formalism would be lost since the treatment would become much more complicated.

The Crystal Field in Racah's model

In Racah's formalism, the crystal field is considered to be strong and cannot be treated as a perturbation. Hence the Hamiltonian to be treated is defined as:

$$\hat{H}_{Racah} = \hat{H}_{free-ion} + \hat{V} \tag{2.15}$$

where $\hat{V}$ is a monoelectronic operator accounting for the crystal field potential and $\hat{H}_{free-ion}$ the free-ion Hamiltonian:

$$\hat{H}_{free-ion} = -\frac{1}{2}\sum_{i=1}^{n}\nabla_i^2 - \sum_{i=1}^{n}\frac{Z_M}{r_{iM}} + \sum_{j>i}^{n}\sum_{i=1}^{n}\frac{1}{r_{ij}} \tag{2.16}$$

where i and j are electron indices, n the number of electrons. M is the metal ion and Z_M its charge, r_{iM} the electron-nucleus distance, and r_{ij} the electron-electron distance. The Racah's Hamiltonian only deals with the d electrons of the metal ion, and acts on determinants expressed with real d orbitals.

The operator accounting for the crystal field potential contains the information of the symmetry of the crystal field. Hence, as in Stevens formalism, the crystal field imposes the symmetry of the wavefunctions and is responsible for the splitting and mixing of the different d^n states. The second-order mixing between configurations belonging to different multiplets in the free-ion is well treated since the complete Hamiltonian is diagonalized. One of the drawbacks of such an approach is that the treatment is more complicated than in the previous case, the diagonalization cannot be done by hand since it involves many couplings between different configurations.

Racah's formalism uses the so-called A, B and C parameters to describe the mono- and bi-electronic interactions of the electrons. These parameters are combinations of the Slater-Condon parameters that are used to describe the radial part of the mono- and bi-electronic integrals. The energy differences between the different d^n states are fully determined by B and C. Hence, A only accounts for monoelectronic integrals, and B and C account for the bielectronic integrals. The basic assumption made by Tanabe and Sugano that $\frac{C}{B}$ is equal to 3.97 and independent of the crystal field strengh allowed them to express the energy dependence of the d^n states as functions of the crystal field and construct the famous Tanabe-Sugano diagrams. However, more precise calculations showed that these relations are only approximatively valid [97]. Therefore, these diagrams will not be used in the present thesis. One may conclude that Abragam's treatment could be improved and that Racah's treatment could be simplified. A compromise has to be found, which is the subject of the next paragraph.

A Usefull Compromize Somewhere in between both Approaches

Both Abragam and Racah approaches describe the splitting and mixing of the d^n states in the presence of a crystal field. In order to define a useful compromize between both approaches for the rationalization of the ZFS, one has to take the advantages of both methods, (i) the simplicity of the treatment of the crystal field in Abragam's approach and (ii) the possibility of treating the effect of spin-orbit free states belonging to excited multiplets in the free-ion as in Racah's model. As a consequence, (i) only the first-order effects of the crystal field on the wavefunctions and energies or the d^n states are considered, and (ii) the d^n states are expressed in terms of the real d orbitals of the metal (and not in terms of the $|L, M_L\rangle$ configurations as in Abragam's treatment). Hence, a monoelectronic SOC Hamiltonian can be applied and the effect of these excited spin-orbit free states on the ZFS can be included in a rather straightforward way (without having to treat the electronic coupling between these excited states and the ground state affected by the ZFS). Example of such treatments will be presented in section 3.2.

2.3.2 The Spin-Orbit Coupling and the ζ Effective Constant

As discussed in the first part of section 2.3, a monoelectronic SOC Hamiltonian has to be used when the coupling of the M_S components of d^n states belonging to different multiplets in the free-ion is considered. In the most rigorous definition, each electron has its proper ζ_i spin-orbit coupling constant:

$$\hat{H}_{SOC} = \sum_i \zeta_i \hat{\mathbf{l}}_i . \hat{\mathbf{s}}_i \tag{2.17}$$

For sake of clarity, the simpler expression of the SOC Hamiltonian given in Eq. 2.13, where ζ is an effective monoelectronic spin-orbit coupling constant used for all electrons and all excitations. Note, however, that the use of an effective spin-orbit coupling constant introduces some approximations both in the results and the interpretation. For example, the effects of the crystal field and the covalency on ζ are far from being trivial. In the first place, the covalency effects reduce ζ in an anisotropic way, *i.e.* the reduction is stronger for orbitals with larger contributions. Moreover, when ζ is expressed as [15]:

$$\zeta = \frac{1}{2}\left(\frac{\hbar}{mc}\right)^2 \frac{1}{r}\frac{dV}{dr} \tag{2.18}$$

arising from the comparison between the monoelectronic Hamiltonian $\zeta\hat{\mathbf{l}}.\hat{\mathbf{s}}$ and the Pauli approximation of the SOC operator:

$$\hat{H}_{Pauli} = \frac{1}{2}\left(\frac{\hbar}{mc}\right)^2 \left(\frac{\nabla V \times \hat{\mathbf{p}}}{\hbar}\right).\hat{\mathbf{s}} \tag{2.19}$$

the potential V associated to the movement of the electron in a self-consistent field has to be spherical to ensure that ζ is equal for all d^n electrons. However, since the crystal field potentials of the cases of interest are anisotropic, it is clear that strictly speaking, the spin-orbit constant should reflect this anisotropy. This effect is neglected when an effective spin-orbit coupling constant is used for all the excitations. Hence, the conclusion that the spin-orbit coupling constant ζ is reduced by covalent bonding oversimplifies the real situation [15]. Since it is not possible to rigorously define an effective spin-orbit coupling constant, the free-ion spin-orbit coupling constant is used. The relevance of this choice will be checked by comparing the relative energies of the resulting model to the energies of the *ab initio* calculations, *i.e.* calculating ϵ of Eq. 2.12.

2.3.3 Analytical Effective Hamiltonian Derivation

The analytical formulae for the ZFS parameters are derived from the second-order Quasi-Degenerate Perturbation Theory (QDPT). The global Hamiltonian $\hat{H} = \hat{H}_{el} + \hat{H}_{SOC}$ is considered, where $\hat{H}_{el}$ is the zeroth order Hamiltonian that accounts for the spin-orbit free interactions. $\hat{H}_{SOC}$ is the perturbation, treated up to second order:

$$\begin{aligned}\langle \Phi_i, M_S|\hat{H}_{eff}|\Phi_j, M_{S'}\rangle &= \delta_{ij}\delta_{M_S M'_S}\langle \Phi_i, M_S|\hat{H}_{el}|\Phi_j, M_{S'}\rangle + \langle \Phi_i, M_S|\hat{H}_{SOC}|\Phi_j, M_{S'}\rangle \\ &+ \sum_{\Phi_k, M_{S_k}} \frac{\langle \Phi_i, M_S|\hat{H}_{SOC}|\Phi_k, M_{S_k}\rangle\langle \Phi_k, M_{S_k}|\hat{H}_{SOC}|\Phi_j, M_{S'}\rangle}{E_{\Phi_j} - E_{\Phi_k}}\end{aligned} \tag{2.20}$$

where δ_{ij} and $\delta_{M_S M'_S}$ are Krönecker δ functions, Φ_i and Φ_j are spin-orbit free states belonging to the model space, Φ_k a spin-orbit free state belonging to the external space, and E_{Φ_k}

and E_{Φ_j} the spin-orbit free energies of the spin-orbit free states Φ_k and Φ_j respectively. The ideal external space includes the most important contributions to the ZFS, presents equilibrated excitations in all directions of space with regard to the model space, and is as smallest as possible to facilitate the analytical derivations. When several spin-orbit free states are considered within the model space, $E_{\Phi_k} - E_{\Phi_j}$ is equalized to $E_{\Phi_k} - E_{\Phi_i}$ to ensure the Hermitian character of the analytical effective Hamiltonian:

$$\Delta\Phi_k = E_{\Phi_k} - \frac{E_{\Phi_i} + E_{\Phi_j}}{2} \tag{2.21}$$

$\Delta\Phi_k$ is a spin-orbit free quantity that includes more effects than included in the analytical model when these excitation energies are extracted from experimental data or by means of *ab initio* calculations. In this work, the denominators will be extracted from a spin-orbit free CASSCF or post-CASSCF calculation, and hence, the denominators also include the effect of (i) scalar relativistic effects, (ii) core electrons, (iii) non-dynamic and sometimes dynamic correlation, and (iv) explicit electronic interactions between the metal atoms and the ligands. One should note that the *ab initio* calculations therefore provide useful information in order to check the validity of the analytical formulae since (i) the number of states that should be included in the model for a quantitative estimate of the ZFS can be checked, (ii) the analytical wavefunctions of the spin-orbit free states can be compared to the ones of the exact electronic Hamiltonian, and (iii) accurate denominators are provided.

The only adjustable parameter of the model that remain at this stage is the effective spin-orbit coupling constant ζ. As already exposed, the free ion spin-orbit constant is taken. If the deviation between the model and *ab initio* spectrum is large, the crystal field approach is not relevant, and hence, there is no meaning in adjusting ζ with an unphysical value. On the other hand, smaller ϵ values validate the model developed to rationalize the ZFS, and only small adjustments of ζ lead to a nearly perfect agreement between the model and reference spectra. As a consequence, the analytical formulae can be rigorously checked, and the pioneering work of Abragam and Bleaney may be revisited and sometimes extended in order to provide quantitative information on the ZFS.

2.4 Computational Details

General Considerations

The magnetic anisotropy is extremely sensitive to the molecular structure used in the calculation. Unless specified, all the *ab initio* results presented in this thesis have been obtained using the crystallographic molecular structure. Indeed, due to the sensitivity of the ZFS parameters to the geometrical structure, it is not possible to use optimized geometries.

The general scheme presented in section 2.1.2 has several computational degrees of freedom. The most important are (i) the size of the active space, (ii) the number of spin-orbit free states included in the SI space, and (iii) the level of theory used to obtain the diagonal energies of the SI matrix. Although general rules exist to obtain a reliable description of the ZFS, some details have to be adapted to the peculiarities of each case. Therefore, the corresponding choices will be presented and validated for each application. In short, the *ab initio* calculation of the ZFS is not a black-box procedure and requires some intervention of the user.

ZFS Calculations with the MOLCAS Program

The general scheme presented in section 2.1.2 is implemented in the MOLCAS program [98] through the Restricted Active Space State-Interaction Spin-Orbit (RASSI-SO) method [83, 99]. The implementation uses the DKH Hamiltonian in the spin-orbit free calculations performed at the CASSCF and CASPT2 levels. In the CASPT2 calculations, unless specified otherwise, the Ionization Potential - Electron Affinitiy (IP-EA) shift in the zeroth-order Hamiltonian [100] is set to zero. It has been shown that a non-zero shift spoils the accuracy obtained in magnetism with the unshifted Hamiltonian [79]. A small imaginary level shift [77], between 0 and 0.2 a.u., is used in all applications to avoid intruder state problems.

The Atomic Natural Orbitals - Relativistically Core Correlated (ANO-RCC) basis sets [101] are used for all atoms. They are especially designed to use the DKH Hamiltonian and to correlate semi-core electrons in the correlated calculations. The following contraction schemes are used: 6s5p4d2f for Transition Metal (TM) atoms, 7s6p4d2f for I atoms, 6s5p3d1f for Br atoms, 5s4p1d for Cl and P atoms, 4s3p1d for O and N atoms (in some calculations for the non-coordinated N atoms the 3s2p1d contraction scheme is used), 3s2p for C atoms and 2s for H atoms.

Spin-Orbit Free Calculations using CASDI

The CASDI program connected to MOLCAS allows one to perform spin-orbit free calculations at the DDCI3 level. The DDCI3 calculations may be iterative in order to relax the MOs under the effect of dynamic correlation [102], and excitation energy dedicated orbitals are used to reduce the computational cost [103].

ZFS Calculations with the ORCA Program

A similar process as the RASSI-SO method is available in the ORCA program [104]. Although a QDPT treatment for the ZFS parameters is also available [46, 62], all ZFS parameters presented in this dissertation have been obtained by diagonalizing the SI matrix. The scalar relativistic effects have been neglected in the application presented in section 4.1.1. This approximation is valid since the present application only concern first-row transition elements and lighter elements and all states considered have the same number of d electrons (scalar relativistic effects are non-negligible for the energy difference between states dominated by $3d^n4s^m$ and $3d^{n\pm1}4s^{m\mp1}$ configurations). Various methods can be used in order to compute the non-relativistic energies used on the diagonal of the SI matrix: CASSCF, NEVPT2, DDCIn (with n=1, 2 or 3). The ORCA implementation allows one to include both the SSC and the SOC in the SI matrix [46].

Def2 split-valence Ahlrichs type basis sets have been used for all atoms [105]. Unless specified, the sv(p) contraction scheme has been used for all atoms, *i.e.* a 5s3p2d1f contraction scheme for TM atoms, a 3s2p1d one for 0, N and C atoms, and a 2s one for H atoms.

Conclusion

The ZFS parameters can be calculated within a two-step SI scheme. While in the first step a spin-orbit free (or non-relativistic) Hamiltonian is used to compute the spin-orbit independent part of the Hamiltonian, a SI matrix is computed and diagonalized in the second step. The ZFS parameters can be extracted through effective Hamiltonian theory taking into account all the information contained in the eigenvalues and projected vectors. In agreement with the spin Hamiltonian philosophy, the complex eigenvectors of the SI Hamiltonian are projected onto the model space, *i.e.* onto the spin degrees of freedom. This extraction process allows

one to check the relevance of the commonly used phenomenological model Hamiltonians. The main interaction leading to ZFS is the SOC, while the SSC can in some cases also play a non-negligible role. This *ab initio* scheme present intrinsic degrees of freedom, (i) the SI space and (ii) the active space sizes as well as (iii) the energies used in the diagonal of the SI matrix. In cases of interest close to ideal geometries it is also possible to derive an analytical effective Hamiltonian using simple models as the crystal field and a monoelectronic spin-orbit coupling operator. Such treatment of the non-relativistic part of the Hamiltonian might be seen as a compromise between Abragam's and Racah's treatments of the crystal field. Such rationalizing works bring new insights on the physical origin of magnetic anisotropy and the way to tune it.

Chapter 3

Mononuclear Complexes

Mononuclear complexes are the smallest systems presenting magnetic anisotropy. A large amount of reliable experimental data exist for mononuclear complexes, hence these systems can be used to first validate the methodology of calculation. The role of dynamic correlation on the ZFS is expected to be less crucial than in binuclear complexes, hence one may expect a good agreement with experimental data at a reasonable computational cost. A series of complexes belonging to different d^n configurations will then be studied for this purpose and to illustrate the extraction of the anisotropic parameters in arbitrary axes frame by using the effective Hamiltonian theory. Since mononuclear units may govern or at least have an important role in the property of larger SMMs, this chapter also aims to propose rationalizations of the ZFS in mononuclear systems. Finally, the limitations of the methodology will be evocated through the study of a series of Ni(II) complexes presenting heavy atom ligands.

All the *ab initio* results presented in this chapter have been obtained using the MOLCAS program [98]. The computational details are presented in section 2.4.1. Part of the data have already been published in the literature [106, 107]. However the presentation of the redundant data may be different, and new material is presented. Hence this chapter may be seen as complementary with the corresponding publications.

3.1 Validation of the Model Hamiltonians and Methodological Considerations

To discuss the peculiarities of the different d^n electronic configurations, three case studies will be presented, namely the $[Ni(HIM2\text{-}Py)_2NO_3]^+$, $[Co(PPh_3)_2Cl_2]$ and $[\gamma\text{-}Mn(acac)_3]$ complexes corresponding to the d^8, d^7 and d^4 configurations, respectively. They will be used to check the validaty of the model Hamiltonians, show the advantage of the effective Hamiltonian theory for the extraction of the ZFS parameters, and also present some methological considerations. After that, other complexes and more general conclusions will be presented in section 3.1.4.

3.1.1 The $[Ni(HIM2\text{-}Py)_2NO_3]^+$ Complex

The $[Ni(HIM2\text{-}Py)_2NO_3]^+$ (HIM2-py=2-(2-pyridyl)-4,4,5,5-tetramethyl-4,5-dihydro-1H-imidazolyl-1-hydroxy) complex has been synthesized and studied experimentally by far infrared spectroscopy, magnetization vs field and HF-EPR spectroscopy in 2005 [40]. The first coordination sphere is a distorted octahedron, and hence, the complex is susceptible to present a relatively large anisotropy. According to the experimental studies, the D parameter is large and negative, and hence this molecular unit might then be an interesting building-block for SMMs and Single Chain Magnets (SCMs). The complex is studied in its experimental structure, although the external methyl groups (*i.e.* far away from the magnetic center) have been replaced by hydrogen atoms (see Fig. 3.1).

The complex has a triplet spin ground state which does not show any (near-) degeneracies. Hence, the ZFS should be accurately described by a model space that only contains the $|1, M_S\rangle$ components of the orbital ground state. Before introducing the methodological considerations, the validity of this model space and the corresponding Hamiltonian will be checked and the extraction process detailed at a given level of theory.

Model Interaction Matrix

The model interaction matrix is built following the process presented in section 2.2.1. The model Hamiltonian has already been presented in Eqs. 1.2 and 2.4 and is reproduced here for clarity:

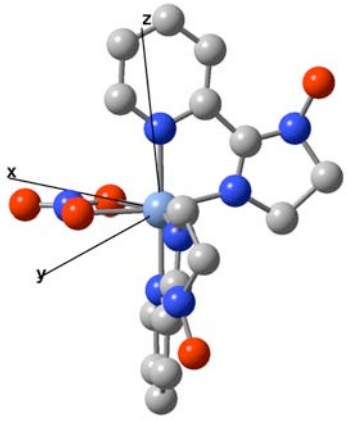

Figure 3.1: The $[Ni(HIM2\text{-}Py)_2NO_3]^+$ (HIM2-py=2-(2-pyridyl)-4,4,5,5-tetramethyl-4,5-dihydro-1H-imidazolyl-1-hydroxy) complex and its magnetic axes frame. The external methyl groups have been replaced by hydrogen atoms and hydrogen atoms are omitted for clarity.

$$\hat{H}_{mod} = \hat{\mathbf{S}}.\overline{\overline{D}}.\hat{\mathbf{S}} \tag{3.1}$$

The model interaction matrix is built by expanding this model Hamiltonian and applying it to the $|1, M_S\rangle$ functions:

$\hat{H}_{mod}$	$\|1,-1\rangle$	$\|1,0\rangle$	$\|1,1\rangle$
$\langle 1,-1\|$	$\frac{1}{2}(D_{xx}+D_{yy})+D_{zz}$	$-\frac{\sqrt{2}}{2}(D_{xz}+iD_{yz})$	$\frac{1}{2}(D_{xx}-D_{yy}+2iD_{xy})$
$\langle 1,0\|$	$-\frac{\sqrt{2}}{2}(D_{xz}-iD_{yz})$	$D_{xx}+D_{yy}$	$\frac{\sqrt{2}}{2}(D_{xz}+iD_{yz})$
$\langle 1,1\|$	$\frac{1}{2}(D_{xx}-D_{yy}-2iD_{xy})$	$\frac{\sqrt{2}}{2}(D_{xz}-iD_{yz})$	$\frac{1}{2}(D_{xx}+D_{yy})+D_{zz}$

(3.2)

Effective Interaction Matrix

The effective interaction matrix is built from a RASSI-SO calculation based on a CAS(12/12) (12 active electrons in 12 active orbitals) reference calculation and a SI space with four triplet spin-orbit free states. The diagonal elements of the SI matrix have been replaced by the energies obtained at the CASPT2 level. After diagonalizing the RASSI-SO matrix, the vectors with the largest projection on the model space are selected. In this case, the projected vectors are simply found by truncating the entire wavefunction to the determinants belonging to the

model space, *i.e.* the M_S components of the triplet spin-orbit free ground state. Here the following energies (in cm^{-1}):

$$\begin{aligned} E_1 &= 0.000 \\ E_2 &= 1.529 \\ E_3 &= 11.369 \end{aligned} \tag{3.3}$$

and the following projected wavefunctions:

$$\begin{aligned} |\widetilde{\Psi}_1\rangle &= (0.045+0.092i)|1,-1\rangle + (-0.668+0.724i)|1,0\rangle + (0.096+0.037i)|1,1\rangle \\ |\widetilde{\Psi}_2\rangle &= (-0.395+0.578i)|1,-1\rangle + (0.062+0.088i)|1,0\rangle + (-0.678+0.173i)|1,1\rangle \\ |\widetilde{\Psi}_3\rangle &= (0.701+0.026i)|1,-1\rangle + (-0.090-0.037i)|1,0\rangle + (-0.519-0.472i)|1,1\rangle \end{aligned} \tag{3.4}$$

are used for the construction of the effective interaction matrix. The norm of the projection can be evaluated with the square root of the diagonal elements of the overlap matrix between the projected vectors:

$$\begin{aligned} \sqrt{S_{11}} &= 0.996 \\ \sqrt{S_{22}} &= 0.996 \\ \sqrt{S_{33}} &= 0.997 \end{aligned} \tag{3.5}$$

meaning that around 99% of the RASSI-SO wavefunctions are carried by the determinants belonging to the model space. Given the large norm of the projections, the use of a spin Hamiltonian is justified, and one may go a step further by building the effective interaction matrix according to the des Cloizeaux formalism [91], as explained in section 2.2.1:

$\hat{H}_{eff}$	$\|1,-1\rangle$	$\|1,0\rangle$	$\|1,1\rangle$
$\langle 1,-1\|$	6.386	$-0.690+0.376i$	$-3.734+3.134i$
$\langle 1,0\|$	$-0.690-0.376i$	0.125	$0.690-0.376i$
$\langle 1,1\|$	$-3.734-3.134i$	$0.690+0.376i$	6.386

(3.6)

where all numbers are expressed in cm^{-1}.

Extraction of the Zero-Field Splitting Parameters and of the Magnetic Axes Frame

The one-to-one comparison of matrices 3.2 and 3.6 show that the model Hamiltonian presented in Eq. 3.1 is perfectly adapted to describe the effective Hamiltonian presented in Eq. 3.6. As in this case no difference can be observed between the model and effective interaction matrices, the model Hamiltonian will exactly reproduce the energy differences ($\epsilon = 0$) and the projected wavefunctions of the *ab initio* Hamiltonian.

The trace of the effective Hamiltonian has been fixed by the arbitrary choice of $E_1 = 0$. In consequence, the trace of the ZFS tensor $\overline{\overline{D}}$ is also arbitrary and will not be discussed in this dissertation.

The components of the ZFS tensor are extracted by solving the system of equations that arises from the equalities between the model and effective interaction matrix elements, leading to:

$$\overline{\overline{D}} = \begin{pmatrix} D_{xx} & D_{xy} & D_{xz} \\ D_{xy} & D_{yy} & D_{yz} \\ D_{xz} & D_{yz} & D_{zz} \end{pmatrix} = \begin{pmatrix} -3.671 & 3.134 & 0.976 \\ 3.134 & 3.797 & -0.532 \\ 0.976 & -0.532 & 6.323 \end{pmatrix} \tag{3.7}$$

where all numbers are expressed in cm^{-1}. The last important step in the extraction process consists in diagonalizing the ZFS tensor:

$$\overline{\overline{D}}_{diag} = P^{-1}\overline{\overline{D}}P \tag{3.8}$$

where the transformation matrix P^{-1} is the eigenvector matrix of the ZFS tensor. This matrix has to be multiplied to the coordinates X of all atoms in order to find the principal axes of the ZFS tensor:

$$X_{diag} = P^{-1}X \tag{3.9}$$

The conventions presented in section 1.3.1 ($|D| > 3E$ and $E > 0$, D and E being defined in Eqs. 1.3 and 1.4) are used in order to define the magnetic axes frame, in which the ZFS tensor is diagonal:

$$\overline{\overline{D}}_{mag} = \begin{pmatrix} D_{XX} & 0 & 0 \\ 0 & D_{YY} & 0 \\ 0 & 0 & D_{ZZ} \end{pmatrix} = \begin{pmatrix} 6.448 & 0 & 0 \\ 0 & 4.920 & 0 \\ 0 & 0 & -4.919 \end{pmatrix} \tag{3.10}$$

where capital letters refer to the magnetic X, Y and Z anisotropy axes (that are represented in Fig. 3.1) and all numbers are expressed in cm^{-1}. The ZFS parameters are then finally extracted:

$$D = D_{ZZ} - \frac{1}{2}(D_{XX} + D_{YY}) = -10.604\ \mathrm{cm}^{-1} \tag{3.11}$$

and

$$E = \frac{1}{2}(D_{XX} - D_{YY}) = 0.764\ \mathrm{cm}^{-1} \tag{3.12}$$

Hence both the ZFS parameters and the magnetic axes frame are accessible in a straightfoward way from the effective Hamiltonian theory.

Direct Extraction of the Zero-Field Splitting Parameters

As already stated in section 2.2.1, the extraction process is much simpler if one only aims at the ZFS parameters D and E in case of even number of electrons. Starting from Eq. 3.2, the model interaction matrix can directly be written in the magnetic axes frame:

$\hat{H}_{mod}$	$\lvert 1,-1\rangle$	$\lvert 1,0\rangle$	$\lvert 1,1\rangle$
$\langle 1,-1\rvert$	$\frac{1}{2}(D_{XX}+D_{YY})+D_{ZZ}$	0	$\frac{1}{2}(D_{XX}-D_{YY})$
$\langle 1,0\rvert$	0	$D_{XX}+D_{YY}$	0
$\langle 1,1\rvert$	$\frac{1}{2}(D_{XX}-D_{YY})$	0	$\frac{1}{2}(D_{XX}+D_{YY})+D_{ZZ}$

(3.13)

Making the matrix traceless and substituting $D = D_{ZZ} - \frac{1}{2}(D_{XX} + D_{YY})$ and $E = \frac{1}{2}(D_{XX} - D_{YY})$, this model matrix transforms to:

$\hat{H}_{mod}$	$\lvert 1,-1\rangle$	$\lvert 1,0\rangle$	$\lvert 1,1\rangle$
$\langle 1,-1\rvert$	$\frac{1}{3}D$	0	E
$\langle 1,0\rvert$	0	$-\frac{2}{3}D$	0
$\langle 1,1\rvert$	E	0	$\frac{1}{3}D$

(3.14)

The diagonalization of this well-known and widely used model matrix lead to:

$$\begin{aligned} E_a &= -\frac{2}{3}D \\ E_b &= \frac{1}{3}D + E \\ E_c &= \frac{1}{3}D - E \end{aligned} \tag{3.15}$$

and to the model Hamiltonian wavefunctions that are identical to the projected vectors of the effective Hamiltonian:

$$\begin{aligned} |\widetilde{\Psi}_a\rangle &= |1,0\rangle \\ |\widetilde{\Psi}_b\rangle &= \frac{1}{\sqrt{2}}|1,-1\rangle + \frac{1}{\sqrt{2}}|1,1\rangle \\ |\widetilde{\Psi}_c\rangle &= \frac{1}{\sqrt{2}}|1,-1\rangle - \frac{1}{\sqrt{2}}|1,1\rangle \end{aligned} \tag{3.16}$$

According to Eq. 3.15:

$$D = \frac{1}{2}(E_b + E_c) - E_a \tag{3.17}$$

and

$$E = \frac{1}{2}(E_b - E_c) \tag{3.18}$$

Where $|\frac{1}{2}(E_b + E_c) - E_a|$ has to be superior to $\frac{3}{2}(E_b - E_c)$ and $\frac{1}{2}(E_b - E_c)$ has to be positive to respect the conventions ($|D| > 3E$ and $E > 0$). In the present example, the following assignments would have to be done:

$$\begin{aligned} E_a &= E_3 \\ E_b &= E_2 \\ E_c &= E_1 \end{aligned} \tag{3.19}$$

leading to the following parameters:

$$D = \frac{1}{2}(E_2 + E_1) - E_3 = -10.604 \text{ cm}^{-1} \tag{3.20}$$

and

$$E = \frac{1}{2}(E_2 - E_1) = 0.764 \text{ cm}^{-1} \tag{3.21}$$

In both approaches, the extracted ZFS parameters are strictly equal since both model Hamiltonians reproduce the eigenvalues of the exact Hamiltonian according to the used extraction process. By considering implicitely the magnetic frame, only the energies of the exact Hamiltonian are necessary to extract the ZFS parameters. This way of extracting the ZFS parameters is only a particular case of the general extraction that considers explicitely the projected wavefunctions and the energies of the exact Hamiltonian. When the general extraction process is used in an arbitrary axes frame, the effective Hamiltonian theory gives access to more information than the D and E parameters since it also provides the magnetic axes frame. Test calculations showed that the ZFS tensor is effectively diagonal when the whole process of calculation and parameter extraction is repeated in the extracted axes frame, proving the tensor character of the ZFS as well as validating the whole approach.

Methodological Considerations

In the previous paragraphs the effective Hamiltonian was obtained from an *ab initio* calculations based on a CAS(12/12) active space, considering four triplet state in the SI space, and the CASPT2 energies were used in the diagonal of the SI matrix. This calculation is considered as the most reliable one of the calculations performed on the $[Ni(HIM2\text{-}Py)_2NO_3]^+$ complex after a small methodological study for which the most important considerations are presented hereafter.

The RASSI-SO approach presents three important intrinsic degrees of freedom, (i) the size of the SI space, (ii) the size of the active space, and (iii) the diagonal energies of the SI matrix. Other computational degrees of freedom such as the size of the basis set were studied in previous test calculations [64], and are considered as fixed in this work. The magnetic axes frame turns out to be only weakly dependent on the three degrees of freedom, and hence, the study focuses only on the ZFS parameters D and E (see Table 3.1).

		$D(\mathrm{cm}^{-1})$		$E(\mathrm{cm}^{-1})$	
SI space	Active space	CASSCF	CASPT2	CASSCF	CASPT2
10T, 14S	(8,10)	-14.15	-10.84	0.94	0.77
10T, 9S	(8,10)	-13.26	-10.03	0.87	0.71
7T, 2S	(8,10)	-15.82	-12.96	1.28	1.22
4T	(8,10)	-13.90	-12.17	0.93	0.87
4T	(12,12)	-12.12	-10.60	0.81	0.76
HF-EPR [40]		-10.15		0.10	

Table 3.1: ZFS parameters in $[Ni(HIM2\text{-}Py)_2NO_3]^+$ as functions of the number of spin-orbit coupled states, active space, and diagonal energies used in the SI matrix. The number and spin multiplicity of the coupled states is indicated as nT (triplets) and mS (singlets).

The first test concerns the size of the SI space. Since the excitations have to be balanced in all directions of space with regard to the ground state, only some particular SI spaces are adequate. Obviously, if the complete d^n manifold is taken into account, all excitations are balanced at the CASSCF level. Hence, the largest SI space for a Ni(II) complex consists of 10 triplet and of 15 singlets, although the highest singlet of the manifold ($^1A_{1g}$ in octahedral symmetry) is never included in the calculations since it lies very high in energy compared to all other d-d states to have any significant contribution to the ZFS of the ground state.

Due to the quasi-octahedral geometry of the complex, the SI space can be truncated easily according to energy criteria while maintaining the excitations balanced in all directions of space. The problem of balanced excitations is actually only critical for small SI spaces. Indeed, in large SI spaces, the lacking excitations (in order to be balanced in all directions of space) lie high in energy so that their contribution to the ZFS are small. As a consequence, the actifact due to an unbalanced truncation is usually not dramatic for large SI spaces.

As shown in Table 3.1, the evolution of the ZFS parameters is not monotonous as a function of the SI space size. Although accuracy is gained by including more states in the SI space, this gain is counterbalanced by the loss of accuracy due to the use of averaged MOs in the CASSCF calculation. Depending on the relative importance of the two effects, the computed ZFS parameters are more or less precise. Hence, a practical compromise has

to be found to obtain the most accurate ZFS parameters possible. One strategy consists in describing accurately the states with the most important contributions to the ZFS. The first three excited triplet states are single excited states (with respect to the ground state) and therefore these two aspects make these triplets strongly coupled by the spin-orbit interaction to the ground state and the SI space with the four lowest triplets (ground state plus three excited triplet) is considered as the best compromise. However, as can be seen in Table 3.1, the results obtained with this SI space does not match perfectly with the experimental data [40], and the influence of the other degrees of freedom has to be considered.

To explore the dependency of the calculated ZFS parameters on the size of the active space, two different choices have been made, namely the CAS(8/10) with the Ni 3d and the so-called 3d' orbitals, and the CAS(12/12), obtained by adding the most interacting ligand orbitals of σ character are added to the 3d and 3d' orbitals in the active space.

The main effect of this extension of the active space is that the covalency effects are better treated, enlarging the delocalization of the d orbitals on the ligands. When the spin-orbit interaction is mainly due to the metal atom, as in the $[Ni(HIM2\text{-}Py)_2NO_3]^+$ complex, this larger delocalization on the ligands causes a reduction of the spin-orbit matrix elements. As a consequence, the computed ZFS parameters are smaller in the CAS(12/12) based calculations than for the smaller CAS. Hence, it is preferable to treat the LMCT configurations variationally by including them in the CASSCF wavefunctions.

Finally, the role of the dynamic correlation has to be commented. Table 3.1 shows that the results obtained by replacing the diagonal elements of the SI matrix are slightly different to those obtained with the CASSCF energies, illustrating the moderate effect of dynamic correlation on the ZFS. Although the present inclusion of dynamic correlation is not complete (only in the energies and not in the wavefunctions), the ZFS parameters obtained with a 4T SI space, the (12/12) active space, and the CASPT2 estimate of the d-d transition energies is in good agreement with the experimental data.

3.1.2 The $[Co(PPh_3)_2Cl_2]$ Complex

To further illustrate the possibilities of the here-presented extraction procedure of the ZFS parameters, the $[Co(PPh_3)_2Cl_2]$ (Ph=phenyl) complex has been studied (see Fig. 3.2). The formal charge of +2 associated to the cobalt atom implies a d^7 electronic configuration, *i.e.*

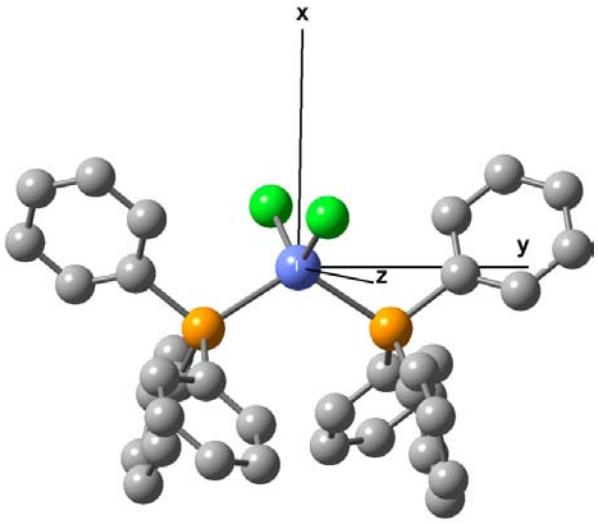

Figure 3.2: The $[Co(PPh_3)_2Cl_2]$ (Ph=phenyl) complex and its magnetic axes frame. Hydrogen atoms are omitted for clarity.

an odd number of electron case. This complex has been synthesized some decades ago [108], and the ZFS parameters have been recently re-extracted by means of HF-EPR spectroscopy [109]. This molecule was presented as a demonstration of the possibilities of HF-EPR since conventional EPR spectroscopy cannot measure the ZFS parameters in such complex due to the large energy differences between the involved spin-orbit levels [109].

Due to the Kramers' degeneracy, the first theoretical study concerning this molecule based on a RASSI-SO calculation was unable to extract the ZFS parameters as well as to get the sign of the D parameter [64]. Only one energy difference is available from the eigenvalues of the SI matrix, which prohibits the extraction of two parameters (here D and E).

A similar methodological study as the one performed on the $[Ni(HIM2\text{-}Py)_2NO_3]^+$ complex lead to the conclusion that the best choice to calculate the ZFS parameters consists in taking seven quartets in the SI space, include the three most interacting σ ligand-metal bonding orbitals, and use the CASPT2 energies on the diagonal elements of the SI matrix [106]. Indeed, in the ideal tetrahedral d^7 configuration, the lowest-lying $^4T_1$ and the $^4T_2$ states are strongly coupled by the SOC to the ground $^4A_2$ state since both excited states have a

partial single excited character compared to this $^4A_2$ state. Because of this, the SI space in the nearly tetrahedral d^7 complex cannot be reduced to four spin-orbit free states as in the nearly octahedral d^8 complexes, and then seven quartets are included in the calculation. A detailed description of the extraction process is presented in the following paragraphs.

The model interaction matrix of the high-spin d^7 configuration is obtained by applying the same Hamiltonian as in section 3.1.1 to the $|\frac{3}{2}, M_S\rangle$ components of the ground state.

$\hat{H}_{mod}$	$\lvert\frac{3}{2},-\frac{3}{2}\rangle$	$\lvert\frac{3}{2},-\frac{1}{2}\rangle$	$\lvert\frac{3}{2},\frac{1}{2}\rangle$	$\lvert\frac{3}{2},\frac{3}{2}\rangle$
$\langle\frac{3}{2},-\frac{3}{2}\rvert$	$\frac{3}{4}(D_{xx}+D_{yy})+\frac{9}{4}D_{zz}$	$-\sqrt{3}(D_{xz}+iD_{yz})$	$\frac{\sqrt{3}}{2}(D_{xx}-D_{yy}+2iD_{xy})$	0
$\langle\frac{3}{2},-\frac{1}{2}\rvert$	$-\sqrt{3}(D_{xz}-iD_{yz})$	$\frac{7}{4}(D_{xx}+D_{yy})+\frac{1}{4}D_{zz}$	0	$\frac{\sqrt{3}}{2}(D_{xx}-D_{yy}+2iD_{xy})$
$\langle\frac{3}{2},\frac{1}{2}\rvert$	$\frac{\sqrt{3}}{2}(D_{xx}-D_{yy}-2iD_{xy})$	0	$\frac{7}{4}(D_{xx}+D_{yy})+\frac{1}{4}D_{zz}$	$\sqrt{3}(D_{xz}+iD_{yz})$
$\langle\frac{3}{2},\frac{3}{2}\rvert$	0	$\frac{\sqrt{3}}{2}(D_{xx}-D_{yy}-2iD_{xy})$	$\sqrt{3}(D_{xz}-iD_{yz})$	$\frac{3}{4}(D_{xx}+D_{yy})+\frac{9}{4}D_{zz}$

(3.22)

The effective Hamiltonian matrix is constructed following exactly the same process as in section 3.1.1. The determinants of the model space, *i.e.* the $|\frac{3}{2}, M_S\rangle$ components of the ground state, provide more than 97% of the wavefunctions of each of the four lowest-lying spin-orbit states. This confirms the adequacy of the model space and that the spin Hamiltonian approach is relevant in this complex. The following effective interaction matrix is obtained from the *ab initio* energies and projected vectors (where all number are expressed in cm^{-1}):

$\hat{H}_{eff}$	$\|\frac{3}{2}, -\frac{3}{2}\rangle$	$\|\frac{3}{2}, -\frac{1}{2}\rangle$	$\|\frac{3}{2}, \frac{1}{2}\rangle$	$\|\frac{3}{2}, \frac{3}{2}\rangle$
$\langle\frac{3}{2}, -\frac{3}{2}\|$	0.203	2.282	−0.889	0.000
$\langle\frac{3}{2}, -\frac{1}{2}\|$	2.282	29.549	0.000	−0.889
$\langle\frac{3}{2}, \frac{1}{2}\|$	−0.889	0.000	29.549	−2.282
$\langle\frac{3}{2}, \frac{3}{2}\|$	0.000	−0.889	−2.282	0.203

(3.23)

By comparing term by term the matrices 3.22 and 3.23, it is clear that both Hamiltonians perfectly suit, even if some non-zero terms in the model Hamiltonians are zero in the effective Hamiltonian. Hence, the ZFS tensor (in cm^{-1}) can be extracted by using both interaction matrices as in the previous Ni(II) example:

$$\overline{\overline{D}} = \begin{pmatrix} D_{xx} & D_{xy} & D_{xz} \\ D_{xy} & D_{yy} & D_{yz} \\ D_{xz} & D_{yz} & D_{zz} \end{pmatrix} = \begin{pmatrix} 8.255 & 0.0 & -1.317 \\ 0.0 & 9.461 & 0.0 \\ -1.317 & 0.0 & -5.815 \end{pmatrix} \tag{3.24}$$

D_{xy} and D_{yz} are both equal to zero because the axes frame used in the calculation is not totally arbitrary. Actually, the $[Co(PPh_3)_2Cl_2]$ complex has C_2 symmetry, and the y axis has been oriented along the two-fold axis for the *ab initio* calculation to take profit of the symmetry of the system, implying that $D_{xy} = D_{yz} = 0$, and that the C_2 axis is one of the magnetic anisotropy axes. However the attribution of the C_2 axis as the X, Y or Z magnetic axis cannot be made only by symmetry arguments. The ZFS tensor (in cm^{-1}) is then diagonalized and the usual conventions applied in order to define the magnetic axes frame:

$$\overline{\overline{D}}_{mag} = \begin{pmatrix} D_{XX} & 0 & 0 \\ 0 & D_{YY} & 0 \\ 0 & 0 & D_{ZZ} \end{pmatrix} = \begin{pmatrix} 9.461 & 0 & 0 \\ 0 & 8.377 & 0 \\ 0 & 0 & -5.937 \end{pmatrix} \tag{3.25}$$

As can be seen in Figure 3.2, the C_2 axis is in fact the X magnetic anisotropy axis. At this stage, the ZFS parameters D:

$$D = D_{ZZ} - \frac{1}{2}(D_{XX} + D_{YY}) = -14.856 \text{ cm}^{-1} \tag{3.26}$$

and E:

$$E = \frac{1}{2}(D_{XX} - D_{YY}) = 0.542 \text{ cm}^{-1} \tag{3.27}$$

are unambiguously extracted. These values are in good agreement with those extracted from HF-EPR spectra ($D = -14.76$ cm^{-1} and $E = 1.14$ cm^{-1}) [109].

The model interaction matrix 3.22 is greatly simplified if the molecule is oriented in the magnetic axes frame. Introducing the axial and rhombic anisotropic parameters, it reduces to [11]:

$\hat{H}_{mod}$	$\lvert\frac{3}{2},-\frac{3}{2}\rangle$	$\lvert\frac{3}{2},-\frac{1}{2}\rangle$	$\lvert\frac{3}{2},\frac{1}{2}\rangle$	$\lvert\frac{3}{2},\frac{3}{2}\rangle$
$\langle\frac{3}{2},-\frac{3}{2}\rvert$	D	0	$\sqrt{3}E$	0
$\langle\frac{3}{2},-\frac{1}{2}\rvert$	0	$-D$	0	$\sqrt{3}E$
$\langle\frac{3}{2},\frac{1}{2}\rvert$	$\sqrt{3}E$	0	$-D$	0
$\langle\frac{3}{2},\frac{3}{2}\rvert$	0	$\sqrt{3}E$	0	D

(3.28)

The energy difference between the two Kramers' doublets is obtained by diagonalizing this model interaction matrix, leading to the well-known formula for ΔE:

$$\Delta E = 2\sqrt{D^2 + 3E^2} \tag{3.29}$$

3.1.3 The [γ-Mn(acac)$_3$] Complex

The high-spin d^4 configuration is particularly interesting since it is the simplest configuration with of fourth order terms in the model Hamiltonian (see section 1.3.1). The strength of these interactions can in principle be determined following the procedure outlined before. However, the extraction of the ZFS parameters and the magnetic axes frame actually faces a problem when both SOC and SSC are considered in the *ab initio* treatment. Whereas both SOC and SSC contribute to the second-order ZFS tensor, the fourth order terms arise exclusively

from the SOC. In the absence of fourth order terms, the second-order tensors arising from the SOC and the SSC can be summed and a common magnetic axes frame can be defined. This is no longer the case when fourth order terms arising only from the SOC come into play. A mathematically strictly correct definition of the axes frame is no longer possible and a pragmatical solution has to be found. There exist several possibilities to avoid this problem, (i) neglect the SSC, (ii) neglect the extradiagonal fourth order terms in the extraction, and (iii) hide the problem by using second-order QDPT instead of diagonalizing the SI matrix. One should note that none of these solutions is fully satisfactory in the general case since the fourth order SOC terms and the second order terms arising from the SSC can be of the same order of magnitude, and since a QDPT treatment can be too crude to provide reliable results. Note that in highly symmetric systems the magnetic axes frame is imposed by symmetry and the problem may disappear without any approximation.

When the SSC is neglected and only the SOC interaction is considered, the extraction process consists in first extracting the magnetic axes frame taking into account the second-order ZFS terms only. After that, the effective Hamiltonian is extracted in this axes frame giving access to all second and fourth order terms. This treatment is equivalent to the extraction with the extended Stevens operators in an arbitrary axes frame given that the fourth-order terms are much smaller than the second-order ones. Otherwise some uncertainties are introduced in the extraction of the magnetic axes frame leading to non-negligible extradiagonal terms in the second effective Hamiltonian that cannot be attributed to the D, E, B_4^0, B_4^2 and B_4^4 parameters only.

When the extradiagonal fourth order terms are neglected while both SOC and SSC are considered, the previous extraction scheme would be applied. However, non-negligible extradiagonal terms might appear in the second extraction, leading to an ambiguous extraction of the D and E parameters.

Description of the System and *Ab Initio* Calculation

The [γ-Mn(acac)$_3$] (acac=acetylacetonato) complex shown in Fig. 3.3 [110] is used to illustrate the peculiarities of the high-spin d^4 configuration. The ZFS of this well known complex has been studied experimentally by means of HF-EPR spectroscopy [111], and theoretically within the DFT and CASSCF frameworks [51]. Test calculations on the [γ-Mn(acac)$_3$] complex re-

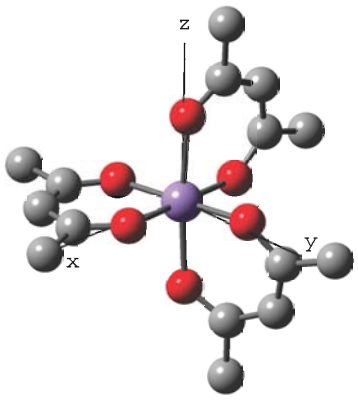

Figure 3.3: The [γ-Mn(acac)$_3$] (acac=acetylacetonato) complex and its magnetic axes frame. Hydrogen atoms are omitted for clarity.

cently showed that the first order SSC contribution to the ZFS was accidentally overestimated in this previous theoretical study, and recent applications confirmed that the SSC actually accounts for around 10% of the total ZFS in Mn(III) complexes [61]. Here, the SSC contribution to the ZFS is neglected.

The calculation of the energies and wavefunctions is based on a CAS(4/10)SCF reference calculation, the CASPT2 energies are used on the diagonal of the SI matrix, and five quintets (5Q), thirteen triplets (13T) and thirteen singlets (13S) are included in the SI space. This SI space is a good compromise between the accuracy in the MO optimization and the treatment of the SOC through SI, even if the truncation is not perfectly balanced in all directions of space. Since the truncation arises relatively high in energy, no noticiable artefact is introduced. A further truncation of the SI space for this configuration will be considered in section 3.2, but is not performed on the [γ-Mn(acac)$_3$] complex.

The model interaction matrix of the high-spin d^4 configuration considering only a second-order ZFS tensor is obtained by applying the same Hamiltonian as in section 3.1.1 and 3.1.2 to the $|2, M_S\rangle$ components of the ground state.

$\hat{H}_{mod}$	$\lvert 2,-2\rangle$	$\lvert 2,-1\rangle$	$\lvert 2,0\rangle$	$\lvert 2,1\rangle$	$\lvert 2,2\rangle$
$\langle 2,-2\rvert$	$D_{xx}+D_{yy}+4D_{zz}$	$-3D_{xz}-3iD_{yz}$	$\frac{\sqrt{6}}{2}(D_{xx}-D_{yy}+2iD_{xy})$	0	0
$\langle 2,-1\rvert$	$-3D_{xz}+3iD_{yz}$	$\frac{5}{2}(D_{xx}+D_{yy})+D_{zz}$	$-\frac{\sqrt{6}}{2}(D_{xz}+iD_{yz})$	$\frac{3}{2}(D_{xx}-D_{yy}+2iD_{xy})$	0
$\langle 2,0\rvert$	$\frac{\sqrt{6}}{2}(D_{xx}-D_{yy}-2iD_{xy})$	$-\frac{\sqrt{6}}{2}(D_{xz}-iD_{yz})$	$3(D_{xx}+D_{yy})$	$\frac{\sqrt{6}}{2}(D_{xz}+iD_{yz})$	$\frac{\sqrt{6}}{2}(D_{xx}-D_{yy}+2iD_{xy})$
$\langle 2,1\rvert$	0	$\frac{3}{2}(D_{xx}-D_{yy}-2iD_{xy})$	$\frac{\sqrt{6}}{2}(D_{xz}-iD_{yz})$	$\frac{5}{2}(D_{xx}+D_{yy})+D_{zz}$	$3D_{xz}+3iD_{yz}$
$\langle 2,2\rvert$	0	0	$\frac{\sqrt{6}}{2}(D_{xx}-D_{yy}-2iD_{xy})$	$3D_{xz}-3iD_{yz}$	$D_{xx}+D_{yy}+4D_{zz}$

(3.30)

The fourth order terms present in the *ab initio* treatment of the ZFS introduce differences between this interaction matrix and the effective Hamiltonian matrix. If these differences are not too large, the second-order ZFS tensor can be extracted and used to find the magnetic axes frame.

The effective interaction matrix is obtained using the des Cloizeaux formalism. The total weight of the $|2, M_S\rangle$ components of the ground state in the five lowest-lying spin-orbit states is more than 99%. Hence a spin Hamiltonian formalism is perfectly adequate in this complex. The following interaction matrix has been obtained in an arbitrary axes frame (with all numbers in cm^{-1}):

$\hat{H}_{eff}$	$\|2,-2\rangle$	$\|2,-1\rangle$	$\|2,0\rangle$	$\|2,1\rangle$	$\|2,2\rangle$
$\langle 2,-2\|$	10.446	$3.350+0.934i$	$-3.778-1.663i$	$0.003-0.006i$	$0.002-0.004i$
$\langle 2,-1\|$	$3.350-0.934i$	6.244	$1.365+0.396i$	$-4.628-2.023i$	$-0.003+0.006i$
$\langle 2,0\|$	$-3.778+1.663i$	$1.365-0.396i$	4.836	$-1.366-0.396i$	$-3.778-1.663i$
$\langle 2,1\|$	$0.003+0.006i$	$-4.628+2.023i$	$-1.366+0.396i$	6.246	$-3.350-0.934i$
$\langle 2,2\|$	$0.002+0.004i$	$-0.003-0.006i$	$-3.778+1.663i$	$-3.350+0.934i$	10.447

(3.31)

The comparison of the matrices 3.30 and 3.31 shows that only tiny deviations exist between the model and effective interaction matrices. As a consequence, it is concluded that here the effective Hamiltonian is dominated by the second-order terms of the ZFS Hamiltonian and the magnetic axes can be obtained by only considering the second-order ZFS tensor. Hence, the ZFS tensor is directly extracted in order to best fit to the effective Hamiltonian (all numbers are in cm^{-1}):

$$\overline{\overline{D}} = \begin{pmatrix} D_{xx} & D_{xy} & D_{xz} \\ D_{xy} & D_{yy} & D_{yz} \\ D_{xz} & D_{yz} & D_{zz} \end{pmatrix} = \begin{pmatrix} -0.736 & -0.679 & -1.117 \\ -0.679 & 2.349 & -0.311 \\ -1.117 & -0.311 & 2.209 \end{pmatrix} \tag{3.32}$$

This effective ZFS tensor is then diagonalized and the magnetic axes frame obtained as in the previous cases (numbers in cm^{-1}):

$$\overline{\overline{D}}_{mag} = \begin{pmatrix} D_{XX} & 0 & 0 \\ 0 & D_{YY} & 0 \\ 0 & 0 & D_{ZZ} \end{pmatrix} = \begin{pmatrix} 2.630 & 0 & 0 \\ 0 & 2.456 & 0 \\ 0 & 0 & -1.264 \end{pmatrix} \tag{3.33}$$

and the second-order effective ZFS parameters are obtained as usual:

$$D = D_{ZZ} - \frac{1}{2}(D_{XX} + D_{YY}) = -3.807 \text{ cm}^{-1} \tag{3.34}$$

and

$$E = \frac{1}{2}(D_{XX} - D_{YY}) = 0.087 \text{ cm}^{-1} \tag{3.35}$$

Once the transformation matrix diagonalizing the second-order ZFS tensor is known, the *ab initio* calculation is repeated in the corresponding axes frame. The following effective Hamiltonian (in cm^{-1}) is then obtained:

$\hat{H}_{eff}$	$\|2,-2\rangle$	$\|2,-1\rangle$	$\|2,0\rangle$	$\|2,1\rangle$	$\|2,2\rangle$
$\langle 2,-2\|$	-15.224	$-0.003+0.001i$	$0.217-0.003i$	0.000	$-0.021-0.013i$
$\langle 2,-1\|$	$-0.003-0.001i$	-3.805	$-0.001+0.001i$	$0.265-0.004i$	0.000
$\langle 2,0\|$	$0.217+0.003i$	$-0.001-0.001i$	0.000	$0.001-0.001i$	$0.217-0.003i$
$\langle 2,1\|$	0.000	$0.265+0.004i$	$0.001+0.001i$	-3.805	$0.003-0.002i$
$\langle 2,2\|$	$-0.021+0.013i$	0.000	$0.217+0.003i$	$0.003+0.002i$	-15.224

(3.36)

where the trace has been shifted in order to put the $\langle 2,0|\hat{H}_{eff}|2,0\rangle$ matrix element at zero energy. This facilitates the identification of the parameters by comparison to the model interaction matrix that includes the second-order and the fourth-order ZFS terms in the magnetic axes frame:

D	-3.807
E	0.089
$10^3 \times B_4^0$	0.007
$10^3 \times B_4^2$	0.040
$10^3 \times B_4^4$	-1.777

Table 3.2: ZFS parameters (in cm^{-1}) of the [γ-Mn(acac)$_3$] complex.

$\hat{H}_{mod}$	$\|2,-2\rangle$	$\|2,-1\rangle$	$\|2,0\rangle$	$\|2,1\rangle$	$\|2,2\rangle$
$\langle 2,-2\|$	$4D-60B_4^0$	0	$\sqrt{6}E+3\sqrt{6}B_4^2$	0	$12B_4^4$
$\langle 2,-1\|$	0	$D-120B_4^0$	0	$3E-12B_4^2$	0
$\langle 2,0\|$	$\sqrt{6}E+3\sqrt{6}B_4^2$	0	0	0	$\sqrt{6}E+3\sqrt{6}B_4^2$
$\langle 2,1\|$	0	$3E-12B_4^2$	0	$D-120B_4^0$	0
$\langle 2,2\|$	$12B_4^4$	0	$\sqrt{6}E+3\sqrt{6}B_4^2$	0	$4D-60B_4^0$

(3.37)

The model and effective interaction matrices are in good agreement (see matrices 3.36 and 3.37). The largest differences between both matrices are about 0.001 cm^{-1}, which can be considered as numerical noise. The ZFS parameters can then be obtained by using both interaction matrices (see Table 3.2). Since the fourth order terms are much smaller than the second-order ones, this process allows to extract unambiguously the ZFS parameters in the d^4 configuration (although the SSC cannot be included in the extraction without loosing the full rigorousity of the procedure).

Despite these problems, the present extraction scheme is the first one allowing the calculation and extraction of fourth order ZFS terms reported in the literature [107]. However, one may question the compromise chosen here to avoid the problem of mismatch between the magnetic axes frame induced by the SOC and SSC interactions. As shown in Table 3.2, the fourth order terms of the ZFS Hamiltonian are negligible in the [γ-Mn(acac)$_3$] complex, while the SSC contribution is not (since about 10 % of the total ZFS arises from the SSC). Hence, the aim of the previous paragraphs was not to reproduce the experimental data, but to illustrate a new extraction process of second- and fourth-order ZFS parameters arising from

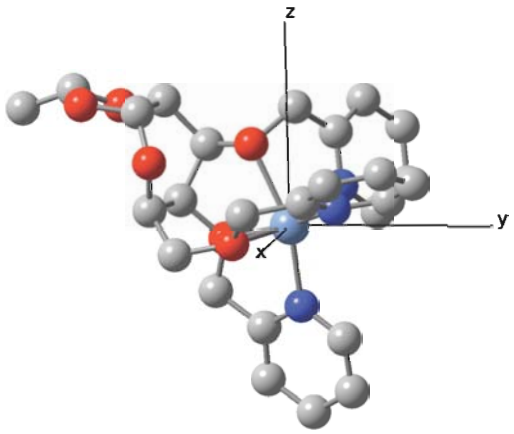

Figure 3.4: The [Ni(glycoligand)]$^{2+}$ (glycoligand=3,4,6-tri-*O*-(2-picolyl)-1,2-*O*-ethylidene-α-D-galactopyranose) complex and its magnetic axes frame. Hydrogen atoms are omitted for clarity.

the SOC interaction.

3.1.4 Other Test Applications and Generalization to all d^n Configurations

Several other complexes have been studied and the most interesting results and conclusions are exposed hereafter. The ZFS parameters are calculated and extracted following the process outlined in sections 3.1.1, 3.1.2, and 3.1.3. A more general conclusion concerning the calculation and extraction of the ZFS parameters in any d^n configuration will be exposed in the final paragraph of the section.

The [Ni(glycoligand)]$^{2+}$ Complex

The [Ni(glycoligand)]$^{2+}$ (glycoligand=3,4,6-tri-*O*-(2-picolyl)-1,2-*O*-ethylidene-α-D-galactopyranose) complex shown in Fig. 3.4 has been synthesized and experimentally studied in 2007 [112]. An intramolecular hydrogen bond is responsible for the geometry of the sugar scaffold, leading to a positive D parameter and underlining the close relation between the structure and the nature of the ZFS [112].

The ZFS parameters have been computed following the methodological conclusions drawn

Parameter	$D(\mathrm{cm}^{-1})$	$E(\mathrm{cm}^{-1})$
CAS(12/12)SCF, 4T	+6.02	0.76
CAS(12/12)PT2, 4T	+8.10	0.58
HF-EPR [112]	+4.40	0.75

Table 3.3: ZFS parameters in $[Ni(glycoligand)]^{2+}$. The number and spin multiplicity of the coupled states is indicated as nT (triplets). Results are compared to HF-EPR data.

from the study of the $[Ni(HIM2\text{-}Py)_2NO_3]^+$ complex (see section 3.1.1). Since the Ni coordination sphere in the $[Ni(glycoligand)]^{2+}$ complex is quasi-octahedral, the SI space can be reduced to four spin-orbit free triplet states. The most interacting σ ligand-metal orbitals are included in the active space, leading to a CAS(12/12)SCF reference calculation. Both the CASSCF and CASPT2 energies on the diagonal of the SI matrix are considered and results are presented in Table 3.3.

As in $[Ni(HIM2\text{-}Py)_2NO_3]^+$, the replacement of the diagonal elements of the SI matrix by the CASPT2 energies slightly modify the result, underlining the effect of the dynamic correlation. Even if such treatment is in principle more accurate than the one with the CASSCF energies on the diagonal (of the SI matrix), one should note however that in this complex the agreement with experiment is worse with CASPT2 energies than with the CASSCF energies, indicating that the use of CASPT2 energies on the diagonal of the SI matrix does not suffice to treat all dynamic correlation effects, and that the CASSCF result suffers from the cancellation of errors phenomenon. The same conclusions were obtained with other SI spaces and active spaces (data not reported here). Hence, it is concluded that in case of relative small ZFS parameters, it is more difficult to find a perfect agreement with experimental data.

The $[Ni(L)]^{2+}$ (L=N,N'-bis(2-aminobenzyl)-1,10-diaza-15-crown-5) Complex

The $[Ni(L)]^{2+}$ (L=N,N'-bis(2-aminobenzyl)-1,10-diaza-15-crown-5) complex is particularly interesting since the Ni^{2+} ion has an unusual coordination sphere, being heptacoodinated. The ideal pentagonal bipyramid geometry is Jahn-Teller active from the orbital point of view in the high-spin d^8 electronic configuration. Moreover, sterical effects make difficult to introduce seven atoms in the first coordination sphere. For these reasons, the heptacoordinated Ni(II)

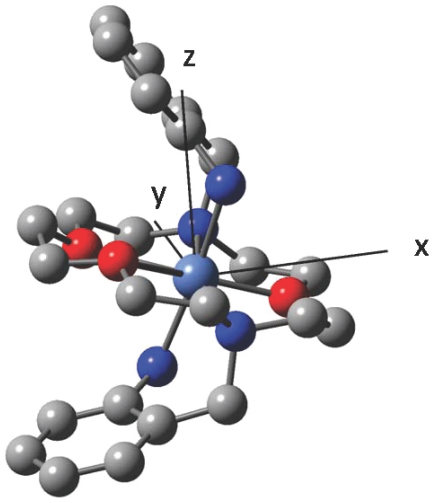

Figure 3.5: The $[Ni(L)]^{2+}$ (L=N,N'-bis(2-aminobenzyl)-1,10-diaza-15-crown-5) complex and its magnetic axes frame. Hydrogen atoms are omitted for clarity.

complexes are largely distorted, quenching the effect of the first order spin-orbit coupling between the orbital configurations that are degenerate in the D_{5h} point group symmetry. Hence, the use of a spin Hamiltonian is justified in such complexes. The synthesis and magnetic study of the $[Ni(L)]^{2+}$ (L=N,N'-bis(2-aminobenzyl)-1,10-diaza-15-crown-5) molecule (see Fig. 3.5) has been presented some years ago in the literature [113]. The magnetic study was based on magnetic susceptibility measurements. Although it is nearly impossible to determine the sign of the D parameter with this technique, a positive sign has been attributed.

The ZFS parameters have been computed through a RASSI-SO calculation that includes four spin-orbit free triplet using the CAS(12/12)PT2 energies on the diagonal of the SI matrix. Only two σ ligand-metal orbitals are included within the active space. The $|1, M_S\rangle$ components of the ground state contribute to more than 98% to the three lowest-lying spin-orbit states, validating the spin Hamiltonian approach in this complex. The magnetic axes frame is presented in Fig. 3.5 and the ZFS parameters in Table 3.4. Since all tests using other SI space and active spaces lead to the same conclusions, the results are considered as robust.

It is actually surprising at first sight to see that the sign of the computed D value is in disagreement with the experimentally reported result. The problem however does not arise

Parameter	$D(\mathrm{cm}^{-1})$	$E(\mathrm{cm}^{-1})$
CAS(12/12)PT2, 4T	-25.86	6.12
χ(T) [113]	+15	-

Table 3.4: ZFS parameters in $[\mathrm{Ni(L)}]^{2+}$ (L=N,N'-bis(2-aminobenzyl)-1,10-diaza-15-crown-5). The number and spin multiplicity of the coupled states is indicated as nT (triplets). Results are compared to experimental data based on magnetic susceptibility (χ(T) curves).

from the calculation but from the experimental data. Recent applications concerning similar Ni(II) heptacoordinated complexes (not reported in this thesis) always lead to negative D parameters. The detailed understanding of the ZFS presented in section 3.2 will clarify this behaviour giving additional evidence to the wrong attribution of the D sign in the experimental study.

The [Ni(*i*Prtacn)Cl_2] Complex

This complex is part of a series of Ni(II) complexes coordinated by the *i*Prtacn (*i*Prtacn=1,4,7-triisotropyl-1,4,7-triazacyclononane) ligand as well as by two chlorine, bromide or thiocyanato ligands [114]. Only the chloride case is studied here. This complex has an intermediate geometry between a square pyramid and a trigonal bipyramid (see Fig. 3.6). While a large positive D parameter is expected in the square pyramid (see section 3.2), the trigonal bipyramid leads to an orbitally degenerate situation. Since the actual geometry of the complex is rather far away from the trigonal bipyramid, the effect of the orbital degeneracy is supposed to be quenched and a spin Hamiltonian is relevant.

Table 3.5 compares the results obtained with a small SI space containing only the lowest four triplets (4T) to those obtained with a large SI space (ten triplets and fourteen singlets; 10T, 14S). Moreover, the results are given with a minimal active space (8/10) and the (12/12) active space containing the two most interacting ligand σ orbitals.

At first sight, it appears that the results obtained with the 4T SI space are better than the ones obtained with the 10T and 14S SI space when one compares the result with the experimental ones. Hence, one may pay attention to the fact that unbalanced SI spaces might sometimes reach to better values compared to experimental data for non relevant reasons.

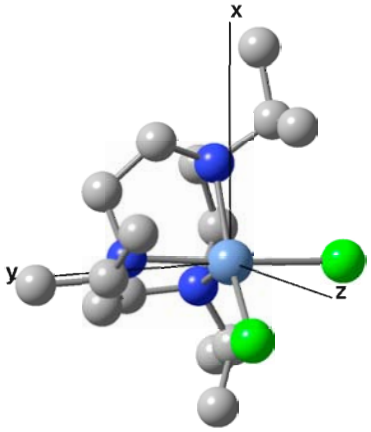

Figure 3.6: The [Ni(*i*Prtacn)Cl_2] (*i*Prtacn=1,4,7-triisotropyl-1,4,7-triazacyclononane) complex and its magnetic axes frame. Hydrogen atoms are omitted for clarity.

		$D(\text{cm}^{-1})$		$E(\text{cm}^{-1})$	
SI space	Active space	CASSCF	CASPT2	CASSCF	CASPT2
10T, 14S	(8,10)	+25.97	+21.44	3.92	1.98
10T, 14S	(12,12)	+22.00	+19.14	3.32	1.22
4T	(8,10)	+19.82	+18.84	5.70	5.71
4T	(12,12)	+17.62	+16.45	5.39	3.82
HF-EPR [114]		+15.70		3.40	

Table 3.5: ZFS parameters in [Ni(*i*Prtacn)Cl_2] as functions of the number of spin-orbit coupled states, active space, and diagonal energies used in the SI matrix. The number and spin multiplicity of the coupled states is indicated as nT (triplets) and mS (singlets).

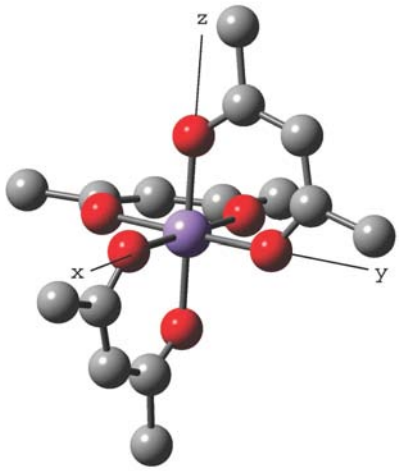

Figure 3.7: The [β-Mn(acac)$_3$] (acac=acetylacetonato) complex and its magnetic axes frame. Hydrogen atoms are omitted for clarity.

When the geometry of a complex prohibits the use of a truncated SI space, as in this largely, angularly distorted complex, one should include the complete d^n manifold in the SI space in order to ensure that the excitations are balanced in all directions of space. The intrinsic best result consists then in the CAS(12/12)PT2 based calculation with the 10T and 14S SI space. This result compare well with experiment, confirming the validity of the whole approach.

The [β-Mn(acac)$_3$] Complex

In addition to the γ isomer characterized by an elongated Jahn-Teller distorted geometry, a second stable form of the Mn(acac)$_3$ complex has been characterized, namely the β form (see Fig. 3.7) [115]. This isomer has a compressed geometry and the experimental information about the ZFS is based on magnetic susceptibility measurements [116]. The sign of the D parameter was obtained with crystal-field calculations and was found to be positive.

The ZFS parameters have been computed following the same procedure as in the γ complex and results are presented in Table 3.1.4. The explanation for the different signs of D in the γ and β forms lies in the structure of the two complexes. As can be seen in Figs. 3.3 and 3.7 the magnetic Z axis is oriented along the elongation axis in the γ case while it is oriented

D	+5.022
E	0.757
$10^3 \times B_4^0$	-0.538
$10^3 \times B_4^2$	1.033
$10^3 \times B_4^4$	-0.917

Table 3.6: ZFS parameters (in cm^{-1}) of the [β-Mn(acac)$_3$] complex.

along the compression axis in the β case. In the γ isomer the easy axis is the Z-axis along the long Mn-O bonds, and the β form the easy axis lies in the XY plane again coinciding with the long Mn-O bonds. Hence, the sign of D is then to the type of Jahn-Teller distortion present in both forms. The observation of this close relation between the structure and the property has motivated an analytical study of nearly octahedral Mn(III) complexes. All the details and conclusions of this analytical study are presented in section 3.2.

Generalization to all d^n Configurations

The theoretical study of the ZFS of a complex with a d^n configuration starts with the validation of the use of the spin Hamiltonian approach. From qualitative arguments, the spin Hamiltonian is relevant if the projections of the lowest spin-orbit states have sufficiently large norms on the $|S, M_S\rangle$ components of the ground state. Such situation occurs for instance in non degenerate and non nearly-degenerate cases. For nearly degenerate cases, the spin Hamiltonian approach is still relevant if no direct spin-orbit interactions can occur between the spin-orbit components of the nearly degenerate states. Otherwise, several orbital configurations have to be included in the model space and the model Hamiltonian should also include operators acting on the orbital degree of freedom. Such situation occurs when the closest ideal geometry present first-order orbital momentum for instance. These situations are not treated in the present thesis, which only focusses on spin Hamiltonians.

Once the spin Hamiltonian approach is proved relevant, a choice has to be made on the appropriate model Hamiltonian. If the ground state has only one unpaired electron, the Kramer's degeneracy prohibits any ZFS, and hence these cases are not interesting in mononuclear complexes. If the complex has two or three unpaired electrons in its ground state, the ZFS can be

described perfectly by using a second-order ZFS tensor. Starting from a SI calculation, effective Hamiltonian theory allows in this case to extract the entire ZFS tensor in any arbitrary axes frame, even in the case of Kramer's degeneracy. Hence, both magnetic axes frame and ZFS parameters are easily extracted in this case. When four or five unpaired electrons are present in the ground state, fourth order terms come into play and should be included in the spin Hamiltonian. These fourth order terms make impossible the rigorous definition of the magnetic axes frame if both SSC and SOC interactions are simultaneously considered. One efficient approximation consists in extracting the five ZFS parameters in an approximate axes frame defined by the SOC only, although no standard approximation can be recommended for all cases. The most appropriate approach always depends on the system and the objectives of the study. In practice the physics is dominated by the second-order ZFS tensor, and the extraction of the fourth order terms in an approximate magnetic axes frame will however give a correct description of the system in most cases. The effective Hamiltonian theory allows to check the approximations by comparing the model and effective interaction matrices.

Concerning the used methodology, it has been showed that the two-step SI approach has a few problems, mainly related with the truncation of the SI space. The excited states included in the SI space have to be balanced in all directions of space, and averaged MOs have to be used. In some particular geometries, it is possible to limit the SI space to a few low-lying excited states, but in general the complete d^n manifold has to be taken into account. This truncation problem is serious, and unbalanced SI spaces can lead to artificial agreement with experiment. Dynamic correlation plays a non-negligible role on the ZFS parameters. However, at this stage, the only possibility to include these effects in the treatment consists in replacing the diagonal elements of the SI matrix by energies computed at a post-CASSCF level. Hence, this treatment is only relevant if dynamic correlation effects are not too strong. Despite the drawbacks and limitations of the method, a good agreemeent with experimental data has been encountered in various complexes if correct choices are made for the computational degrees of freedom. Hence, the methodology is validated for application purposes.

The various examples studied in this section lead to the conclusion that the ZFS is strongly related to the geometry of the first coordination sphere. The next section concentrates on numerical and analytical magnetostructural relations in order to improve the chemical intuition concerning some particular configurations.

3.2 Analytical Derivations of the Model Hamiltonians and Rationalization of the Zero-Field Splitting

It is generally accepted that the anisotropy can be enlarged by (i) maximizing the geometrical distortions, (ii) reducing the d-d excited state energies, or (iii) reducing some particular excited state energies. These factors can be controlled by (i) the use of different ligands in the coordination sphere, (ii) the use of π-donor ligands or (iii) using coordination numbers different than from the more common four or six ones. Such reasoning is based on ligand field approaches, and hence consider that the spin-orbit coupling is dominated by the metal atom. The special case of heavy ligand atoms with important SOC require to go beyond the ligand field, and will be discussed in section 3.3. In this section, analytical expressions for the ZFS are derived to give a firm basis to the mainly empirical rules for enlarging the magnetic anisotropy.

3.2.1 Preliminaries: the Spin-Orbit Coupling Between the d Spin Orbitals

In order to facilitate the analytical derivations as well a the understanding of the effect of the spin-orbit coupling on the ZFS, the interaction matrix between the d spin orbitals is first built. The following SOC Hamiltonian is used:

$$\hat{H}_{SOC} = \zeta \hat{\mathbf{l}}.\hat{\mathbf{s}} = \zeta \left[\frac{1}{2} \left(\hat{l}_+ \hat{s}_- + \hat{l}_- \hat{s}_+ \right) + \hat{l}_z \hat{s}_z \right] \tag{3.38}$$

The real d orbitals can be expressed in terms of the $Y_l^{m_l}$ spherical harmonics in order to facilitate the direct application of this SOC Hamiltonian on the d spin orbitals:

$$\begin{aligned} d_{z^2} &= Y_2^0 \\ d_{x^2-y^2} &= \frac{1}{\sqrt{2}} \left(Y_2^2 + Y_2^{-2} \right) \\ d_{yz} &= \frac{i}{\sqrt{2}} \left(Y_2^1 + Y_2^{-1} \right) \\ d_{xz} &= -\frac{1}{\sqrt{2}} \left(Y_2^1 - Y_2^{-1} \right) \\ d_{xy} &= -\frac{i}{\sqrt{2}} \left(Y_2^2 - Y_2^{-2} \right) \end{aligned} \tag{3.39}$$

The following interaction matrix is obtained between the real d spin orbitals:

$\hat{H}_{SOC}$	$\lvert d_{z^2}\rangle$	$\lvert d_{x^2-y^2}\rangle$	$\lvert d_{yz}\rangle$	$\lvert d_{xz}\rangle$	$\lvert d_{xy}\rangle$	$\lvert \overline{d}_{z^2}\rangle$	$\lvert \overline{d}_{x^2-y^2}\rangle$	$\lvert \overline{d}_{yz}\rangle$	$\lvert \overline{d}_{xz}\rangle$	$\lvert \overline{d}_{xy}\rangle$
$\langle d_{z^2}\rvert$	0	0	0	0	0	0	0	$\frac{i\sqrt{3}}{2}\zeta$	$-\frac{\sqrt{3}}{2}\zeta$	0
$\langle d_{x^2-y^2}\rvert$	0	0	0	0	$-i\zeta$	0	0	$\frac{i}{2}\zeta$	$\frac{1}{2}\zeta$	0
$\langle d_{yz}\rvert$	0	0	0	$\frac{i}{2}\zeta$	0	$-\frac{i\sqrt{3}}{2}\zeta$	$-\frac{i}{2}\zeta$	0	0	$-\frac{1}{2}\zeta$
$\langle d_{xz}\rvert$	0	0	$-\frac{i}{2}\zeta$	0	0	$\frac{\sqrt{3}}{2}\zeta$	$-\frac{1}{2}\zeta$	0	0	$\frac{i}{2}\zeta$
$\langle d_{xy}\rvert$	0	$i\zeta$	0	0	0	0	0	$\frac{1}{2}\zeta$	$-\frac{i}{2}\zeta$	0
$\langle \overline{d}_{z^2}\rvert$	0	0	$\frac{i\sqrt{3}}{2}\zeta$	$\frac{\sqrt{3}}{2}\zeta$	0	0	0	0	0	0
$\langle \overline{d}_{x^2-y^2}\rvert$	0	0	$\frac{i}{2}\zeta$	$-\frac{1}{2}\zeta$	0	0	0	0	0	$i\zeta$
$\langle \overline{d}_{yz}\rvert$	$-\frac{i\sqrt{3}}{2}\zeta$	$-\frac{i}{2}\zeta$	0	0	$\frac{1}{2}\zeta$	0	0	0	$-\frac{i}{2}\zeta$	0
$\langle \overline{d}_{xz}\rvert$	$-\frac{\sqrt{3}}{2}\zeta$	$\frac{1}{2}\zeta$	0	0	$\frac{i}{2}\zeta$	0	0	$\frac{i}{2}\zeta$	0	0
$\langle \overline{d}_{xy}\rvert$	0	0	$-\frac{1}{2}\zeta$	$-\frac{i}{2}\zeta$	0	0	$-i\zeta$	0	0	0

(3.40)

where the overline symbol indicates a $|S = \frac{1}{2}, M_S = -\frac{1}{2}\rangle$ electron/hole. This interaction matrix will be used in the further analytical applications.

3.2.2 Radial Deformations in Distorted Octahedral Nickel(II) Complexes

The State-Interaction Space in the Octahedral Geometry

The ground state of an octahedral Ni(II) complex in an intermediate crystal field is the non-degenerate ${}^3A_{2g}$ state. The reference space contains the $|1, M_S\rangle$ components of this triplet and the maximum M_S components of this state can be expressed as:

$$|T_{0+}\rangle \quad = \quad |d_{xy}\overline{d}_{xy}d_{xz}\overline{d}_{xz}d_{yz}\overline{d}_{yz}d_{x^2-y^2}d_{z^2}\rangle \tag{3.41}$$

where x, y and z correspond to the crystallographic directions. These directions are obviously linked to the magnetic axes frame. In octahedral symmetry x, y and z are equivalent, and hence the magnetic axes frame cannot be defined. As discussed before, the SI space can be limited to the lowest four spin-orbit free triplets. The external space will then consists of the first excited triplet, *i.e.* ${}^3T_{2g}$. The three spatial configurations belonging to this state are expressed as follows:

$$
\begin{aligned}
|T_{1+}\rangle &= -|d_{xy}d_{xz}\overline{d}_{xz}d_{yz}\overline{d}_{yz}d_{x^2-y^2}\overline{d}_{x^2-y^2}d_{z^2}\rangle \\
|T_{2+}\rangle &= \frac{1}{2}|d_{xy}\overline{d}_{xy}d_{xz}\overline{d}_{xz}d_{yz}d_{x^2-y^2}\overline{d}_{x^2-y^2}d_{z^2}\rangle - \frac{\sqrt{3}}{2}|d_{xy}\overline{d}_{xy}d_{xz}\overline{d}_{xz}d_{yz}d_{x^2-y^2}d_{z^2}\overline{d}_{z^2}\rangle \\
|T_{3+}\rangle &= -\frac{1}{2}|d_{xy}\overline{d}_{xy}d_{xz}d_{yz}\overline{d}_{yz}d_{x^2-y^2}\overline{d}_{x^2-y^2}d_{z^2}\rangle - \frac{\sqrt{3}}{2}|d_{xy}\overline{d}_{xy}d_{xz}d_{yz}\overline{d}_{yz}d_{x^2-y^2}d_{z^2}\overline{d}_{z^2}\rangle
\end{aligned}
\tag{3.42}
$$

where the labels 1, 2, and 3 are used to refer to an excitation from the d_{xy}, d_{yz} and d_{xz} orbitals to the $d_{x^2-y^2}$ and/or d_{z^2} orbitals. Since a systematic symmetry lowering will be performed (from O_h to D_{4h} to D_{2h}), the spatial configurations are not labelled according to their irreducible represention. The expressions of the spatial configurations are consistents with the symmetry points O_h, D_{4h} or D_{2h}, and T_1, T_2 and T_3 might be called 'states' in all these point groups even in case of degeneracy between some of these spatial components. In the octahedron, all these three spatial configurations are equivalent, and hence the energy excitations with respect to the ground T_0 state corresponding to T_1, T_2 and T_3, Δ_1, Δ_2 and Δ_3 respectively are equal. Since T_1, T_2 and T_3 are the lowest ones in energy and since they have a pure single excited nature, these states dominate the spin-orbit interaction with the ground state and the other states are neglected in the following derivation.

Since second-order QDPT will be used to rationalize the effect of the SOC on the model space, only a small part of the complete SI matrix has to be calculated, namely the matrix elements between the three M_S components of T_0 on one side and the M_S components of T_1, T_2 and T_3 on the other. Matrix elements between the M_S components of the states in the external space are not included in this second-order treatment. The following matrix elements are obtained:

$\hat{H}_{SOC}$	$\|T_{0+}\rangle$	$\|T_{00}\rangle$	$\|T_{0-}\rangle$	$\|T_{1+}\rangle$	$\|T_{2+}\rangle$	$\|T_{3+}\rangle$	$\|T_{10}\rangle$	$\|T_{20}\rangle$	$\|T_{30}\rangle$	$\|T_{1-}\rangle$	$\|T_{2-}\rangle$	$\|T_{3-}\rangle$
$\langle T_{0+}\|$	0	0	0	$i\zeta$	0	0	0	$\frac{i\sqrt{2}}{2}\zeta$	$-\frac{\sqrt{2}}{2}\zeta$	0	0	0
$\langle T_{00}\|$	0	0	0	0	$\frac{i\sqrt{2}}{2}\zeta$	$\frac{\sqrt{2}}{2}\zeta$	0	0	0	0	$i\frac{\sqrt{2}}{2}\zeta$	$-\frac{\sqrt{2}}{2}\zeta$
$\langle T_{0-}\|$	0	0	0	0	0	0	0	$\frac{i\sqrt{2}}{2}\zeta$	$\frac{\sqrt{2}}{2}\zeta$	$-i\zeta$	0	0

(3.43)

where the second indices +, 0 and - indices are used for the -1, 0 and 1 M_S values respectively. By applying second-order QDPT, an analytical effective Hamiltonian can be obtained in a straightforward way, and simplified by considering that $\Delta_1 = \Delta_2 = \Delta_3$ in an octahedral complex:

$\hat{H}_{eff}$	$\|1,-1\rangle$	$\|1,0\rangle$	$\|1,1\rangle$
$\langle 1,-1\|$	$-\frac{2\zeta^2}{\Delta_1}$	0	0
$\langle 1,0\|$	0	$-\frac{2\zeta^2}{\Delta_1}$	0
$\langle 1,1\|$	0	0	$-\frac{2\zeta^2}{\Delta_1}$

(3.44)

This effective Hamiltonian reproduces the expected degeneracy of the $|1, M_S\rangle$ components of the ground state. The expressions for T_1, T_2 and T_3 in the octahedron are equivalent in Stevens and Racah's languages since no other $^3T_{2g}$ state can be built in this configuration. When the symmetry is lowered, the expressions of T_1, T_2 and T_3 are susceptible to be slightly affected by bielectronic interaction with other excited spatial configurations. Such effect that would be treated in Racah's formalism is neglected in this work which only considers the first order effect of the crystal field on the d-d states, as in Stevens' language used in the rationalizing works of Abragam and Bleaney [15].

Zero-Field Splitting in an Axially Distorted Geometry

An axially distorted crystal field lifts the degeneracy between the T_1 state and the T_2 and T_3 states (assuming that the z axis correspond to the compression or elongation axis). Taking $\Delta_2 = \Delta_3$ the following analytical effective Hamiltonian is obtained using the matrix elements presented in 3.43:

$\hat{H}_{eff}$	$\|1,-1\rangle$	$\|1,0\rangle$	$\|1,1\rangle$
$\langle 1,-1\|$	$-\frac{\zeta^2}{\Delta_1}-\frac{\zeta^2}{\Delta_2}$	0	0
$\langle 1,0\|$	0	$-\frac{2\zeta^2}{\Delta_2}$	0
$\langle 1,1\|$	0	0	$-\frac{\zeta^2}{\Delta_1}-\frac{\zeta^2}{\Delta_2}$

(3.45)

By comparing the analytical effective Hamiltonian to the model Hamiltonian given in Eq. 3.2, and by applying the standard conventions of molecular magnetism, the ZFS tensor is extracted in the magnetic axes frame:

$$\overline{\overline{D}}_{mag} = \begin{pmatrix} D_{XX} & 0 & 0 \\ 0 & D_{YY} & 0 \\ 0 & 0 & D_{ZZ} \end{pmatrix} = \begin{pmatrix} -\frac{\zeta^2}{\Delta_2} & 0 & 0 \\ 0 & -\frac{\zeta^2}{\Delta_2} & 0 \\ 0 & 0 & -\frac{\zeta^2}{\Delta_1} \end{pmatrix} \tag{3.46}$$

where capital letters are used in order to refer to the magnetic X, Y and Z anisotropy axes. The expressions for the ZFS parameters are:

$$D = D_{ZZ} - \frac{1}{2}(D_{XX} + D_{YY}) = -\frac{\zeta^2}{\Delta_1} + \frac{\zeta^2}{\Delta_2} \tag{3.47}$$

and

$$E = \frac{1}{2}(D_{XX} - D_{YY}) = 0 \tag{3.48}$$

Since no rhombic deformation is considered, the rhombic parameter E is zero. The magnetic Z axes correspond to the deformation axis as expected by symmetry arguments. The sign of the D parameter is directly linked to the deformation. If a compression is applied on the z axis, $\Delta_1 < \Delta_2$, and hence D is negative, while in case of elongation $\Delta_1 > \Delta_2$, leading to a positive D value.

One may note that the present derivation is equivalent to the one performed by Abragam and Bleaney [15]. Eq. 3.47 can be expressed in terms of the polyelectronic spin-orbit coupling constant λ, using [15]:

$$\lambda = \pm\frac{\zeta}{2S} \tag{3.49}$$

where S is the spin of the ground free-ion multiplet. The formula of Abragam and Bleaney is then recovered [15]:

$$D = -\frac{4\lambda^2}{\Delta_1} + \frac{4\lambda^2}{\Delta_2} \tag{3.50}$$

Zero-Field Splitting in a Rhombic Geometry

The symmetry of the complex is then lowered to D_{2h} by applying an additional rhombic distortion. In this case, the degeneracy between the three spatial configurations arising from the $^3T_{2g}$ of the octahedron is totally lost, and three different excitation energies have to be

considered, namely Δ_1, Δ_2 and Δ_3. By using the SI matrix elements presented in Eq. 3.43 and second-order QDPT, the following analytical effective Hamiltonian is obtained:

$\hat{H}_{eff}$	$\|1,-1\rangle$	$\|1,0\rangle$	$\|1,1\rangle$
$\langle 1,-1\|$	$-\frac{\zeta^2}{\Delta_1}-\frac{\zeta^2}{2\Delta_2}-\frac{\zeta^2}{2\Delta_3}$	0	$-\frac{\zeta^2}{2\Delta_2}+\frac{\zeta^2}{2\Delta_3}$
$\langle 1,0\|$	0	$-\frac{\zeta^2}{2\Delta_2}-\frac{\zeta^2}{2\Delta_3}$	0
$\langle 1,1\|$	$-\frac{\zeta^2}{2\Delta_2}+\frac{\zeta^2}{2\Delta_3}$	0	$-\frac{\zeta^2}{\Delta_1}-\frac{\zeta^2}{2\Delta_2}-\frac{\zeta^2}{2\Delta_3}$

(3.51)

Equating this effective Hamiltonian to the model Hamiltonian presented in Eq. 3.2, in combination with the stardard conventions of molecular magnetism lead to the following ZFS tensor in the magnetic axes frame:

$$\overline{\overline{D}}_{mag} = \begin{pmatrix} D_{XX} & 0 & 0 \\ 0 & D_{YY} & 0 \\ 0 & 0 & D_{ZZ} \end{pmatrix} = \begin{pmatrix} -\frac{\zeta^2}{2\Delta_2} & 0 & 0 \\ 0 & -\frac{\zeta^2}{2\Delta_3} & 0 \\ 0 & 0 & -\frac{\zeta^2}{\Delta_1} \end{pmatrix} \tag{3.52}$$

The convention $E > 0$ induces that $\Delta_2 > \Delta_3$, fixing not only the attribution of the magnetic anisotropy axes X and Y but also the attribution of the excited states T_2 and T_3. The ZFS parameters are then finally extracted:

$$D = D_{ZZ} - \frac{1}{2}(D_{XX} + D_{YY}) = -\frac{\zeta^2}{\Delta_1} + \frac{\zeta^2}{2\Delta_2} + \frac{\zeta^2}{2\Delta_3} \tag{3.53}$$

and

$$E = \frac{1}{2}(D_{XX} - D_{YY}) = -\frac{\zeta^2}{2\Delta_2} + \frac{\zeta^2}{2\Delta_3} \tag{3.54}$$

In genetal, rhombic distortions leave the average value of Δ_2 and Δ_3 (approximatively) the same as in the axially distorted situation. Accordingly, formula 3.53 shows that the introduction of the rhombic distortion leaves the axial anisotropy parameter almost untouched. The formulae presented for the D_{2h} symmetry point group are also valid in the more symmetric D_{4h} and O_h symmetry point groups. Hence Eqs. 3.53 and 3.54 can be seen as an extension of the formula for D presented by Abragam and Bleaney [15]. Before using these formulae for rationalizing purposes, some numerical tests are performed in order to check their validity.

Numerical Validation of the Analytical Formulae by Confrontation with *Ab Initio* Results

The validations are performed by calculating the ZFS of an octahedral $[Ni(NCH)_6]^{2+}$ model complex. The mean Ni-N distance was fixed to 2.054 Å, the N-C distances to 1.155 Å and the C-H distances to 1.083 Å. The different Ni-N distances are varied to introduce anisotropy, but the mean Ni-N distance is maintained. In order to get a ligand-field picture of the ZFS, the low-lying spin-orbit states are calculated with a CAS(8/5)SCF reference wavefunction and the RASSI-SO calculation considers the four lowest-lying spin-orbit free triplet states in the SI space.

The axial deformation applied to validate Eq. 3.47 is characterised by:

$$\tau_{ax} = \frac{2r(Ni - N_z)}{r(Ni - N_x) + r(Ni - N_y)} \tag{3.55}$$

Δ_1 and Δ_2 are taken from the spin-orbit free calculation. Hence, these effective parameters account for all mono- and bi-electronic interactions inherent to the ligand-field as well as other electronic effects (see section 2.3.3). The model axial ZFS parameter D_{mod} is calculated using the free-ion spin-orbit coupling constant and is compared to the D parameter extracted from the *ab initio* calculation.

According to Table 3.7, the model equations overestimate D by 25%-40% when the free-ion spin-orbit coupling constant is used. The deviations decrease drastically by slightly reducing the coupling constant. The average error between D_{mod} and the value extracted from the *ab initio* calculations is only 4% when ζ is reduced to 86% of its free-ion value. This validates Eq. 3.47 in all D_{4h} Ni(II) complexes under an intermediate crystal field.

The rhombic deformation is characterised by the following parameter:

$$\tau_{rh} = \frac{r(\mathrm{Ni} - \mathrm{N}_y)}{r(\mathrm{Ni} - \mathrm{N}_x)} \tag{3.56}$$

Since the mean Ni-N distance is maintained, the average of Δ_2 and Δ_3 remains practically the same irrespective of τ_{rh}. This implies that the axial deformation parameter is hardly affected by the application of the rhombic deformation. Table 3.8 presents the calculated and model ZFS parameters as functions of τ_{rh} with τ_{ax} fixed to 1.044. The same conclusions are found with other valued of τ_{ax}.

τ_{ax}	D	Δ_1	Δ_2	D_{mod}
0.957	-5.519	8382.4	9692.5	-6.855
0.971	-3.568	8669.7	9559.4	-4.564
0.985	-1.736	8964.0	9416.5	-2.279
1.000	0.000	9266.9	9266.9	0.000
1.015	1.659	9576.9	9110.8	2.271
1.029	3.259	9895.8	8951.8	4.530
1.044	4.814	10224.0	8791.1	6.778

Table 3.7: *Ab initio* axial anisotropy parameter D, *ab initio* excitation energies, and model estimate of the ZFS parameter as functions of the deformation parameter in a model Ni(II) complex. The free-ion spin-orbit coupling constant $\zeta_{free-ion}$ =648 cm^{-1} is used for the estimation of D_{mod}.

τ_{rh}	D	E	$E/\|D\|$	Δ_1	Δ_2	Δ_3	D_{mod}	E_{mod}
1.000	4.814	0.000	0.000	10224	8791	8791	6.778	0.000
1.005	4.819	0.321	0.067	10223	8861	8721	6.777	0.385
1.010	4.834	0.642	0.133	10221	8930	8651	6.781	0.768
1.015	4.860	0.964	0.198	10218	9000	8582	6.781	1.150
1.020	4.896	1.287	0.263	10213	9070	8512	6.783	1.534
1.025	4.941	1.612	0.326	10207	9139	8443	6.785	1.917

Table 3.8: *Ab initio* anisotropy parameters D and E, *ab initio* excitation energies, and model estimate of the ZFS parameters as functions of the rhombic deformation parameter in a model Ni(II) complex. The axial deformation parameter has been fixed to 1.044. The free-ion spin-orbit coupling constant $\zeta_{free-ion}$ =648 cm^{-1} is used for the estimation of D_{mod} and E_{mod}.

The close agreement between the *ab initio* values and those extracted from Eqs. 3.53 and 3.54 validates the analytical expressions based on an intermediate crystal field model. The agreement gets even better when a smaller ζ is used. Note, however, that the deviations in E are smaller than in D, which can be seen as an indication for the anisotropy of the spin-orbit interaction (see section 2.3.2). The introduction of the anisotropy of the spin-orbit interaction is out of the scope of the present rationalization works since it leads to complicated formulae.

How to Enlarge the Magnetic Anisotropy in Nickel(II) complexes

Having validated the analytical formulae for D and E, the previously exposed empiral rules can be verified and provided with a firm theoretical basis.

Observation (i): When different ligands are used in the coordination sphere, the octahedral symmetry is lost and the Δ_1, Δ_2 and Δ_3 excitation energies are not equal anymore. As a consequence, magnetic anisotropy is created. If the ligand field along one axis is significantly different than along the others, this axis becomes the easy or hard axes of magnetization and a strong axial anisotropy is observed. If the ligand field is stronger along this axis than along the two others, the situation is analogous to the compressed case in the model complex, and a negative D parameter appears. The introduction of a rhombic anisotropy does not practically affect the axial anisotropy, and hence, both axial and rhombic parameters can be controlled separately.

Observation (ii): If π-donor ligands are used, the Δ_1, Δ_2 and Δ_3 excitation energies are diminished. Hence, larger ZFS parameters are expected in these cases.

Observation (iii): The use of non-standard coordination numbers is best illustrated with the square pyramid example. In this case, the formulae presented in Eq. 3.47 is valid and Δ_1 is much larger than Δ_2. As a consequence, a large positive D parameter is expected, as already commented in section 3.1.4. Eq. 3.47 can also be used to further discuss the $[Ni(L)]^{2+}$ (L=N,N'-bis(2-aminobenzyl)-1,10-diaza-15-crown-5) heptacoordinated complex, already introduced in section 3.1.4. As in compressed D_{4h} and D_{2h} structures, the first excited triplet is mainly characterized by an excitation from the d_{xy} orbital to the $d_{x^2-y^2}$ orbital compared to the ground triplet. As T_1 in Eq. 3.47 and 3.53, such an excitation gives a negative contribution to the ZFS, and the total ZFS is negative since this excitation is the dominant one according to energy criteria.

Hence, the anisotropy of Ni(II) complexes is in principle tunable through controlled changes in the ligand field. However, the occurrence of angular deformations complicates the situation drastically, and hence, a calculation or an experiment is still required in an arbitrary complex to confirm the sign of the D parameter and the values of D and E.

3.2.3 Radial Deformations in Distorted Octahedral Manganese(III) Complexes

Zero-Field Splitting in the Octahedral Geometry

The ground state of octahedral high-spin Mn(III) complexes is orbitally doubly degenerate. The maximum M_S components of the two spatial configurations of this ${}^5E_g$ can be written as follows in a crystal field approach:

$$\begin{aligned} |Q_1, 2\rangle &= |d_{x^2-y^2} d_{xy} d_{xz} d_{yz}\rangle \\ |Q_2, 2\rangle &= |d_{z^2} d_{xy} d_{xz} d_{yz}\rangle \end{aligned} \tag{3.57}$$

where Q stands for quintet. These degenerate configurations are split in an axially distorted complex such that the two configurations wavefunctions are correct for the Q_1 or Q_2 ground states. Since the ground state is orbitally degenerate, the spin Hamiltonian approach is not relevant in the octahedral geometry. According to Eq. 3.40, no direct (*i.e.* first order) spin-orbit interaction is possible between Q_1 and Q_2. However, second order spin-orbit interactions couple certain spin-orbit components belonging to Q_1 and Q_2, causing a non-zero ZFS in the octahedron. Note that ZFS is used here in its general meaning, *i.e.* the splitting of spin-orbit states in the absence of a magnetic field. The x, y and z directions are equivalent in the octahedron, and hence, this ZFS has nothing to do with magnetic anisotropy.

To demonstrate the origin of this ZFS (already mentionned by Abragam and Bleaney [15]), an effective Hamiltonian between the $|S, M_S\rangle$ components of Q_1 and Q_2 is built by means of second-order QDPT. The external space consists of the excited ${}^5T_{2g}$ and the lowest-lying single excited ${}^3T_{1g}$. *Ab initio* calculations allowed to validate this model space, and will be presented later (see Table 3.9). In a crystal field approach, the maximum M_S components of these excited states are:

$$
\begin{aligned}
|Q_3, 2\rangle &= |d_{x^2-y^2} d_{z^2} d_{xz} d_{yz}\rangle \\
|Q_4, 2\rangle &= |d_{x^2-y^2} d_{z^2} d_{xy} d_{xz}\rangle \\
|Q_5, 2\rangle &= |d_{x^2-y^2} d_{z^2} d_{xy} d_{yz}\rangle \\
|T_1, 1\rangle &= |d_{xy} \overline{d}_{xy} d_{xz} d_{yz}\rangle \\
|T_2, 1\rangle &= |d_{xy} d_{xz} \overline{d}_{xz} d_{yz}\rangle \\
|T_3, 1\rangle &= |d_{xy} d_{xz} d_{yz} \overline{d}_{yz}\rangle
\end{aligned} \tag{3.58}
$$

The expressions can be used in the O_h, D_{4h} and D_{2h} geometries, although the expression for T_1, T_2 and T_3 are approximate compared with those obtained in the Racah's formalism, since the second-order crystal field terms are neglected here. On the other hand, the inclusion of T_1, T_2 and T_3 is an extension of the treatment of Abragam and Bleaney that only considered the effect of excited states with the same spin moment as the ground state. This case study nicely illustrates the compromise between Racah's and Abragam's approaches outlined in Chapter 2.

The total space, consisting on both the model space and the external space, has a 34x34 dimension, and hence the SI matrix is not reported in this dissertation. The effect of the external space on the model space is introduced by means of second-order QDPT, leading to the following effective Hamiltonian:

$\hat{H}_{eff}$	$\lvert Q_1,-2\rangle$	$\lvert Q_1,-1\rangle$	$\lvert Q_1,0\rangle$	$\lvert Q_1,1\rangle$	$\lvert Q_1,2\rangle$	$\lvert Q_2,-2\rangle$	$\lvert Q_2,-1\rangle$	$\lvert Q_2,0\rangle$	$\lvert Q_2,1\rangle$	$\lvert Q_2,2\rangle$
$\langle Q_1,-2\rvert$	$-\frac{3\zeta^2}{8Q}-\frac{\zeta^2}{2T}$	0	0	0	0	0	0	$\frac{3\zeta^2}{8\sqrt{2}Q}+\frac{\zeta^2}{2\sqrt{2}T}$	0	0
$\langle Q_1,-1\rvert$	0	$-\frac{15\zeta^2}{16Q}-\frac{5\zeta^2}{4T}$	0	0	0	0	0	0	$\frac{3\sqrt{3}\zeta^2}{16Q}+\frac{\sqrt{3}\zeta^2}{4T}$	0
$\langle Q_1,0\rvert$	0	0	$-\frac{9\zeta^2}{8Q}-\frac{3\zeta^2}{2T}$	0	0	$\frac{3\zeta^2}{8\sqrt{2}Q}+\frac{\zeta^2}{2\sqrt{2}T}$	0	0	0	$\frac{3\zeta^2}{8\sqrt{2}Q}+\frac{\zeta^2}{2\sqrt{2}T}$
$\langle Q_1,1\rvert$	0	0	0	$-\frac{15\zeta^2}{16Q}-\frac{5\zeta^2}{4T}$	0	0	$\frac{3\sqrt{3}\zeta^2}{16Q}+\frac{\sqrt{3}\zeta^2}{4T}$	0	0	0
$\langle Q_1,2\rvert$	0	0	0	0	$-\frac{3\zeta^2}{8Q}-\frac{\zeta^2}{2T}$	0	0	$\frac{3\zeta^2}{8\sqrt{2}Q}+\frac{\zeta^2}{2\sqrt{2}T}$	0	0
$\langle Q_2,-2\rvert$	0	0	$\frac{3\zeta^2}{8\sqrt{2}Q}+\frac{\zeta^2}{2\sqrt{2}T}$	0	0	$-\frac{9\zeta^2}{8Q}-\frac{3\zeta^2}{2T}$	0	0	0	0
$\langle Q_2,-1\rvert$	0	0	0	$\frac{3\sqrt{3}\zeta^2}{16Q}+\frac{\sqrt{3}\zeta^2}{4T}$	0	0	$-\frac{9\zeta^2}{16Q}-\frac{3\zeta^2}{4T}$	0	0	0
$\langle Q_2,0\rvert$	$\frac{3\zeta^2}{8\sqrt{2}Q}+\frac{\zeta^2}{2\sqrt{2}T}$	0	0	0	$\frac{3\zeta^2}{8\sqrt{2}Q}+\frac{\zeta^2}{2\sqrt{2}T}$	0	0	$-\frac{3\zeta^2}{8Q}-\frac{\zeta^2}{2T}$	0	0
$\langle Q_2,1\rvert$	0	$\frac{3\sqrt{3}\zeta^2}{16Q}+\frac{\sqrt{3}\zeta^2}{4T}$	0	0	0	0	0	0	$-\frac{9\zeta^2}{16Q}-\frac{3\zeta^2}{4T}$	0
$\langle Q_2,2\rvert$	0	0	$\frac{3\zeta^2}{8\sqrt{2}Q}+\frac{\zeta^2}{2\sqrt{2}T}$	0	0	0	0	0	0	$-\frac{9\zeta^2}{8Q}-\frac{3\zeta^2}{2T}$

(3.59)

where Q stands for the excitation energy between the ground state and the excited states belonging to ${}^5T_{2g}$:

$$Q = \frac{E_{Q_3} + E_{Q_4} + E_{Q_5}}{3} - min\left(E_{Q_1}, E_{Q_2}\right) \tag{3.60}$$

and T stands for the excitation energy between the ground state and the excited states belonging to ${}^3T_{1g}$:

$$T = \frac{E_{T_3} + E_{T_4} + E_{T_5}}{3} - min\left(E_{Q_1}, E_{Q_2}\right) \tag{3.61}$$

The diagonalization of the effective Hamiltonian presented in Eq. 3.59 leads to the following eigenvectors and eigenvalues:

$$\begin{aligned}
|\Phi_1\rangle &= \frac{1}{2}\Big[\sqrt{2}|Q_1,0\rangle - |Q_2,-2\rangle - |Q_2,2\rangle\Big] \\
|\Phi_2\rangle &= \frac{1}{2}\sqrt{2}\Big[|Q_2,-2\rangle - |Q_2,2\rangle\Big] \\
|\Phi_3\rangle &= \frac{1}{2}\Big[|Q_1,-1\rangle - \sqrt{3}|Q_2,1\rangle\Big] \\
|\Phi_4\rangle &= \frac{1}{2}\Big[|Q_1,1\rangle - \sqrt{3}|Q_2,-1\rangle\Big] \\
|\Phi_5\rangle &= \frac{1}{2}\Big[\sqrt{2}|Q_1,0\rangle + |Q_2,-2\rangle + |Q_2,2\rangle\Big] \\
|\Phi_6\rangle &= \frac{1}{2}\Big[-|Q_1,-2\rangle - |Q_1,2\rangle + \sqrt{2}|Q_2,0\rangle\Big] \\
|\Phi_7\rangle &= \frac{1}{2}\Big[|Q_1,-1\rangle + \sqrt{3}|Q_2,1\rangle\Big] \\
|\Phi_8\rangle &= \frac{1}{2}\Big[|Q_1,1\rangle + \sqrt{3}|Q_2,-1\rangle\Big] \\
|\Phi_9\rangle &= \frac{1}{2}\sqrt{2}\Big[|Q_1,-2\rangle - |Q_1,2\rangle\Big] \\
|\Phi_{10}\rangle &= \frac{1}{2}\Big[|Q_1,-2\rangle + |Q_1,2\rangle + \sqrt{2}|Q_2,0\rangle\Big]
\end{aligned} \tag{3.62}$$

$$\begin{aligned}
E_1 &= 4\left(\frac{-4Q\zeta^2 - 3T\zeta^2}{8QT}\right) \\
E_2 = E_3 = E_4 &= 3\left(\frac{-4Q\zeta^2 - 3T\zeta^2}{8QT}\right) \\
E_5 = E_6 &= 2\left(\frac{-4Q\zeta^2 - 3T\zeta^2}{8QT}\right)
\end{aligned}$$

$$
\begin{aligned}
E_7 = E_8 = E_9 &= \frac{-4Q\zeta^2 - 3T\zeta^2}{8QT} \\
E_{10} &= 0
\end{aligned}
\tag{3.63}
$$

Most of the ten spin-orbit states of the model space have large contributions from the two spatial configurations Q_1 and Q_2, invalidating the use of a spin Hamiltonian. The effect of the first excited triplet state, $^3T_{1g}$, is large but strictly proportional to the effect of the excitet quintet state $^5T_{2g}$. As a consequence, the wavefunctions here obtained are equivalent to the ones obtained by Abragam and Bleaney and the same pattern is observed for the spin-orbit spectrum [15].

The Axial Distortion and the Spin Hamiltonian

A careful inspection of the effective Hamiltonian presented in Eq. 3.59 leads in a few steps to the formula presented by Gerritsen and Sabisky in 1963 for the ZFS in axially distorted high-spin d^4 complex with D_{4h} symmetry point group [117]. In this case the degeneracy between Q_1 and Q_2 is lost and if the distortion is large enough, the second-order SOC between the Q_1 and Q_2 M_S components vanish according to second-order QDPT. Consequently the spin Hamiltonian approach applies to the ground state. If the small energy difference between Q_3, Q_4 and Q_5, as well as between T_1, T_2 and T_3 are neglected (*i.e.* the distortion is not too large), the diagonal elements of the effective matrix presented in Eq. 3.59 correspond directly to the diagonal elements of the effective spin Hamiltonian, since the off-diagonal elements become zero (the interaction between Q_1 and Q_2 disappears with the distortion).

If a compression along the z-axis is considered, Q_1 is the ground state, and the following effective spin Hamiltonian is obtained:

$\hat{H}_{eff}$	$\lvert Q_1,-2\rangle$	$\lvert Q_1,-1\rangle$	$\lvert Q_1,0\rangle$	$\lvert Q_1,1\rangle$	$\lvert Q_1,2\rangle$
$\langle Q_1,-2\rvert$	$-\frac{3\zeta^2}{8Q} - \frac{\zeta^2}{2T}$	0	0	0	0
$\langle Q_1,-1\rvert$	0	$-\frac{15\zeta^2}{16Q} - \frac{5\zeta^2}{4T}$	0	0	0
$\langle Q_1,0\rvert$	0	0	$-\frac{9\zeta^2}{8Q} - \frac{3\zeta^2}{2T}$	0	0
$\langle Q_1,1\rvert$	0	0	0	$-\frac{15\zeta^2}{16Q} - \frac{5\zeta^2}{4T}$	0
$\langle Q_1,2\rvert$	0	0	0	0	$-\frac{3\zeta^2}{8Q} - \frac{\zeta^2}{2T}$

(3.64)

while in case of elongation, Q_2 is the ground state and the following effective spin Hamiltonian is obtained:

$\hat{H}_{eff}$	$\|Q_2,-2\rangle$	$\|Q_2,-1\rangle$	$\|Q_2,0\rangle$	$\|Q_2,1\rangle$	$\|Q_2,2\rangle$
$\langle Q_2,-2\|$	$-\frac{9\zeta^2}{8Q}-\frac{3\zeta^2}{2T}$	0	0	0	0
$\langle Q_2,-1\|$	0	$-\frac{9\zeta^2}{16Q}-\frac{3\zeta^2}{4T}$	0	0	0
$\langle Q_2,0\|$	0	0	$-\frac{3\zeta^2}{8Q}-\frac{\zeta^2}{2T}$	0	0
$\langle Q_2,1\|$	0	0	0	$-\frac{9\zeta^2}{16Q}-\frac{3\zeta^2}{4T}$	0
$\langle Q_2,2\|$	0	0	0	0	$-\frac{9\zeta^2}{8Q}-\frac{3\zeta^2}{2T}$

(3.65)

Comparing these matrices with the model Hamiltonian given in Eq. 3.37 and after adjusting the trace of the effective and model Hamiltonians, the axial D parameter can be extracted in both cases and the following general formula obtained:

$$D = \pm\zeta^2\left[\frac{3}{16Q}+\frac{1}{4T}\right] \tag{3.66}$$

where the positive sign correspond to a compressed structure and a negative sign to an elongated structure. The formula of Gerritsen and Sabisky [117] is obtained by expressing the ζ monoelectronic spin-orbit constant in terms of the λ polyelectronic one.

If the distortion is large, the effect of the loss of degeneracy between the excited spin-orbit free multiplets can play *a priori* a non-negligible role on the ZFS parameter. In order to check this hypothesis numerically, it is indeed necessary to include this degeneracy lift in the derivation. Figure 3.8 explicits the excitation energies considered in both compressed and elongated cases. Neglecting the second-order SOC between Q_1 and Q_2, the effective Hamiltonians of the 5x5 model Hamiltonians are given in 3.67 for the compressed complex and in 3.68 for the elongated case.

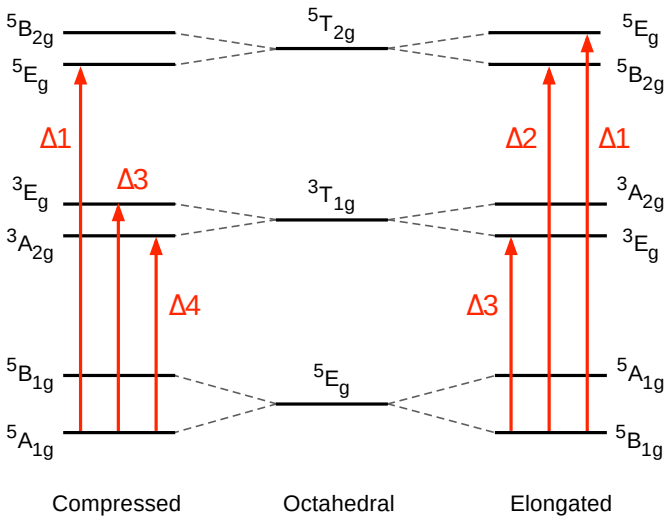

Figure 3.8: Splitting of the spin-orbit free states considered in the LFT derivations for axially distorted Mn(III) complexes leading to compressed or elongated structures.

$\hat{H}_{eff}$	$\lvert Q_1,-2\rangle$	$\lvert Q_1,-1\rangle$	$\lvert Q_1,0\rangle$	$\lvert Q_1,1\rangle$	$\lvert Q_1,2\rangle$
$\langle Q_1,-2\rvert$	$-\frac{3\zeta^2}{8\Delta_1}-\frac{\zeta^2}{2\Delta_3}$	0	0	0	0
$\langle Q_1,-1\rvert$	0	$-\frac{15\zeta^2}{16\Delta_1}-\frac{\zeta^2}{4\Delta_3}-\frac{\zeta^2}{\Delta_4}$	0	0	0
$\langle Q_1,0\rvert$	0	0	$-\frac{9\zeta^2}{8\Delta_1}-\frac{\zeta^2}{6\Delta_3}-\frac{4\zeta^2}{3\Delta_4}$	0	0
$\langle Q_1,1\rvert$	0	0	0	$-\frac{15\zeta^2}{16\Delta_1}-\frac{\zeta^2}{4\Delta_3}-\frac{\zeta^2}{\Delta_4}$	0
$\langle Q_1,2\rvert$	0	0	0	0	$-\frac{3\zeta^2}{8\Delta_1}-\frac{\zeta^2}{2\Delta_3}$

(3.67)

$\hat{H}_{eff}$	$\lvert Q_2,-2\rangle$	$\lvert Q_2,-1\rangle$	$\lvert Q_2,0\rangle$	$\lvert Q_2,1\rangle$	$\lvert Q_2,2\rangle$
$\langle Q_2,-2\rvert$	$-\frac{\zeta^2}{8\Delta_1}-\frac{\zeta^2}{\Delta_2}-\frac{3\zeta^2}{2\Delta_3}$	0	0	0	0
$\langle Q_2,-1\rvert$	0	$-\frac{5\zeta^2}{16\Delta_1}-\frac{\zeta^2}{4\Delta_2}-\frac{3\zeta^2}{4\Delta_3}$	0	0	0
$\langle Q_2,0\rvert$	0	0	$-\frac{3\zeta^2}{8\Delta_1}-\frac{\zeta^2}{2\Delta_3}$	0	0
$\langle Q_2,1\rvert$	0	0	0	$-\frac{5\zeta^2}{16\Delta_1}-\frac{\zeta^2}{4\Delta_2}-\frac{3\zeta^2}{4\Delta_3}$	0
$\langle Q_2,2\rvert$	0	0	0	0	$-\frac{\zeta^2}{8\Delta_1}-\frac{\zeta^2}{\Delta_2}-\frac{3\zeta^2}{2\Delta_3}$

(3.68)

From the matrices, analytical formulae for D can be derived in both the compressed and the elongated cases:

$$D_{comp} = \frac{\zeta^2}{16}\left[\frac{3}{\Delta_1} - \frac{4}{3\Delta_2} + \frac{16}{3\Delta_4}\right] \tag{3.69}$$

$$D_{elong} = \frac{\zeta^2}{16}\left[\frac{1}{\Delta_1} - \frac{4}{\Delta_2} - \frac{4}{\Delta_3}\right] \tag{3.70}$$

The formula for D_{elong} was already obtained by Dugad *et al.* some decades ago [118]. However the formula for D_{comp} is new, and as in the Ni(II) case study all existing formulae are derived again for illustrative purposes. By accounting for the loss of the degeneracy between the excited states, the compressed and elongated cases are not symmetrical anymore, contrary to the Gerritsen and Sabisky formula.

In the regime of small distortions, there is another source of asymmetry between elongated and compressed cases. Since the distortion is considered small, the excited states Q_3, Q_4 and Q_5, as well as T_1, T_2 and T_3 can be considered to be degenerate, respectively. However, the lack of degeneracy between Q_1 and Q_2 has to be taken into account, and is described as follows:

$$a = \frac{|E_{Q1} - E_{Q2}|}{2} \tag{3.71}$$

The coupling of the M_S components of Q_1 and Q_2 is treated at second order of QDPT by using the matrix elements between Q_1 and Q_2 M_S components obtained in the octahedral case (3.59). Since $a << Q$ and $a << T$, the effect of the energy difference between Q_1 and Q_2 on the excitation energies concerning other spin-orbit free states is neglected. Moreover, the zeroth order effect of the spin-orbit coupling on the excitation energies between the $|Q_1, M_S\rangle$ and $|Q_2, M'_S\rangle$ components is neglected. As a consequence, the effective Hamiltonians for both compressed and elongated cases are Hermitian and given in 3.72 and 3.73.

$\hat{H}_{eff}$	$\lvert Q_1,-2\rangle$	$\lvert Q_1,-1\rangle$	$\lvert Q_1,0\rangle$	$\lvert Q_1,1\rangle$	$\lvert Q_1,2\rangle$
$\langle Q_1,-2\rvert$	$-a-\frac{3\zeta^2}{8Q}-\frac{\zeta^2}{2T}-\frac{b^2}{2a}$	0	0	0	$-\frac{b^2}{2a}$
$\langle Q_1,-1\rvert$	0	$-a-\frac{15\zeta^2}{16Q}-\frac{5\zeta^2}{4T}-\frac{3b^2}{4a}$	0	0	0
$\langle Q_1,0\rvert$	0	0	$-a-\frac{9\zeta^2}{8Q}-\frac{3\zeta^2}{2T}-\frac{b^2}{a}$	0	0
$\langle Q_1,1\rvert$	0	0	0	$-a-\frac{15\zeta^2}{16Q}-\frac{5\zeta^2}{4T}-\frac{3b^2}{4a}$	0
$\langle Q_1,2\rvert$	$-\frac{b^2}{2a}$	0	0	0	$-a-\frac{3\zeta^2}{8Q}-\frac{\zeta^2}{2T}-\frac{b^2}{2a}$

(3.72)

$\hat{H}_{eff}$	$\lvert Q_2,-2\rangle$	$\lvert Q_2,-1\rangle$	$\lvert Q_2,0\rangle$	$\lvert Q_2,1\rangle$	$\lvert Q_2,2\rangle$
$\langle Q_2,-2\rvert$	$-a-\frac{9\zeta^2}{8Q}-\frac{3\zeta^2}{2T}-\frac{b^2}{2a}$	0	0	0	$-\frac{b^2}{2a}$
$\langle Q_2,-1\rvert$	0	$-a-\frac{9\zeta^2}{16Q}-\frac{3\zeta^2}{4T}-\frac{3b^2}{4a}$	0	0	0
$\langle Q_2,0\rvert$	0	0	$-a-\frac{3\zeta^2}{8Q}-\frac{\zeta^2}{2T}-\frac{b^2}{a}$	0	0
$\langle Q_2,1\rvert$	0	0	0	$-a-\frac{9\zeta^2}{16Q}-\frac{3\zeta^2}{4T}-\frac{3b^2}{4a}$	0
$\langle Q_2,2\rvert$	$-\frac{b^2}{2a}$	0	0	0	$-a-\frac{9\zeta^2}{8Q}-\frac{3\zeta^2}{2T}-\frac{b^2}{2a}$

(3.73)

where:

$$b = \frac{3\zeta^2}{8\sqrt{2}Q} + \frac{\zeta^2}{2\sqrt{2}T} \tag{3.74}$$

After shifting the traces of both analytical effective Hamiltonians to facilitate the identification of the ZFS parameters by comparison with Eq. 3.37, the following formulae emerge:

$$D = \pm\zeta^2\left[\frac{3}{16Q} + \frac{1}{4T}\right] + \frac{3b^2}{28a} \tag{3.75}$$

$$B_4^0 = -\frac{b^2}{840a} \tag{3.76}$$

$$B_4^4 = -\frac{b^2}{24a} \tag{3.77}$$

The near degeneracy of Q_1 and Q_2 introduces fourth order terms in the spin Hamiltonian. Moreover, the formula for D has an opposite effect in the compressed and elongated cases. In the former case, D is enlarged in absolute value and in the latter case the D parameter is diminished in absolute value. Although the sign of D could possibly change in the elongated case, when the fourth order terms cannot be considered as a perturbation to the second order terms in the spin Hamiltonians. A relation appears in Eqs 3.76 and 3.77 between B_4^0 and B_4^4:

$$B_4^4 = 35B_4^0 \tag{3.78}$$

Hence, even if the B_4^0 interaction has larger prefactors, the main fourth order term is B_4^4. This B_4^4 term plays a non negligible role in high-spin d^4 complexes close to the octahedral geometry since it lifts the degeneracy between the states dominated by the $|2,2\rangle \pm |2,-2\rangle$ determinants in the absence of any rhombic distortion.

Zero-Field Splitting in a Rhombic Geometry

The effect of the rhombic distortions on the ZFS is studied starting with an axially distorted complex where the distortion is large enough to remove all near degeneracy effects such as the fourth order terms in the spin Hamiltonian. Although Q_1 and Q_2 belong to the same spatial symmetry in the D_{2h} symmetry point group, the larger axial distortion keeps the two states sufficiently separated in energy to avoid problems due to the mixing of the two components arising from the SOC as in the octahedral case.

Two models are considered in the rationalization of the rhombic distortion. In model 1, both axial and rhombic distortions are considered large and all the degeneracy lifts are treated while the mixing between the Q_1 and Q_2 configurations is neglected. In model 2, both distortions are considered as intermediate, hence all degeneracy lifts are neglected while the mixing between the Q_1 and Q_2 configurations is taken into account.

The approximations in model 1 lead to the following analytical formulae:

$$D_{comp} = \frac{\zeta^2}{16}\left[\frac{3}{2\Delta Q_4}+\frac{3}{2\Delta Q_5}+\frac{16}{3\Delta T_1}-\frac{2}{3\Delta T_2}-\frac{2}{3\Delta T_3}\right] \quad (3.79)$$

$$E_{comp} = \frac{\zeta^2}{16}\left[\frac{3}{2\Delta Q_5}-\frac{3}{2\Delta Q_4}+\frac{2}{3\Delta T_3}-\frac{2}{3\Delta T_2}\right] \quad (3.80)$$

$$D_{elong} = \frac{\zeta^2}{16}\left[-\frac{4}{\Delta Q_3}+\frac{1}{2\Delta Q_4}+\frac{1}{2\Delta Q_5}-\frac{2}{\Delta T_2}-\frac{2}{\Delta T_3}\right] \quad (3.81)$$

$$E_{elong} = \frac{\zeta^2}{16}\left[\frac{1}{2\Delta Q_5}-\frac{1}{2\Delta Q_4}+\frac{2}{\Delta T_3}-\frac{2}{\Delta T_2}\right] \quad (3.82)$$

These formulae reduce to the formulae presented in Eqs. 3.69 and 3.70 for D_{4h} symmetry.

The mixing of Q_1 and Q_2 taken into account in model 2 is expressed in the wavefunctions in the same way as done by Abragam and Bleaney [15]:

$$\begin{aligned}|\Phi_1\rangle &= \cos\delta|Q_1\rangle+\sin\delta|Q_2\rangle\\ |\Phi_2\rangle &= -\sin\delta|Q_1\rangle+\cos\delta|Q_2\rangle\end{aligned} \quad (3.83)$$

Under the assumption of one excitation energy for the excited triplets (T) and one for the excited quintets (Q), the effective Hamiltonian is constructed and the following formulae for D and E are derived:

$$D = \zeta^2\cos 2\delta\left[\frac{3}{16Q}+\frac{1}{4T}\right] \quad (3.84)$$

$$E = \zeta^2|\sin 2\delta|\left[\frac{\sqrt{3}}{16Q}+\frac{\sqrt{3}}{12T}\right] \quad (3.85)$$

Again, these formulae reduce to those derived for the D_{4h} case, where $\delta = 0$ or $\delta = 90°$ for the compressed or elongated structures, respectively. As in the D_{4h} case, the effect of

the excited triplet states is proportional to the effect of the excited quintet states. As a consequence, the analytical formula found by Abragam and Bleaney for $\frac{E}{|D|}$ is confirmed [15]:

$$\frac{E}{|D|} = \frac{\sqrt{3}}{3}|tan(2\delta)| \tag{3.86}$$

Numerical Validation of the Analytical Formulae by Confrontation with *Ab Initio* Results

The numerical validation of the analytical formulae is performed for the $[Mn(NCH)_6]^{3+}$ model complex with a mean Mn-N distance of 2.061 Å, all N-C distances equal to 1.155 Å and all C-H distances equal to 1.083 Å. The RASSI-SO calculations are based on CAS(4/5)SCF reference calculations, the CASSCF energies are used on the diagonal elements of the SI matrix, and a large SI space consisting of 5Q, 13T and 13S (see section 3.1.3) is considered.

The analytical expressions presented in this work are all based on a smaller SI space, and hence, the validity of the 5Q, 3T SI space has to be established. Table 3.9 lists the energies of the lowest-lying spin-orbit states obtained from *ab initio* calculations dealing with three different SI spaces, (i) the smallest with only 5Q that was used by Abragam and Bleaney [15], (ii) the intermediate one consists of 5Q and 3T and is used in the analytical derivations presented here and in other works [117, 118], and (iii) the large one, taken as a reference, consisting of 5Q, 13T and 13S. The differences between the spectra obtained with reduced SI spaces and the reference spectrum is summurized in the ϵ error parameter, defined in Eq. 2.12. Table 3.10 reports D and E for various axial or rhombic systems estimated from the three SI spaces.

From both tables the intermediate SI space appears accurate enough for rationalizing purposes. The SI space used by Abragam and Bleaney, *i.e.* the quintet states only, only accounts for about 50% of the ZFS parameters, and is not sufficient for quantitative purposes. However, as shown in the previous paragraphs, this SI space is qualitatively correct since all the patterns and behaviours obtained with it were confirmed with the intermediate SI space. In the following paragraphs and Tables, 'model' refers to the results of the analytical formulae derived in the preceding paragraphs using the CASSCF spin-orbit free energies and the free-ion spin-orbit coupling constant $\zeta_{free-ion}$=352 cm^{-1}.

In Table 3.11, the model and *ab initio* spectrum are compared for the strictly octahedral

	SI space		
Energies	Small	Intermediate	Large
E_1	11.89	1.00	0.00
$E_2 = E_3 = E_4$	15.39	9.89	9.48
$E_5 = E_6$	18.90	18.78	18.90
$E_7 = E_8 = E_9$	22.27	27.18	27.22
E_{10}	25.65	35.59	35.36
ϵ (%)	17	0.9	0

Table 3.9: Relative energies (in cm^{-1}) of the lowest spin-orbit states issued from the ^5E_g spin-orbit free state of an octahedral $[Mn(NCH)_6]^{3+}$ model complex for different SI spaces.

		SI space		
Structure	Parameter	Small	Intermediate	Large
Elongated (D_{4h})	D	-1.60	-3.97	-4.12
Compressed (D_{4h})	D	1.58	4.00	4.18
Rhombic (D_{2h})	D	1.35	3.40	3.55
	E	0.47	1.14	1.17

Table 3.10: Axial and rhombic ZFS parameters (in cm^{-1}) for three distortions of the $[Mn(NCH)_6]^{3+}$ model complex for different SI spaces.

Energies	Model	*Ab initio*
E_1	2.628	0.000
$E_2 = E_3 = E_4$	10.762	9.477
$E_5 = E_6$	18.897	18.897
$E_7 = E_8 = E_9$	27.032	27.217
E_{10}	35.167	35.355
Error (%)	2.3	0

Table 3.11: Relative energies (in cm^{-1}) of the spin-orbit states of the ^5E_g spin-free states in an octahedral $[Mn(NCH)_6]^{3+}$ model complex obtained with QDPT in the SI space spanned by ^5E_g, $^5T_{2g}$ and $^3T_{1g}$. The model spectra is compared to the *ab initio* results obtained with the large SI space.

complex. Both model and computed spectra are in good agreement. The small difference between both spectra (ϵ=2.3%) is attributed to higher excited configurations that are neglected in the model while included in the *ab initio* calculation.

For large axial distortions, the loss of degeneracy of the excited triplet and quintet states can be included in the analytical expression. Table 3.12 compares the model ZFS parameters obtained with and without degenerated excited states (*i.e.* by using Eqs. 3.66 and 3.69 or 3.70) to the *ab initio* results for an axial distorted system. Even in this largely distorted system, the degeneracy loss in the excited Q_3, Q_4 and Q_5 as well as in the T_1, T_2 and T_3 can be safely neglected, validating the formula of Gerritsen and Sabisky in axially distorted high-spin d^4 complexes.

To validate the analytical formulae presented for small distortions, a slightly compressed and a slightly elongated structure are considered in Table 3.13. The numerical values arising from the model are in good agreement with the *ab initio* ones, validating the previous analytical work.

The last confirmation deals with the physical origin of the rhombic anisotropy. While model 1 includes the loss of degeneracy between all excited states but neglects the mixing between the Q_1 and Q_2 spatial configurations, model 2 includes the mixing between Q_1 and Q_2 while it neglects the absence of strict degeneracy in the other excited states. Table 3.14

Structure	$\Delta1 = \Delta2$ $\Delta3 = \Delta4$	$\Delta1 \neq \Delta2$ $\Delta3 \neq \Delta4$	*Ab initio*
Compressed	+4.08	+4.10	+4.12
Elongated	-4.08	-4.11	-4.18

Table 3.12: Axial ZFS parameter in cm^{-1} for $[Mn(NCH)_6]^{3+}$ D_{4h} distorted structures (τ_{ax}=0.9702, 1.0284) extracted under the assumption that the excited states are degenerate (left colum), and taking into account the lift of degeneracy between excited states (middle column). Results are compared to the *ab initio* result obtained using the large SI space.

Structure	Parameter	Model	*Ab initio*
Compressed	D	4.15	4.58
(τ_{ax}=0.9991)	B_4^0	$-1.2\cdot10^{-3}$	$-3.6\cdot10^{-3}$
	B_4^4	-0.042	-0.043
Elongated	D	-3.96	-4.35
(τ_{ax}=1.0012)	B_4^0	$-9.2\cdot10^{-4}$	$3.3\cdot10^{-4}$
	B_4^4	-0.032	-0.044

Table 3.13: Axial ZFS parameters in cm^{-1} for the $[Mn(NCH)_6]^{3+}$ D_{4h} distorted structures. The degeneracy breaking of the excited states is not included. Results are compared to the *ab initio* result with the large SI space.

Structure	Extraction	D	E	E/$\|D\|$
τ_{ax}=0.9792	Model 1	+4.09	0.01	0.000
	Model 2	+3.91	0.61	0.156
	Ab initio	+4.01	0.62	0.155
τ_{ax}=1.0284	Model 1	-4.10	0.01	0.000
	Model 2	-3.89	0.68	0.175
	Ab initio	-3.93	0.70	0.178

Table 3.14: Axial and rhombic ZFS parameters D and E in cm^{-1} for two $[Mn(NCH)_6]^{3+}$ D_{2h} distorted structures with τ_{rh}=1.0096 and τ_{ax} as indicated. Results of models 1 and 2 (see text) are compared to the *ab initio* result with the large SI space.

shows undoubtedly that the rhombicity appears through the mixing between the Q_1 and Q_2 spatial configurations giving a nearly zero E value in model 1. This mixing also induces that the axial ZFS parameter is affected by the rhombic deformation, contrary to the Ni(II) case study.

Correlation between the ZFS parameters and the deformation parameters

Before concluding on how to enlarge the anisotropy in Mn(III) complexes, some curves are built to establish a possible correlation between the ZFS and the deformation. As in the study for Ni(II), τ_{ax} and τ_{rh} (defined in Eqs. 3.55 and 3.56) are used to characterize the distortions. The y axis is chosen such that τ_{rh} is positive and may not correspond the the Y magnetic anisotropy axis. Indeed, according to Eq. 3.85 the sign of E is not linked to the relative energies of the spin-orbit free states arising from the excited quintet states, and hence the magnetic anisotropy axes X and Y cannot be attributed from the spin-orbit free spectrum contrary to the Ni(II) case.

The first curve depicted in Fig. 3.9 shows the axial D parameter as a function of the axial deformation parameter τ_{ax}. Since the D parameter cannot be defined in the octahedral situation, the curve is discontinuous in this point. The D parameter is nearly independent of the deformation, although for compressed structures the D parameter is enlarged close to the octahedron by the near degeneracy effects (see Eq. 3.75). The two parts of the curve, *i.e.* the

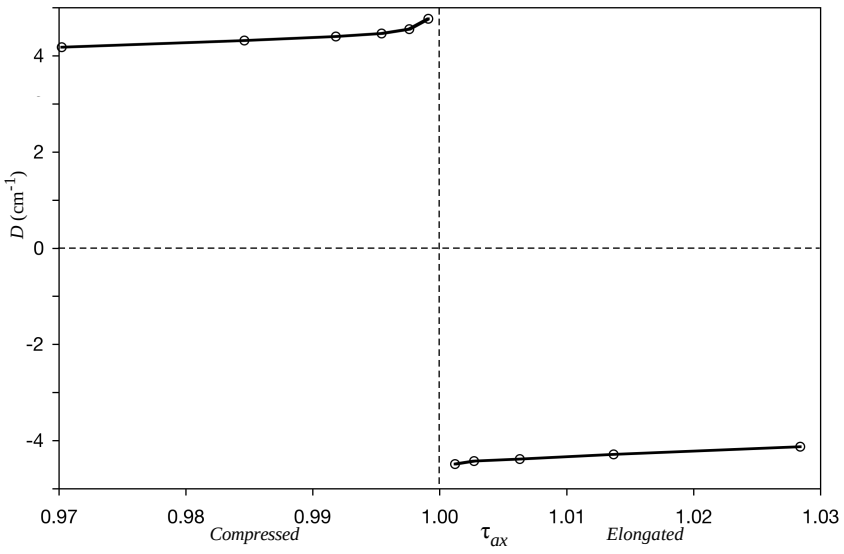

Figure 3.9: The axial anisotropy parameter D as a function of τ_{ax} in the $[Mn(NCH)_6]^{3+}$ model complex.

compressed one and the elongated one, are almost symmetrical as expected from the equation of Gerritsen and Sabisky, which applies for all intermediate and largely distorted systems.

Fig. 3.10 shows the evolution of D and E as functions of the rhombic deformation parameter τ_{rh}. As expected (after deriving and validating the analytical formulae), the introduction of rhombicity diminishes the axial anisotropy, contrary to the Ni(II) case, underlining the specificities of the d^4 configuration.

The introduction of:

$$\Delta\tau_{ax} = |1 - \tau_{ax}| \tag{3.87}$$

and

$$\Delta\tau_{rh} = |1 - \tau_{rh}| \tag{3.88}$$

reveals a relation between $|D|$ and E. Fig. 3.11 reports $\frac{E}{|D|}\frac{1}{\Delta\tau_{rh}}$ as a function of $\frac{1}{\Delta\tau_{ax}}$ for various distorted structures, from which the following approximation for $\frac{E}{|D|}$ is deduced:

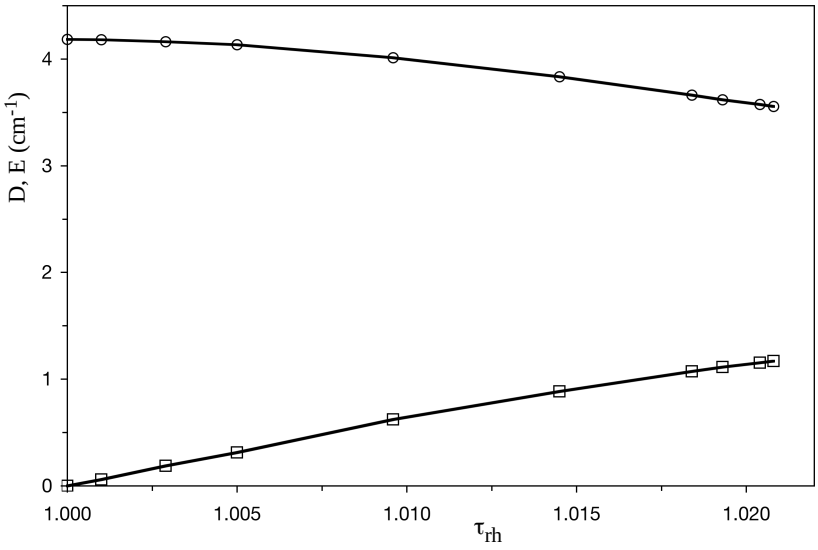

Figure 3.10: The anisotropy parameters D (circles) and E (squares) as function of τ_{rh} for a fixed τ_{ax}=0.9702 $[Mn(NCH)_6]^{3+}$ model complex.

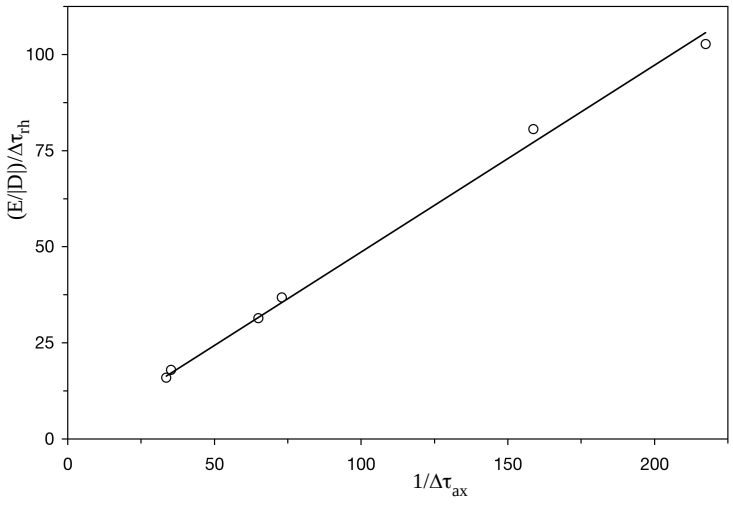

Figure 3.11: Correlation between the anisotropy parameters and the deformation applied on a $[Mn(NCH)_6]^{3+}$ model complex. The solid line is a guide to the eye obtained by a linear regression with R^2=0.9964.

$$\frac{E}{|D|} \simeq \frac{1}{2}\frac{\Delta\tau_{rh}}{\Delta\tau_{ax}} \tag{3.89}$$

According to Eq. 3.86, $\frac{E}{|D|}$ can be evaluated directly from the angle δ defining the mixing of the Q_1 and Q_2 spatial configurations. Hence, the ratio of the anisotropy parameters can be linked to both the geometry and the electronic structure of the system.

How to Enlarge the Magnetic Anisotropy in Manganese(III) complexes

The analytical formulae derived (and validated) so far only consider radial distortions. In real complexes, there are of course also angular distortions and the behaviour of the ZFS is possibly slightly more complicated than expressed by the analytical formulae. However, it should be kept in mind that the d^4 configuration is Jahn-Teller active. While the second-order SOC between Q_1 and Q_2 tends to minimize the distortions by introducing a mixing of the two different spatial components, the Jahn-Teller effect imposes an important radial distortion, and hence, the behaviour is dominated or at least oriented by the radial deformations. Therefore, the results obtained with the radial deformations are used to discuss the standard empirical rules to enlarge the anisotropy.

(i) As soon as the system is distorted from the octahedral geometry, the effect of the orbital degeneracy practically disappears and the spin Hamiltonian approach applies, since the spin-orbit interaction occurs at second-order between the degenerate orbital configurations. This is not true in case of first-order spin-orbit coupling such as in octahedral Co(II) complexes. However, contrary to the Ni(II) case, the axial anisotropy parameter remains practically constant irrespective of the axial distortion. Moreover, rhombic distortions diminishes the axial anisotropy. Hence it not recommendable to enlarge the distortions in order to maximize the anisotropy.

(ii) Since both the excited quintet states and the lowest-lying triplet states have a similar effect on the ZFS, any kind of ligand (from π-donor to π-acceptor) can be used without any significant effect. In fact, π-donor ligands stabilize the excited quintets while the lowest-lying triplets are destabilized with respect to the ground state. For π-acceptor ligands, the situation is inverted, leading to similar ZFS parameters.

(iii) Non-standard coordination numbers are less interesting than in the case of Ni(II)

complexes. Such complexes lead to largely distorted coordination spheres, which has been found to diminish $|D|$.

As a consequence, Mn(III) complexes do not obey to the standard empirical rules used to enlarge the ZFS parameters. Actually, the largest anisotropy is observed for geometries with quasi-octahedral symmetry. As a consequence the ZFS parameters are always small in Mn(III) complexes, and the absolute value of D never exceeds 6 cm^{-1} in any reported complex [11].

3.2.4 General Considerations on Angular Deformations

The rationalization of the angular deformations on the ZFS is complicated, and nearly impossible in the case of several combined angular distortions. If such a deformation lowers the symmetry of the complex to a low-symmetry point group (a subgroup of D_{2h}, for instance), many configurations participate in the ground and excited states wavefunctions. In consequence, many spin-orbit free states have a (partial) singly excited character with respect to the ground state, all playing an important role on the ZFS and the SI space would then consist of numerous spin-orbit free states. Obviously, it is not easy to derive analytical expressions involving a lot of spin-orbit free states, but an extra complication arises writing down the effect of the crystal field on the d-d states, which becomes highly non-trivial for any but the very simplest angular distortions. To overcome this problem, one may use a numerical solution of the crystal field problem, for instance the energies and wavefunctions of a CASSCF calculation. In other words, the solution is known and then expressed in a simpler model. Such rationalizing work is actually more illustrative than rationalizing, and do not provide basic new insight since they only reproduce the *ab initio* SOC calculation in a more crude way. A more pragmatic approach consists in directly calculating the state-by-state contributions to the ZFS parameters at second-order of perturbation in the *ab initio* calculation to illustrate the contribution of each individual spin-orbit free state. Such approach is for instance implemented in the ORCA code [104]. Hence, in case of important angular distortions, it is preferable to use state-of-the-art calculations and/or an experiment to determine the ZFS parameters and an *a priori* prediction of the result is beyond the present possibilities.

3.3 When Covalency and Charge Transfer Play an Important Role: the Special Case of Heavy Atom Ligands

3.3.1 Two visions of the same phenomenon

The covalency of the metal ligand bond can be approached from two different yet complementary viewpoints. From one side it can be seen as the result of the partial delocalization of the electrons in the molecular orbitals. This effect is represented by the non-zero contribution of the basis functions centered on the ligands in the mainly metal orbitals and vice versa in the mainly ligand orbitals. The second point of view considers the covalency as the appearance of charge transfer configurations in the N-electron wavefunctions with non-negligible weights. The CASSCF wavefunctions typically adopt an intermediate position between the two extremes; the metal orbitals have significant tails on the ligands and the charge transfer configurations gain certain weight in the wave function of the ground state. Note however that the two viewpoints are mathematically equivalent and one can gradually switch between them by unitary transformations of the N-electron wavefunction.

For not too strong covalency, the lower part of the spectrum of the transition metal complexes treated in this thesis is dominated by the different d^n states and at higher energy the ligand-to-metal charge transfer states (LMCT) appear. Whereas the d^n states are dominated by the configurations with n electrons in the orbitals that can be characterized as TM-d orbitals, the LMCT states have strong contributions from configurations with one electron transferred from the (mainly) ligand orbitals to the TM-d orbitals.

Covalency effects on the *ab initio* calculations of the ZFS

Two cases have to be considered, (i) the spin-orbit interaction is only or mainly caused by the metal atom (light atoms in the first coordination sphere) and (ii) some atoms of the ligands are expected to contribute to the spin-orbit coupling (heavy atom(s) in the first coordination sphere).

When the SOC only arises from the metal atom, the ZFS can be described almost from the interaction of the ground state with the other d^n states. However, mean-field calculations such as CASSCF generally underestimate the metal to ligand delocalization in the d MOs if

one considers a minimal active space with the five 3d orbitals and the n electrons of the d^n configuration. As a consequence, the ZFS is overestimated, and additional steps are required to improve the covalency treatment. In section 3.1, the active space was enlarged with metal d' and the most important σ orbitals of the ligand. In other studies dealing with the g matrix the LMCT states involving these σ bonding ligand-metal orbitals are explicitely included through Multi-State (MS) CASPT2 calculations [119]. Either of the two strategies lead to a better description of the covalency and the ZFS can be treated according to the methodology used in section 3.1 and it is also possible to rationalize the property through ligand-field approaches as in section 3.2.

The situation becomes much more complicated when SOC on the ligand is important to describe the ZFS of the complex. As mentionned before, for not too strong covalent metal-ligand bonds, the charge transfer states lie higher in energy than the d^n states, and a rough description of the ZFS can be obtained from a SI calculation involving these d^n states. However, if the covalency effects are important, the charge transfer states appear in the same energy interval as the d^n states and the SI space can no longer be limited to the d^n states only. An extra complication is the fact that the excited states actually adquire a mixed character with large contributions from the d^n and LMCT configurations. This makes extremely difficult to construct a spatially balanced SI space.

The relevance of the RASSI-SO method to study the ZFS in case of heavy ligand atoms have been checked on a series of Ni(II) complexes with one normal, multidentate ligand and one halogen atom coordinated to the metal. The halogen atom is changed from Cl to Br to I along the series. The study starts with real complexes (see section 3.3.2), but due to the elevated computational cost, model complexes have been used to study the effect of the LMCT states on the ZFS of the complexes (see section 3.3.3).

3.3.2 Covalency Effects in $[Ni(iPrtacn)X]^+$ (X=Cl, Br, I) Complexes

The $[Ni(iPrtacn)X]^+$ (X=Cl, Br, I and *i*Prtacn=1,4,7-triisotropyl-1,4,7-triazacyclononane) complexes are taken in their experimental structures [120]. The macrocyclic ligand is identical to the previously studied $[Ni(iPrtacn)Cl_2]$ complex (see section 3.1.4), but here only one halide ligand is coordinated to the nickel atom. The geometry of the three complexes is close to C_{3v} symmetry, and are mainly differentiated between them by their Ni-X distance which is 2.146,

Complex	Parameter	CAS(8/10)		CAS(14/13)		HF-EPR [120]
		CASSCF	CASPT2	CASSCF	CASPT2	
$[Ni(i\text{Prtacn})Cl]^+$	D	+20.9	+16.6	+17.4	+13.8	+9.2
	E	1.8	1.3	1.5	1.1	2.1
$[Ni(i\text{Prtacn})Br]^+$	D	+14.5	+11.5	+11.9	+9.3	+4.4
	E	3.1	1.3	2.5	1.3	1.1
$[Ni(i\text{Prtacn})I]^+$	D	+7.1	+5.1	+5.3	+4.2	-2.1
	E	1.4	1.1	1.0	1.0	0.2

Table 3.15: Calculated ZFS parameters in $[Ni(i\text{Prtacn})X]^+$ (X=Cl, Br, I) complexes as a function of the active space size and diagonal energies of the spin-orbit coupling matrix used in the RASSI-SO calculations. The results are compared with the HF-EPR ones.

2.284 and 2.490 Å for X=Cl, Br and I, respectively. The magnetic Z-axis coincides with the Ni-X bond which is the C_3 pseudo symmetry element.

The *ab initio* calculations consider all the d^8 states (10 triplets and 15 singlets) except for the X=I case where the fifteenth singlet is neglected. Two active spaces are considered, first the (8/10) space (8 electrons in 10 orbitals) and secondly, three occupied ligand orbitals are added to give a (14/13) active space. The results are condensed in Table 3.15.

For the complexes with Cl and Br ligands, a similar agreement with experiment is obtained as in all other complexes studied so far. However, when X=I, the experimental sign of D is not reproduced.

Since the SOC due to the ligand is especially important in the latter case, it is interesting to see if the inclusion in the SI calculation of the states dominated by the LMCT configurations improves the description of ZFS through a more marked contribution of the SOC due to the ligand.

3.3.3 Covalency and Charge Transfer Effects in Model $[Ni(NH_3)_3X]^+$ (X=Cl, Br, I) Complexes

To reduce the computational cost implying this extension of the SI space, model complexes are built by replacing the *i*Prtacn ligand by three NH_3 ligands. In the first place, the same

study is performed as in the real complexes (see Table 3.16, columns 3-6, entry "d^8 states"). Obviously, the σ-donor character of the *i*Prtacn ligand is not exactly reproduced by the NH_3 ligands and the computed ZFS parameters are rather different in the models. Therefore, no comparison with the experimental data will be made and they only aim at the illustration of the role of the charge transfer states on the ZFS.

The optimal active space includes the σ-orbitals of the three N atoms, and the np orbitals of the halogen involved in the LMCT states. Together with the ten orbitals of the metal, this leads to an active space with at least 16 orbitals and 20 electrons. This is far beyond the computational possibilities and only the np orbitals of the halogen are added, accepting the fact that the covalency between Ni and the NH_3 groups is only approximatively described. The smallest SI space equilibrated in all directions of space consists in 25T and 29S. One should note that when only the d^8 states are considered in the SI space, the three ligand orbitals included in the active space include also covalency effects attributed to the N atoms, while they only include halogen contributions when the d^8 and LMCT states are considered in the SI space.

The inclusion of the LMCT states largely affects the ZFS parameters (see Table 3.16, last two columns), even in the case of X=Cl and Br, where only small changes are expected. This can be explained by the lack of N-σ orbitals in the active space and by the state average procedure followed to optimize the orbitals. The addition of the LMCT states lakes that the average is made for many more states, which obviously not improves the description of the d^8 states. This artificially enlarges the ZFS parameters in the complexes with the lighter halogens.

Complex	Parameter	d^8 states				d^8 + LMCT states	
		CAS(8/10)		CAS(14/13)		CAS(14/13)	
		CASSCF	CASPT2	CASSCF	CASPT2	CASSCF	CASPT2
$[Ni(NH_3)_3Cl]^+$	D	+25.1	+21.7	+22.6	+20.3	+31.7	+27.7
	E	1.7	1.2	1.4	1.0	2.0	1.5
$[Ni(NH_3)_3Br]^+$	D	+18.7	+16.4	+17.0	+15.7	+19.4	+17.7
	E	2.4	1.1	2.0	1.1	2.0	1.5
$[Ni(NH_3)_3I]^+$	D	+10.5	+8.8	+10.6	+11.5	-2.5	+6.9
	E	1.2	1.0	1.2	1.1	0.5	0.7

Table 3.16: Calculated ZFS parameters in model complexes $[Ni(NH_3)_3X]^+$ (X=Cl, Br, I) as a function of the active space size, diagonal elements of the spin-orbit coupling matrix used in the RASSI-SO calculations, and the type of states included in the state interaction space.

This artefact is of course also present in the X=I case. Nevertheless, the change in D is in the opposite direction and its sign even changes when charge transfer states are included in the SI space. A second indication of the important role of the LMCT states in the iodine complex is the huge difference between the CASSCF and the CASPT2 results. The use of energies obtained with these two methods leads to almost equivalent ZFS parameters when the d^8 states dominate the physics (X=Cl and Br), or when the LMCT states are not considered in the SI space (columns 3-6). However, when the CASSCF energies in the SI matrix are replaced with the CASPT2 energies, the computed ZFS parameters are drastically changed in the X=I case. The CASPT2 energies of the LMCT states are significantly different than at the CASSCF level. Combined with the large SOC effect of iodine, the large effect on the ZFS can be explained. Having in mind the shortcomings in the treatment of the Ni-N covalency and the artifacts due to the averaging procedure of the orbital optimization, which tends to artificially raise the ZFS, it is not surprising to see that our final estimate of D overestimates the experimental value.

Alternatives to the RASSI-SO methodology in this case are not available nowadays. A better approach should overcome the difficulties that arise from truncation problems (on both the active space and SI space) and from averaging effects in order to consistently treat the complexes with heavy ligand atoms that participate to the SOC. This methodological perspective would be of utmost importance to go beyond the two-step SI procedure succesfully applied to all the other transition metal complexes.

Conclusion

The two-step SI approach is well adapted to compute the ZFS parameters in mononuclear transition metal complexes provided that correct choices are made for the computational degrees of freedom. When a spatially balanced SI space and a large active space is used, the computed ZFS parameters are in good agreement with experimental data. The effect of the dynamic correlation can be introduced by substituting the diagonal elements of the SI matrix with post-CASSCF energies. This methodology encounters its limits of applicability when heavy ligand atom(s) are present in the first coordination sphere. In this situation, covalency and charge transfer effects have to be accurately treated, which is not possible in the two-step

SI procedure due to the computational cost. The effective Hamiltonian theory is a powerful tool to extract ZFS parameters since it allows to validate the use of spin Hamiltonians in the interpretation of the ZFS. Moreover, it allows to verify that all interactions of the exact electronic Hamiltonian are included in the model. The ZFS parameters and the magnetic axes frame can be extracted after diagonalizing the SI matrix in any d^n configuration, including those with Kramers' degeneracy since the information contained in the energies and the wavefunctions is used. Such *ab initio* calculations can be used in order to predict the ZFS parameters in largely distorted systems. In more symmetric systems, ligand field analytical derivations can be used to rationalize the ZFS. It has been demonstrated that Ni(II) complexes follow all common rules to enlarge the anisotropy, contrary to the Mn(III) complexes. Finally, a promising way of enlarging the ZFS is the use of non-standard coordination modes of the transition metal ion.

Chapter 4

Binuclear Complexes

Binuclear complexes are particularly interesting since they may pave the way for the study of larger systems. Indeed, they introduce the main features responsible for the anisotropy of SMMs (local and intersite anisotropies), and fragment based approaches can be envisaged for the study of large SMMs. Due to the intersite interactions, the binuclear complexes are susceptible to be more complicated to treat. In order to analyze the main difficulties that can arise in binuclear complexes, this chapter is separated in two parts dealing with the $d^9 - d^9$ and $d^8 - d^8$ configurations respectively.

Unless specified, all the *ab initio* calculations have been performed using the MOLCAS package [98]. The computational details are presented in section 2.4.1. The majority of the results presented in this chapter have already been published [121–124]. The presentation of the results is here slightly different than in the articles. Only homobinuclear complexes are considered since they usually have higher symmetry than heterobinuclear complexes and are therefore easier to study. However, the treatment of heterobinuclear complexes would not introduce more conceptual difficulties *a priori* and the conclusions of this chapter are transferable to such cases.

4.1 The $d^9 - d^9$ Configuration

As the high-spin d^8 configuration in monometallic complexes, the $d^9 - d^9$ configuration in binuclear complexes is the simplest situation since it presents only two unpaired electrons. However, since the unpaired electrons are localized on two different magnetic sites, the phe-

nomenological model Hamiltonian introduces more interactions than in the case of mononuclear complexes:

$$\hat{H}_{mod} = J\hat{\mathbf{S}}_a \cdot \hat{\mathbf{S}}_b + \hat{\mathbf{S}}_a \overline{\overline{D}}_{ab} \hat{\mathbf{S}}_b + \overline{d} \cdot \hat{\mathbf{S}}_a \times \hat{\mathbf{S}}_b \tag{4.1}$$

where J is the isotropic exchange coupling, $\overline{\overline{D}}_{ab}$ is the second-order symmetric exchange tensor and $\overline{d}$ is the Dzyaloshinskii-Moriya pseudo-vector (DM vector). While the exchange tensor has a similar role as the ZFS tensor in Ni(II) mononuclear complexes (see section 4.1.1), the isotropic exchange and the DM vector are specific to binuclear complexes. The isotropic exchange accounts for the isotropic coupling between the local spins that gives rise to the lowest-lying magnetic states with spin quantum numbers $|S_a - S_b| \leq S \leq S_a + S_b$ (with S_a and S_b the local spin quantum numbers on site a and b respectively). This term accounts then for the energy difference between the lowest-lying triplet and singlet states. The DM vector, often called 'antisymmetric exchange', is an anisotropic interaction that occurs in particular symmetry point groups [5, 31]. In order to introduce separately the methodological and interpretation difficulties arising from the anisotropic intersite interactions, namely the symmetric and antisymmetric exchanges, two case studies will be extensively presented. In section 4.1.1, the crucial role of dynamic correlation on the isotropic exchange couplings in excited states and its consequences on the anisotropic parameters will be studied on the copper acetate monohydrate complex. In section 4.1.2, several deformations will be considered in a model complex in order to study the antisymmetric exchange magnitude as a function of the geometrical structure.

4.1.1 The Symmetric Exchange in Copper Acetate Monohydrate

Introduction and Description of the System

The copper acetate monohydrate complex is one of the most famous molecules of molecular magnetism, and hence a case study of interest for introducing the symmetric exchange. Actually, the molecular structure presented in Fig. 4.1 was unknown in the first experimental studies. It was assumed in the late forties that this complex was mononuclear, with a $[Cu(CH_3COO)_2]H_2O$ crystal formula. In 1951, Guha published a magnetic susceptibility curve which was exhibiting unusual features for a mononuclear complex [1]. Indeed, the curve

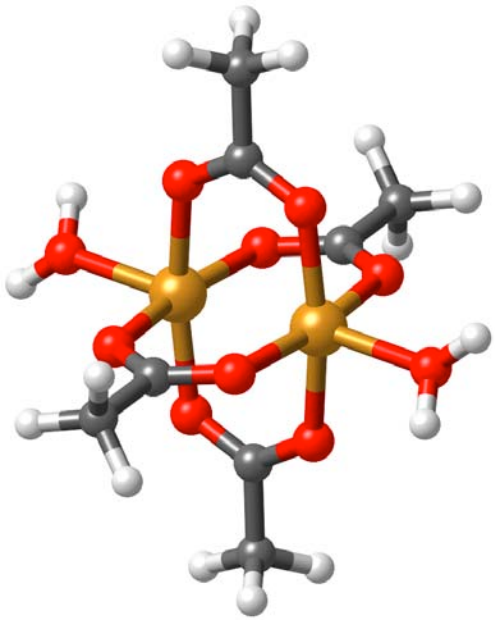

Figure 4.1: Ball and stick representation of $[Cu(CH_3COO)_2]_2(H_2O)_2$. The easy axis of magnetization almost coincides with the Cu-Cu direction.

showed a maximum at room temperature and a dramatic decrease when the temperature was lowered. Such behaviour motivated Bleaney and Bowers to study the copper acetate monohydrate by means of EPR spectroscopy [125]. In order to explain the observed EPR spectrum at room temperature as well as the 'Christmas tree' structure arising from the hyperfine interaction, Bleaney and Bowers formulated the hypothesis of interacting pairs of copper ions [2]. The decrease of the susceptibility when the temperature was lowered was then attributed to the population of a singlet ground state and the maximum at room temperature due to the population of the triplet state. One year later, the crystal structure was published for the first time, validating the hypothesis of interacting pairs of copper ions [3].

Fig. 4.1 shows the refined structure of copper acetate that is used in this work [126]. The molecular structure presents an inversion center, prohibiting the appearance of the DM vector [5, 31]. The original paper of Bleaney and Bowers already provided an estimate of the J magnetic coupling ruling the energetic ordering of the lowest singlet and triplet states as well as the D and E ZFS parameters of the triplet state [2]. Moreover, they provided an analytical formula that was used in order to determine the sign of the D parameter. The D sign was

then found positive, as in another work dealing with the copper acetate pyrazine complex presenting a similar structure as the monohydrate one [127]. During many years, the D sign was always assumed to be positive in the extraction process and never directly determined from experiment. In 2008, Ozarowski determined the ZFS parameters by means of HF-EPR [33]. The D sign was then unambiguously found negative in both copper acetate complexes (the monohydrate and the pyrazine ones). However, the reasons for which the analytical formula used over the years in order to indirectly determine the D sign are not clarified in the paper of Ozarowski. An analysis of the validity of this analytical formula is then of first importance and constitutes one of the objectives of the present section.

The computation of the ZFS in the copper acetate monohydrate is particularly challenging since it concentrates most of the difficulties that can occur in transition metal complexes, (i) both SOC and SSC have to be considered in the calculations (due to the smallness of the D and E parameters) and (ii) the role of dynamic correlation is in this case particularly crucial.

Relation between the Symmetric Tensors in the Multispin and Giant Spin Models

In order to avoid any confusion between the multispin and giant spin Hamiltonians, it is preferable to start by expliciting the relation between the ZFS tensors of both models. The model multispin Hamiltonian explicitely considers the local spins $\mathbf{S}_a$ and $\mathbf{S}_b$ which are effectively coupled through the isotropic and symmetric exchanges:

$$\hat{H}_{mod} = J\hat{\mathbf{S}}_a \cdot \hat{\mathbf{S}}_b + \hat{\mathbf{S}}_a \overline{\overline{D}}_{ab} \hat{\mathbf{S}}_b \tag{4.2}$$

The model interaction matrix calculated in the $|S_a, M_{Sa}, S_b, M_{Sb}\rangle$ uncoupled basis set is:

$\hat{H}_{mod}$	$\lvert -\frac{1}{2}, -\frac{1}{2}\rangle$	$\lvert -\frac{1}{2}, \frac{1}{2}\rangle$	$\lvert \frac{1}{2}, -\frac{1}{2}\rangle$	$\lvert \frac{1}{2}, \frac{1}{2}\rangle$
$\langle -\frac{1}{2}, -\frac{1}{2}\rvert$	$\frac{1}{4}(J + D^{ab}_{zz})$	$-\frac{1}{4}(D^{ab}_{xz} + iD^{ab}_{yz})$	$-\frac{1}{4}(D^{ab}_{xz} + iD^{ab}_{yz})$	$\frac{1}{4}(D^{ab}_{xx} - D^{ab}_{yy} + 2iD^{ab}_{xy})$
$\langle -\frac{1}{2}, \frac{1}{2}\rvert$	$-\frac{1}{4}(D^{ab}_{xz} - iD^{ab}_{yz})$	$-\frac{1}{4}(J + D^{ab}_{zz})$	$\frac{1}{2}J + \frac{1}{4}(D^{ab}_{xx} + D^{ab}_{yy})$	$\frac{1}{4}(D^{ab}_{xz} + iD^{ab}_{yz})$
$\langle \frac{1}{2}, -\frac{1}{2}\rvert$	$-\frac{1}{4}(D^{ab}_{xz} - iD^{ab}_{yz})$	$\frac{1}{2}J + \frac{1}{4}(D^{ab}_{xx} + D^{ab}_{yy})$	$-\frac{1}{4}(J + D^{ab}_{zz})$	$\frac{1}{4}(D^{ab}_{xz} + iD^{ab}_{yz})$
$\langle \frac{1}{2}, \frac{1}{2}\rvert$	$\frac{1}{4}(D^{ab}_{xx} - D^{ab}_{yy} - 2iD^{ab}_{xy})$	$\frac{1}{4}(D^{ab}_{xz} - iD^{ab}_{yz})$	$\frac{1}{4}(D^{ab}_{xz} - iD^{ab}_{yz})$	$\frac{1}{4}(J + D^{ab}_{zz})$

(4.3)

The following change of basis matrix U is used:

$$U = \begin{pmatrix} 1 & 0 & 0 & 0 \\ 0 & \frac{1}{\sqrt{2}} & 0 & -\frac{1}{\sqrt{2}} \\ 0 & \frac{1}{\sqrt{2}} & 0 & \frac{1}{\sqrt{2}} \\ 0 & 0 & 1 & 0 \end{pmatrix} \tag{4.4}$$

in order to transform the model interaction matrix into the coupled $|S, M_S\rangle$ basis by applying the following relation:

$$\hat{H}_{mod}(coupled) = \widetilde{U}.\hat{H}_{mod}(uncoupled).U \tag{4.5}$$

where $\widetilde{U}$ is the transpose matrix of U. The Hamiltonian matrix in the coupled basis is:

$\hat{H}_{mod}$	$\|1,-1\rangle$	$\|1,0\rangle$	$\|1,1\rangle$	$\|0,0\rangle$
$\langle 1,-1\|$	$\frac{1}{4}J + \frac{1}{4}D_{zz}^{ab}$	$-\frac{1}{2\sqrt{2}}(D_{xz}^{ab} + iD_{yz}^{ab})$	$\frac{1}{4}(D_{xx}^{ab} - D_{yy}^{ab} + 2iD_{xy}^{ab})$	0
$\langle 1,0\|$	$-\frac{1}{2\sqrt{2}}(D_{xz}^{ab} - iD_{yz}^{ab})$	$\frac{1}{4}J - \frac{1}{2}D_{zz}^{ab}$	$\frac{1}{2\sqrt{2}}(D_{xz}^{ab} + iD_{yz}^{ab})$	0
$\langle 1,1\|$	$\frac{1}{4}(D_{xx}^{ab} - D_{yy}^{ab} - i2D_{xy}^{ab})$	$\frac{1}{2\sqrt{2}}(D_{xz}^{ab} - iD_{yz}^{ab})$	$\frac{1}{4}J + \frac{1}{4}D_{zz}^{ab}$	0
$\langle 0,0\|$	0	0	0	$-\frac{3}{4}J$

(4.6)

The J parameter is related to the singlet-triplet energy difference, while the symmetric ZFS tensor $\overline{\overline{D}}_{ab}$ accounts for the splitting and mixing of the spin-orbit components of the triplet state.

The giant spin model only deals with the ZFS of the triplet state. Its expression is:

$$\hat{H}_{mod} = \hat{\mathbf{S}}\overline{\overline{D}}\hat{\mathbf{S}} \tag{4.7}$$

where S=1 in the considered case. This model Hamiltonian is the same as in mononuclear complexes. The same interaction matrix as in the Ni(II) mononuclear complexes is then obtained:

$\hat{H}_{mod}$	$\|1,-1\rangle$	$\|1,0\rangle$	$\|1,1\rangle$
$\langle 1,-1\|$	$\frac{1}{2}D_{zz}$	$-\frac{1}{\sqrt{2}}(D_{xz} + iD_{yz})$	$\frac{1}{2}(D_{xx} - D_{yy} + 2iD_{xy})$
$\langle 1,0\|$	$-\frac{1}{\sqrt{2}}(D_{xz} - iD_{yz})$	$-D_{zz}$	$\frac{1}{\sqrt{2}}(D_{xz} + iD_{yz})$
$\langle 1,1\|$	$\frac{1}{2}(D_{xx} - D_{yy} - 2iD_{xy})$	$\frac{1}{\sqrt{2}}(D_{xz} - iD_{yz})$	$\frac{1}{2}D_{zz}$

(4.8)

where the trace has been shifted compared to Eq. 3.2 in order to facilitate the identification between the multispin and the giant spin interaction matrices. According to matrices 4.6 and 4.8, the following relation appears between $\overline{\overline{D}}_{ab}$ and $\overline{\overline{D}}$:

$$\overline{\overline{D}} = \frac{1}{2}\overline{\overline{D}}_{ab} \tag{4.9}$$

One may notice that the same relation is obtained when using the coupling coefficients of Eq. 1.12 ($2C_{ab} = 1$) (see section 1.4.1) [11, 23]. In the $d^9 - d^9$ configuration, the symmetric terms of the spin Hamiltonian cannot bring any spin mixing effects. Hence, no distinction between the strong- and weak-exchange limits can be done, and both treatments (calculation of the interaction matrix in the uncoupled basis and change of basis to the coupled one or the use of the coupling coefficients) are perfectly equivalent.

Analytical Derivation of the Spin-orbit Contribution to the Symmetric Exchange

In copper acetate, the geometrical structure is very close to D_{2h}. The most particular direction which here corresponds to the easy axis of magnetization is along the Cu-Cu direction. Another consequence of this almost highly symmetric structure is that both the SOC and SSC induce almost the same magnetic axes frame while considered separately. The total D and E parameters calculated in a joint $SOC + SSC$ treatment can be approximated by the sum of the parameters obtained in separate SOC and SSC calculations:

$$\begin{aligned} D_{SSC+SOC} &\approx D_{SSC} + D_{SOC} \\ E_{SSC+SOC} &\approx E_{SSC} + E_{SOC} \end{aligned} \tag{4.10}$$

Since the SSC and the SOC interactions can be considered separately, and since the SSC contribution is not the dominant one, the analytical derivations only deal with the SOC. Such a rationalization of the SOC effect is important in order to illustrate the challenge of the theoretical calculation of the SOC contribution to the ZFS in the copper acetate. The SSC, which also contributes to the ZFS will be included in the *ab initio* calculations.

Analytical expressions for D_{SOC} already exist in the literature [2, 127]. However, no expression was provided for E_{SOC}, and hence the entire derivations for D_{SOC} and E_{SOC} are

provided for the sake of clarity. In the D_{2h} symmetry point group and in a crystal field approach, the electronic configuration in the lowest-lying singlet and triplet states contains two unpaired electrons in the local $d_{x^2-y^2}$ atomic orbitals (on site a and b). The M_S=1 component of the lowest A_u triplet state is:

$$|\Phi^T_{x^2-y^2}, 1\rangle = |d_{x^2-y^2}(a)d_{x^2-y^2}(b)\rangle \tag{4.11}$$

where only the orbitals of the unpaired electrons are specified and the letter T is used to indicate the triplet spin multiplicity (triplet state). The model space is spanned by the three M_S components of this state. In order to rationalize the ZFS, the external space has to be defined. The same criteria as in the mononuclear cases are used. Only the 'neutral' states in the valence bond sense are considered. Such states are characterized by a dominant d^9-d^9 local configuration (while the 'ionic' states would have dominant d^8-d^{10} local configurations). Only the local singly excited states of A_u symmetry are considered since the states of A_g symmetry cannot be coupled with the model space for symmetry reasons. Four triplet and four singlet spin-orbit free states are then considered in the external space, the maximum M_S components of which can be expressed as follows:

$$\begin{aligned}
|\Phi^T_n, 1\rangle &= \frac{1}{\sqrt{2}}[|d_n(a)d_{x^2-y^2}(b)\rangle + |d_{x^2-y^2}(a)d_n(b)\rangle] \\
|\Phi^S_n, 0\rangle &= \frac{1}{2}[|d_n(a)\bar{d}_{x^2-y^2}(b)\rangle - |\bar{d}_n(a)d_{x^2-y^2}(b)\rangle - |d_{x^2-y^2}(a)\bar{d}_n(b)\rangle + |\bar{d}_{x^2-y^2}(a)d_n(b)\rangle]
\end{aligned} \tag{4.12}$$

where the index n is used in order to characterize the local excitation from a d_n atomic orbital ($n = xz$, yz, xy or z^2) and where S stands for singlet spin state.

As in section 3.2, the monoelectronic SOC Hamiltonian is applied and the analytical effective interaction matrix is built using the QDPT at second-order.

$\hat{H}_{eff}$	$\lvert 1,-1\rangle$	$\lvert 1,0\rangle$	$\lvert 1,1\rangle$
$\langle 1,-1\rvert$	$-\frac{2\zeta^2}{\Delta\Phi^T_{xy}}-\frac{\zeta^2}{4\Delta\Phi^T_{xz}}-\frac{\zeta^2}{4\Delta\Phi^S_{xz}}-\frac{\zeta^2}{4\Delta\Phi^T_{yz}}-\frac{\zeta^2}{4\Delta\Phi^S_{yz}}$	0	$\frac{\zeta^2}{4\Delta\Phi^T_{xz}}-\frac{\zeta^2}{4\Delta\Phi^S_{xz}}-\frac{\zeta^2}{4\Delta\Phi^T_{yz}}+\frac{\zeta^2}{4\Delta\Phi^S_{yz}}$
$\langle 1,0\rvert$	0	$-\frac{2\zeta^2}{\Delta\Phi^S_{xy}}-\frac{\zeta^2}{2\Delta\Phi^T_{xz}}-\frac{\zeta^2}{2\Delta\Phi^T_{yz}}$	0
$\langle 1,1\rvert$	$\frac{\zeta^2}{4\Delta\Phi^T_{xz}}-\frac{\zeta^2}{4\Delta\Phi^S_{xz}}-\frac{\zeta^2}{4\Delta\Phi^T_{yz}}+\frac{\zeta^2}{4\Delta\Phi^S_{yz}}$	0	$-\frac{2\zeta^2}{\Delta\Phi^T_{xy}}-\frac{\zeta^2}{4\Delta\Phi^T_{xz}}-\frac{\zeta^2}{4\Delta\Phi^S_{xz}}-\frac{\zeta^2}{4\Delta\Phi^T_{yz}}-\frac{\zeta^2}{4\Delta\Phi^S_{yz}}$

(4.13)

with:

$$\Delta\Phi_n^{T,S} = E\left(\Phi_n^{T,S}\right) - E\left(\Phi_{x^2-y^2}^T\right) \tag{4.14}$$

the excitation energies between the $\Phi_n^{T,S}$ spin-orbit free states and the triplet ground state $\Phi_{x^2-y^2}^T$.

The D parameter is calculated as follows:

$$\begin{aligned}
D &= \langle\Phi_{x^2-y^2}^T, \pm1|H_{eff}|\Phi_{x^2-y^2}^T, \pm1\rangle - \langle\Phi_{x^2-y^2}^T, 0|H_{eff}|\Phi_{x^2-y^2}^T, 0\rangle \\
D &= +\frac{2\zeta^2}{\Delta\Phi_{xy}^S} - \frac{2\zeta^2}{\Delta\Phi_{xy}^T} - \frac{\zeta^2}{4\Delta\Phi_{xz}^S} + \frac{\zeta^2}{4\Delta\Phi_{xz}^T} - \frac{\zeta^2}{4\Delta\Phi_{yz}^S} + \frac{\zeta^2}{4\Delta\Phi_{yz}^T} \\
D &= \frac{2\zeta^2\left(\Delta\Phi_{xy}^T - \Delta\Phi_{xy}^S\right)}{\Delta\Phi_{xy}^T\Delta\Phi_{xy}^S} - \frac{\zeta^2\left(\Delta\Phi_{xz}^T - \Delta\Phi_{xz}^S\right)}{4\Delta\Phi_{xz}^T\Delta\Phi_{xz}^S} - \frac{\zeta^2\left(\Delta\Phi_{yz}^T - \Delta\Phi_{yz}^T\right)}{4\Delta\Phi_{yz}^S\Delta\Phi_{yz}^S}
\end{aligned} \tag{4.15}$$

The $\Delta E_{x^2-y^2,n}$ are the geometric means between the $\Delta\Phi_n^T$ and $\Delta\Phi_n^S$ excitation energies and the $J_{x^2-y^2,n}$ are the magnetic couplings between the Φ_n^T and Φ_n^S excited states:

$$\begin{aligned}
\Delta E_{x^2-y^2,n} &= \sqrt{\Delta\Phi_n^T.\Delta\Phi_n^S} \\
J_{x^2-y^2,n} &= E\left(\Phi_n^T\right) - E\left(\Phi_n^S\right)
\end{aligned} \tag{4.16}$$

Finally, the expression of the D parameter is:

$$D = 2\frac{\zeta^2 J_{x^2-y^2,xy}}{\Delta E_{x^2-y^2,xy}^2} - \frac{1}{4}\frac{\zeta^2 J_{x^2-y^2,xz}}{\Delta E_{x^2-y^2,xz}^2} - \frac{1}{4}\frac{\zeta^2 J_{x^2-y^2,yz}}{\Delta E_{x^2-y^2,yz}^2} \tag{4.17}$$

The E parameter is calculated from:

$$\begin{aligned}
E &= \langle\Phi_{x^2-y^2}^T, \pm1|H_{eff}|\Phi_{x^2-y^2}^T, \mp1\rangle \\
E &= -\frac{\zeta^2}{4\Delta\Phi_{xz}^S} + \frac{\zeta^2}{4\Delta\Phi_{xz}^T} + \frac{\zeta^2}{4\Delta\Phi_{yz}^S} - \frac{\zeta^2}{4\Delta\Phi_{yz}^T} \\
E &= -\frac{\zeta^2\left(\Delta\Phi_{xz}^T - \Delta\Phi_{xz}^S\right)}{4\Delta\Phi_{xz}^T\Delta\Phi_{xz}^S} + \frac{\zeta^2\left(\Delta\Phi_{yz}^T - \Delta\Phi_{yz}^S\right)}{4\Delta\Phi_{yz}^T\Delta\Phi_{yz}^S}
\end{aligned} \tag{4.18}$$

which leads to the following expression:

$$E = \frac{1}{4}\frac{\zeta^2 J_{x^2-y^2,yz}}{\Delta E^2_{x^2-y^2,yz}} - \frac{1}{4}\frac{\zeta^2 J_{x^2-y^2,xz}}{\Delta E^2_{x^2-y^2,xz}} \quad (4.19)$$

Since the $d_{x^2-y^2}$ and d_{z^2} atomic orbitals cannot be coupled by the monoelectronic SOC, $\Phi^T_{z^2}$ and $\Phi^S_{z^2}$ do not contribute to the ZFS at second-order of perturbation, and hence does not appear in the obtained analytical formulae of D and E.

Eqs. 4.17 and 4.19 provide useful information concerning the physical origin of the ZFS and the difficulty to accurately calculate D_{SOC} and E_{SOC} using *ab initio* calculations. Indeed, the ZFS is directly linked to the $\Delta E_{x^2-y^2,n}$ and the $J_{x^2-y^2,n}$ parameters. While both quantities are sensitive to dynamic correlation (as the excitation energies in mononuclear complexes), the accurate descriptions of magnetic couplings which are generally very small require the use of highly correlated methods. This methodological challenge is the subject of the next paragraph.

The Crucial Role of the Dynamic Correlation on the Spin Hamiltonian Parameters

According to matrix 4.6, the value of J extracted after a SI calculation can be slightly different than the one extracted from a spin-orbit free calculation if the SOC has a differential effect on the singlet and triplet components. However, as it will be shown in section 4.1.2, in practice, this effect is neglible and one may directly extract the J parameter of the spin Hamiltonian from the spin-orbit free calculations. Since the lowest singlet state belongs to the A_g symmetry, it will of course not be considered in the SI space.

Various post-CASSCF calculations are performed using a CAS(2/2)SCF reference wavefunctions of the lowest-lying ^1A_g and ^3A_u. The DDCI2 and DDCI3 calculations use the following thresholds [82]: T_{pre}=10^{-5} a.u. and T_{sel}=10^{-8} a.u., *i.e.* tight values. The $J_{x^2-y^2,x^2-y^2}$ parameter is extracted using Eq. 4.16. Results are reported in Table 4.1.

As usual, the CASSCF value is far from the experimental one. The NEVPT2 method does not introduce enough dynamic correlation to provide an estimate of the magnetic coupling and the corresponding J value is also far away from the experimental one. According to the large difference between the DDCI2 and DDCI3 values, the 2h-1p and 1h-2p play a crucial role on this magnetic coupling, and have to be treated variationnaly in order to relax the 1h and 1p

Method	$J_{x^2-y^2,x^2-y^2}$
CASSCF	+18.9
NEVPT2	+39.8
DDCI2	+67.5
DDCI3	+271.3
Experiment [128]	+292.2

Table 4.1: Ground state magnetic coupling (in cm^{-1}) in copper acetate monohydrate computed using different methods.

excitations [71–73]. At the DDCI3 level, the computed value is very close to the experimental one, as already noticed in previous studies of magnetic couplings.

The role of the dynamic correlation on the ZFS in binuclear complexes has never been studied theoretically by means of state-of-art *ab initio* calculations. In order to perform such a study, various post-CASSCF methods are considered on top of a CAS(18/10)SCF reference calculation. The effects of the SOC, SSC and joint treatment of the SOC and SSC on the ZFS parameters are included in SI calculations. Dynamic correlation is introduced by replacing the diagonal elements of the SI matrix by the energies obtained at the post-CASSCF levels (see Table 4.2). As in the analytical derivation, the SI space consists in five ^3A_u and four ^1A_u spin-orbit free states. The ZFS parameters are extracted from the eigenvalues of the SI matrix.

Since the effect of dynamic correlation is included only though a shift of the diagonal of the SI matrix and since the SSC is only a first order effect (the second order contributions are non zero but their numerical contributions are negligible), the contribution of the SSC is identical at all levels of theory in Table 4.2. The approximation of Eq. 4.10 is relevant at all levels of theory. The ZFS parameters are well reproduced by the DDCI3 method since the $J_{x^2-y^2,n}$ parameters are well treated at this level of theory.

Since dynamic correlation obviously plays a crucial role on the ZFS in copper acetate, one may think that the use of correlated wavefunctions in the calculation of the off-diagonal elements of the SI matrix would improve the results. Test calculations performed at the DDCI2 and DDCI3 levels are presented in Table 4.3. Although the results seem disappointing at

Method	D_{SSC}	D_{SOC}	$D_{SSC+SOC}$	E_{SSC}	E_{SOC}	$E_{SSC+SOC}$
CASSCF	-0.118	-0.017	-0.137	0.000	0.001	0.000
NEVPT2	-0.118	-0.026	-0.144	0.000	0.003	0.003
DDCI2	-0.118	-0.172	-0.291	0.000	0.002	0.002
DDCI3	-0.118	-0.200	-0.319	0.000	0.006	0.006
Experiment [33]	-	-	-0.335	-	-	0.01

Table 4.2: ZFS parameters (in cm^{-1}) in copper acetate monohydrate extracted from either SOC or SSC calculations separately or combining both SOC and SSC in the SI matrix. Wavefunctions are the CAS(18,10)SCF ones while the energies used in the SI matrix are those of the indicated methods.

Method	D_{SSC}	D_{SOC}	$D_{SSC+SOC}$	E_{SSC}	E_{SOC}	$E_{SSC+SOC}$
DDCI2	-0.100	-3.321	-3.442	0.000	0.066	0.006
DDCI3	-0.091	-2.303	-2.394	0.000	0.052	0.052

Table 4.3: ZFS parameters (in cm^{-1}) in copper acetate monohydrate extracted from separate SOC or SSC calculations, or from combining SOC and SSC in the SI matrix. Correlated energies and wave functions of the indicated methods are used in the SI matrix.

first sight, they deserve to be commented. Concerning the SSC, dynamic correlation plays a moderate role, justifying its calculation with the CASSCF wavefunctions as done in Table 4.2. The treatment of the SOC is problematic: the calculated values are very far from the experimental one when using the correlated wavefunctions. This effect is attributed to truncation problems. As already mentionned, the excitations have to be perfectly balanced in all directions of space in order to avoid any artefacts. The used correlated wavefunctions are here solutions of truncated CI and nothing guarantees that the excitation selected are sufficiently well balanced in space for a correct treatment of the anisotropy, while the CASSCF wavefunctions are solutions of a full CI interaction within a certain active space, and then well balanced if the active space is properly chosen. Hence, at this stage, the only recommended solution in two-step SI approaches consists in shifting the diagonal elements of the SI matrix with correlated energies.

Method	D_{SOC} (Eq. 4.17)	D_{SOC} (*Ab initio*)	E_{SOC} (Eq. 4.19)	E_{SOC} (*Ab initio*)
CASSCF	0.047	-0.017	0.005	0.001
NEVPT2	0.025	-0.026	0.003	0.003
DDCI2	-0.143	-0.172	0.005	0.001
DDCI3	-0.179	-0.200	0.003	0.006

Table 4.4: SOC contributions to the ZFS parameters in copper acetate monohydrate calculated with Eqs. 4.17 and 4.19 with $J_{x^2-y^2,n}$ and $\Delta E_{x^2-y^2,n}$ obtained from CASSCF, NEVPT2, DDCI2 and DDCI3 calculations. Results are compared with the *ab initio* ZFS parameters. All values are given in cm^{-1}.

Numerical Validation of the Analytical Formulae for the Zero-Field Splitting Parameters

In order to validate the analytical formulae presented in Eqs. 4.17 and 4.19, the D_{SOC} and E_{SOC} values obtained using the *ab initio* $\Delta E_{x^2-y^2,n}$ and $J_{x^2-y^2,n}$, the $\zeta_{free-ion}$=829 cm^{-1} spin-orbit constant and these formulae are compared to the computed ones. The results obtained at all levels of theory are in good agreement with the *ab initio* values (see Table 4.4) even if at the CASSCF and NEVPT2 levels, the sign of the D parameter is not reproduced. The differences between the computed and reproduced values may be attrituted to the use of the spin-orbit constant of the free-ion and to higher than second order effects.

The contribution of each orbital excitation to the D_{SOC} parameter obtained at the DDCI3 level with Eq. 4.17 are detailed in Table 4.5. As expected according to Eq. 4.17, the $n = xy$ excitation dominates the axial ZFS (its contribution having both a larger prefactor and a smaller denominator than the others). Since the $n = xz$ and $n = yz$ excitations have similar $J_{x^2-y^2,n}$ and $\Delta E_{x^2-y^2,n}$ values, their contributions to D_{SOC} are almost identical at second-order of perturbation and almost cancel in E_{SOC}, leading to a particularly small rhombic parameter.

Bleaney and Bowers [2], as well as Ross *et al.* [127] already used a similar expression of D to determine its sign and magnitude from experimental measurements. However, they found it positive, while it is actually negative [33]. The reasons why they found a wrong sign is linked to the use of wrong values of $J_{x^2-y^2,n}$ in the formula. Bleaney and Bowers considered

n	$\Delta E_{x^2-y^2,n}$	$J_{x^2-y^2,n}$	$D_{SOC}(n)$
xy	12280	-29.9	-0.276
z^2	13313	-359.0	0.000
xz	15090	-64.0	+0.048
yz	15510	-63.9	+0.045
Total			-0.179
Ab initio			-0.200

Table 4.5: $\Delta E_{x^2-y^2,n}$, $J_{x^2-y^2,n}$ and their contributions to D_{SOC} decomposed into contributions arising from the different excited states. Spin free quantities are obtained at the DDCI3 level. All values are given in cm^{-1}.

that all the $J_{x^2-y^2,n}$ parameters were equal to $J_{x^2-y^2,x^2-y^2}$. Since, as shown in Tables 4.1 and 4.5, $J_{x^2-y^2,x^2-y^2}$ and the other $J_{x^2-y^2,n}$ parameters have opposite sign, the correct expression of Eq. 4.17 led to the wrong sign of D. Concerning the work of Ross *et al.*, the $J_{x^2-y^2,xy}$ parameter that is responsible for the D sign was extracted from the A_g symmetry states and had the wrong sign as well.

The ZFS in copper acetate has been consistenly revisited by both the experimental work of Ozarowski [33] and the present theoretical work. From a methodological point of view, the computation of the ZFS in copper acetate happened to be particularly challenging since (i) a highly accurate spin-orbit free spectrum had to be computed and (ii) both SOC and SSC provide non-negligible contributions to the ZFS parameters. The crucial role of the dynamic correlation has been related to the analytical expressions of D and E that involve magnetic couplings in excited states. Hence, the control of the anisotropic exchange appears complicated in binuclear complexes since it is related to the synergistic or antagonist effects of various contributions that are linked to the magnetic couplings between excited states.

4.1.2 Antisymmetric Exchange in $[Cu_2O(H_2O)_6]^{2+}$ Model Complexes

Introduction and Description of the Models

The antisymmetric exchange, first introduced by Dzyaloshinskii in 1958 [4], and Moriya in 1960 [5], occurs in polynuclear species. For binuclear complexes, the symmetry rules allowing

or prohibiting this interaction are well known [31]. However, the norm of the DM vector is still far from being predictable in any given structure, not even in bi-, tri- and tetra-nuclear complexes [129]. The extraction of the DM vector from experiment is problematic, since all interactions of the spin Hamiltonian (isotropic, symmetric and antisymmetric) are difficult to separate from EPR spectroscopy [130]. One may however quote some experimental evidences on a differic binuclear complex [131], and a trinuclear Cu(II) complex for instance [132].

Insights from theory could help in experimental extractions and in interpretations of the physical origin of the antisymmetric exchange. However, the DM vector has never been determined from *ab initio* calculations although the two-step SI approach can be used to calculate the antisymmetric anisotropy. The extraction of the DM vector requires the use of the effective Hamiltonian theory. The present section aims to apply this methodology and evaluate its ability to determine the DM vector.

Since no experimental data exists for Cu(II) binuclear systems, the full study is performed on model complexes. In order to propose magneto-structural correlations and provide more insights on the mechanisms leading to antisymmetric anisotropy, the studied geometries have systematically been varied. Two deformations are applied to the $[Cu_2O(H_2O)_6]^{2+}$ model, mimicking the main deformations observed in the real copper oxide materials. The first one, characterized by the ϑ_1 angular deformation plays with the Cu-O-Cu angle while the second one plays with the twist angle ϑ_2 between the two copper planes (see Fig. 4.2). The Cu-O distances have been fixed to 2 Å and the O-H distances are 0.96 Å. The mechanisms discussed first by Moriya [5], and more recently by Moskvin [34] will be studied for structures having different ϑ_1 values.

In order to keep a consistent SI space all along the studied deformations, all the 'neutral' valence states have been included in the SI space for the CAS(18/10) calculations. The minimal CAS(2/2) active space and the corresponding SI space has also been considered, in order to get more insights on the origin of the DM vector.

The Multispin Hamiltonian and the Model Interaction Matrix

The model interaction matrix should also take into account the antisymmetric exchange interaction. One convenient way consists in rewriting the model Hamiltonian presented in Eq. 4.1 in the following form:

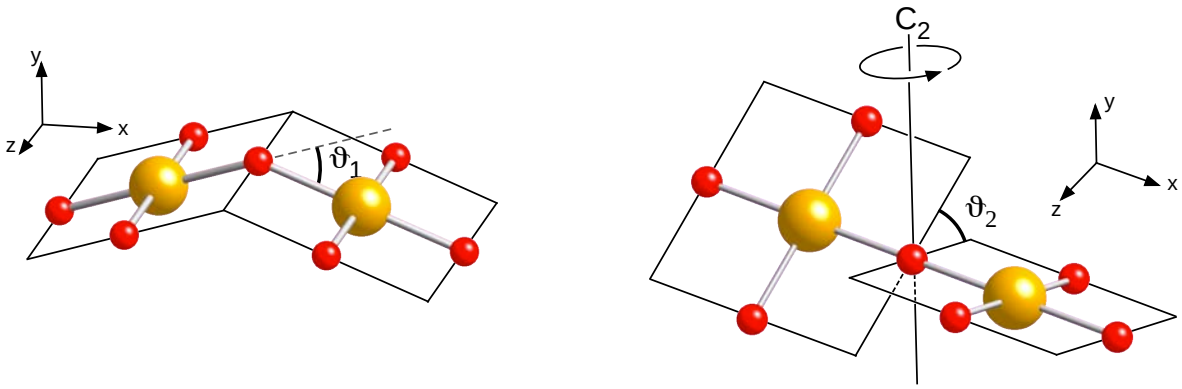

Figure 4.2: Schematic representation of the distortions applied to the $[Cu_2O(H_2O)_6]^{2+}$ model complex. Large spheres represent Cu and smaller spheres are oxygens.

$$\hat{H}_{mod} = J\hat{\mathbf{S}}_a \cdot \hat{\mathbf{S}}_b + \hat{\mathbf{S}}_a \overline{\overline{T}} \hat{\mathbf{S}}_b \tag{4.20}$$

where $\overline{\overline{T}}$ is a non-symmetric second-order tensor (*i.e.* $T_{ij} \neq T_{ji}$). The same process as in section 4.1.1 is used in order to built the model interaction matrix in both uncoupled and coupled basis sets.

$\hat{H}_{mod}$	$\lvert -\frac{1}{2}, -\frac{1}{2}\rangle$	$\lvert -\frac{1}{2}, \frac{1}{2}\rangle$	$\lvert \frac{1}{2}, -\frac{1}{2}\rangle$	$\lvert \frac{1}{2}, \frac{1}{2}\rangle$
$\langle -\frac{1}{2}, -\frac{1}{2}\rvert$	$\frac{1}{4}(J + T_{zz})$	$-\frac{1}{4}(T_{zx} + iT_{zy})$	$-\frac{1}{4}(T_{xz} + iT_{yz})$	$\frac{1}{4}[T_{xx} - T_{yy} + i(T_{xy} + T_{yx})]$
$\langle -\frac{1}{2}, \frac{1}{2}\rvert$	$-\frac{1}{4}(T_{zx} - iT_{zy})$	$-\frac{1}{4}(J + T_{zz})$	$\frac{1}{2}J + \frac{1}{4}[T_{xx} + T_{yy} + i(T_{yx} - T_{xy})]$	$\frac{1}{4}(T_{xz} + iT_{yz})$
$\langle \frac{1}{2}, -\frac{1}{2}\rvert$	$-\frac{1}{4}(T_{xz} - iT_{yz})$	$\frac{1}{2}J + \frac{1}{4}[T_{xx} + T_{yy} - i(T_{yx} - T_{xy})]$	$-\frac{1}{4}(J + T_{zz})$	$\frac{1}{4}(T_{zx} + iT_{zy})$
$\langle \frac{1}{2}, \frac{1}{2}\rvert$	$\frac{1}{4}[T_{xx} - T_{yy} - i(T_{xy} + T_{yx})]$	$\frac{1}{4}(T_{xz} - iT_{yz})$	$\frac{1}{4}(T_{zx} - iT_{zy})$	$\frac{1}{4}(J + T_{zz})$

(4.21)

$\hat{H}_{mod}$	$\lvert 1, -1\rangle$	$\lvert 1, 0\rangle$	$\lvert 1, 1\rangle$	$\lvert 0, 0\rangle$
$\langle 1, -1\rvert$	$\frac{1}{4}(J + T_{zz})$	$-\frac{\sqrt{2}}{8}[T_{xz} + T_{zx} + i(T_{yz} + T_{zy})]$	$\frac{1}{4}[T_{xx} - T_{yy} + i(T_{xy} + T_{yx})]$	$-\frac{\sqrt{2}}{8}[T_{xz} - T_{zx} + i(T_{yz} - T_{zy})]$
$\langle 1, 0\rvert$	$-\frac{\sqrt{2}}{8}[T_{xz} + T_{zx} - i(T_{yz} + T_{zy})]$	$\frac{1}{4}(J + T_{xx} + T_{yy} - T_{zz})$	$\frac{\sqrt{2}}{8}[T_{xz} + T_{zx} + i(T_{yz} + T_{zy})]$	$-\frac{i}{4}(T_{xy} - T_{yx})$
$\langle 1, 1\rvert$	$\frac{1}{4}[T_{xx} - T_{yy} - i(T_{xy} + T_{yx})]$	$\frac{\sqrt{2}}{8}[T_{xz} + T_{zx} - i(T_{yz} + T_{zy})]$	$\frac{1}{4}(J + T_{zz})$	$-\frac{\sqrt{2}}{8}[T_{xz} - T_{zx} - i(T_{yz} - T_{zy})]$
$\langle 0, 0\rvert$	$-\frac{\sqrt{2}}{8}[T_{xz} - T_{zx} - i(T_{yz} - T_{zy})]$	$\frac{i}{4}(T_{xy} - T_{yx})$	$-\frac{\sqrt{2}}{8}[T_{xz} - T_{zx} + i(T_{yz} - T_{zy})]$	$\frac{1}{4}(-3J - T_{xx} - T_{yy} - T_{zz})$

(4.22)

The symmetric and antisymmetric components of the second-order ZFS tensor $\overline{\overline{T}}$ are then separated as follows:

$$\begin{aligned} D_{ii} &= T_{ii} \\ D_{ij} = D_{ji} &= \frac{1}{2}(T_{ij} + T_{ji}) \\ d_{ij} = -d_{ji} &= \frac{1}{2}(T_{ij} - T_{ji}) \end{aligned} \tag{4.23}$$

The antisymmetric terms appear in the singlet-triplet off-diagonal elements between the singlet and the triplet components. The antisymmetric second-order tensor is usually reduced as a pseudo-vector (the DM one), whose components might be expressed as follow:

$$d_x = d_{yz} \qquad d_y = -d_{xz} \qquad d_z = d_{xy} \tag{4.24}$$

Extraction of the Spin Hamiltonian

In order to check the validity of the model spin Hamiltonian presented in Eqs. 4.1 and 4.20 (the two expressions being equivalent), and to illustrate the extraction process, the effective Hamiltonian is detailed in the specific case $\vartheta_1 = \vartheta_2 = 45°$. The projection of the four lowest-lying SO states onto the model space are close to 98%, showing that the spin Hamiltonian approach is relevant in this case (the structures have been chosen in order to prohibit any near degeneracy effects in all the studied structures). The following effective interaction matrix (in cm^{-1}) is obtained in the coupled basis set:

$\hat{H}_{eff}$	$\|1,-1\rangle$	$\|1,0\rangle$	$\|1,1\rangle$	$\|0,0\rangle$
$\langle 1,-1\|$	50.557	0.024	0.168	$0.657i$
$\langle 1,0\|$	0.024	49.781	-0.024	$7.015i$
$\langle 1,1\|$	0.168	0.024	50.557	$-0.657i$
$\langle 0,0\|$	$-0.657i$	$7.015i$	$0.657i$	1.006

(4.25)

This interaction matrix perfectly matches matrix 4.22, demonstrating the validity of the spin Hamiltonian presented in Eqs. 4.1 and 4.20. The non-symmetric ZFS tensor is then extracted after having substracted J=49.292 cm^{-1} and fixed $T_{xx}+T_{yy}+T_{zz} = 0$ for convenience (numbers in cm^{-1}):

$$\overline{\overline{T}} = \begin{pmatrix} T_{xx} & T_{xy} & T_{xz} \\ T_{yx} & T_{yy} & T_{yz} \\ T_{zx} & T_{zy} & T_{zz} \end{pmatrix} = \begin{pmatrix} -0.181 & 14.030 & -0.068 \\ -14.030 & -0.853 & -1.858 \\ -0.068 & 1.858 & 1.034 \end{pmatrix} \tag{4.26}$$

and separated into a symmetric part (numbers in cm^{-1}):

$$\overline{\overline{D}} = \begin{pmatrix} D_{xx} & D_{xy} & D_{xz} \\ D_{xy} & D_{yy} & D_{yz} \\ D_{xz} & D_{yz} & D_{zz} \end{pmatrix} = \begin{pmatrix} -0.181 & 0 & -0.068 \\ 0 & -0.853 & 0 \\ -0.068 & 0 & 1.034 \end{pmatrix} \tag{4.27}$$

and an antisymmetric one (numbers in cm^{-1}):

$$\overline{\overline{d}} = \begin{pmatrix} 0 & d_{xy} & d_{xz} \\ -d_{yx} & 0 & d_{yz} \\ -d_{zx} & -d_{zy} & 0 \end{pmatrix} = \begin{pmatrix} 0 & 14.030 & 0 \\ -14.030 & 0 & -1.858 \\ 0 & 1.858 & 0 \end{pmatrix} \tag{4.28}$$

As usual, zero terms in the ZFS tensors (symmetric and antisymmetric) are characteristics of the symmetry of the system and the axes frame used in the *ab initio* calculation. Indeed, the model structure possesses a C_2 symmetry axis that has been oriented along the y axis in the calculation. As a consequence, $D_{xy} = D_{yz} = 0$, and $d_{xz} = 0$ [31]. Indeed, one of the magnetic axis determined with the symmetric ZFS tensor has to be oriented along the C_2 axis, and the DM vector has to be perpendicular to this C_2 axis. In the C_2 symmetry point group, the DM vector has no reason to coincide with one of the magnetic axis. The DM vector might be finally expressed as follow (numbers in cm^{-1}):

$$\overline{d} = \begin{pmatrix} d_{yz} \\ -d_{xz} \\ d_{xy} \end{pmatrix} = \begin{pmatrix} -1.858 \\ 0 \\ 14.030 \end{pmatrix} \tag{4.29}$$

If one defines the magnetic axes frame with the symmetric ZFS tensor, the DM vector can be expressed in this frame by following the same transformation as the coordinates (see Eq. 3.9, the conventions for D and E have also to be applied for the attribution of X, Y, and Z). Hence, the 10 parameters of the spin Hamiltonian that appear in any arbitrary axes frames can be extracted safely from the effective Hamiltonian theory. The magnetic axes frame is still defined with the symmetric part of the ZFS tensor. The DM vector, by allowing to mix

	J(Spin-free)		J(RASSI-SO)	
$\vartheta_1 = \vartheta_2$	CASSCF	CASPT2	CASSCF	CASPT2
0°	153	562	151	557
15°	138	515	136	509
45°	50	236	49	232
75°	−18	−19	−17	−20
90°	−20	−97	−21	−96

Table 4.6: Spin-free and RASSI-SO J parameter (in cm^{-1}) for several model geometries. RASSI-SO calculations were performed with 25 triplet and 25 singlet spin-free states and using the CAS(18/10)SCF and CAS(18/10)PT2 energies on the diagonal of the SI matrix.

effectively the triplet components with the singlet one then play an important role on the property, particularly in the case of weak-exchange limit. From a methodological point of view, the role of the dynamic correlation on the ZFS parameters has to be studied. This is the subject of the next paragraph.

Role of Dynamic Correlation on the Spin Hamiltonian Interactions

The role of dynamic correlation on the different parameters of the spin Hamiltonian have been studied for several geometries in which $\vartheta_1 = \vartheta_2$.

The role of dynamic correlation on the magnetic coupling J has already been commented in the copper acetate study. Table 4.6 reports the values of J obtained at the CAS(18/10)SCF and CAS(18/10)PT2 levels before and after the SI calculation. As usual, the J parameter is deeply affected by dynamic correlation as shown by the comparison of the CASSCF and CASPT2 results. The extraction of the magnetic coupling parameter is independent in practice on the inclusion of the SOC. The deformation affects drastically J, which is large and antiferromagnetic in the $\vartheta_1 = \vartheta_2 = 0$ structure and becomes small and ferromagnetic for $\vartheta_1 = \vartheta_2 = 90°$. The ϑ_1 deformation dominates this effect, as expected from the Goodenough-Kanamori-Anderson rules [133–135].

Table 4.7 shows the results obtained at the CASSCF and CASPT2 levels for the D and E parameters. Here again, dynamic correlation plays an important role on the magnitude

	CASSCF		CASPT2	
$\vartheta_1 = \vartheta_2$	D	E	D	E
0°	−1.62	0.08	−0.90	0.02
15°	−1.52	0.02	−0.71	0.14
45°	1.56	0.33	−1.66	0.20
75°	3.38	0.10	−3.27	0.57
90°	4.60	0.27	−4.10	1.22

Table 4.7: Symmetric anisotropy parameters D and E (in cm^{-1}) for several model geometries extracted from the RASSI-SO calculations with 25 triplet and 25 singlet spin-free states. The use of CAS(18/10)SCF energies for the spin-free states is compared to the use of CASPT2 energies.

of the ZFS parameters. While the attribution of the magnetic anisotropy axes X, Y and Z is susceptible for changes along the deformation, the principal axes of the second-order symmetric ZFS tensor are similar in all structures whatever the level of calculation is.

While the J, D and E parameters are sensitive to dynamic correlation and particularly difficult to calculate accurately, the $|\overline{d}|$ and φ values presented in Table 4.8 are consistent at all levels of calculation. With the minimal active space and SI space, the replacement of the diagonal elements of the SI matrix cannot change the computed $|\overline{d}|$ and φ values since the DM vector components originate at first order of SOC. Using a larger active space and introducing the excited states in the SI space could however modify the DM vector through second-order effects. However, since the results obtained from CAS(2/2)SCF, CAS(18/10)SCF and CAS(18/10)PT2 calculations are in good agreement, one may conclude that the first order effects are dominant.

One may therefore use minimal active and SI spaces in order to calculate relevant estimates of the antisymmetric exchange. In the next paragraph both the ϑ_1 and ϑ_2 angles will be varied and magneto-structural correlations will be proposed.

	CAS(2/2)		CAS(18/10)		CAS(18/10)PT2	
$\vartheta_1 = \vartheta_2$	$\lvert\overline{d}\rvert$	φ	$\lvert\overline{d}\rvert$	φ	$\lvert\overline{d}\rvert$	φ
0°	0.00	0.0	0.00	0.0	0.00	0.0
15°	8.35	−0.7	6.98	0.7	9.77	17.2
45°	17.58	−8.5	14.15	−7.5	17.75	7.4
75°	7.78	−17.1	4.97	−16.5	6.76	6.6
90°	7.58	−16.5	7.32	−15.3	6.75	−28.3

Table 4.8: Norm of the DM vector $|\overline{d}|$ (in cm^{-1}) and angle φ (in degrees) of the DM vector with the cartesian z-axis (perpendicular to the Cu-O-Cu plane) for several model geometries.

Deformation	ϑ_1 (°)	ϑ_2 (°)	Point group	d_x	d_z	$\lvert\overline{d}\rvert$
None	0	0	D_{2h}	0	0	0
ϑ_1	$0 < \vartheta_1 \leq 90$	0	C_{2v}	0	$\neq 0$	$\neq 0$
ϑ_2	0	$0 < \vartheta_1 < 90$	D_2	$\neq 0$	0	$\neq 0$
	0	90	D_{2d}	0	0	0
ϑ_1+ϑ_2	$0 < \vartheta_1 \leq 90$	$0 < \vartheta_2 \leq 90$	C_2	$\neq 0^a$	$\neq 0^a$	$\neq 0$

Table 4.9: Symmetry rules for the appearance of the DM vector as functions of the ϑ_1 and ϑ_2 deformation angles. [a] The C_2 axis can here exchange the two magnetic centers.

Relation between the structure and the antisymmetric interaction

All the structures have been calculated using a same axes frame. The y-axis is oriented along the C_2 symmetry axis, the z-axis is perpendicular to the Cu-O-Cu plane. In order to further analyse the hypersurface drawn in Fig. 4.3, the symmetry rules for the appearance of the DM vector are given in Table 4.9 [31]. Since the C_2 axis is maintained in all structures, the d_y component always vanishes.

These symmetry rules can also be seen in Fig. 4.3. The ϑ_1 deformation (as defined in Table 4.9, *i.e.* $\vartheta_2 = 0$ all along the deformation) starts with a vanishing DM vector due to the inversion center. It is non-zero for $\vartheta_1 = 90°$ and passes through a maximum for $\vartheta_1 \approx 40°$. The DM vector has to be perpendicular to the C_2 axis and to the Cu-O-Cu plane (since this

symmetry plane includes both magnetic centers). As a consequence, the DM vector is oriented in this case along the cartesian z-axis.

The ϑ_2 deformation (as defined in Table 4.9, *i.e.* $\vartheta_1 = 0$ all along the deformation) starts and ends with a vanishing DM vector. For $\vartheta_2 = 0$ the appearence of any antisymmetric terms is prohibited due to the inversion center (as in the ϑ_1 deformation), while for $\vartheta_2 = 90°$ the DM vector is prohibited due to the presence of two orthogonal symmetry planes that include the two magnetic centers. In the D_2 symmetry point group, the DM vector has to be colinear to the Cu-Cu direction since this C_2 axis joints the two magnetic centers. Hence, only the d_x components is non-zero in the considered axes frame.

When both deformations are applied simultaneously (deformation $\vartheta_1+\vartheta_2$ in Table 4.9), the only symmetry element that remains, *i.e.* the C_2 axis, can exchange the two magnetic centers. Hence, the DM vector is perpendicular to this cartesian y-axis, and lies in the xz plane. While the ϑ_2 deformation does not induce spectacular antisymmetric terms when applied alone, a synergistic effect between the two deformations leads to a maximal norm of the DM vector for the $(\vartheta_1 = 45°, \vartheta_2 = 90°)$ structure. The norm of the DM vector is in this case around 25 cm^{-1}, showing that this interaction can be very important, as stated recently by Boča [129].

The Main Origin of the Antisymmetric Exchange

As suggested by Table 4.8, it is here considered that the DM vector is dominated at first order of perturbation by the direct coupling between the lowest-lying triplet and singlet state. As a consequence, the DM vector is practically independent on the J value (except that some magneto-structural correlations may be found for J and for the DM vector, but no obvious correlation appears between both interactions). From expressions 4.22, 4.23 and 4.24, the total DM vector can be approximated as follows:

$$\begin{aligned} d_x &\approx -2\sqrt{2}Im\left(\langle 1,-1|\hat{H}_{SOC}|0,0\rangle\right) \\ d_y &\approx 2\sqrt{2}Re\left(\langle 1,-1|\hat{H}_{SOC}|0,0\rangle\right) \\ d_z &\approx -2Im\left(\langle 1,0|\hat{H}_{SOC}|0,0\rangle\right) \end{aligned} \tag{4.30}$$

where 'Im' refers to the imaginary part and 'Re' to the real one.

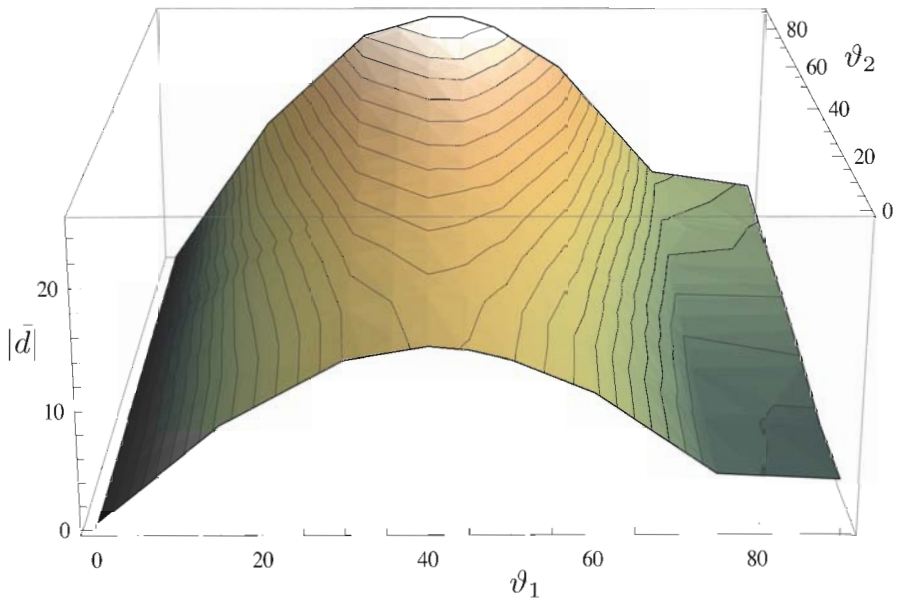

Figure 4.3: Norm of the DM vector (in cm^{-1}) in the $[Cu_2O(H_2O)_6]^{2+}$ model complexes as a function of the ϑ_1 and ϑ_2 deformation angles (in degrees) obtained at the CAS(2/2)/RASSI-SO level.

In order to illustrate the main mechanisms leading to antisymmetric exchange, only the ϑ_1 deformation is considered. According to the used cartesian axes frame, only the d_z component of the DM vector is non-zero (see Table 4.9). Hence, only the $|1,0\rangle$ component of the triplet is involved. The wavefunctions of the triplet and singlet along the ϑ_1 deformation vary along the angular deformations. In order to numerically illustrate the importance of all types of mechanisms, the CASSCF wavefunctions are used to derive the DM vector.

The following CASSCF wavefunctions of the triplet and singlet $M_S = 0$ components are expressed as:

$$\begin{aligned} |1,1\rangle &= |\phi_s\phi_a\rangle \\ |0,0\rangle &= \lambda|\phi_s\overline{\phi}_s\rangle - \mu|\phi_a\overline{\phi}_a\rangle \end{aligned} \tag{4.31}$$

where the λ and μ coefficients vary along the deformation, and ϕ_s and ϕ_a are the symmetric and antisymmetric (with respect to the C_2 axis) symmetry adapted orbitals (see Fig. 4.4):

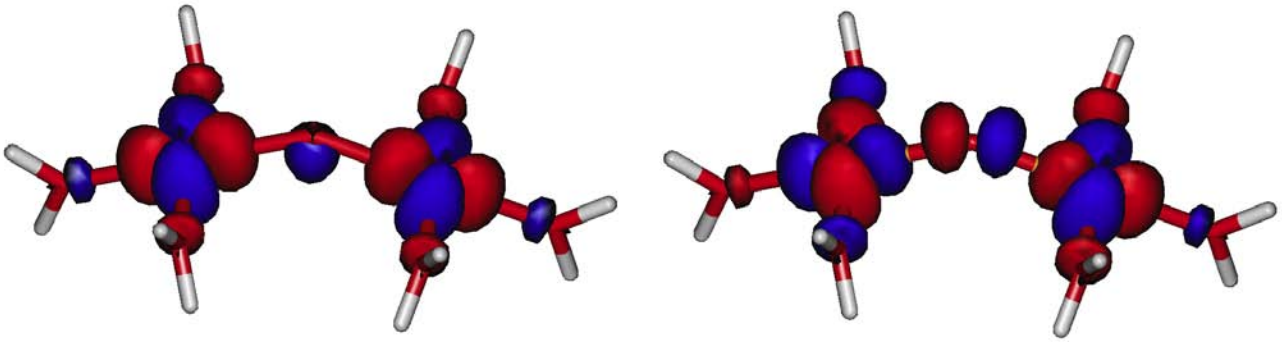

Figure 4.4: Symmetric (ϕ_s) and antisymmetric (ϕ_a) magnetic orbitals for the $\vartheta_1 = 40°, \vartheta_2 = 0°$ model $[Cu_2O(H_2O)_6]^{2+}$ structure.

$$\begin{aligned} \phi_s &= \sum_i c_i[3d_i(l) \pm 3d_i(r)] + c_y 2p_y + \ldots \\ \phi_a &= \sum_i c'_i[3d_i(l) \mp 3d_i(r)] + c_x 2p_x + \ldots \end{aligned} \tag{4.32}$$

where the c_i, c'_i, c_x and c_y coefficients differ for the singlet and triplet states and depend on θ_1. The $d_i(l,r)$ orbitals are pure local atomic orbitals centered on site l (left) and r (right) respectively. The $2p_y$ and $2p_x$ orbitals are localized on the bridging oxygen.

The following renormalized orbitals for the $\theta_1 = 40°$ structure are used in the derivation:

$$\begin{aligned} \phi_s^T &= 0.2260(d^l_{xy} - d^r_{xy}) + 0.5941(d^l_{z^2} + d^r_{z^2}) - 0.3023(d^l_{x^2-y^2} + d^r_{x^2-y^2}) - 0.0952p_y \\ \phi_a^T &= -0.2285(d^l_{xy} + d^r_{xy}) - 0.5868(d^l_{z^2} - d^r_{z^2}) + 0.2898(d^l_{x^2-y^2} - d^r_{x^2-y^2}) - 0.1973p_x \\ \phi_s^S &= 0.2313(d^l_{xy} - d^r_{xy}) + 0.5939(d^l_{z^2} + d^r_{z^2}) - 0.2992(d^l_{x^2-y^2} + d^r_{x^2-y^2}) - 0.0919p_y \\ \phi_a^S &= -0.2327(d^l_{xy} + d^r_{xy}) - 0.5860(d^l_{z^2} - d^r_{z^2}) + 0.2872(d^l_{x^2-y^2} - d^r_{x^2-y^2}) - 0.2001p_x \end{aligned} \tag{4.33}$$

The simultaneous presence of $d_{x^2-y^2}$ and d_{xy} atomic orbitals on sites l and r in ϕ_s and in ϕ_a, as well as the simultaneous presence of the p_y and p_x atomic orbitals in ϕ_s and ϕ_a respectively are responsible for the existence of the DM vector arising from several classes of mechanisms (see Table 4.10). The entire derivation is laborious and will not be detailed here.

Class	SO applied on	ϑ_1=40°	ϑ_1=90°
d-d (neutral)	copper atoms	13.1	0.0
d-d (ionic)	copper atoms	−0.2	0.0
p-d (copper)	copper atoms	0.1	0.0
p-d (oxygen)	oxygen atom	0.4	1.2
p-p	oxygen atom	−0.1	0.0
Total		13.3	1.2
RASSI-SO		14.8	3.6

Table 4.10: Contributions to the d_z component of the DM vector (in cm^{-1}) of the different type of mechanisms at the CASSCF level for the ($\vartheta_1 = 40°, 90°; \vartheta_2 = 0°$) structures. The spin-orbit operator is acting on the copper $d_i(l, r)$ atomic orbitals in the d-d (neutral), d-d (ionic) and p-d (copper) mechanisms, while it is acting on the bridging oxygen atom $p_{x,y}$ atomic orbitals in the p-d (oxygen) and p-p mechanisms. The mechanisms are labelled according to the nature of the involved determinants and the atom(s) on which the spin-orbit coupling is applied.

The contribution of all types of mechanisms is presented in Table 4.10. The free-ion spin-orbit coupling constants $\zeta_{Cu^{2+}}$, $\zeta_{Cu^{3+}}$, and ζ_O are used (ζ_{O^-} is considered equal to ζ_O).

According to Table 4.10, the total DM vector is dominated by the d-d (neutral) mechanisms. This result is not surprising since the majority of the wavefunctions is carried by the 'neutral' d-d determinants and since the copper contribution dominates by far the SOC. The p-p mechanisms are almost negligible since the spin-orbit coupling constant of the oxygen atom is small and since the p-p determinants have negligible weights in the wavefunctions. All these mechanisms have already been analyzed by Moskvin [34], but numerical estimates are here provided for the first time.

The $\vartheta = 90°$ structure is particularly interesting since it prohibits any copper contribution. Hence the DM vector only arises from the oxygen contributions. Since the *ab initio* estimate is non negligible (d_z=3.6 cm^{-1}), an important role of the central oxygen atom is here demonstrated, in agreement with the previous analytical study provided by Moskvin [34].

When $\vartheta_1 = 0$, all contributions vanish, and no DM vector is possible (which is in agreement

with the symmetry rules). The mechanisms illustrated previously explain several points of the curve as a function of ϑ_1, and can be used in order to rationalize its shape. Since the d-d (neutral) mechanisms dominate, the maximum of the curve is expected around $\vartheta_1 = 45°$ (where the d_{xy} and $d_{x^2-y^2}$ atomic orbitals are maximal in the wavefunctions). Since other mechanisms can play a small role and since the λ and μ coefficients also influence the result, the maximum is actually found for $\vartheta_1 = 40°$. For $\theta_1 = 90°$, since the dominant mechanisms vanish, the curve ends with a non-zero but small d_z value.

The DM vector can be calculated *ab initio* and an analysis provides useful information on the leading mechanisms. One of the perspectives of this thesis would be to further analyze real complexes. One may conclude from this section that all terms of the spin Hamiltonian can be calculated and extracted safely by using effective Hamiltonian theory. While the determination of the symmetric tensor components require high-cost and highly correlated calculations, the DM vector can be determined from relatively low-cost calculations.

4.2 The Magnetic Anisotropy in Centrosymmetric d^8-d^8 Complexes

In order to focuss on the symmetric anisotropic terms in the high-spin $d^8 - d^8$ configuration, a centrosymmetric complex is considered. In this configuration, several difficulties arise. As in high-spin Mn(III) mononuclear complexes, four unpaired electrons are effectively coupled, and hence fourth order terms may appear in the model Hamiltonians. Moreover, contrary to the $d^9 - d^9$ configuration, the symmetric exchange should account for spin-mixing effects. In other words, the weak-exchange limit introduces new features that prohibit the use of standard extractions that are only valid in the strong-exchange limit. In the high-spin $d^8 - d^8$ configuration both local and intersite anisotropic tensors are present. One should note that other compounds presenting antisymmetric exchange can be studied in the same way, since these antisymmetric terms can be extracted independently, as shown in section 4.1.2.

The standard multispin model Hamiltonian which describes centrosymmetric Ni(II) binuclear complexes has the following expression:

$$\hat{H}_{mod} = J\hat{\mathbf{S}}_a \cdot \hat{\mathbf{S}}_b + \hat{\mathbf{S}}_a \overline{\overline{D}}_a \hat{\mathbf{S}}_a + \hat{\mathbf{S}}_b \overline{\overline{D}}_b \hat{\mathbf{S}}_b + \hat{\mathbf{S}}_a \overline{\overline{D}}_{ab} \hat{\mathbf{S}}_b \tag{4.34}$$

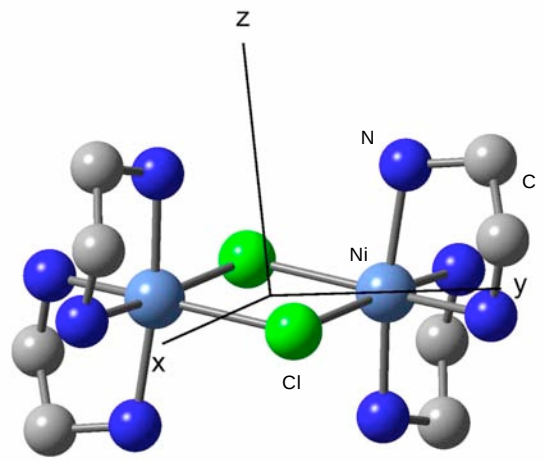

Figure 4.5: Ball and stick representation of $[Ni_2(en)_4Cl_2]^{2+}$ (en=ethylenediamine). Hydrogen atoms are omitted for clarity. The magnetic anisotropy axes are shown.

where $\overline{\overline{D}}_a$ and $\overline{\overline{D}}_b$ are the local anisotropy tensors. Three different models will be extracted: the multispin, the block spin and the giant spin Hamiltonians from the *ab initio* study of the weakly ferromagnetic $[Ni_2(en)_4Cl_2]^{2+}$ (en=ethylenediamine) complex (see Fig. 4.5). According to a recent experimental study [44], this complex exhibits a very small ferromagnetic coupling between the two Ni(II) ions. Only the J, D_a and D_{ab} parameters have been extracted from a joint HF-EPR and magnetic susceptibility study, *i.e.* the rhombic terms have been neglected.

As stated several times by Boča [11, 23, 129], the weak-exchange limit had to be solved while the approximations made in standard models should be questionned. The present section aims to adress these questions by an extensive study of the $[Ni_2(en)_4Cl_2]^{2+}$ complex. The study of such complex from *ab initio* calculations is particularly interesting and promising, but also challenging. The next section is devoted to the *ab initio* study while the extraction of the different models is presented in sections 4.2.2-4.2.4.

4.2.1 *Ab Initio* Strategy

All the CASSCF, CASPT2 and RASSI-SO calculations presented in this section have been performed using the MOLCAS program [98], while the DDCI3 results have been obtained using the CASDI code (see section 2.4.1). Spin-mixing effects are important in the weak-exchange limit. As a consequence, accurate spin-orbit free energy differences between the

lowest-lying quintet, triplet and singlet must be used in the diagonal of the SI matrix. The first part of the study is therefore devoted to the accurate calculation of the spin-orbit free magnetic coupling J value.

Determination of the Isotropic Exchange Parameter

As already mentioned, the isotropic exchange parameter J is very sensitive to dynamic correlation. In the weak-exchange limit, the CASPT2 treatment of dynamic correlation is not recommended since it often generates artificial deviations to the Landé intervals (*i.e.* non-Heisenberg behaviours) [79] and DDCI3 calculations are usually necessary. Unfortunately, the large size of the system is not compatible with a full DDCI3 calculation and two approximate strategies were used to compute J, (i) perform a truncated DDCI3 calculation on the full system, and (ii) perform a full DDCI3 calculation on a simplified model complex.

(i) In order to truncate the DDCI3 calculation on the full system, the so-called energy difference dedicated orbitals are used [103]. In this approach, a unitary transformation is performed on the natural orbitals such that the resulting orbitals can be ordered in terms of their importance on the considered energy differences. These orbitals are here obtained by diagonalizing a difference density matrix defined as $\rho_{diff} = 2\rho_Q - \rho_T - \rho_S$, where the indices Q, T and S respectively refer to the quintet, triplet and singlet lowest-lying spin-orbit free states. Once the orbitals are ordered according to their importance on the quintet-triplet and quintet-singlet energy differences (*i.e.* on J), the external space used in the DDCI3 calculation can be safely reduced by 'freezing' some inactive and virtual MOs. The results obtained from different truncated spaces are presented in Fig. 4.6. As expected, severe truncations of the external space strongly affect the computed J value. However, J rapidly converges to a value close to -6 cm^{-1}.

(ii) In this approach the $[Ni_2(en)_4Cl_2]^{2+}$ complex is modeled by a $[Ni_2(NH_3)_8Cl_2]^{2+}$ symmetrized model (belonging to the C_{2h} point group). Such modelization and symmetrization is not expected to affect strongly the magnetic coupling between the two magnetic sites since the first coordination sphere is conserved [136], and the real first coordination sphere is close to the C_{2h} symmetry (see Fig. 4.5). An Iterative DCCI3 (IDDCI) calculation is performed [102]. At each iteration, a new set of MOs is obtained by diagonalizing the averaged density matrix $\rho_{avg} = \rho_Q + \rho_T + \rho_S$. After six iterations, the J value also converges to -6 cm^{-1} (see

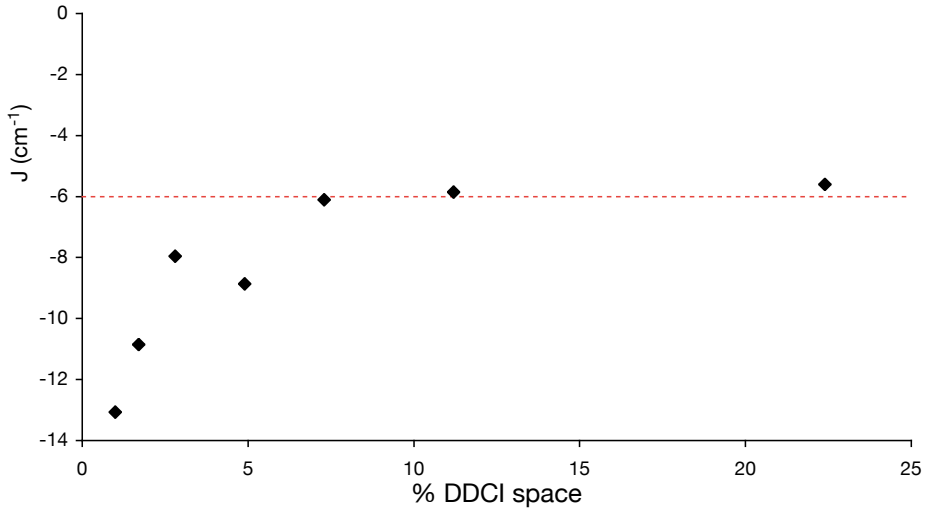

Figure 4.6: Magnetic coupling J (in cm^{-1}) as a function of the size of the DDCI space (expressed in percentage of the total DDCI space) computed for the $[Ni_2(en)_4Cl_2]^{2+}$ complex.

Table 4.11). Since no significant deviations to the Landé intervals is observed, the isotropic exchange is assumed to follow the Heisenberg behaviour in the rest of the section. The -6.00 cm^{-1} value obtained from both strategies is chosen as a reference for the SI calculations.

Computation of Excited States

In order to compute the lowest-lying spin-orbit spectrum with the RASSI-SO method, both the SI space and the level of theory used for the diagonal energies of the SI matrix have to be defined. CAS(16/10)SCF calculations will be used in order to compute the spin-orbit free states while the CASPT2 energies will be used on the diagonal of the SI matrix. As in the $d^9 - d^9$ configuration, only 'neutral' states are considered. Since the local environment of the magnetic centers is close to the octahedral symmetry, only three local single excitations are considered (as in nearly octahedral Ni(II) mononuclear complexes). However, since the lowest-lying spin-orbit free states belong to both A_g and A_u symmetry (being actually ^5A_g, ^3A_u and ^1A_g), excitations leading to A_g or A_u excited states must be considered (contrary to the copper acetate case). Finally, the SI space consists in 21 spin-orbit free states: four ^5A_g, three ^5A_u, three ^3A_g, four ^3A_u, four ^1A_g and three ^1A_u.

Iteration	J(Q-T)	J(T-S)
1	-2.00	-2.13
2	-3.30	-3.37
3	-4.44	-4.49
4	-5.22	-5.29
5	-5.70	-5.77
6	-5.99	-6.06

Table 4.11: IDDCI magnetic coupling parameter (in cm^{-1}) for $[Ni_2(NH_3)_8Cl_2]^{2+}$ model complex.

The diagonal elements of the SI matrix have been replaced by the CASPT2 energies except for the lowest quintet, triplet and singlet states for which the DDCI3 energy differences were used. The spin-orbit spectrum is then obtained from the diagonalization of the SI matrix.

Determination of the Magnetic Axes Frame

Although all the conclusions presented in this section can be obtained in any arbitrary axes frame, it is preferable to present the results in the magnetic axes frame for the sake of clarity. Indeed, the attribution of the spin-orbit energy levels is ambiguous unless the computed wavefunctions are expressed in the magnetic axes frame, that has then to be determined before any further analysis.

From a theoretical point of view, the procedure of determination of the magnetic axes frame in such high-spin $d^8 - d^8$ binuclear complex is linked to a series of hypothesis that will be confirmed afterwards (see section 4.2.3):

- All the tensors involved in the multispin Hamiltonian have the same magnetic anisotropy axes.

- These anisotropy axes are those of the $\overline{\overline{D}}_2$ giant spin tensor (where the index 2 refers to spin quantum number of the considered state).

- The $\overline{\overline{D}}_S$ tensors of all spin states of the configuration have the same magnetic anisotropy axes (see sections 1.4.1 and 4.2.4 for more details concerning the block spin tensors).

- The spin mixing between the quintet and singlet components does not affect the $\overline{\overline{D}}_2$ anisotropy axes.

In order to determine the magnetic anisotropy axes of the quintet state, the giant spin effective interaction matrix free of any spin-mixing effect has been determined using the effective Hamiltonian theory. Since this matrix can in principle be modeled by and $\hat{\mathbf{S}}.\overline{\overline{D}}.\hat{\mathbf{S}}$ Hamiltonian, the extraction of the magnetic axes frame can be performed as in mononuclear species. In order to eliminate the spin-mixing effects, the following three-step procedure has been adopted:

- The effective Hamiltonian is built in the coupled $|S, M_S\rangle$ basis that contain all spin-orbit components of the spin-orbit free Q, T and S states.

- The matrix elements between spin-orbit components belonging to different spin states are set to zero and this 'spin decoupled Hamiltonian' is diagonalized.

- The giant spin effective interaction matrix between the $|2, M_S\rangle$ components of the ground spin state is then calculated from the eigenvalues and eigenvectors of the 'spin decoupled Hamiltonian'.

The second-order giant spin tensor $\overline{\overline{D}}_2$ is then extracted from the 'spin decoupled giant spin effective interaction matrix' and its principal axes are determined.

4.2.2 The Standard Multispin Hamiltonian in the Weak-Exchange Limit

Usually, the extractions of the standard multispin model parameters are only performed using the strong-exchange limit approximation [11, 23]. In order to solve the weak-exchange limit and show the effect of the spin-mixing on the spectrum, both extractions will be presented and a strategy to extract a common parameter set from both approaches will be proposed.

Extraction Scheme in the Strong-Exchange Limit

In the strong exchange limit, the spin-mixing is negligible. Hence, only the matrix elements between same-spin spin-orbit components are required to obtain the model spectrum. The extraction is easily done using the tabulated coupling coefficients (see section 1.4.1) [11, 23].

From Eqs. 1.11, 1.12, 1.13 and 1.14, one may generate the C_a and C_{ab} coefficients for all the spin states [23, 30], and obtain the following relations for the block spin tensors $\overline{\overline{D}}_2$ (for S=2) and $\overline{\overline{D}}_1$ (for S=1):

$$\begin{aligned} \overline{\overline{D}}_2 &= \frac{1}{6}\overline{\overline{D}}_a + \frac{1}{6}\overline{\overline{D}}_b + \frac{1}{3}\overline{\overline{D}}_{ab} \\ \overline{\overline{D}}_1 &= -\frac{1}{2}\overline{\overline{D}}_a - \frac{1}{2}\overline{\overline{D}}_b + \overline{\overline{D}}_{ab} \end{aligned} \tag{4.35}$$

Considering that all tensors are traceless and have the same magnetic axes frame, one gets the following relations:

$$\begin{aligned} D_2 &= \frac{1}{3}\left(D_a + D_{ab}\right) \\ E_2 &= \frac{1}{3}\left(E_a + E_{ab}\right) \\ D_1 &= -D_a + D_{ab} \\ E_1 &= -E_a + E_{ab} \end{aligned} \tag{4.36}$$

Using the D_2, E_2, D_1 and E_1 values extracted from the spectrum, one may access to the D_a, E_a, D_{ab} and E_{ab} parameters. In order to extract the same parameters even in the case of weak-exchange limit, these parameters must be extracted from the six energy levels that are not affected by the spin-mixing, as shown in Fig. 4.7. As it will be shown in the next paragraph, the $|0,0\rangle$, $|2,0\rangle$ and $\frac{1}{\sqrt{2}}\left(|2,2\rangle + |2,-2\rangle\right)$ projected spin states are affected by the spin-mixing and are therefore not considered in the extraction. As a consequence, the modelization of the energy levels of these states from the extracted parameters is of course not reliable.

The Resolution of the Weak-Exchange Limit

In order to solve the weak-exchange limit, the complete interaction matrix in the uncoupled $|M_{Sa}, M_{Sb}\rangle$ basis is built and the anisotropic parameters are extracted using the effective Hamiltonian theory and only the energies of the low-lying spectrum. This common strategy in magnetism, suggested recently by Boča in order to solve the weak-exchange limit [11], is applied in this section. The following model interaction matrix is obtained in the uncoupled basis set:

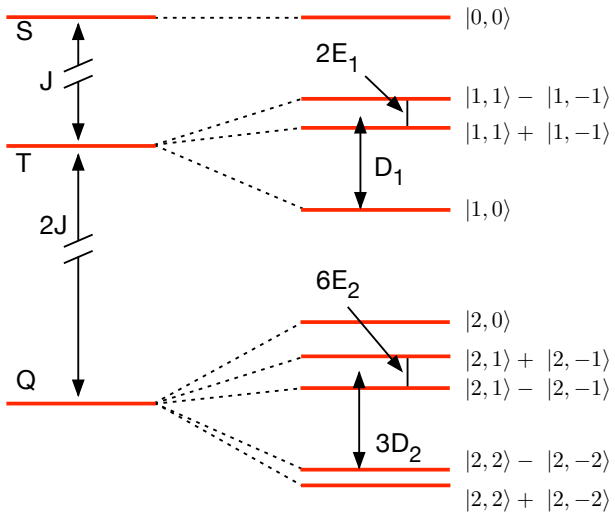

Figure 4.7: Energy levels of the "quintet", "triplet" and "singlet" state components after introducing the spin-orbit coupling in the strong exchange limit. $D_1 = -D_a + D_{ab}$; $3D_2 = D_a + D_{ab}$; $E_1 = -E_a + E_{ab}$; $3E_2 = E_a + E_{ab}$ [11, 23].

$\hat{H}_{mod}$	$\lvert -1,-1\rangle$	$\lvert -1,0\rangle$	$\lvert 0,-1\rangle$	$\lvert -1,1\rangle$	$\lvert 0,0\rangle$	$\lvert 1,-1\rangle$	$\lvert 1,0\rangle$	$\lvert 0,1\rangle$	$\lvert 1,1\rangle$
$\langle -1,-1\rvert$	$J+\frac{2}{3}(D_a+D_{ab})$	0	0	E_a	E_{ab}	E_a	0	0	0
$\langle -1,0\rvert$	0	$-\frac{1}{3}D_a$	$J-\frac{1}{3}D_{ab}$	0	0	0	E_a	E_{ab}	0
$\langle 0,-1\rvert$	0	$J-\frac{1}{3}D_{ab}$	$-\frac{1}{3}D_a$	0	0	0	E_{ab}	E_a	0
$\langle -1,1\rvert$	E_a	0	0	$-J+\frac{2}{3}(D_a-D_{ab})$	$J-\frac{1}{3}D_{ab}$	0	0	0	E_a
$\langle 0,0\rvert$	E_{ab}	0	0	$J-\frac{1}{3}D_{ab}$	$-\frac{4}{3}D_a$	$J-\frac{1}{3}D_{ab}$	0	0	E_{ab}
$\langle 1,-1\rvert$	E_a	0	0	0	$J-\frac{1}{3}D_{ab}$	$-J+\frac{2}{3}(D_a-D_{ab})$	0	0	E_a
$\langle 1,0\rvert$	0	E_a	E_{ab}	0	0	0	$-\frac{1}{3}D_a$	$J-\frac{1}{3}D_{ab}$	0
$\langle 0,1\rvert$	0	E_{ab}	E_a	0	0	0	$J-\frac{1}{3}D_{ab}$	$-\frac{1}{3}D_a$	0
$\langle 1,1\rvert$	0	0	0	E_a	E_{ab}	E_a	0	0	$J+\frac{2}{3}(D_a+D_{ab})$

(4.37)

The following matrix U is used in order to transform the model interaction matrix from the uncoupled to the coupled basis:

$$U = \begin{pmatrix} 0 & 0 & 0 & 0 & 1 & 0 & 0 & 0 & 0 \\ 0 & 0 & 0 & \frac{1}{\sqrt{2}} & 0 & 0 & 0 & -\frac{1}{\sqrt{2}} & 0 \\ 0 & 0 & 0 & \frac{1}{\sqrt{2}} & 0 & 0 & 0 & \frac{1}{\sqrt{2}} & 0 \\ 0 & 0 & \frac{1}{\sqrt{6}} & 0 & 0 & 0 & -\frac{1}{\sqrt{2}} & 0 & \frac{1}{\sqrt{3}} \\ 0 & 0 & \sqrt{\frac{2}{3}} & 0 & 0 & 0 & 0 & 0 & -\frac{1}{\sqrt{3}} \\ 0 & 0 & \frac{1}{\sqrt{6}} & 0 & 0 & 0 & \frac{1}{\sqrt{2}} & 0 & \frac{1}{\sqrt{3}} \\ 0 & \frac{1}{\sqrt{2}} & 0 & 0 & 0 & \frac{1}{\sqrt{2}} & 0 & 0 & 0 \\ 0 & \frac{1}{\sqrt{2}} & 0 & 0 & 0 & -\frac{1}{\sqrt{2}} & 0 & 0 & 0 \\ 1 & 0 & 0 & 0 & 0 & 0 & 0 & 0 & 0 \end{pmatrix} \tag{4.38}$$

The model interaction matrix is finally obtained in the coupled basis by using Eq. 4.5:

$\hat{H}_{mod}$	$\|2,2\rangle$	$\|2,1\rangle$	$\|2,0\rangle$	$\|2,-1\rangle$	$\|2,-2\rangle$
$\langle 2,2\|$	$J+\frac{2}{3}(D_a+D_{ab})$	0	$\sqrt{\frac{2}{3}}(E_a+E_{ab})$	0	0
$\langle 2,1\|$	0	$J-\frac{1}{3}(D_a+D_{ab})$	0	E_a+E_{ab}	0
$\langle 2,0\|$	$\sqrt{\frac{2}{3}}(E_a+E_{ab})$	0	$J-\frac{2}{3}(D_a+D_{ab})$	0	$\sqrt{\frac{2}{3}}(E_a+E_{ab})$
$\langle 2,-1\|$	0	E_a+E_{ab}	0	$J-\frac{1}{3}(D_a+D_{ab})$	0
$\langle 2,-2\|$	0	0	$\sqrt{\frac{2}{3}}(E_a+E_{ab})$	0	$J+\frac{2}{3}(D_a+D_{ab})$
$\langle 1,1\|$	0	0	0	0	0
$\langle 1,0\|$	0	0	0	0	0
$\langle 1,-1\|$	0	0	0	0	0
$\langle 0,0\|$	$\frac{1}{\sqrt{3}}(2E_a-E_{ab})$	0	$\frac{\sqrt{2}}{3}(2D_a-D_{ab})$	0	$\frac{1}{\sqrt{3}}(2E_a-E_{ab})$

$\hat{H}_{mod}$	$\|1,1\rangle$	$\|1,0\rangle$	$\|1,-1\rangle$	$\|0,0\rangle$
$\langle 2,2\|$	0	0	0	$\frac{1}{\sqrt{3}}(2E_a-E_{ab})$
$\langle 2,1\|$	0	0	0	0
$\langle 2,0\|$	0	0	0	$\frac{\sqrt{2}}{3}(2D_a-D_{ab})$
$\langle 2,-1\|$	0	0	0	0
$\langle 2,-2\|$	0	0	0	$\frac{1}{\sqrt{3}}(2E_a-E_{ab})$
$\langle 1,1\|$	$-J-\frac{1}{3}(D_a-D_{ab})$	0	$-E_a+E_{ab}$	0
$\langle 1,0\|$	0	$-J+\frac{2}{3}(D_a-D_{ab})$	0	0
$\langle 1,-1\|$	$-E_a+E_{ab}$	0	$-J-\frac{1}{3}(D_a-D_{ab})$	0
$\langle 0,0\|$	0	0	0	$-2J$

(4.39)

Parameter	*Ab initio*	Experiment [44]
J	-5.415	-9.66
D_a	-9.437	-4.78
E_a	2.042	-
D_{ab}	0.367	-0.64
E_{ab}	-0.052	-

Table 4.12: Multispin parameters (in cm^{-1}) of the $[Ni_2(en)_4Cl_2]^{2+}$ complex.

The main conclusion that can be dressed from this matrix is that the strong-exchange limit extraction is recovered when one sets to zero all off-diagonal elements between spin-orbit components belonging to different spin states. As a consequence, the same parameters can be obtained from both extraction schemes if the extraction only deals with the projected spin states that are not affected by the spin-mixing. The spin-mixing is expressed in terms of the local and intersite anisotropic parameters, and then its effect on the spectrum can be numerically evaluated from the extracted parameters.

The Spin-mixing and the Spectrum

The extracted parameters are presented in Table 4.12. The J value has slightly been modified by the effect of the SOC, while being still close to the spin-orbit free value. As in the experimental study [44], the intersite anisotropy is non-negligible.

Using the experimental values reported in Table 4.12, the experimental spectrum has been constructed and represented in Fig. 4.8. The main difference between the experimental and the computed spectra concern the value of the isotropic exchange J. However, even if these values are different such an accuracy on the J value (a few cm^{-1}) is quite remarkable. The other important difference comes from the rhombic terms that are not considered in the experimental extraction. Since according to the *ab initio* estimates of E_a and E_{ab} such interactions are non-negligible, their neglect in the experimental extraction process may have affected the other extracted parameters. As a consequence, a comparison between the computed and experimental results is difficult. The experimental extraction included the spin-mixing by introducing an additional Δ_2 parameters accounting for the energy difference between the

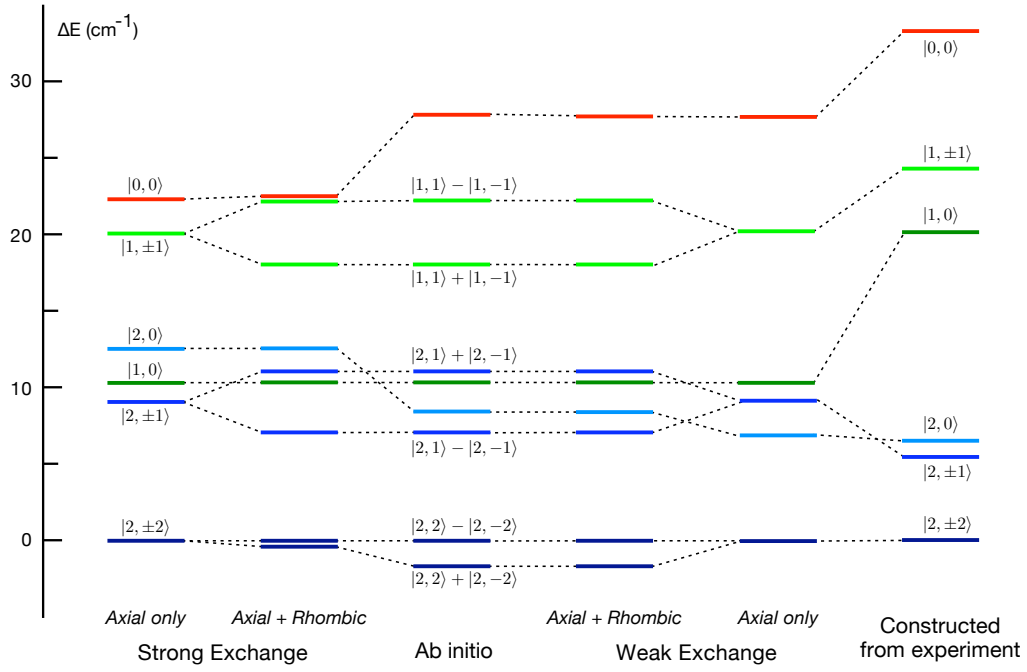

Figure 4.8: Comparison of the *ab initio* spectrum and model spectra obtained using different parametrizations.

$|2,0\rangle$ and $|2,\pm1\rangle$ projected spin states. By using the experimental J, D_a and D_{ab} parameters in the weak-exchange limit scheme, the experimental Δ_2 parameter can be calculated (Δ_2=1.1 cm^{-1}). In the *ab initio* spectrum, since the J value is smaller than the experimental one, the spin-mixing affects more importantly the spectrum and hence Δ_2 is diminished (the projected $|2,0\rangle$ states is more stabilized by its coupling with the $|0,0\rangle$ projected state) and even changes its sign (Δ_2=-0.65 cm^{-1}).

The effect of both rhombic interactions and of spin-mixing on the model spectrum can be appreciated from Fig. 4.8 and Table 4.13. Rhombic interactions play a crucial role by directly splitting the $|S,\pm M_S\rangle$ projected spin states and by enlarging the tunnel splitting between the $\frac{1}{\sqrt{2}}(|2,2\rangle \pm |2,-2\rangle)$ combinations through the spin-mixing. When both the rhombicity and the spin-mixing are consistently included in the model Hamiltonian, the model spectrum perfectly reproduces the *ab initio* one (ϵ=0.07%). Since only few parameters were needed in order to fully determine the multispin Hamiltonian, only the *ab initio* energies were used in the extraction process. The extracted parameter set allows to reproduce all the spectrum,

Model	Terms	ϵ (%)
Strong-exchange	Axial	7.2
	Axial+rhombic	3.1
Weak-exchange	Axial	1.7
	Axial+rhombic	0.07

Table 4.13: Comparison of the model and *ab initio* spectra for several models. The error ϵ between the model and *ab initio* spectra are evaluated using Eq. 2.12.

indicating that the model Hamiltonian would be valid, justifying *a priori* the previously made hypothesis. In order to fully validate this Hamiltonian and hypothesis, a deeper analysis should be performed.

4.2.3 The Effective Hamiltonian in the Magnetic Axes Frame

From the effective Hamiltonian theory, it is also possible to use the information contained in the wavefunctions in order to compare all interactions of the model Hamiltonian to those of the effective Hamiltonian built from the *ab initio* results. This process allows a more rigorous check of the accuracy of the studied model.

Confrontation Between the Model and the Effective Interaction Matrices

The effective interaction matrices are built in both the coupled and uncoupled basis (numbers in cm^{-1}):

H_{eff}	$\|2,2\rangle$	$\|2,1\rangle$	$\|2,0\rangle$	$\|2,-1\rangle$	$\|2,-2\rangle$	$\|1,1\rangle$	$\|1,0\rangle$	$\|1,-1\rangle$	$\|0,0\rangle$
$\langle 2,2\|$	1.670	$0.001+0.003i$	1.616	0.000	0.002	0.000	0.000	0.000	$-2.367+0.020i$
$\langle 2,1\|$	$0.001-0.003i$	10.742	0.000	1.989	0.000	0.000	0.000	0.000	$-0.024-0.086i$
$\langle 2,0\|$	1.616	0.000	13.793	0.000	1.616	0.000	0.000	0.000	$9.057-0.001i$
$\langle 2,-1\|$	0.000	1.989	0.000	10.742	$-0.001-0.003i$	0.000	0.000	0.000	$0.024-0.086i$
$\langle 2,-2\|$	0.002	0.000	1.616	$-0.001+0.003i$	1.670	0.000	0.000	0.000	$-2.366-0.020i$
$\langle 1,1\|$	0.000	0.000	0.000	0.000	0.000	21.814	$0.020+0.070i$	$-2.095+0.025i$	0.000
$\langle 1,0\|$	0.000	0.000	0.000	0.000	0.000	$0.020-0.070i$	12.021	$-0.021-0.070i$	0.000
$\langle 1,-1\|$	0.000	0.000	0.000	0.000	0.000	$-2.095-0.025i$	$-0.021+0.070i$	21.814	0.000
$\langle 0,0\|$	$-2.367-0.020i$	$-0.024+0.086i$	$9.057+0.001i$	$0.024+0.086i$	$-2.366+0.020i$	0.000	0.000	0.000	24.125

(4.40)

H_{eff}	$\|-1,-1\rangle$	$\|-1,0\rangle$	$\|0,-1\rangle$	$\|-1,1\rangle$	$\|0,0\rangle$	$\|1,-1\rangle$	$\|1,0\rangle$	$\|0,1\rangle$	$\|1,1\rangle$
$\langle -1,-1\|$	1.670	$-0.001+0.002i$	$-0.001+0.002i$	$-0.706-0.011i$	$2.686+0.011i$	$-0.706-0.011i$	0.000	0.000	0.002
$\langle -1,0\|$	$-0.001-0.002i$	16.278	-5.536	0.000	$-0.010+0.035i$	$0.020-0.070i$	$2.042+0.013i$	$-0.053-0.012i$	0.000
$\langle 0,-1\|$	$-0.001-0.002i$	-5.536	16.278	$0.020-0.070i$	$-0.010+0.035i$	0.000	$-0.053-0.012i$	$2.042+0.013i$	0.000
$\langle -1,1\|$	$-0.706+0.011i$	0.000	$0.020+0.070i$	20.621	-1.309	8.599	$-0.020+0.070i$	0.000	$-0.706-0.012i$
$\langle 0,0\|$	$2.686-0.011i$	$-0.010-0.035i$	$-0.010-0.035i$	-1.309	8.698	-1.309	$0.010-0.035i$	$0.010-0.035i$	$2.686+0.012i$
$\langle 1,-1\|$	$-0.706+0.011i$	$0.020+0.070i$	0.000	8.599	-1.309	20.621	0.000	$-0.020+0.070i$	$-0.707-0.012i$
$\langle 1,0\|$	0.000	$2.042-0.013i$	$-0.053+0.012i$	$-0.020-0.070i$	$0.010+0.035i$	0.000	16.278	-5.536	$0.001-0.002i$
$\langle 0,1\|$	0.000	$-0.053+0.012i$	$2.042-0.013i$	0.000	$0.010+0.035i$	$-0.020-0.070i$	-5.536	16.278	$0.001-0.002i$
$\langle 1,1\|$	0.002	0.000	0.000	$-0.707+0.012i$	$2.686-0.011i$	$-0.707+0.012i$	$0.001+0.002i$	$0.001+0.002i$	1.670

(4.41)

While the same information is present in both basis (since both interaction matrices are linked by a unitary transformation), the coupled basis is more adequate in order to compare the magnetic axes frames of the tensor, while the uncoupled one provides additional information on the interactions of the multispin Hamiltonian.

As it can be seen in matrix 4.40, the block spin $\overline{\overline{D}}_2$ tensor of the quintet block is diagonal in the magnetic axes frame defined through the 'spin decoupled giant spin effective interaction matrix'. As a consequence, all tensors of the multispin Hamiltonian have the same magnetic axes frame, *i.e.* the one of the $\overline{\overline{D}}_2$ giant spin tensor. The triplet block shows some tiny off-diagonal terms in the effective interaction matrix. However, since these terms are much smaller than the diagonal ones, it can be safely considered that all block spin $\overline{\overline{D}}_S$ tensors have the same anisotropy axes. One may notice that the magnetic X and Y axes are inverted between $\overline{\overline{D}}_1$ and $\overline{\overline{D}}_2$. Moreover, the quintet-singlet off-diagonal terms are dominated by diagonal terms of the spin Hamiltonian, and hence all hypothesis made in section 4.2.1 concerning the magnetic axes frame are numerically validated.

The comparison of matrices 4.37 and 4.41 (the model and effective interaction matrices) reveals the existence of non-zero interactions that are not considered by the model. One may quote for instance the $\langle -1, 1|\hat{H}_{eff}|1, -1\rangle$ matrix element that is the most important off-diagonal element in the effective Hamiltonian (8.599 cm^{-1}) while it is zero in the model interaction matrix. Other important differences appear between both interaction matrices, showing definitely that, as already said in section 2.2.1, phenomenological Hamiltonians can miss part of the physics. Test calculations on complexes in the strong-exchange limit exhibited the same differences, showing that the results presented in this section are not specific to the weak-exchange limit and may concern all high-spin $d^8 - d^8$ binuclear complexes.

Proposition of a New Model Hamiltonian

The problem of the model Hamiltonian comes from the neglect of biquadratic spin operators that could arise since the four unpaired electons of the lowest-lying states may effectively be coupled. One way to introduce such operators in the model Hamiltonian consists in defining the biquadratic anisotropic exchange tensor as the fourth order tensor that couples the local second order spin tensors. Such a model operator is then added to the standard model Hamiltonian (already presented in Eq. 4.34), leading to the following Hamiltonian:

$$\hat{H}_{mod} = J\hat{\mathbf{S}}_a \cdot \hat{\mathbf{S}}_b + \hat{\mathbf{S}}_a \overline{\overline{D}}_a \hat{\mathbf{S}}_a + \hat{\mathbf{S}}_b \overline{\overline{D}}_b \hat{\mathbf{S}}_b + \hat{\mathbf{S}}_a \overline{\overline{D}}_{ab} \hat{\mathbf{S}}_b + \left(\hat{\mathbf{S}}_a \otimes \hat{\mathbf{S}}_a\right) \overline{\overline{\overline{\overline{D}}}}_{aabb} \left(\hat{\mathbf{S}}_b \otimes \hat{\mathbf{S}}_b\right) \quad (4.42)$$

The symmetry of the $\overline{\overline{\overline{\overline{D}}}}_{aabb}$ tensor can be obtained by making an analogy with elasticity. According to Hooke's law, the second-order stress and strain tensors are coupled through a fourth order tensor [137]. Due to the centrosymmetry of the whole systems and the symmetry of the local tensors, the $\overline{\overline{\overline{\overline{D}}}}_{aabb}$ tensor has the same symmetry properties as the elasticity tensors in an orthorhombic crystal. In the principal axes frame, only nine independant parameters have to be considered [137], namely the non-equivalent D_{iiii}, D_{iijj} and D_{ijij} terms (where i=X, Y or Z and j≠i). Indeed, due to the inversion center, $D_{iijj} = D_{jjii}$ and due to the local symmetries $D_{ijij} = D_{jiij} = D_{ijji} = D_{jiji}$. In the principal axes frame, the 21 non-zero components of the tensor reduce to a set of nine independent parameters, namely the D_{XXXX}, D_{YYYY}, D_{ZZZZ}, D_{XXYY}, D_{XXZZ}, D_{YYZZ}, D_{XYXY}, D_{XZXZ} and D_{YZYZ} parameters.

In an arbitrary axes frame, the 81 elements of the $\overline{\overline{\overline{\overline{D}}}}_{aabb}$ tensor reduces to 21 independent components. Indeed, since the local tensors are symmetric, the fourth order tensor is symmetric and $D_{ijkl} = D_{jikl} = D_{ijlk} = D_{jilk}$, hence the number of independant elements is 36. Moreover, due to the inversion center, $\hat{\mathbf{S}}_a \otimes \hat{\mathbf{S}}_a = \hat{\mathbf{S}}_b \otimes \hat{\mathbf{S}}_b$, and the two local indices can be interchanged from site a to site b, leading finally to 21 independent components.

Determination of the New Model Hamiltonian Interaction

In order to find the new model Hamiltonian interaction of Eq. 4.42 in the magnetic axes frame, the model interaction matrix is built by adding the fourth order terms to matrix 4.37:

$\hat{H}_{mod}$	$\|-1,1\rangle$	$\|-1,0\rangle$	$\|0,-1\rangle$	$\|-1,1\rangle$	$\|0,0\rangle$	$\|1,-1\rangle$	$\|1,0\rangle$	$\|0,1\rangle$	$\|1,1\rangle$
$\langle -1,1\|$	$J+\frac{2}{3}(D_a+D_{ab})+(1)$	0	0	$E_a+(2)$	$E_{ab}+(3)$	$E_a+(2)$	0	0	$0+(4)$
$\langle -1,0\|$	0	$-\frac{1}{3}D_a+(5)$	$J-\frac{1}{3}D_{ab}+(6)$	0	0	0	$E_a+(7)$	$E_{ab}-(3)$	0
$\langle 0,-1\|$	0	$J-\frac{1}{3}D_{ab}+(6)$	$-\frac{1}{3}D_a+(5)$	0	0	0	$E_{ab}-(3)$	$E_a+(7)$	0
$\langle -1,1\|$	$E_a+(2)$	0	0	$-J+\frac{2}{3}(D_a-D_{ab})+(1)$	$J-\frac{1}{3}D_{ab}-(6)$	$0+(8)$	0	0	$E_a+(2)$
$\langle 0,0\|$	$E_{ab}+(3)$	0	0	$J-\frac{1}{3}D_{ab}-(6)$	$-\frac{4}{3}D_a+(9)$	$J-\frac{1}{3}D_{ab}-(6)$	0	0	$E_{ab}+(3)$
$\langle 1,-1\|$	$E_a+(2)$	0	0	$0+(8)$	$J-\frac{1}{3}D_{ab}-(6)$	$-J+\frac{2}{3}(D_a-D_{ab})+(1)$	0	0	$E_a+(2)$
$\langle 1,0\|$	0	$E_a+(7)$	$E_{ab}-(3)$	0	0	0	$-\frac{1}{3}D_a+(5)$	$J-\frac{1}{3}D_{ab}+(6)$	0
$\langle 0,1\|$	0	$E_{ab}-(3)$	$E_a+(7)$	0	0	0	$J-\frac{1}{3}D_{ab}+(6)$	$-\frac{1}{3}D_a+(5)$	0
$\langle 1,1\|$	$0+(4)$	0	0	$E_a+(2)$	$E_{ab}+(3)$	$E_a+(2)$	0	0	$J+\frac{2}{3}(D_a+D_{ab})+(1)$

(4.43)

where:

$$
\begin{aligned}
(1) &= \frac{1}{4}(D_{XXXX}+D_{YYYY})+\frac{1}{2}D_{XXYY}+D_{XXZZ}+D_{YYZZ}+D_{ZZZZ}\\
(2) &= \frac{1}{4}(D_{XXXX}-D_{YYYY})+\frac{1}{2}(D_{XXZZ}-D_{YYZZ})\\
(3) &= \frac{1}{2}(D_{XZXZ}-D_{YZYZ})\\
(4) &= \frac{1}{4}(D_{XXXX}+D_{YYYY})-\frac{1}{2}D_{XXYY}-D_{XYXY}\\
(5) &= \frac{1}{2}(D_{XXXX}+D_{YYYY})+D_{XXYY}+D_{XXZZ}+D_{YYZZ}\\
(6) &= \frac{1}{2}(D_{XZXZ}+D_{YZYZ})\\
(7) &= \frac{1}{2}(D_{XXXX}-D_{YYYY})\\
(8) &= \frac{1}{4}(D_{XXXX}+D_{YYYY})+D_{XYXY}-\frac{1}{2}D_{XXYY}\\
(9) &= D_{XXXX}+D_{YYYY}+2D_{XXYY}
\end{aligned}
\tag{4.44}
$$

By comparing the effective interaction matrix (4.41) to the model interaction one (4.43), one may conclude that the model Hamiltonian presented in Eq. 4.42 perfectly reproduces all features of the effective Hamiltonian. The $\langle -1,1|\hat{H}_{mod}|1,-1\rangle$ matrix element is now affected by a linear combination of fourth-order terms (see matrix 4.43 and Eq. 4.44), explaining its non-zero value in the effective Hamiltonian. All other features of the effective Hamiltonian that were unexplained with the standard model Hamiltonian are now well described with the biquadratic exchange tensor.

However, one may notice that the model Hamiltonian presented in Eq. 4.42 contains 14 parameters in the magnetic axes frame (J, D_a, E_a, D_{ab}, E_{ab} and the 9 fourth order terms). Such a large number of parameters makes this Hamiltonian not usable in practice. Even worse, the parameters cannot be extracted from matrices 4.41, 4.43 and Eq. 4.44 due to a lack of independent equations. Hence, even if the model Hamiltonian presented in Eq. 4.42 is relevant, its full extraction is not possible and one has to find an alternative approach in order to describe the magnetic properties of such systems.

4.2.4 From the Multispin to the Block Spin and Giant Spin Models in the Weak-Exchange Limit

Since the newly proposed multispin Hamiltonian is not usable for high-spin $d^8 - d^8$ binuclear complexes, alternatives based on block spin and giant spin approaches are necessary. The giant spin approach which is equivalent to the block spin one when only one projected spin state is considered will be further commented after the study of the block spin approach. In order to distinguish the interactions due to spin-mixing from the others, the spin-mixing is neglected in the first approach, and then introduced.

The Block Spin Model Interaction in the Absence of Spin-mixing

In the case of strong-exchange limit, or when the spin-mixing effects are intentionaly removed ('spin decoupled block spin effective Hamiltonian'), the model Hamiltonian presented in Eq. 1.14 has to be revised in order to account for all features of the newly proposed multispin Hamiltonian:

$$\hat{H}_{mod} = \sum_{S}[\frac{1}{2}(\hat{\mathbf{S}}^2 - \hat{\mathbf{S}}_a^2 - \hat{\mathbf{S}}_b^2)J + \hat{\mathbf{S}}\overline{\overline{D}}_S\hat{\mathbf{S}} + \sum_{k=4}^{2S}\sum_{q=-k}^{k} B_k^q \hat{O}_k^q] \tag{4.45}$$

In this model Hamiltonian, second-order tensors are involved in order to describe the main anisotropy of each spin block and the extended Stevens operators accounts for higher order anisotopic terms for all spin states with $S \geq 2$. One may remind that the extended Stevens operators may reduce in this case to the standard ones due to the symmetry of the system in the magnetic axes frame.

The model interaction matrix involving the J, D_1, E_1, D_2, E_2, B_4^0, B_4^2 and B_4^4 parameters in then built assuming that all the second-order block spin tensors are traceless and all the block spin tensors have the same magnetic anisotropy axes:

$\hat{H}_{mod}$	$\|2,2\rangle$	$\|2,1\rangle$	$\|2,0\rangle$	$\|2,-1\rangle$	$\|2,-2\rangle$	$\|1,1\rangle$	$\|1,0\rangle$	$\|1,-1\rangle$	$\|0,0\rangle$
$\langle 2,2\|$	$J+2D_2+60B_4^0$	0	$\sqrt{6}E_2+3\sqrt{6}B_4^2$	0	$12B_4^4$	0	0	0	0
$\langle 2,1\|$	0	$J-D_2$	0	$3E_2-12B_4^2$	0	0	0	0	0
$\langle 2,0\|$	$\sqrt{6}E_2+3\sqrt{6}B_4^2$	0	$J-2D_2+120B_4^0$	0	$\sqrt{6}E_2+3\sqrt{6}B_4^2$	0	0	0	0
$\langle 2,-1\|$	0	$3E_2-12B_4^2$	0	$J-D_2$	0	0	0	0	0
$\langle 2,-2\|$	$12B_4^4$	0	$\sqrt{6}E_2+3\sqrt{6}B_4^2$	0	$J+2D_2+60B_4^0$	0	0	0	0
$\langle 1,1\|$	0	0	0	0	0	$-J+\frac{1}{3}D_1$	0	E_1	0
$\langle 1,0\|$	0	0	0	0	0	0	$-J-\frac{2}{3}D_1$	0	0
$\langle 1,-1\|$	0	0	0	0	0	E_1	0	$-J+\frac{1}{3}D_1$	0
$\langle 0,0\|$	0	0	0	0	0	0	0	0	$-2J$

(4.46)

Extraction of the Block Spin Model without Spin-mixing

In order to determine the block spin interaction matrix (4.46), the 'spin decoupled effective interaction matrix' is built. As already commented in section 4.2.1, such an interaction matrix can be obtained as follows:

- A first effective interaction matrix is built in the coupled $|S, M_S\rangle$ basis.
- All the matrix elements between projected spin states belonging to difference spin-orbit free states are set to zero and this 'spin decoupled Hamiltonian' is diagonalized.
- The 'spin decoupled effective interaction matrix' is then obtained in the coupled $|S, M_S\rangle$ basis with the eigenvalues and eigenvectors of the 'spin decoupled Hamiltonian'.

After such a treatment, the obtained effective interaction matrix is block diagonal, each block corresponds to a state. This matrix is (in cm^{-1}):

H_{eff}	$\|2,2\rangle$	$\|2,1\rangle$	$\|2,0\rangle$	$\|2,-1\rangle$	$\|2,-2\rangle$	$\|1,1\rangle$	$\|1,0\rangle$	$\|1,-1\rangle$	$\|0,0\rangle$
$\langle 2,2\|$	1.670	$0.001+0.002i$	1.623	0.000	0.002	0.000	0.000	0.000	0.000
$\langle 2,1\|$	$0.001-0.002i$	10.742	0.000	1.989	0.000	0.000	0.000	0.000	0.000
$\langle 2,0\|$	1.623	0.000	13.793	0.000	1.610	0.000	0.000	0.000	0.000
$\langle 2,-1\|$	0.000	1.989	0.000	10.742	$-0.001-0.003i$	0.000	0.000	0.000	0.000
$\langle 2,-2\|$	0.002	0.000	1.610	$-0.001+0.003i$	1.670	0.000	0.000	0.000	0.000
$\langle 1,1\|$	0.000	0.000	0.000	0.000	0.000	21.814	$0.020+0.070i$	$-2.095+0.025i$	0.000
$\langle 1,0\|$	0.000	0.000	0.000	0.000	0.000	$0.020-0.070i$	12.021	$-0.021-0.070i$	0.000
$\langle 1,-1\|$	0.000	0.000	0.000	0.000	0.000	$-2.095-0.025i$	$-0.021+0.070i$	21.814	0.000
$\langle 0,0\|$	0.000	0.000	0.000	0.000	0.000	0.000	0.000	0.000	24.125

(4.47)

The only mismatch between this matrix and the model interaction matrix concerns some small off-diagonal terms that appear in the triplet block. These terms come from the use of the magnetic axes frame of the quintet block. Spin blocks can have different magnetic anisotropy axes. Since these off-digonal terms are lower than 0.1 cm^{-1}, their effect on the spin-orbit spectrum is expected to be negligible. It is therefore considered that the magnetic anisotropy axes of the quintet block is satisfactory for all spin states (see sections 4.2.1 and 4.2.3). The Stevens fourth order terms are non-zero even if they are quite small in the considered case. One should conclude that fourth order interactions are not only necessary to describe spin-mixing effects and could in principle accounts for some direct anisotropic effects inherent to the quintet state components.

The Introduction of the Spin-mixing in the Block Spin Model

The objective of the present section is to add the effect of the spin-mixing in the model interaction matrix. The block spin Hamiltonian is derived at second-order of QDPT starting from the multispin model interaction matrix. The model interaction matrix (4.43) is then transformed in the coupled $|S, M_S\rangle$ basis:

$\hat{H}_{mod}$	$\|2,2\rangle$	$\|2,1\rangle$	$\|2,0\rangle$	$\|2,-1\rangle$	$\|2,-2\rangle$
$\langle 2,2\|$	$J+\frac{2}{3}(D_a+D_{ab})+(1)$	0	$\sqrt{\frac{2}{3}}[E_a+E_{ab}+(2)+(3)]$	0	(4)
$\langle 2,1\|$	0	$J-\frac{1}{3}(D_a+D_{ab})+(5)+(6)$	0	$E_a+E_{ab}-(3)+(7)$	0
$\langle 2,0\|$	$\sqrt{\frac{2}{3}}[E_a+E_{ab}+(2)+(3)]$	0	$J-\frac{2}{3}(D_a+D_{ab})+\frac{1}{3}[(1)-4(6)+(8)+2(9)]$	0	$\sqrt{\frac{2}{3}}[E_a+E_{ab}+(2)+(3)]$
$\langle 2,-1\|$	0	$E_a+E_{ab}-(3)+(7)$	0	$J-\frac{1}{3}(D_a+D_{ab})+(5)+(6)$	0
$\langle 2,-2\|$	(4)	0	$\sqrt{\frac{2}{3}}[E_a+E_{ab}+(2)+(3)]$	0	$J+\frac{2}{3}(D_a+D_{ab})+(1)$
$\langle 1,1\|$	0	0	0	0	0
$\langle 1,0\|$	0	0	0	0	0
$\langle 1,-1\|$	0	0	0	0	0
$\langle 0,0\|$	$\frac{1}{\sqrt{3}}[2E_a-E_{ab}+2(2)-(3)]$	0	$\frac{\sqrt{2}}{3}[2D_a-D_{ab}+(1)-(6)+(8)-(9)]$	0	$\frac{1}{\sqrt{3}}[2E_a-E_{ab}+2(2)-(3)]$

$\hat{H}_{mod}$	$\|1,1\rangle$	$\|1,0\rangle$	$\|1,-1\rangle$	$\|0,0\rangle$
$\langle 2,2\|$	0	0	0	$\frac{1}{\sqrt{3}}[2E_a-E_{ab}+2(2)-(3)]$
$\langle 2,1\|$	0	0	0	0
$\langle 2,0\|$	0	0	0	$\frac{\sqrt{2}}{3}[2D_a-D_{ab}+(1)-(6)+(8)-(9)]$
$\langle 2,-1\|$	0	0	0	0
$\langle 2,-2\|$	0	0	0	$\frac{1}{\sqrt{3}}[2E_a-E_{ab}+2(2)-(3)]$
$\langle 1,1\|$	$-J-\frac{1}{3}(D_a-D_{ab})+(5)-(6)$	0	$-E_a+E_{ab}-(3)-(7)$	0
$\langle 1,0\|$	0	$-J+\frac{2}{3}(D_a-D_{ab})+(1)-(8)$	0	0
$\langle 1,-1\|$	$-E_a+E_{ab}-(3)-(7)$	0	$-J-\frac{1}{3}(D_a-D_{ab})+(5)-(6)$	0
$\langle 0,0\|$	0	0	0	$-2J+\frac{1}{3}[2(1)+4(6)+2(8)+(9)]$

(4.48)

where the (i) (with $1 \leq i \leq 9$) linear combinations of fourth order terms are explicited in Eq. 4.44.

Since the block spin Hamiltonian without spin-mixing has been validated, all direct anisotropic terms in each block are expressed according to the model Hamiltonian presented in Eq. 4.45. The effect of the spin-mixing is then expressed at second-order of QDPT as follows:

$\hat{H}_{mod}$	$\|2,2\rangle$	$\|2,1\rangle$	$\|2,0\rangle$	$\|2,-1\rangle$	$\|2,-2\rangle$	$\|1,1\rangle$	$\|1,0\rangle$	$\|1,-1\rangle$	$\|0,0\rangle$
$\langle 2,2\|$	$J+2D_2+60B_4^0+B^{rh}$	0	$\sqrt{6}E_2+3\sqrt{6}B_4^2+B^{ax,rh}$	0	$12B_4^4+B^{rh}$	0	0	0	0
$\langle 2,1\|$	0	$J-D_2$	0	$3E_2-12B_4^2$	0	0	0	0	0
$\langle 2,0\|$	$\sqrt{6}E_2+3\sqrt{6}B_4^2+B^{ax,rh}$	0	$J-2D_2+B^{ax}+120B_4^0$	0	$\sqrt{6}E_2+3\sqrt{6}B_4^2+B^{ax,rh}$	0	0	0	0
$\langle 2,-1\|$	0	$3E_2-12B_4^2$	0	$J-D_2$	0	0	0	0	0
$\langle 2,-2\|$	$12B_4^4+B^{rh}$	0	$\sqrt{6}E_2+3\sqrt{6}B_4^2+B^{ax,rh}$	0	$J+2D_2+60B_4^0+B^{rh}$	0	0	0	0
$\langle 1,1\|$	0	0	0	0	0	$-J-\frac{1}{3}D_1$	0	E_1	0
$\langle 1,0\|$	0	0	0	0	0	0	$-J+\frac{2}{3}D_1$	0	0
$\langle 1,-1\|$	0	0	0	0	0	E_1	0	$-J-\frac{1}{3}D_1$	0
$\langle 0,0\|$	0	0	0	0	0	0	0	0	$-2J-B^{ax}-2B^{rh}$

(4.49)

where:

$$
\begin{aligned}
B^{ax} &= \frac{2[(1)+2D_a-D_{ab}-(6)+(8)-(9)]^2}{27J} \\
B^{rh} &= \frac{[2(2)-(3)+2E_a-E_{ab}]^2}{9J} \\
B^{ax,rh} &= \frac{\sqrt{6}[2(2)-(3)+2E_a-E_{ab}][(1)+2D_a-D_{ab}-(6)+(8)-(9)]}{27J}
\end{aligned}
\tag{4.50}
$$

The spin-mixing parameters have been labelled according to their main interpretation in terms of the multispin picture given in Eq. 4.50. In order to get a Hermitian operator, the denominators have been set to the spin-orbit free energy differences between the quintet and the singlet (*i.e.* $3J$).

One should note that the spin-mixing does not affect the quintet block in a form compatible with the Stevens operators (see matrix 4.49). As a consequence one may conclude that the Stevens operators cannot be used for a consistent treatment of the spin-mixing. In standard extractions, the fourth order Stevens terms are used in order to account for the spin-mixing effects. In such a case, the second-order extracted terms are artificially affected by the inclusion of the spin-mixing, leading to unphysical values. Indeed, one may remind that renormalization of second-order effects are only physically based if the higher order terms affect the same matrix elements than the second-order ones, which is not the case in the present study. One may then conclude that the spin-mixing cannot be described by the Stevens operators.

Extraction of the Block Spin Parameters

The J, D_1, E_1, D_2, E_2, B_4^0, B_4^2 and B_4^4 parameters are extracted in order to provide the best matching between matrices 4.46 and 4.47. In order to obtain the spin-mixing parameters, it is necessary to include effectively the spin-mixing in the spin blocks. The giant effective Hamiltonian matrix of the quintet block in the presence of spin-mixing (in cm^{-1}) is then built in order to further extract all the remaining parameters:

H_{eff}	$\|2,2\rangle$	$\|2,1\rangle$	$\|2,0\rangle$	$\|2,-1\rangle$	$\|2,-2\rangle$
$\langle 2,2\|$	1.553	$0.000+0.011$i	$2.493-0.008$i	$0.002+0.007$i	-0.116
$\langle 2,1\|$	$0.000-0.011$i	10.742	$0.012+0.047$i	1.988	$-0.002-0.008$i
$\langle 2,0\|$	$2.493+0.008$i	$0.012-0.047$i	8.657	$-0.012-0.047$i	$2.493-0.009$i
$\langle 2,-1\|$	$0.002-0.007$i	1.988	$-0.012+0.047$i	10.742	$0.000-0.011$i
$\langle 2,-2\|$	-0.116	$-0.002+0.008$i	$2.493+0.009$i	$0.000+0.011$i	1.553

(4.51)

By comparing this Hamiltonian to the quintet block in matrix 4.49, and by using the previously extracted J, D_1, E_1, D_2, E_2, B_4^0, B_4^2 and B_4^4 parameters, the B^{ax}, $B^{ax,rh}$ and B^{rh} are finally extracted. The results are presented in Table 4.2.4.

J	-5.487
D_2	-3.035
E_2	0.663
D_1	9.793
E_1	-2.093
$60B_4^0$	$<10^{-3}$
$3\sqrt{6}B_4^2$	$<10^{-3}$
$12B_4^4$	0.002
B^{ax}	-5.136
$B^{ax,rh}$	0.870
B^{rh}	-0.116

Table 4.14: Block spin parameters (in cm^{-1}) of the $[Ni_2(en)_4Cl_2]^{2+}$ complex.

As expected, the spin-mixing is important in the weak-exchange limit since it can affect the block spin matrix elements by a few cm^{-1}. A consistent and accurate block spin model has been rationally conceived for the weak-exchange limit. Its derivation at the second-order of perturbation from the newly proposed multispin Hamiltonian introduces the effect of the fourth order tensor. The whole set of parameters can be easily extracted from *ab initio* calculations from the effective Hamiltonian theory. An interesting pespective of this work would be to generalize its expression to all $d^n - d^n$ configurations.

Application to the Giant Spin Hamiltonian

Once the block spin Hamiltonian is reached, the definition of a new and consistent giant spin Hamiltonian is particularly straightforward. Indeed, it consists in a reduction of the model space of the block spin Hamiltonian to the M_S components of the ground spin state. The model Hamiltonian can be expressed as follows if one shifts the isotropic part:

$$\hat{H}_{mod} = D\hat{S}_z^2 + E(\hat{S}_x^2 - \hat{S}_y^2) + \sum_{k=0}^{4} B_4^k \hat{O}_4^k + B^{ax}\hat{O}^{ax} + B^{ax,rh}\hat{O}^{ax,rh} + B^{rh}\hat{O}^{rh} \qquad (4.52)$$

where the $\hat{O}^{ax}$, $\hat{O}^{ax,rh}$ and $\hat{O}^{rh}$ operators have the following expressions:

$$
\begin{aligned}
\hat{O}^{ax} &= \frac{1}{96}(M_S+2)(M_S+1)(M_S-1)(M_S-2)(\hat{S}_+\hat{S}_+\hat{S}_-\hat{S}_- + \hat{S}_-\hat{S}_-\hat{S}_+\hat{S}_+) \\
\hat{O}^{ax,rh} &= \frac{1}{4\sqrt{6}}(\hat{S}_-\hat{S}_z\hat{S}_z\hat{S}_- + \hat{S}_+\hat{S}_z\hat{S}_z\hat{S}_+) \\
\hat{O}^{rh} &= \frac{1}{24}[\hat{S}_+\hat{S}_+\hat{S}_+\hat{S}_+ + \hat{S}_-\hat{S}_-\hat{S}_-\hat{S}_- + (M_S-1)(M_S+1)(\hat{S}_z\hat{S}_+\hat{S}_z\hat{S}_- + \hat{S}_z\hat{S}_-\hat{S}_z\hat{S}_+)]
\end{aligned}
\tag{4.53}
$$

The corresponding D_2, E_2, B_4^0, B_4^2, B_4^4, B^{ax}, $B^{ax,rh}$ and B^{rh} parameters are then extracted with the 'spin decoupled giant spin effective interaction matrix' and the giant spin effective interaction matrix that effectively includes spin-mixing effects. Such extraction of the giant spin parameters without passing through the block spin approach lead to a slightly different B_4^4 value than the one presented in Table 4.2.4. Indeed, the model spaces used in the construction of both 'spin decoupled effective interaction matrices' are different, leading to slightly different values of the Stevens interactions. Since the Stevens fourth order terms are very small compared to all other terms (the second-order ones and the spin-mixing terms), the uncertainty on the extracted parameters is not problematic, and all the conclusions presented with the block spin approach remain valid in the giant spin one.

In binuclear complexes, the use of a giant spin Hamiltonian is not justified in case of weak-exchange limit since the different spin blocks may be populated and therefore affect the measured properties. In this case, it is recommanded to use a block spin approach in order to account effectively for all spin states. The spin-mixing cannot be treated consistently with the Stevens operators, and hence new operators have to be defined as it has been done in the present case. In case of strong-exchange limit, and if the ground state is not a spin singlet, the giant spin approach is relevant provided that correct operators (including higher than two order terms) are used, and the spin-mixing can be safely neglected. As a consequence, the Stevens operators alone are sufficient to describe all features of the effective Hamiltonian. One may also notice that some high order terms can be attributed to direct anisotropic terms (and not only to the spin-mixing as it is the case for the B_4^4 interaction).

In larger systems, such as real SMMs, the block spin Hamiltonian would become too difficult to handle due to the large number of states generated by the HDVV Hamiltonian. One may however envisage to restrict the number of spin states described by the Hamiltonian

to the lowest in energy ones.

Conclusion

Two main situations can be distinguihed in binuclear transition metal complexes. When one magnetic center has two or less unpaired electrons and the other one only one unpaired electron (as in the $d^9 - d^9$ and $d^8 - d^9$ configurations for instance), the standard model Hamiltonians applies and both multispin and giant spin Hamiltonians can be used safely. However, when two or more unpaired electrons are present in each magnetic sites (as in the high-spin $d^8 - d^8$ configuration for instance), the situation is more complicated. The multispin Hamiltonian can involve anisotropic exchange tensor up to the order $2\,(S_a + S_b)$ when $S_a = S_b$. Test calculations in the $d^7 - d^7$ configurations actually evidenced for the presence of a sixth order anisotropic exchange tensor! Hence, the multispin Hamiltonian becomes unusable in practice, and alternative models such as the block spin and giant spin approaches can be used. The two step SI approach and the extraction scheme based on the effective Hamiltonian theory enables one to consistently calculate and extract the anisotropic parameters (when possible). The weak-exchange limit has been studied for the first time from *ab initio* calculations, allowing to question and improve the standard models used in molecular magnetism. More importantly, the antisymmetric exchange has been extracted for the first time from such *ab initio* calculations. This work opened the way for the study of larger systems, which is the subject of future researches. Moreover, the crucial role of the dynamic correlation on the anisotropic exchange has been illustrated through the well known copper acetate complex. While an important progress has been done in the present work on binuclear complexes, further researches are necessary to adress larger polynuclear complexes.

Conclusion and perspectives

The theoretical study of the magnetic anisotropy in transition metal complexes is difficult but highly interesting. This task has been pursued in the present thesis with an extensive study of several mono- and bi-nuclear complexes. This work has lead to the following main conclusions:

1. A two-step procedure to treat relativistic effects and electron correlation has been validated for the calculation of the anisotropic parameters in mono- and bi-nuclear transition metal complexes. The computational degrees of freedom have been studied, allowing to obtain parameters in good agreement with experimental data when adequate choices are made for these degrees of freedom.

2. The anisotropic spin Hamiltonians have been extracted using effective Hamiltonian theory. This extraction procedure has given rise to three main results, (i) the Zero-Field Splitting (ZFS) parameters can be extracted in case of Kramers' degeneracy, (ii) the antisymmetric interaction has been extracted from an *ab initio* calculation for the first time, and (iii) the model Hamiltonians in binuclear complexes have been revised for systems with more than one unpaired electron in each magnetic center.

3. The ZFS has been rationalized in Ni(II) and Mn(III) complexes, showing that the former case follows intuitive rules to enlarge the anisotropy while the ZFS in the latter case is ruled by less obvious rules. Moreover, insights have been given on the intersite anisotropy in binuclear complexes through the analytical derivation of the ZFS in copper acetate monohydrate and through the study of models mimicking deformations present in CuO.

4. The study of the ZFS in complexes with heavy atom ligands that can contribute to the ZFS through covalency and charge transfer has been established to be at (or beyond) the limit of the two-step State-Interaction (SI) procedure.

These main conclusions are further worked out in the following paragraphs.

Concerning the methodology, the two-step SI scheme has been succesfully applied to several standard cases. The results are only moderately affected by the different choices of the computational degrees of freedom, and accurate values can be obtained when adequate choices are made. However, the limitations of the methodology has been reached in two special cases. When the dynamic correlation plays a crucial role, as in the copper acetate complex, highly accurate calculations have to be performed on several spin-orbit free states. These calculations cannot be performed for any binuclear complex due to the high computational cost. Moreover, the dynamic correlation is not treated completely when the CASSCF wavefunctions are used in the construction of the SI matrix. For both reasons, an alternative computational approach is necessary to calculate more accurately and with a smaller computational cost the effects of the dynamic correlation on the ZFS parameters. Another difficult situation arises when heavy ligand atoms contribute to the ZFS. In this case, both the different d^n states and the charge transfer states have to be considered, while a practical and consistent truncation of the SI space is far from being obvious. Moreover, the dynamic correlation also plays a crucial role in this situation by acting on the covalency and charge transfer effects. The two-step SI procedure can only provide approximate values and a more precise method is required.

The magnetic anisotropy is usually described using phenomenological model Hamiltonians. The originality of the present work comes from the use of effective Hamiltonian theory in the parameter extraction process. Such approach allows to validate and in some cases improve the models use to describe the ZFS. It provides a bridge between the full electronic Hamiltonian and the model Hamiltonians that only considers spin degrees of freedom. By accounting for all the information contained in the energy levels and in the projected wavefunctions, effective Hamiltonian theory provides a rigorous procedure to design new and approximate Hamiltonians when a full model Hamiltonian is not usable in practise. In this case, all the approximations can be justified by comparing the model interaction matrix to the effective interaction matrix. The two most appealing achievements in this aspect concern binuclear complexes. In the $d^9 - d^9$ configuration, the extraction of the DM antisymmetric interaction has been performed for the first time from *ab initio* calculations and in the $d^8 - d^8$ configuration, the standard model Hamiltonians have been improved to take into account all the features of the exact Hamiltonian, invalidating some previous experimental works. More efforts have still

to be done on other configurations and larger systems to advance on the way to polynuclear complexes.

An important part of this dissertation is dedicated to magneto-structural correlations, rationalizations and applications dealing with the ZFS in transition metal complexes. Even though interesting progress have been made concerning analytical derivations of the ZFS parameters, the ZFS remains difficult to predict in the general case. In mononuclear complexes, non-standard coordination numbers are promising, since they allow to reach larger ZFS parameters than in the usual coordinations. Moreover insight have been given on the magnetic intersite interaction and in particular on the antisymmetric exchange. Other cases and other applications have to be performed to extend this work and provide more useful informations to experimentalists. As this stage, a close collaboration between theorists and experimentalists appears more necessary and possible than ever. Since the property seems to be difficult to predict *a priori* through general analytical expressions, the use of computational chemistry can provide deeper insights into the origin of the property.

While the present work was devoted to the ZFS in transition metal complexes, other interesting applications have to be mentioned. The magnetic anisotropy also arises in materials. The methodology presented in this dissertation can be applied in materials through the so-called embedded cluster approach. Such task is the subject of ongoing researches in the group of Pr. Broer in Groningen (Netherlands). Concerning transition metal complexes, recent highlights uses not only the spin but also the orbital degree of freedom. Bistability of the magnetization can occur for instance in case of first-order angular momentum in first-row transition metal systems [138], or lanthanide based SMMs [139]. These new systems imagined by chemists and theorists can provide new interesting properties and can be studied from a theoretical point of view. The bis(phthalocyaninato)terbium complex is for instance currently studied with the two-step SI approach used in this work, and new insights can be expected in the near future.

Bibliography

[1] B. C. Guha, *Magnetic properties of some paramagnetic crystals at low temperatures*, Proc. Roy. Soc. London Ser. A **206**, 353–373 (1951).

[2] B. Bleaney, and K. D. Bowers, *Anomalous paramagnetism of copper acetate*, Proc. Roy. Soc. London Ser. A **214**, 451–465 (1952).

[3] J. N. Van Niekerk, and F. R. L. Schoenig, *A new type of copper complex as found in the crystal structure of cupric acetate*, Acta Cryst. **6**, 227–232 (1953).

[4] I. Dzyaloshinskii, *A thermodynamic theory of weak ferromagnetism of antiferromagnetism*, J. Phys. Chem. Solids **4**, 241–255 (1958).

[5] T. Moriya, *Anisotropic superexchange interaction and weak ferromagnetism*, Phys. Rev. **120**, 91–98 (1960).

[6] C. A. Hutchison, and B. W. Mangum, *Paramagnetic resonance absorption in naphtalene in its phosphorescent state*, J. Chem. Phys. **34**, 908–922 (1961).

[7] T. Lis, *Preparation, structure, and magnetic properties of a dodecanuclear mixed-valence manganese carboxylate*, Acta Cryst. Sect. B **36**, 2042–2046 (1980).

[8] A. Caneschi, D. Gatteschi, R. Sessoli, A. L. Barra, L. C. Brunel, and M. Guillot, *Alternating current susceptibility, high field magnetization, and millimeter band EPR evidence for a ground $S = 10$ state in $[Mn_{12}O_{12}(CH_3COO)_{16}(H_2O)_4].2CH_3COOH.4H_2O$*, J. Am. Chem. Soc. **113**, 5873–5874 (1991).

[9] J. Friedman, M. P. Sarachik, J. Tejada, and R. Ziolo, *Macroscopic measurement of*

resonant magnetization tunneling in high-spin molecules, Phys. Rev. Lett. **76**, 3830–3833 (1996).

[10] L. Thomas, F. Lionti, R. Ballou, D. Gatteschi, R. Sessoli, and B. Barbara, *Macroscopic quantum tunneling of magnetization in single crystal of nanomagnets*, Nature **383**, 145–147 (1996).

[11] R. Boča, *Zero-field splitting in metal complexes*, Coord. Chem. Rev. **248**, 757–815 (2004).

[12] E. Ruiz, J. Cirera, J. Cano, S. Alvarez, C. Loose, and J. Kortus, *Can large magnetic anisotropy and high spin really coexist?*, Chem. Commun. pp. 52–54 (2008).

[13] O. Waldmann, *A criterion for the anisotropy barrier in Single-Molecule Magnets*, Inorg. Chem. **46**, 10 035–10 037 (2007).

[14] J. Telser, *A perspective on applications of ligand-field analysis: inspiration from electron paramagnetic resonance spectroscopy of coordination complexes of transition metal ions*, J. Braz. Chem. Soc. pp. 1501–1515 (2006).

[15] A. Abragam, and B. Bleaney, *Electron paramagnetic resonance of transition ions* (Dover Publications, Dover, New York) (1986).

[16] M. N. Leuenberger, and D. Loss, *Quantum computing in molecular magnets*, Nature **410**, 789–793 (2001).

[17] S. Hill, S. Datta, J. Liu, R. Inglis, C. Milios, P. L. Feng, J. J. Henderson, E. del Barco, E. K. Brechin, and D. N. Hendrickson, *Magnetic quantum tunneling: Insights from simple molecule-based magnets*, Dalton Trans. **39**, 4693–4707 (2010).

[18] J. H. Van Vleck, *The theory of electric and magnetic susceptibilities* (Oxford University Press, Oxford) (1932).

[19] M. L. H. Pryce, *A modified perturbation procedure for a problem in paramagnetism*, Proc. Phys. Soc. Ser. A **63**, 25–29 (1950).

[20] A. Abragam, and M. H. L. Pryce, *Theory of the nuclear hyperfine structure of paramagnetic resonance spectra in crytals*, Proc. Roy. Soc. London Ser. A **206**, 135–153 (1951).

[21] A. Abragam, and M. H. L. Pryce, *The theory of the nuclear hyperfine structure of paramagnetic resonance spectra in the copper tutton salts*, Proc. Roy. Soc. London Ser. A **206**, 164–172 (1951).

[22] B. Bleaney, and K. W. H. Stevens, *Paramagnetic resonance*, Rep. Prog. Phys. **16**, 108–159 (1953).

[23] R. Boča, *Theoretical foundations of molecular magnetism* (Elsevier, Amsterdam) (1999).

[24] A. Abragam, *The principles of nuclear magnetism* (Clarendon Press, Oxford) (1961).

[25] O. Kahn, *Molecular Magnetism* (VCH Publishers) (1993).

[26] R. McWeeny, *On the origin of the spin-Hamiltonian parameters*, J. Chem. Phys. **42**, 1717–1725 (1965).

[27] K. G. Dyall, and K. Faegri Jr, *Introduction to relativistic quantum chemistry* (Oxford University Press, New York) (2007).

[28] A. Trueba, P. Garcia-Fernandez, F. Senn, C. A. Daul, J. A. Aramburu, M. T. Barriuso, and M. Moreno, *High magnetic anisotropy of Fe^+ ions in $KTaO_3$ and $SrCl_2$*, Phys. Rev. B **81**, 075 107 (2010).

[29] J. Titiš, and R. Boča, *Magnetostructural D correlation in nickel(II) complexes: reinvestigation of the zero-field splitting*, Inorg. Chem. **49**, 3971–3973 (2010).

[30] A. Bencini, and D. Gatteschi, *EPR of exchange coupled systems* (Springer, Berlin) (1990).

[31] A. D. Buckingham, P. Pyykko, J. B. Robert, and L. Wiesenfeld, *Symmetry rules for the indirect nuclear spin-spin coupling tensor revisited*, Mol. Phys. **46**, 177–182 (1982).

[32] C. Riplinger, P. Y. Kao, G. M. Rosen, V. Kathirvelu, G. R. Eaton, S. Eaton, A. Kutaleadze, and F. Neese, *Interaction of radical pairs through-bond and through-space: scope and limitations of the point-dipole approximation in electron paramagnetic resonance spectroscopy*, J. Am. Chem. Soc. **131**, 10 092–10 106 (2009).

[33] A. Ozarowski, *The Zero-field splitting parameter D in binuclear copper(II) carboxylates is negative*, Inorg. Chem. **47**, 9760–9762 (2008).

[34] A. S. Moskvin, *Dzyaloshinsky-Moriya antisymmetric exchange coupling in cuprates: Oxygen Effects*, J. Exp. Theor. Phys. **104**, 913–927 (2007).

[35] E. Liviotti, S. Carreta, and G. Amoretti, *S-mixing contributions to the high-order anisotropy terms in the effective spin Hamiltonian for magnetic clusters*, J. Chem. Phys. **117**, 3361–3368 (2002).

[36] O. Waldmann, and H. U. Güdel, *Many-spin effects in inelastic neutron scattering and electron paramagnetic resonance of molecular nanomagnets*, Phys. Rev. B **72**, 094 422 (2005).

[37] A. L. Barra, A. Caneschi, A. Cornia, D. Gatteschi, L. Gorini, L.-P. Heiniger, R. Sessoli, and L. Sorace, *The origin of transverse anisotropy in axially symmetric single molecule magnets*, J. Am. Chem. Soc. **129**, 10 754–10 762 (2007).

[38] A. Wilson, J. Lawrence, E.-C. Yang, M. Nakano, D. N. Hendrickson, and S. Hill, *Magnetization tunneling in high-symmetry single-molecule magnets: limitations of the giant spin approximation*, Phys. Rev. B **74**, 140 403 (2006).

[39] A. L. Barra, D. Gatteschi, , and R. Sessoli, *High-frequency EPR spectra of a molecular nanomagnet: understanding quantum tunneling of the magnetization*, Phys. Rev. B **56**, 8192–8198 (1997).

[40] G. Rogez, J.-N. Rebilly, A.-L. Barra, L. Soraca, G. Blondin, N. Kirchner, M. Duran, J. van Slageren, S. Parsons, L. Ricard, A. Marvilliers, and T. Mallah, *Very large Ising-type magnetic anisotropy in a mononuclear Ni^{II} complex*, Angew. Chem. Int. Ed. **44**, 1876–1879 (2005).

[41] W. Wernsdofer, N. E. Chakov, and G. Christou, *Determination of the magnetic anisotropy axes of single-molecule magnets*, Phys. Rev. B **70**, 132 413 (2004).

[42] J. Krzystek, A. Ozarowski, and T. J., *Multi-frequency, high-field EPR as a powerful tool to accurately determine zero-field splitting in high-spin transition metal complexes*, Coord. Chem. Rev. **250**, 2308–2324 (2006).

[43] Q. Scheifele, C. Riplinger, F. Neese, H. Weihe, A.-L. Barra, F. Juranyi, A. Podlesnyak, and P. L. W. Tregenna-Piggoot, *Spectroscopic and theoretical study of a mononuclear manganese(III) complex exhibiting a tetragonally compressed geometry*, Inorg. Chem. pp. 439–447 (2008).

[44] R. Herchel, R. Boča, J. Krzystek, A. Ozarowski, Durán, and J. van Slageren, *Definitive determination of zero-field splitting and exchange interactions in Ni(II) dimer: investigation of $[Ni_2(en)_4Cl_2]Cl_2$ using magnetization and tunable-frequency high-field electron paramagnetic resonance*, J. Am. Chem. Soc. **129**, 10 306–10 307 (2007).

[45] S. Piligkos, E. Bill, D. Collison, E. J. L. McInnes, G. A. Timco, H. Weihe, R. E. P. Winpenny, and F. Neese, *Importance of the anisotropic exchange interaction for the magnetic anisotropy of polymetallic systems*, J. Am. Chem. Soc. **129**, 760–761 (2006).

[46] D. Ganyushin, and F. Neese, *First-principles calculations of zero-field splitting parameters*, J. Chem. Phys. **125**, 024 103 (2006).

[47] M. R. Pederson, and S. N. Khanna, *Magnetic anisotropy barrier for spin tunneling in $Mn_{12}O_{12}$ molecules*, Phys. Rev. B **60**, 9566–9572 (1999).

[48] M. Atanasov, C. A. Daul, and C. Rauzy, *New insights into the effects of covalency on the ligand-field parameters: A DFT study*, Chem. Phys. Lett. **367**, 737–746 (2003).

[49] A. Borel, L. Helm, and C. A. Daul, *Hybrid ligand-field theory/quantum chemical calculation of the fine structure and ZFS in lanthanide(III) complexes*, Chem. Phys. Lett. **383**, 584–591 (2004).

[50] F. Aquino, and J. H. Rodriguez, *First-principle computation of zero-field splittings: Application to a high valent Fe(IV)-oxo model of nonheme iron proteins*, J. Chem. Phys. **123**, 204 902 (2005).

[51] F. Neese, *Importance of direct spin-spin coupling and spin-flip excitations for the zero-field splittings of transition metal complexes: A case study*, J. Am. Chem. Soc. **128**, 10 213–10 222 (2006).

[52] F. Neese, *Calculation of the zero-field splitting tensor on the basis of hybrid density functional and Hartree-Fock theory*, J. Chem. Phys. **127**, 164 112 (2007).

[53] J. Kortus, T. Baruah, N. Bernstein, and M. R. Pederson, *Magnetic ordering, electronic structure, and magnetic anisotropy energy in the high-spin Mn_{10} single molecule magnet*, Phys. Rev. B **66**, 092 403 (2002).

[54] T. Baruah, and M. R. Pederson, *Density Functional Study of the conformers of Co_4-based single molecule magnet*, Int. J. Quantum Chem. **93**, 324–331 (2003).

[55] J. Kortus, M. R. Pederson, T. Baruah, N. Bernstein, and C. S. Hellberg, *Density functional studies of singlet molecule magnets*, Polyhedron **22**, 1871–1876 (2003).

[56] K. Park, M. R. Pederson, S. L. Richardson, N. Aliaga-Alcalde, and G. Christou, *Density-functional theory calculation of the intermolecular exchange interaction in the magnetic Mn_4 dimer*, Phys. Rev. B **68**, 020 405 (2003).

[57] J. Ribas-Ariño, T. Baruah, and M. R. Pederson, *Density-functional study of two Fe_4-based single-molecule magnets*, J. Chem. Phys. **123**, 044 303 (2005).

[58] J. Ribas-Ariño, T. Baruah, and M. R. Pederson, *Toward the control of the magnetic anisotropy of Fe^{II} Cubes: A DFT study*, J. Am. Chem. Soc. **128**, 9497–9505 (2006).

[59] S. Zein, C. Duboc, W. Lubitz, and F. Neese, *A systematic density functional study of the zero-field splitting in Mn(II) coordination compounds*, Inorg. Chem. **47**, 134–142 (2008).

[60] S. Zein, and F. Neese, *Ab initio and coupled-perturbed density functional theory estimation of zero-field splittings in MnII transition metal complexes*, J. Phys. Chem. A **112**, 7976–7983 (2008).

[61] C. Duboc, D. Ganyushin, K. Sivalingam, M.-N. Collomb, and F. Neese, *Systematic theoretical study of the zero-field splitting in coordination complexes of Mn(III). Density functional theory versus multireference wave-function approaches*, J. Phys. Chem. A **114**, 10 750–10 758 (2010).

[62] F. Neese, and E. I. Solomon, *Calculation of the zero-field splitting, g-values, and the relativistic nephelauxetic effect in transition metal complexes. Application to high-spin ferric complexes*, Inorg. Chem. **37**, 6568–6582 (1998).

[63] S. P. Webb, and M. S. Gordon, *The effect of spin-orbit coupling on the magnetic properties of $H_2Ti(\mu\text{-}H)_2TiH_2$*, J. Chem. Phys. **109**, 919–927 (1998).

[64] C. de Graaf, and C. Sousa, *Assesssing the zero-field splitting in magnetic molecules by wave function-based methods*, Int. J. Quantum Chem. **106**, 2470–2478 (2006).

[65] K. Sugisaki, K. Toyota, K. Sato, D. Shiomi, M. Kitagawa, and T. Takui, *Ab initio calculations of spin–orbit contribution to the zero-field splitting tensors of $n\pi^*$ excited states by the CASSCF method with MRMP2 energy correction*, Chem. Phys. Lett. **477**, 369–373 (2009).

[66] K. Fink, C. Wang, and V. Staemmler, *Superexchange and spin-orbit coupling in chlorine-bridged binuclear cobalt(II) complexes*, Inorg. Chem. **38**, 3847–3856 (1999).

[67] S. Petit, G. Pilet, D. Luneau, L. Chibotaru, and L. Ungur, *A dinuclear cobalt(II) complex of calix[8]arenes exibiting strong magnetic anisotropy*, Dalton Trans. pp. 4582–4588 (2007).

[68] L. Chibotaru, L. Ungur, C. Aronica, H. Elmoll, G. Pilet, and D. Luneau, *Structure, magnetism, and theoretical study of a mixed-valence $Co_3^{II}Co_4^{III}$ heptanuclear wheel: Lack of SMM behavior despite negative magnetic anisotropy*, J. Am. Chem. Soc. **130**, 12 445–12 455 (2008).

[69] L. Chibotaru, L. Ungur, and A. Soncini, *The origin of nonmagnetic Kramers doublets in the ground state of dysprosium triangles : Evidence for a toroidal magnetic moment*, Angew. Chem. Int. Ed. **47**, 4126–4129 (2008).

[70] A. Soncini, and L. Chibotaru, *Toroidal magnetic states in molecular wheels: Interplay between isotropic exchange interactions and local magnetic anisotropy*, Phys. Rev. B **77**, 220 406 (2008).

[71] C. J. Calzado, J. Cabrero, J. P. Malrieu, and R. Caballol, *Analysis of the magnetic coupling in binuclear complexes. I. Physics of the coupling*, J. Chem. Phys. **116**, 2728 (2002).

[72] C. J. Calzado, J. Cabrero, J. P. Malrieu, and R. Caballol, *Analysis of the magnetic coupling in binuclear complexes. II. Derivation of valence effective Hamiltonians from ab initio CI and DFT calculations*, J. Chem. Phys. **116**, 3985 (2002).

[73] C. J. Calzado, C. Angeli, D. Taratiel, R. Caballol, and J.-P. Malrieu, *Analysis of the magnetic coupling in binuclear systems. III. The role of the ligand to metal charge transfer excitations revisited*, J. Chem. Phys. **131**, 2009 (2009).

[74] R. Bastardis, N. Guihéry, and C. de Graaf, *Microscopic origin of isotropic non-Heisenberg behaviour in S=1 magnetic systems*, Phys. Rev. B **76**, 132 412 (2007).

[75] K. Andersson, P.-A. Malmqvist, and B. O. Roos, *Second-order perturbation theory with a complete active space self-consistent field reference function*, J. Chem. Phys. **96**, 1218–1226 (1992).

[76] C. Angeli, R. Cimiraglia, S. Evangelisti, T. Leinenger, and J.-P. Malrieu, *Introduction of n-electron valence states for multireference perturbation theory*, J. Chem. Phys. **114**, 10 252–10 264 (2001).

[77] N. Forsberg, and P.-Å. Malmqvist, *Multiconfigurational perturbation theory with imaginary level shift*, Chem. Phys. Lett. **274**, 196–204 (1997).

[78] C. Angeli, M. Pastore, and R. Cimiraglia, *New perspectives in multireference perturbation theory: the n-electron valence state approach*, Theo. Chem. Acc. **56**, 743–754 (1997).

[79] N. Queralt, D. Taratiel, C. de Graaf, R. Caballol, R. Cimiraglia, and C. Angeli, *On the applicability of multireference second-order perturbation theory to study weak magnetic coupling in molecular complexes*, J. Comp. Chem. **29**, 994–1003 (2008).

[80] J. Miralles, O. Castell, R. Caballol, and J.-P. Malrieu, *Specific CI calculation of energy differences : transition energies and bond energies*, Chem. Phys. **172**, 33–43 (1993).

[81] B. Huron, J.-P. Malrieu, and P. Rancurel, *Iterative perturbation calculations of ground and excited state energies from multiconfigurational zeroth-order wavefunctions*, J. Chem. Phys. **58**, 5745–5759 (1973).

[82] F. Neese, *A spectroscopy oriented configuration interaction procedure*, J. Chem. Phys. **119**, 9428 (2003).

[83] B. O. Roos, and P.-Å. Malmqvist, *Relativistic quantum chemistry: the multiconfigurational approach*, Phys. Chem. Chem. Phys. **6**, 2919–2927 (2004).

[84] N. Douglas, and N. M. Kroll, *Quantum electrodynamical corrections to fine-structure of helium*, Ann. Phys. (Leipzig) **82**, 89–155 (1974).

[85] B. A. Hess, *Relativistic electronic structure calculations employing a two-component no-pair formalism with external-field projection operators*, Phys. Rev. A **33**, 3742–3748 (1986).

[86] G. Jansen, and B. A. Hess, *Revision of the Douglas-Kroll transformation*, Phys. Rev. A **39**, 6016–6017 (1989).

[87] B. A. Hess, C. M. Marian, U. Wahlgren, and O. Gropen, *A mean-field spin-orbit method applicable to correlated wavefunctions*, Chem. Phys. Lett. **251**, 365–371 (1996).

[88] O. Christiansen, J. Gauss, and B. Schimmelpfenning, *Spin-orbit coupling constants from coupled-cluster response theory*, Phys. Chem. Chem. Phys. **2**, 965–971 (2000).

[89] R. Llusar, M. Casarrubios, Z. Barandiarán, and L. Seijo, *Ab initio model potential calculations on the electronic spectrum of Ni^{2+} doped MgO including correlation, spin-orbit and embedding effects*, J. Chem. Phys. **105**, 5321–5330 (1996).

[90] C. Bloch, *Sur la théorie des perturbations des états liés*, Nucl. Phys. **6**, 329–347 (1958).

[91] J. des Cloizeaux, *Extension d'une formule de Lagrange à des problèmes de valeurs propres*, Nucl. Phys. **20**, 321–346 (1960).

[92] R. Bastardis, N. Guihéry, N. Suaud, and C. de Graaf, *Competition between double exchange and purely magnetic Heisenberg models in mixed valence systems: Application to half-doped manganites*, J. Chem. Phys. **76**, 194 708 (2007).

[93] N. Suaud, Gaita-Ariño, J. M. Clemente-Juan, J. Sánchez-Marín, and E. Coronado, *Electron delocalization in mixed-valence Keggin polyoxometalates. Ab initio calculation*

of the local effective tranfer integrals and its consequences on the spin coupling, J. Am. Chem. Soc. **124**, 15 134–15 140 (2002).

[94] C. J. Calzado, J. M. Clemente-Juan, E. Coronado, A. Gaita-Ariño, and N. Suaud, *Role of the electron transfer and magnetic exchange interactions in the magnetic properties of mixed-valence polyoxovanadate complexes*, Inorg. Chem. **47**, 5889–5901 (2008).

[95] N. Suaud, Y. Masaro, E. Coronado, J. M. Clemente-Juan, and N. Guihéry, *Origin of the paramagnetic properties of the mixed-valenced polyoxometalate* $[GeV_{14}O_{40}]^{8-}$ *reduced by two electrons: wave function theory and model Hamiltonian calculations*, Eur. J. Inorg. Chem. pp. 5109–5114 (2009).

[96] K. W. H. Stevens, *Matrix elements and operator equivalents connected with the magnetic properties of rare earth ions*, Proc. Roy. Soc. A **65**, 209–15 (1952).

[97] H.-H. Schmidkte, *The variation of Slater-Condon parameters* F^k *and Racah parameters B and C with chemical bonding in transition group complexes*, Structure and Bonding pp. 19–35 (2004).

[98] G. Karlström, R. Lindh, P.-Å. Malmqvist, B. O. Roos, U. Ryde, V. Veryazov, P.-O. Widmark, M. Cossi, B. Schimmelpfennig, P. Neogrady, and L. Seijo, *MOLCAS: a program package for computational chemistry*, Comput. Mater. Sci. **28**, 222–239 (2003).

[99] P.-Å. Malmqvist, B. O. Roos, and B. Schimmelpfennig, *The restricted active space (RAS) state interaction approach with spin-orbit coupling*, Chem. Phys. Lett. **357**, 230–240 (2002).

[100] G. Ghigo, B. O. Roos, and P.-Å. Malmqvist, *A modified definition of the zeroth order Hamiltonian in multiconfigurational perturbation theory (CASPT2)*, Chem. Phys. Lett. **396**, 142–149 (2004).

[101] B. O. Roos, R. Lindh, P.-Å. Malmqvist, V. Veryazov, and P.-O. Widmark, *New relativistic ANO basis sets for transition metal atoms*, J. Phys. Chem. A **109**, 6575–6579 (2005).

[102] V. M. García, O. Castell, R. Caballol, and J.-P. Malrieu, *An iterative difference-dedicated configuration interaction. Proposal and test studies*, Chem. Phys. Lett. **238**, 222–229 (1995).

[103] C. J. Calzado, J. P. Malrieu, J. Cabrero, and R. Caballol, *Excitation energy dedicated molecular orbitals. Methods and applications to magnetic systems*, J. Phys. Chem. A **104**, 11 636–11 643 (2000).

[104] *Neese, F.; ORCA – An ab initio, density functional and semiempirical program package, Version 2.7. University of Bonn, 2010.*

[105] F. Weigend, and R. Ahlrichs, *Balanced basis set of split valence, triple zeta and quadruple zeta valence quality for H to Rn: design and assessment of accuracy*, Phys. Chem. Chem. Phys. **7**, 3297–3305 (2005).

[106] R. Maurice, R. Bastardis, C. de Graaf, N. Suaud, T. Mallah, and N. Guihéry, *Universal theoretical approach to extract anisotropic spin Hamiltonians*, J. Chem. Theory Comput. **5**, 2977–2984 (2009).

[107] R. Maurice, C. de Graaf, and N. Guihéry, *Magnetostructural relations from a combined ab initio and ligand field analysis for the nonintuitive zero-field splitting in Mn(III) complexes*, J. Chem. Phys. **133**, 084 307 (2010).

[108] R. L. Carlin, R. D. Chirico, E. Sinn, G. Mennenga, and L. J. de Jongh, *Magnetic ordering in cobalt chloride-triphenylphosphine ($CoCl_2.2P(C_6H_5)_3$) and cobalt bromide-triphenylphosphine ($CoBr_2.2P(C_6H_5)_3$)*, Inorg. Chem. **131**, 2218–2222 (2009).

[109] J. Krzystek, S. A. Zvyagin, A. Ozarowski, A. T. Fiedler, T. C. Brunold, and T. J., *Definitive spectroscopic determination of the Zero-Field Splitting in high-spin Cobalt (II)*, J. Am. Chem. Soc. **126**, 2148–2155 (2004).

[110] B. R. Stults, R. S. Marianelli, and V. W. Day, *Distortions of the coordination polyhedron in high-spin Manganese (III) complexes. 3. Crystal and molecular structure of γ-tris(acetylacetonato)manganese(III): A tetragonally elongated octahedral form*, Inorg. Chem. **18**, 1853–1858 (1979).

[111] J. Krzystek, G. J. Yeagle, J.-H. Park, R. D. Britt, M. W. Meisel, L.-C. Brunel, and J. Telser, *High-frequency and -field EPR spectroscopy of tris(2,4-pentanedionato)manganese(III): Investigation of solid-state versus solution Jahn-Teller effects*, Inorg. Chem. **42**, 4610–4618 (2003).

[112] G. Charron, F. Bellot, F. Cisnetti, G. Pelosi, J.-N. Rebilly, E. Rivière, A.-L. Barra, T. Mallah, and C. Policar, *Glycoligands tuning the magnetic anisotropy of Ni^{II} complexes*, Chem. Eur. J. **13**, 2774–2782 (2007).

[113] C. Platas-Iglesias, L. Vaiana, D. Esteban-Gómez, F. Avecilla, J. A. Real, A. de Blas, and T. Rodríguez-Blas, *Electronic structure study of seven-coordinate first-row transition metal complexes derived from 1,10-diaza-15-crown-5: A successful marriage of theory with experiment*, Inorg. Chem. **44**, 9704–9713 (2005).

[114] J.-N. Rebilly, G. Charron, R. Rivière, E. Guillot, A.-L. Barra, M. D. Serrano, J. van Slageren, and T. Mallah, *Large magnetic anisotropy in pentacoordinate Ni^{II} complexes*, Chem. Eur. J. **14**, 1169–1177 (2008).

[115] J. P. Fackler Jr., and A. Avdeef, *Crystal and molecular structure of tris(2,4-pentanedionato)manganese(III), $Mn(O_2C_5H_7)_3$, a distorted complex as predicted by Jahn-Teller arguments*, Inorg. Chem. **13**, 1864–1875 (1974).

[116] A. K. Gregson, D. M. Doddrell, and P. C. Healy, *Low-temperature magnetic properties of three vanadium(III) and maganese(III) β-diketonate complexes*, Inorg. Chem. **17**, 1216–1219 (1978).

[117] H. J. Gerritsen, and E. S. Sabisky, *Paramagnetic resonance of trivalent Manganese in Rutile (TiO_2)*, Phys. Rev. **132**, 1507–1512 (1963).

[118] L. B. Dugad, D. V. Behere, V. R. Marathe, and S. Mitra, *Magnetic properties and electronic structure of Manganese(III) porphyrins*, Chem. Phys. Lett. **104**, 353–356 (1984).

[119] S. Vancoillie, and K. Pierloot, *Multiconfigurational g tensor calculation as a probe for the covalency of the copper-ligand bonds in copper(II) complexes: $[CuCl_4]^{2-}$, $[Cu(NH_3)_4]^{2+}$ and plastocyanin*, J. Phys. Chem. A **112**, 4011–4019 (2008).

[120] J.-N. Rebilly, *Synthèse de molécules à haut spin anisotropes à ponts cyanure*, Ph.D. thesis, Université Paris Sud, Orsay, Equipe du Pr. Talal Mallah (2005).

[121] R. Maurice, N. Guihéry, R. Bastardis, and C. de Graaf, *Rigorous extraction of the anisotropic multispin Hamiltonian in bimetallic complexes from the exact electronic Hamiltonian*, J. Chem. Theory Comput. **6**, 55–65 (2010).

[122] R. Maurice, C. de Graaf, and N. Guihéry, *Magnetic anisotropy in binuclear complexes in the weak-exchange limit: From the multispin to the giant-spin Hamiltonian*, Phys. Rev. B **81**, 214 427 (2010).

[123] R. Maurice, A. M. Pradipto, N. Guihéry, R. Broer, and C. de Graaf, *Antisymmetric magnetic interactions in oxo-bridged copper(II) bimetallic systems*, J. Chem. Theo. Comput. **6**, 3092–3101 (2010).

[124] R. Maurice, K. Sivalingam, D. Ganyushin, N. Guihéry, C. de Graaf, and F. Neese, *Theoretical determination of the zero-field splitting in copper acetate monohydrate*, Inorg. Chem. **50**, 6229–6236 (2011).

[125] B. Bleaney, *A citation classic commentary on Anomalous paramagnetism of copper acetate by Bleaney, B. and Bowers, K. D.*, Current Contents **30**, 20 (1990).

[126] G. M. Brown, and C. R., *Dinuclear copper(II) acetate monohydrate: A redetermination of the structure by neutron-diffraction analysis*, Acta Cryst. **B29**, 2393–2403 (1973).

[127] P. K. Ross, M. D. Allendorf, and E. I. Solomon, *Detailed spectral studies of copper acetate: Excited-state interactions in copper dimers*, J. Am. Chem. Soc. **111**, 4009–4021 (1989).

[128] A. Elmali, *The magnetic super-exchange coupling in copper(II) acetate monohydrate and a redetermination of the crystal structure*, Turk. J. Phys. **24**, 667–672 (2000).

[129] R. Boča, and R. Herchel, *Antisymmetric exchange in polynuclear metal complexes*, Coord. Chem. Rev. **254**, 2973–3025 (2010).

[130] A. Bencini, and D. Gatteschi, *The effect of antisymmetric exchange on the E.P.R. spectra of coupled pairs of transition metal ions*, Mol. Phys. **47**, 161–169 (1982).

[131] K. E. Kauffmann, C. V. Popescu, Y. Dong, J. D. Lipscomb, L. Que Jr., and E. Münck, *Mössbauer evidence for antisymmetric exchange in a diferric synthetic complex and diferric methane monooxygenase*, J. Am. Chem. Soc. **120**, 8739–8746 (1998).

[132] J. Yoon, L. M. Mirica, D. P. Stack, and E. I. Solomon, *Spectroscopic demonstration of a large antisymmetric exchange contribution to the spin-frustrated ground state of a D_3 symmetric hydroxy-bridged trinuclear Cu(II) complex: Ground-to-excited state superexchange pathways*, J. Am. Chem. Soc. **126**, 12 586–12 595 (2004).

[133] P. W. Anderson, *Antiferromagnetism. Theory of superexchange interaction*, Phys. Rev. **79**, 350–356 (1950).

[134] J. B. Goodenough, *Theory of the role of covalence in the perovskite-type manganites [La,M(II)]MnO_3*, Phys. Rev. **100**, 564–573 (1955).

[135] J. Kanamori, *Superexchange interaction and symmetry properties of electron orbitals*, J. Phys. Chem. Solids **10**, 87–98 (1959).

[136] E. Bordas, C. Caballol, and C. de Graaf, *Ab initio study of the magnetic coupling in oxalato-bridged dinuclear Ni(II) complexes*, J. Mol. Struct.-THEOCHEM **727**, 173–179 (2005).

[137] J. F. Nye, *Physical properties of crystals: Their representation by tensors and matrices* (Clarendon Press, Oxford) (1985).

[138] G. Juhász, R. Matsuda, S. Kanegawa, K. Inoue, O. Sato, and K. Yoshizawa, *Bistability of magnetization without spin-transition in a high-spin Cobalt(II) complex due to angular momentum quenching*, J. Am. Chem. Soc. **131**, 4560–4561 (2009).

[139] N. Ishikawa, M. Sugita, and W. Wernsdorfer, *Quantum tunneling of the magnetization in lanthanide Single-Molecule Magnets: Bis(phthalocyaninato)terbium and bis(phthalocyaninato)dysprosium anions*, Angew. Chem. Int. Ed. **117**, 2991–2995 (2005).

AUTEUR: Rémi MAURICE

TITRE: Zero-Field Anisotropic Spin Hamiltonians in First-Row Transition Metal Complexes: Theory, Models and Applications

DIRECTEURS DE THESE: Pr. Nathalie Guihéry (Toulouse) et Dr. Coen de Graaf (Tarragone)

LIEU ET DATE DE SOUTENANCE: le lundi 20 juin 2011 à Toulouse

Abstract

Magnetic anisotropy is responsible for the slow relaxation of the magnetization in single molecule magnets. The main goal of this work is to understand the factors that govern local and intersite anisotropies in polynuclear compounds. For this purpose, correlated relativistic calculations are performed in mono- and bi-nuclear species. The main degrees of freedoms of the two-step state-interaction ab initio method have been optimized in order to obtain anisotropic parameters in good agreement with the spectroscopic data. The effective Hamiltonian theory provides a universal procedure of extraction of these parameters. It has therefore been used to check the accuracy of the standard model and to propose improved models when necessary. Finally, the anisotropy parameters have been rationalized in several cases by using the quasi-degenerate perturbation theory.

Keywords: relativistic and correlated *ab initio* calculations, magnetic anisotropy, transition metal complexes, ligand-field theory

---

Résumé

L'anisotropie magnétique est à l'origine de la lente relaxation de l'aimantation des aimants moléculaires. L'objectif principal de ce travail est de comprendre les facteurs qui gouvernent les anisotropies locales et intersites dans les composés polynucléaires. Des calculs relativistes et corrélés ont été effectués sur des systèmes mono- et bi-nucléaires. Les dégrés de liberté principaux de la méthode *ab initio* d'interaction d'états en deux étapes ont été optimisés pour obtenir des paramètres d'anisotropie en bon accord avec les résultats spectroscopiques. La théorie des hamiltoniens effectifs procure un procédé universel d'extraction de ces paramètres. Elle a donc été utilisée pour vérifier la validité des modèles usuels et proposer des éventuelles améliorations aux modèles. Enfin, les paramètres d'anisotropies ont été rationalisés dans certains cas à l'aide de la théorie des perturbations quasi-dégénérées.

Mots-clés: calculs *ab initio* relativistes et corrélés, anisotropie magnétique, complexes de métaux de transition, théorie du champ cristallin

---

DISCIPLINE ADMINISTRATIVE: Physico-chimie théorique

INTITULE ET ADRESSE DU LABORATOIRE: Laboratoire de Chimie et de Physique Quantiques, Bât. 3R1B4, Université Paul Sabatier, 118 route de Narbonne, TOULOUSE Cédex 4, France